MODELLING AND MONITORING OF SUSPENDED MATTER IN SURFACE WATERS USING REMOTELY SENSED DATA

Asif Mumtaz Bhatti

A dissertation submitted to
Kochi University of Technology
in partial fulfillment of the requirements
for the degree of

Doctor of Philosophy

Graduate School of Engineering
Kochi University of Technology
Kochi, Japan

March 2008

Modelling and Monitoring of Suspended Matter in Surface Waters Using Remotely Sensed Data **Asif M. Bhatti**

MODELLING AND MONITORING OF SUSPENDED MATTER IN SURFACE WATERS USING REMOTELY SENSED DATA

Asif Mumtaz Bhatti

A dissertation submitted to
Kochi University of Technology
in partial fulfillment of the requirements
for the degree of

Doctor of Philosophy

Special Course for International Students
Department of Engineering
Graduate School of Engineering
Kochi University of Technology
Kochi, Japan

March 2008

ABSTRACT

Water is one of the most precious natural resources and the lifeblood for sustained economic development in any country. Water resources & environmental management is essential for sustaining quality of life on earth. In the future, therefore, it will be important to incorporate water quality assessment as an integral part of water resources and environmental planning, development and management. Without this approach the problems of the water & environmental sector are going to compound in the future. Modeling and monitoring of suspended matters in water bodies is a difficult task because of many influencing factors. Synoptic information on water quality is difficult to obtain from a routine in situ monitoring network. The conventional point sampling campaigns do not give either the spatial or temporal view of water quality needed for accurate assessment and management of water bodies. New sources of data must be explored to complement traditional data collection techniques. Remote sensing makes it possible to monitor the water bodies effectively and efficiently and, identifying areas with significant water quality problems. Remote sensing has been used extensively for the delineation of the water bodies and has an important role in water quality evaluation and management strategy. Monitoring large areas on a frequent basis can only be achieved economically with remote sensing. The aim of this study was to develop the monitoring system that can be used to monitor suspended matters, efficiently and effectively, in water bodies on seasonal bases and during floods.

Spectral reflectance for different types and concentration of suspended sediments are unique. Magnitude and spectral shape varied with type, texture, grain size and concentration of suspended sediments in surface water. The reflectance in the red and near- infrared (NIR) wavelength 700-900 is a useful range for determining the amount of suspended sediments. However, the wavelength range 525-665 provides information about sediments type. Band ration models allow the accurate quantification of suspended sediments. At a depth of 60 cm, in the visible domain, there is no bottom effect when suspended sediment concentrations were above 400mg/l. The selection of ASTER 3B-NIR image can be the solution to overcome the effects of surface roughness for studying water bodies. Under windy conditions and waves on the water surface, the spectrum average and ratio of bands may decrease the effect of waves on the observed spectral signals. The above-water measurements are problematic because of inefficient methods for the removal of surface reflection effects from the total upwelling radiance signals. It is strongly recommended that the subsurface spectral reflectance measurement is better option for the researcher who attempt to analyze water by using remotely sensed data.

Many inland and coastal waters are affected by water quality problems. The simple band ratio algorithms do not function well in optically complex waters. It is obvious that more sophisticated remote sensing models and approach is needed to establish the relationship between water quality parameters and spectral signatures. Water bodies in general reflect (as subsurface irradiance reflectance) in the range of 1 to 10% of downwelling irradiance. To improve the understanding of coastal and inland waters, optical remote sensing is a helpful tool and technique. The proposed 2 band model approach is considered to be the

best predictor of SSC. The reflectance peak in red domain and ratio of ALOS/AVNIR2 Band 1 and Band 3 is well correlated with chlorophyll concentration The ratio of NIR and green domain is best predictor of TSS. The optical depth is found to be strongly correlated with Chl-a and TSS concentration. The research work demonstrates an example for effective and efficient application of remotely sensed data for monitoring total suspended sediments (TSS), chlorophyll-a, colored dissolved organic matter (CDOM), secchi depth, and turbidity in water bodies. The successful application of remote sensing in water quality monitoring necessitate for suitable sensors with spatial and spectral resolution that are compatible with the features to be monitored, complementary in situ data and experimental methodology that is carefully designed.

Remote sensing makes it possible to monitor the water bodies effectively & efficiently and is most successfully used as part of a multidisciplinary approach to addressing natural resource questions. The application of developed 2 band model for assessment of suspended sediment concentration is promising. Integrated optical modeling technique is a useful tool for collection of information over large areas and to monitor river waters carrying heavy suspended sediments in the absence of ground truth data. Algorithms based on the fundamentals of hydrological optics are strongly advocated. The performance of such algorithms is always subject to compatibility between the waters under study and the waters from which data were obtained for algorithm development. The Indus River, Pakistan is selected as case study. The integration of satellite data, in situ data, and optical models is an effective tool for monitoring erosion, deposition areas, sediment distribution, and suspended matter in water bodies. The proposed system offers an ideal opportunity to consolidate various parameters such as chlorophyll, suspended sediments and CDOM. The present research work is successful example for the researchers to substantiate the utility of remotely sensed data for water quality monitoring and modeling of inland and coastal waters.

Acknowledgement

Foremost, I would like to express my sincere gratitude to my advisor Prof. Seigo Nasu for giving me chance to continue doctoral course under his kind guidance. With innovative ideas, broad vision and clear sense of direction, he has always an answer for everything. His utmost patient support on each and every step helped me to make this research possible. I think he is the best professor and advisor.

I am really grateful to my second advisor Professor Masataka TAKAGI for extremely fruitful discussions and guidance.

Special thanks go to Prof. Dr. Donald C. Rundquist, Director, Center for Advanced Land Management Information Technologies (CALMIT), University of Nebraska-Lincoln for providing opportunity to work together and willingness for data support to purse the research.

I gratefully acknowledge the financial assistance provided by Kochi University of Technology (KUT), Japan, without which this research would not have been possible.

Thanks to my committee members, International Relation Center (IRC) at KUT, Prof. Masahiro Murakami, Rieko TOBISAKI, MIZOBUCHI Michiko and everyone at KUT who gave their valuable time, skills and suggestions to complete this research.

Many thanks are directed to my father and mother, the best parents ever.

Finally and most of all I would like to sincerely thank my wife Sabah for her endless love, patience, sacrifice and incredible support, which kept me going throughout the ordeal. I also want to thank my daughter Eman and son Shayan for all the love and happiness they give me.

TABLE of C O N T E N T S

List of Figures

List of Table

CHAPTER 1

INTRODUCTION

1.1 BACKGROUND

Water is one of the most precious natural resources and the lifeblood for sustained economic development in any country. Water distinguishes the planet earth from all other plants by giving it its blue colour. Of all the water on the earth, 97.5% is in the oceans, thus the total fresh water is only 2.5%, most of which (68.7%) is in the form of snow and ice. Almost all of it is practically inaccessible in the polar ice caps. About 31.1% of freshwater is underground, much of it in deep aquifers. The most accessible fresh water contained in lakes, reservoirs and rivers is only 0.26% of the total amount of fresh water or 0.007% of all water (Ishfaq A., 2002). It is universal truth that meagre resources compel for their better utilization and preservation. Water resources & environmental management is essential for sustaining quality of life on earth.

Synoptic information on water quality is difficult to obtain from a routine in situ monitoring network. The conventional point sampling campaigns do not give either the spatial or temporal view of water quality needed for accurate assessment and management of water bodies. Therefore, the difficulty of overall and successive water quality sampling becomes a barrier in water quality monitoring, forecasting and management. Remote sensing makes it possible to monitor the water bodies effectively, efficiently, and identifying areas with significant water quality problems. Remote sensing is a tool and technique that provides a platform for large-scale synoptic observations and continuous monitoring of water bodies. Remote sensing provides a synoptic view of the spatial distribution of water quality parameters (WQP) present in water bodies. This knowledge of the distribution is imperative in environmental water studies as well as for resource management.

Many inland and coastal waters are affected by water quality problems. The simple band ratio algorithms do not function well in optically complex waters. It is obvious that more sophisticated remote sensing models and approach is needed to establish the relationship between water quality parameters and spectral signatures. Water bodies in general reflect (as subsurface irradiance reflectance) in the range of 1 to 10% of downwelling irradiance. The majority of waters bodies reflect between 2 and 6% of downwelling irradiance. To improve the understanding of coastal and inland waters, optical remote sensing is a helpful tool and technique. The successful application of remote sensing in water quality monitoring necessitate for suitable sensors with spatial and spectral resolution that are compatible with the features to be monitored, complementary in situ data and experimental methodology that is carefully designed.

Remote sensing is a useful tool for large-scale monitoring of inland and coastal water quality and its advantages have long been recognized. Review of intensive literature reveals that the majority of work addressed the water quality parameters with the aim to develop algorithms by processing remotely sensed data. Most of the already done works have no multitemporal or multi-site applicability. The change in water quality parameters, both in space and time as well as in reflectance signature from point to point, makes the

field applicability of remotely sensed data more difficult. The new developed remote sensing sensors with higher sensitivity and more flexible band widths allowed researchers to monitor efficiently and effectively water quality of coastal and inland waters. The rigorous understanding of that "What can water-leaving remotely sensing signals really give us, and with what accuracy?" is vital for application of remote sensing and development of water quality monitoring system. The techniques and approaches for remotely data collection and application are insufficient to address and overcome the filed problems. This research emphasis on measurement protocols, methodology and application of remotely sensed data with necessary accuracy for modeling and monitoring of suspended matters in surface waters.

1.2 THE PROBLEM

Modeling and monitoring of suspended matters in water bodies is a difficult task because of many influencing factors. The monitoring stations are generally fairly sparse, thus any extensive spatial resolution cannot be obtained. Some ad-hoc spatial monitoring campaigns do take place, however, their expense and logistical difficulty prohibits extensive use. Traditional methods of sampling and analysis are time consuming, labour intensive and provide only point data where measurements at any location on one lake, or even on many lakes, are generally necessary (Lodhi, 1997). The word suspended matter represents the all type of matter, inorganic and organic, present in water bodies. The water quality problems of different watr bodies and at different sampling points of the same water body are not same and have unique characteristics. The field campaign and prime water quality parameter under consideration depends on the objective of the study. In case of dams, sediments are one of the most important environmental problem throughout the world. High concentration of suspended matter in water is a critical element in the economic feasibility of a project and could shorten the useful life of reservoirs & dams. The sedimentation has engineering consequences because it leads to a reduction of the storage capacity of the reservoir and, hence, of its efficiency.

In coastal and inland waters the other water quality parameters such as total suspended sediments, chlorophyll-a and colored dissolved organic matters are of great importance. However, the water quality parameters individual and in combination effects the water resources and the assessment of these parameters is imperative for sustainable water resources development and management. In this era, the traditional methods are not enough to address the water quality distribution pattern in water bodies and to highlight the regional and global water quality issues. Remote sensing makes it possible to monitor the water bodies effectively and efficiently and identifying areas with significant water quality problems. Remote sensing is the observation of objects without being in physical contact with the object. Remotely sensed data and techniques enhance the efficiency and reliability of the data, as well as complement traditional data collection techniques. Remote sensing has been used extensively for the delineation of the water bodies and has an important role in water quality evaluation and management strategy. Today's remote sensing technology can detect a much larger portion of the electromagnetic spectrum with high special and spectral resolution, but there is still a need for new and more efficient analysis methods for extracting as much useful information as possible from captured signature.

1.3 STUDY AREA

The Indus River, Pakistan is one of the largest sediment producing rivers in the world. The Indus rises in Tibet, in the snow-clad Kailas range of the Himalayas, is about 5,500 m above mean sea level. The river slope from the headwaters to Attock is approximately 1/ 300; from Attock to Mithankot it is 1/4,000; and from Mithankot to the sea it averages 1/7,000. The total length of the Indus is about 2,900 km. The Indus River alone provides 65% of total river flows, while the contribution of River Jhelum is 17 %. The main source of sediment is from the glacial landscape and erosion from steep sided barren slopes.

The Monobe River has its source at Mt. Akagioyama (1,436 m) in Tsurugi mountain range; the length of the river is 68.12km and the basin area is 508.2 km^2 , in which , mountain forest is 461.8 km^2, flat land is 38.2 km^2 and water course is 8.2 km^2. The Monobe River has three dams and two head works, namely Nagase Dam, Yoshino Dam, Suita Dam, Godo Weir and Togo Weir from upstream to downstream.

The Altamaha River in Georgia, USA drains one of the largest basins on the east coast. The watershed area of the river including its tributaries is 36,260 sq km. There is no dam on the river. The St. Marys river is in the southeastern United States. The river is approximately 144 km long. It rises in the southeastern Okefenokee Swamp, and flows into the Atlantic Ocean near St. Marys, Georgia and Fernandina Beach, Florida. Apalachicola Bay is an estuary and lagoon, covering an area of about 208 sq. mile, located on northwest coast of Florida. The Apalachicola River is the largest source of fresh water to the estuary. The lagoon has been designated as a National Estuarine Research Reserve.

1.4 OBJECTIVES

The main theme of the research is the development of suspended matter monitoring system with necessary data and accuracy by processing remotely sensed data. In this research work the optical models and spatial information available from the satellite data is integrated to improve the accuracy for quantification of suspended matters. The purpose of the study is to evaluate the capabilities and potential of remotely sensed data for modeling and monitoring of water quality variables in surface waters. The feasibility of the remotely sensed data in the absence of ground truth data is demonstrated.

1.5 STATE OF THE ART

The water bodies with different optically active substances are complex and require sophisticated models and precise approach for monitoring and modeling of water constituents. To make quantitative statements about the light field in the water, the inherent optical properties of the water body must be estimated depending on wavelength by means of specific optical properties of the water constituents - phytoplankton, suspended matter, and colored dissolved organic matter and their concentrations. The absence of ground truth data force to advocate the use of valuable time series remote sensing data. Data from remote sensing can easily indicate a spatial pattern of a parameter, which is not possible though traditional measurement campaign. Numerous researchers have developed algorithms for the relationship between the water quality parameters and

radiance or reflectance. A few studies have taken the next step and used these algorithms to estimate parameters for another time or place. In this research work attention is paid to develop the monitoring system for retrieval of suspended matters by integrating multispectral data, hyperspectral data and optical modeling. The correction of atmospheric effects plays an important role in case of multispectral remotely sensed data. The study leads to a robust and effective monitoring system for assessment of suspended matters/suspended sediments in water bodies.

The research study will have the following major outcomes:

1- The research work demonstrates the feasibility of remotely sensed data for efficient and effective monitoring of water bodies. The study is first an extensive remotely sensed work on Indus River, Pakistan and provides practical tools for modeling and monitoring of suspended matters.

2- The research emphasis on new concepts, techniques and approaches for monitoring of water quality parameters by means of remote sensing.

3- The research work provides model for monitoring suspended matter distribution in water bodies on seasonal bases and during floods.

4- The study identifies key limiting factors and set directions to solve potential problems that may be encountered in the field application of the remote sensing technology.

5- The developed monitoring system will prove to be a useful tool for sustainable water resources and environmental management.

1.6 STUDY FRAMEWORK

The dissertation consists of mainly four parts. The first part emphasis on the importance of remotely sensed data in water quality management and highlights the objective of the present research study.

The second part deals with hyperspectral remote sensing and thoroughly explains calibration of hyperspectral spectroradiometer equipment, effect of influencing factors on remotely sensed signatures, measurement protocols and suspended sediment concentration models developed in controlled conditions with different types and concentration of suspended sediments.

The third part describes the application of hyperspectral data in field and elucidates the influence of various influencing parameters on spectral signatures in field conditions. The optical modeling and development of water quality models for effective and efficient monitoring of water quality parameters is investigated in detail.

The forth part, research and analysis part, mainly concentrate on techniques and approaches for the retrieval of suspended sediments by using ALOS, ASTER and SPOT multispectral remotely sensed data. In this part of the thesis, the suspended sediment monitoring system is developed.

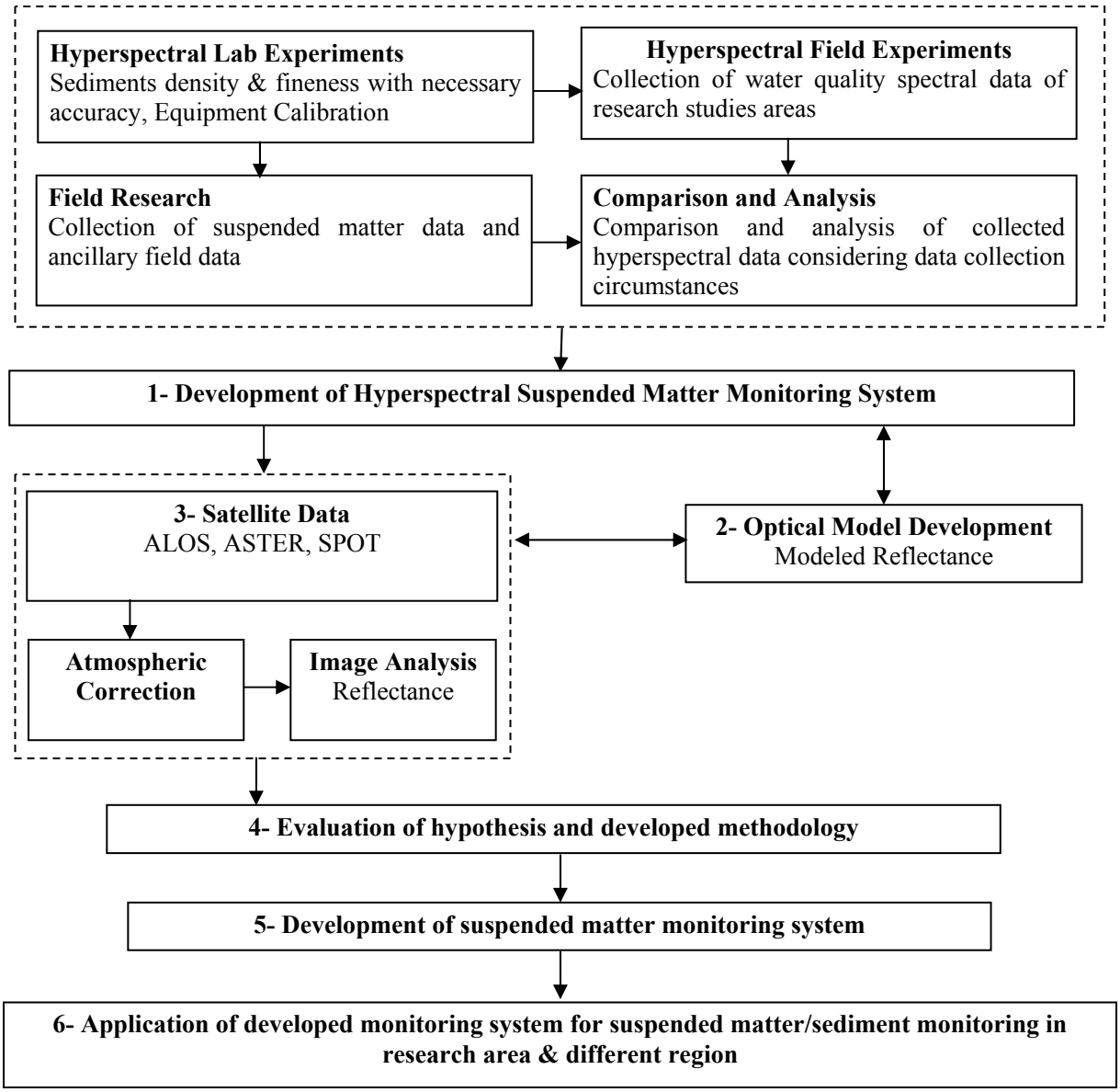

Figure 1.1 Study Framework

1.7 ORGANIZATION OF THE THESIS

The chapter wise description of the thesis is as follow:

Chapter 1 describes the introduction, research study area, nature of problem, study frame work and the objective of the research study. This chapter advocates the use of valuable time series remote sensing in the research areas. In order to take into account the variety of environmental conditions, the research area in Japan, USA and Pakistan was selected.

Chapter 2 mainly deals with hyperspectral remote sensing and work is based on lab experiments in controlled conditions. Lab experiments were performed at Kochi University of Technology. The fundamental characteristics of suspended sediment as a

function of wavelength are introduced. Effect of different concentration of suspended sediments on spectral signals were investigated by numerous researchers, however, the relationship between different types of soil and spectral signatures in black dark room and in field conditions with different sensors were first time investigated and discussed in detail. The relationship between simulated satellite data, derivative of reflectance and SSC was also explained. Laboratory based model for measurement of chlorophyll- a was also developed. In this chapter the emphasis is placed on the formulation of methodology and feasibility of remotely sensed signals for measurement of water quality parameters. The quality of remotely sensed signatures plays a critical role in the accuracy of retrieved parameters.

Chapter 3 emphasis on application of hyperspectral data in field and delineate the effect of varying field conditions on remotely sensed data. Unique characteristics of hyperspectral remotely sensed data are introduces. Different experiments were made to elucidate the effect of wave, surface roughness, field of view, the interaction between light and water, and surface reflection effects on the acquired remotely sensed data. The comparison between above water surface and subsurface reflectance is also explained in details and the surface reflection effects were also quantified. The effect of view geometry on ASTER data is also explored.

Chapter 4 describes the practical application of hyperspectral remotely sensed data in water quality modeling. The water quality models for total suspended sediments (TSS), chlorophyll-a, turbidity, colored dissolved organic matters (CDOM) are presented. The developed algorithms have shown high accuracy and the same models were applied on other places. In this chapter the effect of water variables on remotely sensed signals were identified and investigated in details. This chapter mainly consists of our joint research work with Center for Advanced Land Management Information Technologies (CALMIT), University of Nebraska-Lincoln, USA.

Chapter 5 focused on the concept of water remote sensing and optical modeling approach. The impact of water quality parameters, size distribution and composition of particulate matter and/or dissolved constituents on inherent optical properties (IOPs) is discussed. Based on the in situ measurements, the modeled spectra were developed for all the sampling points. The comparisons of developed modeled spectra with in situ hyperspectral data acquired by spectroradiometer are presented. The comparison of inverse and forward modeling approach is explained in detailed in this chapter.

Chapter 6 is considered to be more useful for practical purpose. The synthesis of this research is given in chapter 6. This chapter identifies the applicability of multispectral data (ALOS, SPOT, and ASTER) for quantification of suspended sediments in rivers and reservoirs. In this chapter the integration of multispectral data and modeled spectra was adopted to estimate the suspended sediment concentration along the river reach, which is not possible through traditional measurement campaigns. Application of selected satellites data (ALOS, ASTER & SPOT) were discussed in detail and model was developed for assessment of SSC along the Indus River, Pakistan.

Finally in *Chapter 7* the conclusions of this research work are highlighted, leading to recommendations for water quality monitoring and useful application of remotely sensed data in hydrology and water management.

CHAPTER 2

HYPERSPCTRAL REMOTE SENSING – LAB EXPERIMENTS

2.1 Introduction

Remote sensing holds potential for monitoring and estimating suspended sediments in surface water. Traditional methods of sampling and analysis are time consuming, labor intensive and provide only the point data where measurements at many locations on one lake, or even on many lakes, are generally necessary (Lodhi, 1997). The strength of remote sensing techniques lies in their ability to provide both spatial and temporal views of surface water quality parameters that is typically not possible from in situ measurements. Remote sensing makes it possible to monitor the water bodies effectively and efficiently and, identifying areas with significant water quality problems. Remote sensing has been used extensively for the delineation of the water bodies. Remote sensing has an important role in water quality evaluation and management strategy. Monitoring large areas on a frequent basis can only be achieved economically with remote sensing (Engam 1991).

Numerous researchers have developed algorithms for the relationship between the concentration of suspended sediments and radiance or reflectance. A few studies have taken the next step and used these algorithms to estimate suspended sediments for another time or place (Ritchie, 1988). The suspended sediment concentration and reflectance relationship depends on many factors including physical and optical properties of sediment type and sensor zenith angle (Kuo and Cheng 1978, Chen et al. 1991). The absorption and scattering properties of sediment type affect water reflectance (Novo et al. 1989). The presence of sediment in water changes the backscattering characteristics of the water dramatically. The synoptic view provided by remote sensing gives resource managers different type of data owing to large area coverage, timeliness and repetitive nature of satellite image, which is not possible from traditional surface data collection campaigns. The spectral reflectance of suspended sediment in surface water is a function of both the quantity and characteristics (particle size, texture, absorption) of sediments

2.2 Purpose of the Study

It is imperative to determine the quantity and type of suspended matters and optimal wavelength to enhance the reliability and applicability of remotely sensed data for water quality monitoring. The calibration of hyperspectral Field SpecPro FR Spectroradiometer is the first step to improve the accuracy and reliability of the data. Controlled experiments were conducted in order to investigate hyperspectral spectroradiometer equipment characteristics and the effects of varying concentrations and types of suspended sediments on the spectral signature of the surface water. The effect of various concentrations of chlorophyll-a on spectral reflectance was also investigated. The purpose of the research was to demonstrate the relationship of varying concentration of suspended sediments and chlorophyll-a on detected hyperspectral reflectivity.

2.3 Hyperspectral Spectroradiometer Equipment

2.3.1 Equipment characteristics

Field SpecPro FR Spectroradiometer (Analytical Devices, Inc., Boulder, CO) was used to collect the upwelling radiance from the water surface. This portable spectrometer combines three spectrometers to cover the wavelength range from 350 to 2500 nm. A photodiode array spectrometer is used to cover the 350 to 1000 nm spectral range (UV/VNIR), while two fast-scanning (0.1 sec) spectrometers provide coverage for the two wavelength ranges from 1001 to 1800 nm and 1801 to 2500 nm (SWIR 1 and SWIR 2). The sampling interval is 1.4 nm and spectral resolution of 3 nm from 350-100 nm, which meet the nominal sampling and resolution requirements for hyperspectral remote sensing applications (Curtiss, 1994). For hyperspectral remote sensing, a spectral resolution of about 10 nm and a spectral sampling interval of about 2 to 3 nm is required (Goetz and Calvin, 1987, Goetz, 1992b).

Radiation input to the ASD FieldSpec FR spectrometers is through a fiber optic bundle, 5 meters in length. The fiber optic cable provides the ability to quickly and easily point the spectrometer field of view at different targets, especially when using the pistol grip.

Table 2.1 ASD Field SpecPro FR Spectroradiometer Specification

Parameter	Range
Spectral range	350-2500 nm
Sampling Interval	1.4 nm for range 350-1000 nm) 2 nm for range 1000-2500 nm
Spectral Resolution	3 nm for range 350-1000 nm 10 nm for range 1000-2500 nm
Field of View	25° nominal with 1^o, 8^o option
Scan Time	0.1 sec
Power Source	External NiCad rechargeable batteries
Size	35 x 29 x 13 cm
Weight	7 kg + 2.2 kg battery pack

2.3.2 Data acquisition and management

Data acquisition and management is time-consuming when done properly. Accurate technical approach for data acquisitioning, data analysis and data management is the first step to reach the full potential of spectroscopic remote sensing for target identification. The operating software for the FieldSpec FR spectroradiometer instrument is called RS^3. The RS^3 software provides a graphical user interface for collection of remote sensing data and displays the spectra of the target. ASD View SpecPro provides post-acquisition utilities. The software is sued for analysis of the acquired spectral data. The software is DOS-based and provided with the Instrument. The features and utility of the both softwares and interface is explained in detail in users manual.

2.4 Factors Affecting Hyperspectral Measurements

2.4.1 Introduction

The definition of accurate methodology and overall experimental design is the base for precise research. The collection of accurate spectra requires an awareness of the influences of the various sources owing to sensitivity of the instrument. If the formulation of an appropriate experimental design is not obvious, the results may lead to the errors. Technical issues such as equipment calibration, effect of environmental factors, target viewing and illumination geometry, and sampling strategy need to be considered; keeping in view the overall objective of the research. The experimental design must be developed to account for the characteristics of the equipment. The characteristics of equipment and the influence on spectral measurements limit the practical use of the spectroradiometer. The ASD FieldSpec FR spectroradimeter is calibrated in the laboratory to achieve maximum accuracy of radiance measurements. The calibration room was completely darkened; the only source of illumination was the halogen lamp.

2.4.2 Factors Affecting Measurements

2.4.2.1 Warm-up time

The sensitivity of the equipment changes significantly during warming up time. The sensitivity of the spectroradiometer is examined in the laboratory under controlled conditions. The reflectance of the white reference panel was acquired after every 10 minutes. During the warming up time the signals acquired by the sensor changed with time, however, become stable after 120 minutes.

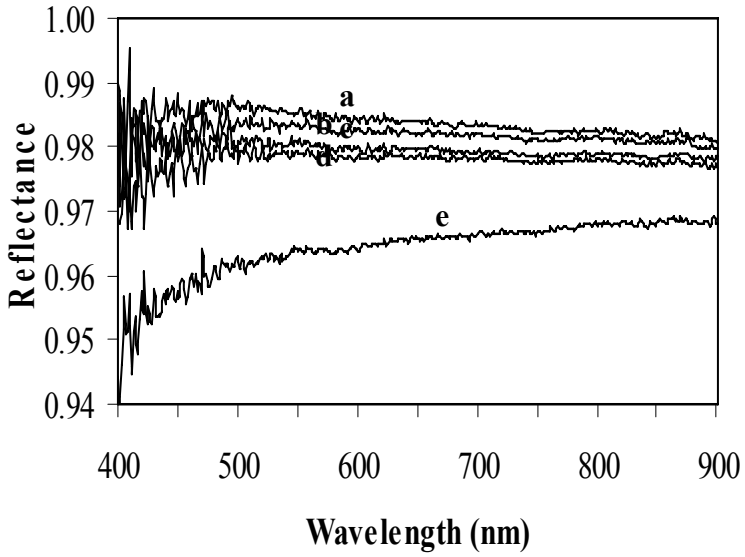

Figure 2.1 Reflectance measurement of reference panel with different warm up time after the spectroradiometer was turned on, a: After 90 minutes b: After 30 minutes c: After 120 minutes d: After 150 minutes e: At start

Figure 2.1 depicts the spectral reflectance of white reference panel at different time intervals. Also, ten spectral curves of reference panels were acquired after every 10 minutes and compared. Figure 2.2 illustrate variation in spectral reflectance of white reference panel at start, after 30, 60, 90, 120 and 150 minutes. It is seen that at start there is little difference between the acquired ten spectral curves. However, at 30minutes, 60 and 90 minutes the equipment becomes more sensitive showing variation between the curves. After 120 minutes the collected spectral reflectance become stable and little variation is seen between the signals. The warming up time of 120 to 150 minutes is recommended.

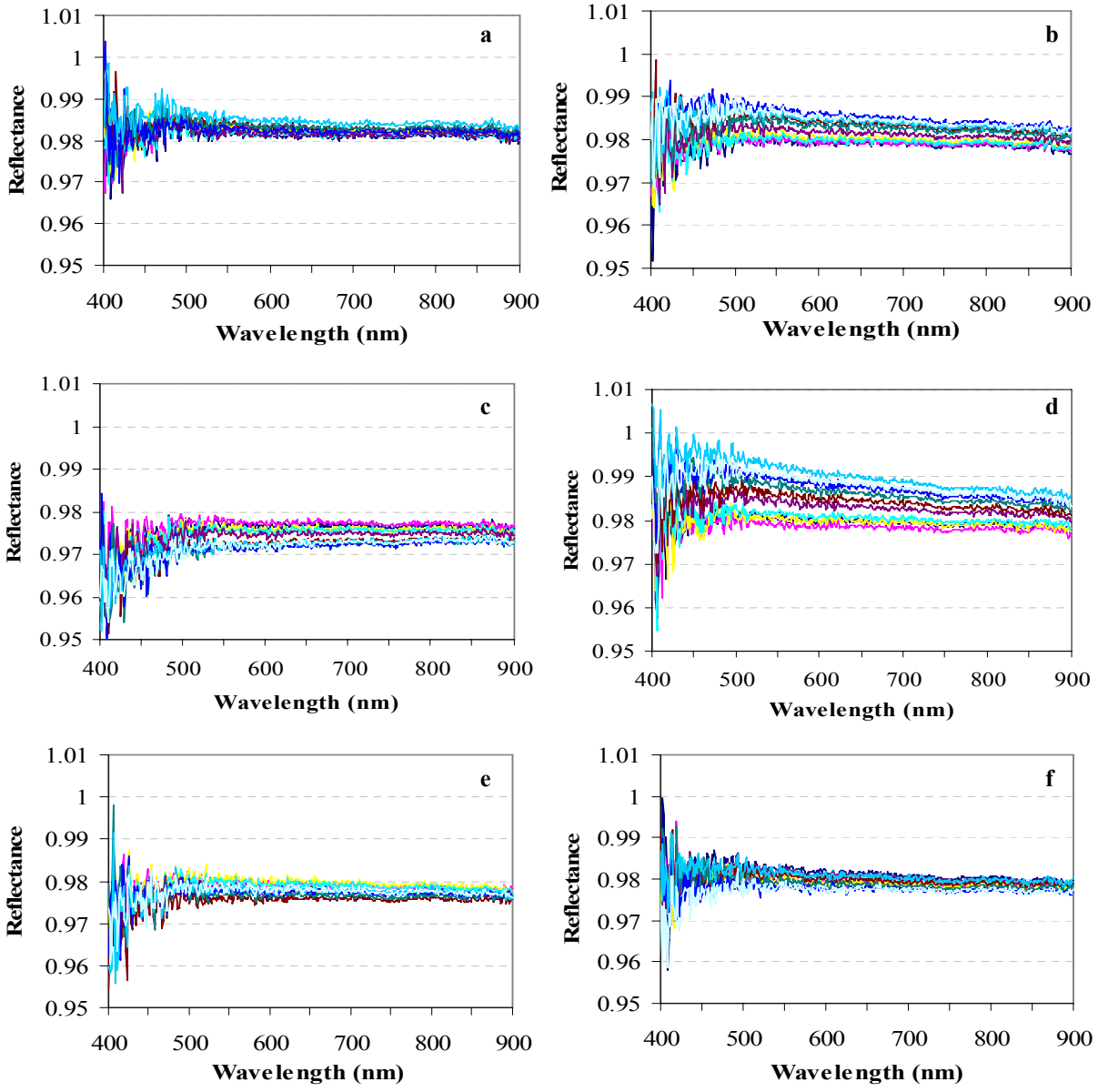

Figure 2.2 Variation in spectral reflectance of reference panel with different warm up time after the spectroradiometer was turned on a: At start b: After 30 minutes c: After 60 minutes d: After 90 minutes e: After 120 minutes e: After 150 minutes

2.4.2.2 Cable flexure test

ASD FieldSpec FR spectrometers receive spectral signatures through attached fiber optic bundle, nominally 1.2 m in length. The small size of the fore optics greatly reduces error associated with instrument self-shadowing. However, in our case the length of the fiber is 5 meters, which provides flexibility to quickly and easily point the spectrometer field of view at variety of targets, especially when using the pistol grip.
Buntzen (1996) measured this effect by recording the digital number (DN) level with the cable coiled vs. the cable extended, while viewing a constant source. He found the flexure effect, even in this extreme flexure case, to be quite small. The ratio of DN extended to DN coiled yielded a negative fractional difference of up to 3% at the extreme short wavelength end of the VNIR (350 nm), and only about 1% at 400 nm. The effects of flexure on the received data need to be explored.

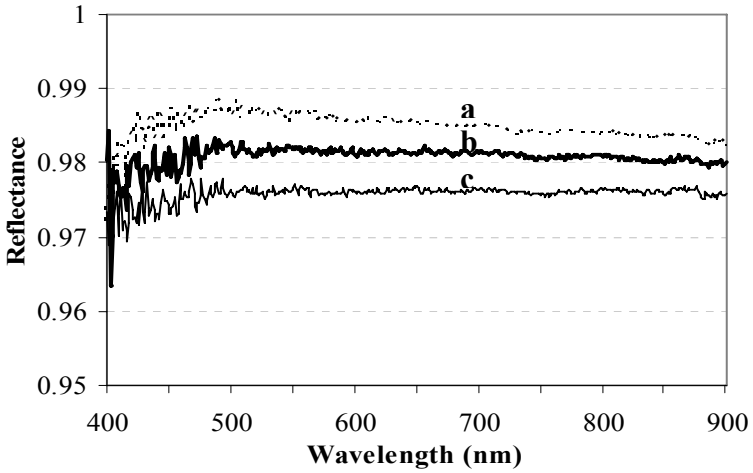

Figure 2.3 Spectral reflectance of white reference panel with different cable positions a: coiled b: zig-zag position c: straight cable

Experiments were carried out under controlled conditions in order to elucidate the cable flexure effects associated with radiance or reflectance measurements. It is observed that that position of cable slightly observed the signals and the straight cable position is recommend for field measurements.

2.4.2.3 Illumination Angle

In order to examine the effect of the illumination angle of the spectral reflectance; experiments were performed in lab under controlled conditions. Halogen Lamp was the source of illumination and reflectance of white reference panel was collected with different angle. The instrument's fiber optic probe with 1degree FOV is placed in a stationary position at 15, 30, 45 and 60 degree angle to the white spectralon panel. The consistent illumination geometry is necessary for accurate measurements. With the change in angle, the reflectance pattern also changed. To avoid errors caused by the illumination source, it is recommended that to update white reference and target measurement

frequently. The artificial illumination angle of 30 to 45 degree is recommended for collecting spectral signals under controlled conditions.

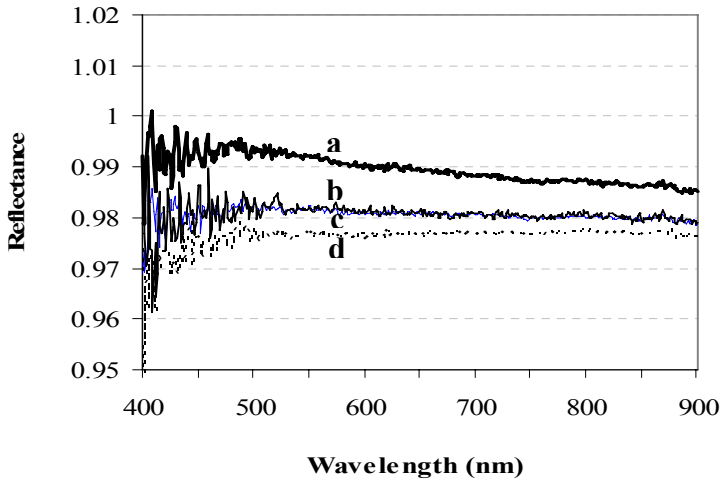

Figure 2.4 Reflectance measurement of reference panel with different illumination angle; a: 15 degree b: 30 degree c: 60 degree c: 45 degree

2.4.3.4 Spectrum average

The reflectance of white reference panel with different spectrum average is carried out in lab. The spectrum average improves the quality of data and influencing parameters may minimize. In any case, averaging multiple measurements of a target is a good practice to compensate for heterogeneity (which may be too subtle for the eye to note), and so that scans with spectral artifacts can be discarded (Sulisbury, 1998). It is recommended that average of 10 to 20 spectra be adopted for collection of remote sensing data. In this study, average of 20 spectra is selected for lab and field experiments.

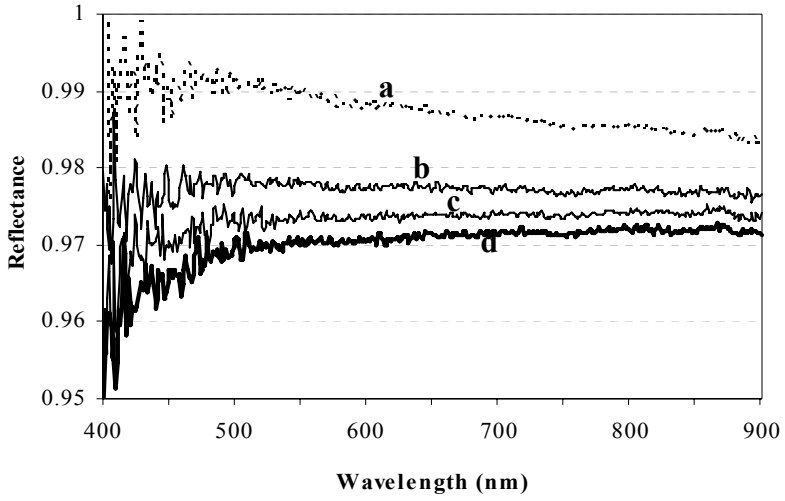

Figure 2.5 Reflectance measurement of reference panel with different spectrum average; a: Average of 20 spectra b: Average of 15 spectra c: Average of 5 spectra d: Average of 10 spectra

2.4.3.5 Type of sensor

The choice of the sensor depends on the objective of the study. The contact probe is used for analysis of mineral, grain, and granule applications. However, the 1 degree fore optic is used in the study of water bodies. The advantage of the contact probe is that it is in contact with the target. Its optical design minimizes the errors and the influence of extraneous reflectance associated with stray light. The Contact Probe is lightweight (1.5 lbs or .68 kg) with easy-grip handle. The spot size of the probe is 10mm with built in halogen bulb for light source. With hand held pistol grip one degree fore optic probe relatively large area may observed. The FOV depends on the sensor height above the target. Figure 2.6 describe the spectral pattern of white reference panel with two kinds of optical probe of 1 degree FOV is placed 1 meter above the reference panel. The contact probe proves to be effective for collection of remote sensing data. However, in case of monitoring water bodies, it is not possible to apply contact prob.

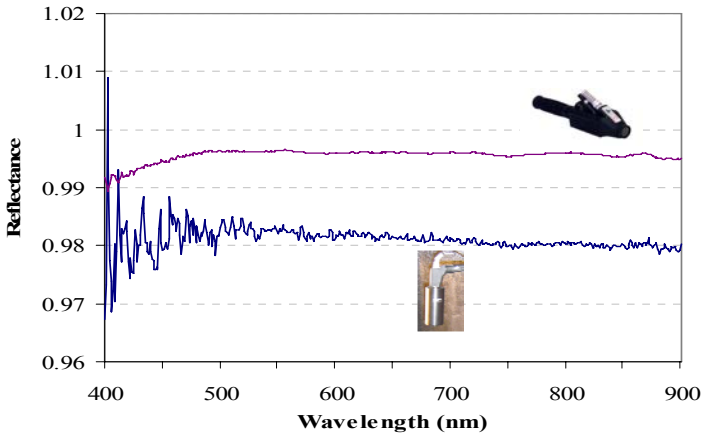

Figure 2.6 Reflectance measurement of reference panel with different probes; a: contact probe b: 1 degree optical probe

2.4.3.6 Sensor height above the target

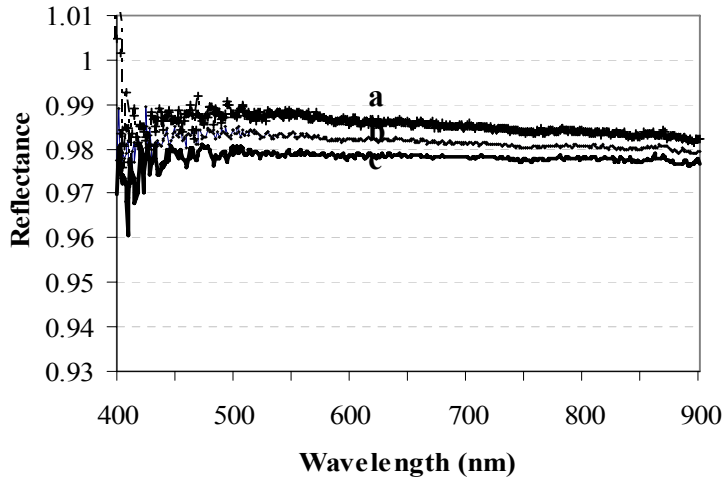

Figure 2.7 Reflectance measurement of reference panel with different sensor heights above the target; a: 1.5 meter b: 0.5 meter c: 1.0 meter above the target

The sensor height above the target is associated with field of view and affects the spectral signatures. The FOV changes with different fore optics and distance from the target. The reflectance pattern of white reference with sensor height of 0.5 meter, 1.0 and 1.5 meter above the target is examined. It is observed that with the change in height there is a slight effect of the spectral signature in lab under controlled conditions. However, in field work, different behavior is expected.

2.4.3.7 Surface Roughness

Surface roughness is the source of error in the measurements of reflectance or radiance and causes surface reflection and disturb the signals received by the sensor. To examine the effect of surface roughness on spectral signals, experiments were carried out in the laboratory under controlled conditions. In the black coated tank, waves were made by using diffuser. The diffuser makes the surface rough and the spectral reflectance was collected from the water surface with 1000mg/l suspended sediment concentration (SSC). The height of sensor above the water surface was 1m. The same methodology was adopted for water with suspended sediment concentration of 500 mg/l. However, the same kind of trend is observed in both cases. With the increase in surface roughness, the spectral reflectance increase. Near the mouth of the diffuser the reflectance was more and tends to decrease as move away from the diffuser. Under such conditions, it is recommended that several spectra of such targets be averaged to reduce the effects of these variables.

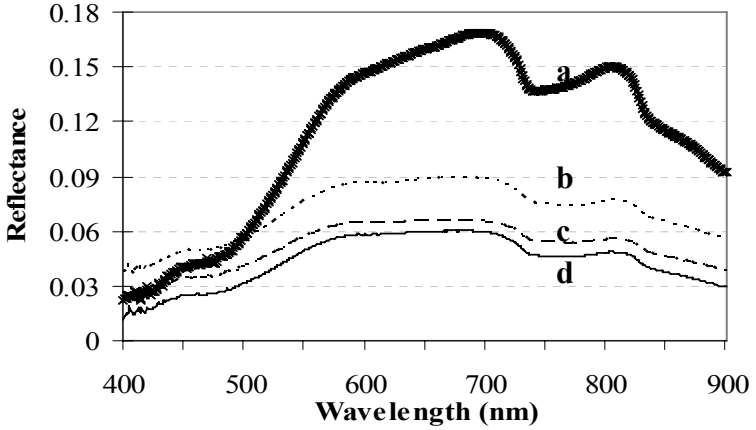

Figure 2.8 Spectral reflectance of water surface with SSC 1000mg/l with different warm up time a: Near the mouth of diffuser b: 15 cm away from the diffuser c: 30 cm away from the diffuser d: Without diffuser (Normal Surface)

2.5 Spectral Characteristic of Different Dry Soils in controlled Conditions

Soil is unconsolidated material at the surface of the earth and it is vital to the earth's life-support system on the land. Soil is s mixture of mineral particles and organic matter of varying size and composition (Jensen, 2000).

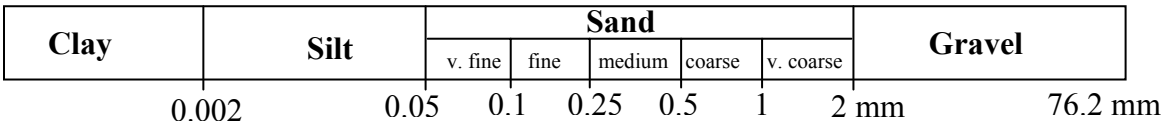

There are three universally recognized soil grain size classes: sand, silt, and clay. Above classification depicts the U.S. department of Agriculture scale used to classify soil particles based on their diameters (Loynachan et al., 1999).

In an effort to demonstrate the relationship between different types of dry soil and spectral signature in the spectral range on 400 nm to 2500 nm, the experiments are carried out under controlled conditions in the laboratory at Kochi University of Technology, Kochi, Japan. The soil samples were placed in black containers (15 cm in diameter and 6 cm in height). Six cases were examined: clayey red soil, silty red soil, kaolin, silty red soil (50%) and kaolin (50%), very fine sand and coarse sand. In this case the contact probe was used to measure reflectance of the soil samples. The advantage of the contact probe is extraneous errors can be eliminated and controlled. The contact probe spot size is 10mm with built in halogen bulb for light source. Many authors including Streck et al. 2003 have delineated the spectral signature of different type of soils. Spectral signatures of different dry soils sample are unique. It is possible to differentiate between different dry soils samples with varying texture and colors owing to distinct spectral pattern of reflectance as depicted in Fig 2.9.

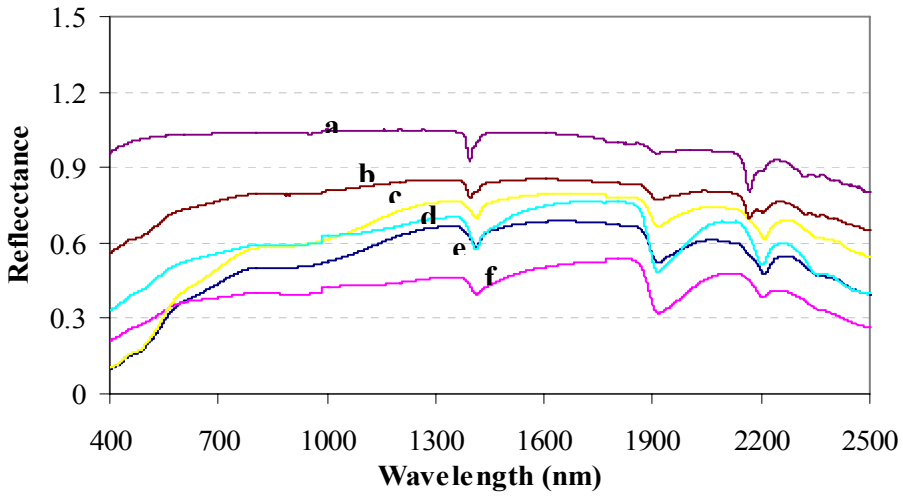

Figure 2.9 Spectral Reflectance of dry soils (a) Kaolin (b) Kaolin 50% and Silty red soil 50% (c) Silty red soil (d) Very fine sand (e) Clayey red soil (f) Coarse sand

All types of soils show a consistent characteristic signature. The reflectance value increase with the increase in wavelength in the visible and NIR domain. Kaolin (Curve a) has the highest reflectance, with about 25 % more reflectance than the mixture kaolin and silty red soil 50-50%. Dry fine sand showed higher reflectance as compared to clayey red soil and silty red soil. The higher reflectance of sand is because it is composed of quartz, which has higher reflectance VIS, NIR, and MIR compared to agricultural soils (Streck, 2003). Owing to soil characteristics and dark color of clayey soil the reflectance value of

silty red soil was found to be more than clayey red soil. The organic matter content in the dry soils samples was not measured as it was out of the scope of present study. However, previous studies have shown that organic matter content has a strong influence on the soil reflectance.

2.6 Spectral Signatures of Different Types of Suspended Sediments with Varying Concentration of SS in Controlled Condition

2.6.1 Literature Review

Variations of sediment type (grain size and refractive index) and changing illumination conditions affect the reflectance signal of coastal waters and limit the accuracy of sediment-concentration estimations from remote-sensing measurements (Doxaran, 2003). It is believed that the main differences between the two types of waters are located in the 0.4–0.7 m spectral range (R. Li, 2003), where the turbid water has significantly larger reflectance than the clear water. This formed the basis for the detection of turbid water and SSC estimation algorithms.

If the range of suspended sediments is between 0 and 50 mg/l, reflectance from almost any wavelength will be significantly related to suspended sediment concentrations (Ritchie, 2000). As the range of suspended sediments increases to 200 mg/l or higher, curvilinear relationships have to be developed with reflectance in the longer wavelength. Significant relationships have been shown between suspended sediments and radiance or reflectance from spectral wave bands or combinations of wave bands on satellite sensors. Ritchie et al. (Ritchie, 1976) using in situ studies concluded that wavelengths between 700 and 800 nm were most useful for determining suspended sediments in surface waters.
Suspended sediments are the most common pollutant both in terms of weight and volume in surface waters of freshwater systems. Suspended sediments may serve as a surrogate contaminant in agricultural watersheds since phosphorus, insecticides, and metals adhere to fine sediment particles. Remote sensing is an effective tool for the assessment of suspended sediment in surface water. Numerous researchers have developed algorithms for the relationship between the concentration of suspended sediments and radiance or reflectance. A few studies have taken the next step and used these algorithms to estimate suspended sediments for another time or place (Ritchie, 1988). Also, a few studies actually address how different sediment types and size affect spectral reflectance (Lodhi 1997, Bhargava 1990, 1991). The aim of the study was simply to investigate the relationship between suspended sediment concentration (SSC) and reflectance in a column of water. The objective was to understand the change in reflectance pattern with different types of soils and varying suspended sediment concentration in constant volume of water. The change in reflectance signatures for the same SSC with time is also examined.

2.6.2 Material & methodology

The research is based on the experiments conducted indoor at Kochi University of Technology, Kochi, Japan. The purpose of this research was to estimate the suspended sediment concentration by means of remote sensing. In this research work five cases were examined: clayey red soil, silty red soil, kaolin, silty red soil (50%) and kaolin (50%) and very fine sand. The red soil samples were collected from the central area of Okinawa

Island (coordinates: 26º23´N and 127º73´E). Subsurface geology is diverse in this area with limestone, sandstone, phyllite, and gravels (Kubotera, 2006). The physical properties of the collected red soil were expected to be various, reflecting the diversity of parent materials. The percentage of clay was higher in the clayey soil. Kaolin and very fine sand was ordered commercially. The soil samples were air dried, pulverized and manually sieved to ensure a uniform particle size. To minimize extraneous reflectance, the experiments were performed in black room designed for experimental purpose using black coated tank. Two 500 watt tungsten halogen lamps, uniformly illuminated from 1 meter above water surface with a beam inclination of 30^{o}, were the sources of illumination during the experiment. The water tank is also black coated to reduce the influence of extraneous reflectance.

Radiation input to the ASD Field Spec FR spectrometers is through a fiber optic, nominally 5 meters in length. The spectroradiometer was linked to a laptop, which stores the scans for each sample. The experiment was consisted of two parts. In the first part, the radiance of selected dry soil samples and in the second part radiance of water surface with varying concentration and types of suspended sediments was performed. In case of water with varying suspended sediment concentration 1 degree sensor was used. The experimental design and setup is depicted in the figure 2.10.

The sieved soil samples were weighted to produce fifty concentrations of suspended sediments in each case ranging from 20 to 1000 mg/l. Initial reflectance readings were taken for the water tank prior to the addition of any suspended sediments and subsequently after sediments were mixed into the tank. The addition of each soil sediment produces suspended sediment concentration of level of 20 mg/l. The depth of water column was 60 cm and was kept constant for all experiments. The soil sediments were kept in suspension by means of a mechanical diffuser and manually stirring at regular intervals. Homogeneity of the suspended sediments in the water is imperative for accurate estimation of concentration. A stopwatch was used to monitor sampling intervals to ensure equal mixing times for each sediment addition and scanned time in order to minimize settling of input sediments. To improve the signal to noise ratio mean of ten scans were used in the analysis. All variables and procedure are kept identical for each case. Turbidity was measured by using PARTECH turbidity meter in mg/l in order to verify the homogeneity of suspended sediments and for comparison with SSC levels (M.A. Lodhi, 1997).

Reflectance was calculated as a simple ratio between target and reference panel using following equation.

$$\% \ R(\lambda) = \frac{L(\lambda)}{S(\lambda)} \times Cal \quad (\lambda)$$

Where L (λ) is the radiance measured from the water surface, S (λ) is the radiance from the reference panel measured under the same illumination conditions and Cal (λ) is the calibration factor for the reference panel. The reference plaque was a Labsphere white Spectralon of dimensions 12.5cm x 12.5cm. Using this method, all parameters that are multiplicative in nature, such as the spectral irradiance of the illumination source and the optical throughput of the field spectrometer, and present in both the spectral response of a reference sample and the target material, are mathematically eliminated.

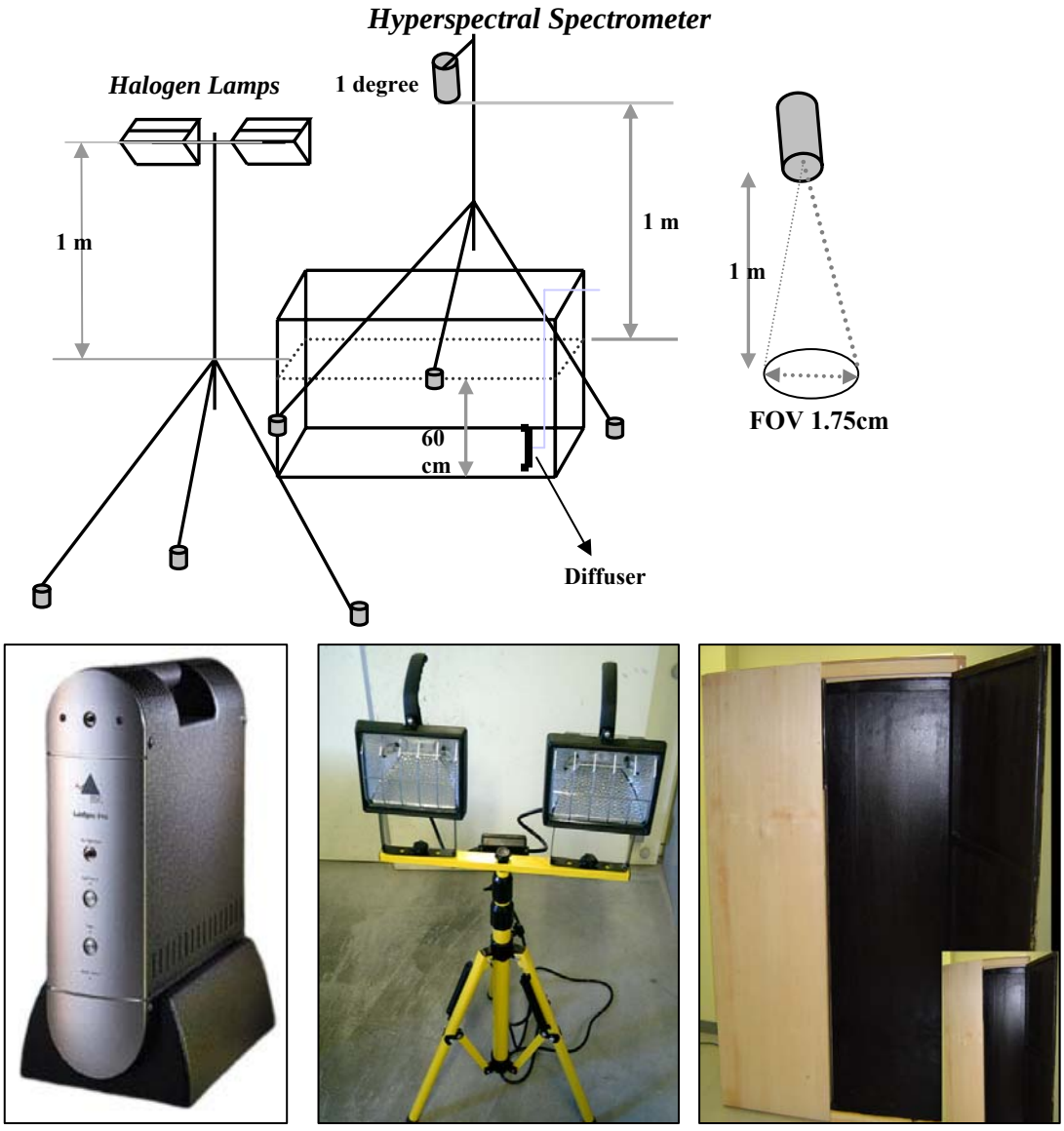

Figure 2.10 Experimental design and setup

2.6.3 Result and discussion

It is desirable to examine the spectral characteristic of the suspended sediments in the laboratory under controlled environment. This could be useful to provide methodology to monitor the type, amount and spatial distribution of suspended sediments in water bodies. In order to investigate the concentration and type of suspended sediments in surface water, series of reflectance measurements in the spectral range between 400 and 900 nm was carried out in a black coated tank. Reflectance is the function of quantity and characteristics of suspended sediments. There is no standard algorithm for the estimation of suspended sediments due to the complex nature and composition of the suspended sediments. The spectral reflectance of water with different types of suspended sediments and concentration of 1000mg/l is shown in figure 2.11.

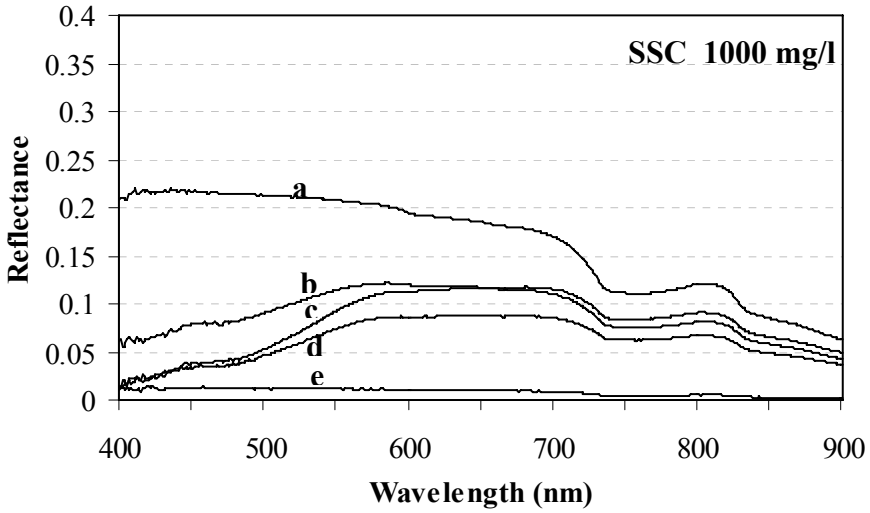

Figure 2.11 Spectral reflectance of water with different type of suspended sediments (a) Kaolin (b) Kaolin 50% and Silty red soil 50% (c) Silty red soil (d) Clayey red soil (e) Find sand

An asymptote exists for sediment loading in surface waters, and the asymptote is different for various types of soil. Therefore, amount of suspended material and type are important factors in volume reflectance (Lodhi, 1997). The reflectance value of kaolin as suspended sediments is higher as compared to other types of soils. Fine sand as suspended sediments has low value of reflectance. The find sand settle in the water and affect the accurate estimation of suspended sediment concentration. The reflectance of silty red soil as suspended sediments is more than the clayey red soil, which conforms with the results of numerous researchers. The reflectance tends to increase with the increase in SSC, with a few minor exceptions. The wavelengths of peak reflectance were plotted against varying SSC of silty red soil (Figure 2.12).

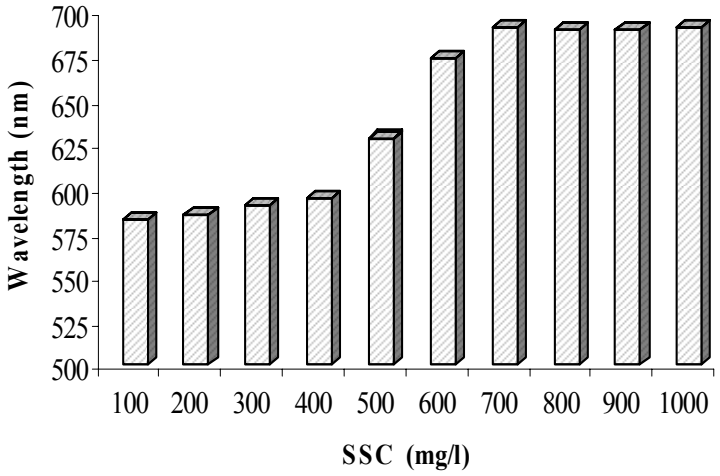

Figure 2.12 Wavelength of peak reflectance with varying SSC

Ritchie et al. (1976) using in situ studies concluded that wavelengths between 700 and 800 nm were most useful for determining suspended sediments in surface waters. It

was observed that the red and near-infrared (NIR) wavelength 700-900 is a useful range for determining the amount of suspended sediments. However, the wavelength range 525-665 provides information about sediments type.

Graphs were plotted to describe the variation of spectral reflectance with wavelength for different suspended sediment concentration (SSC) caused by different types of sediments (Figure 2.13).

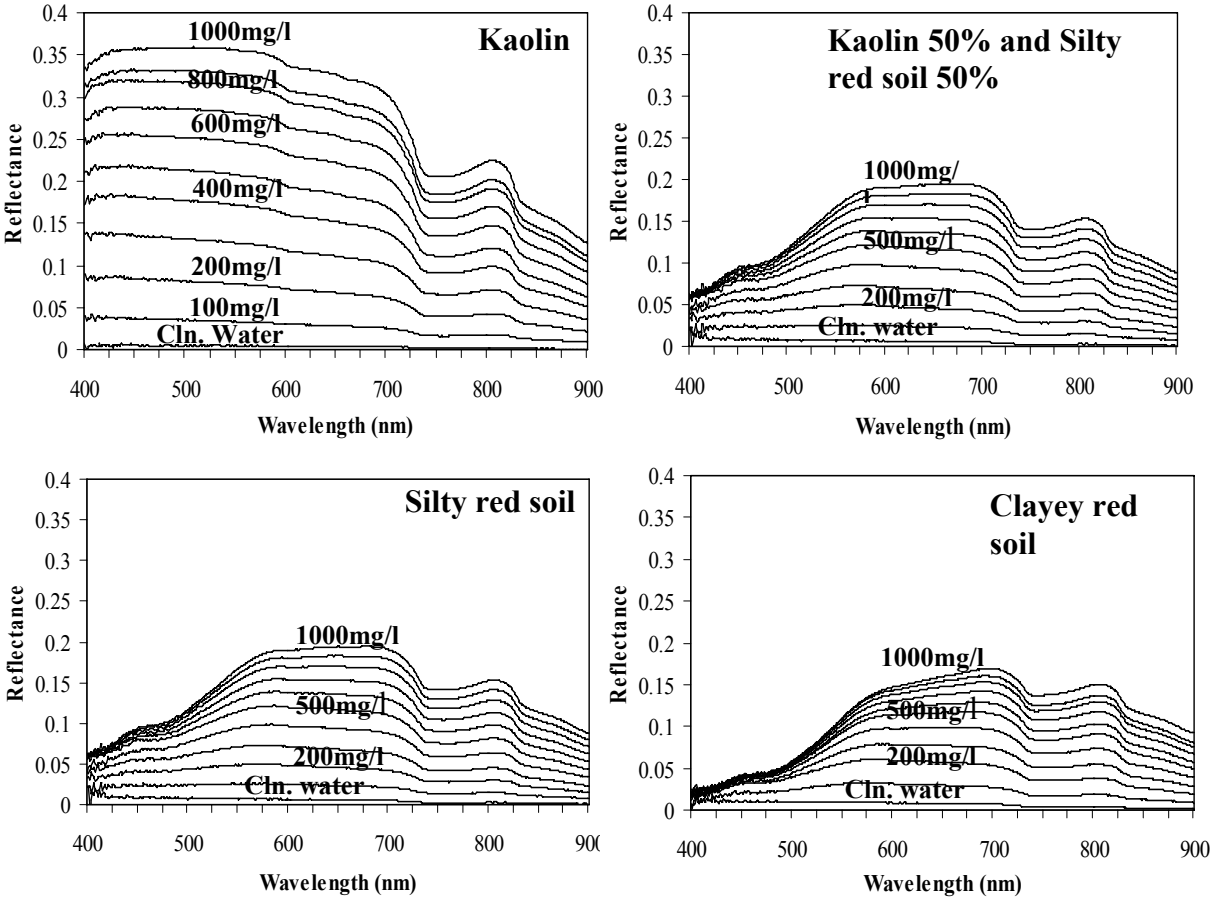

Figure 2.13 Spectral reflectance of water with different types and varying concentration of SSC (mg/l)

The comparison of the graphs showed that optical signature trends are almost similar in case of kaolin, kaolin 50% and silty red soil 50%, clayey red soil, and silty red soil. A consistent increasing trend in reflectance was observed with the increase in SSC. Suspended sediment in water has greater absorption of radiation at longer wavelength (Chen et al. 1991). It was observed that within the visible domain suspended sediments have no characteristic absorption. Fischer and Kronfeld (1990) suggested that scattering depends strongly on the complex refractive index and the size distribution of the particles. The mean refractive index of clay and non-clay minerals is higher than the refractive index of water (1.335). The mean refractive index of the clay minerals (1.540) is higher than the non-clay minerals (1.523) and the effect of variation in the refractive index is expected on the relation between the suspended sediment concentration and the reflectance.

The results obtained from the laboratory experiment indicated that the visible region were more useful than the longer near-infrared wavelengths for the information about type of the soil. When SSC is low the peak reflectance occurred at short visible wavelengths, but when SSC is high the peak reflectance shifted towards longer wavelength. Below 400 mg/l, the reflectance occurred around 575 nm with only minor differences. Above 400 mg/l the peak reflectance shifted to 675 nm and increase slightly with increase in sediment load. Maximum reflectance was observed in the visible domain and high absorption is in the NIR as depicted in figure 2.14. With the increase in the suspended sediments the qualitative nature of the spectral curves are similar in all cases, however, there is considerable variance in the magnitude of spectral reflectance. The low reflectance value is due to the black coated inner walls of the tank, which absorb much of the incident light. At levels of 600 mg/l SSC and above, the spectral profile becomes somewhat irregular in all cases, suggesting that the relationship between reflectance and SSC was found to be nonlinear.

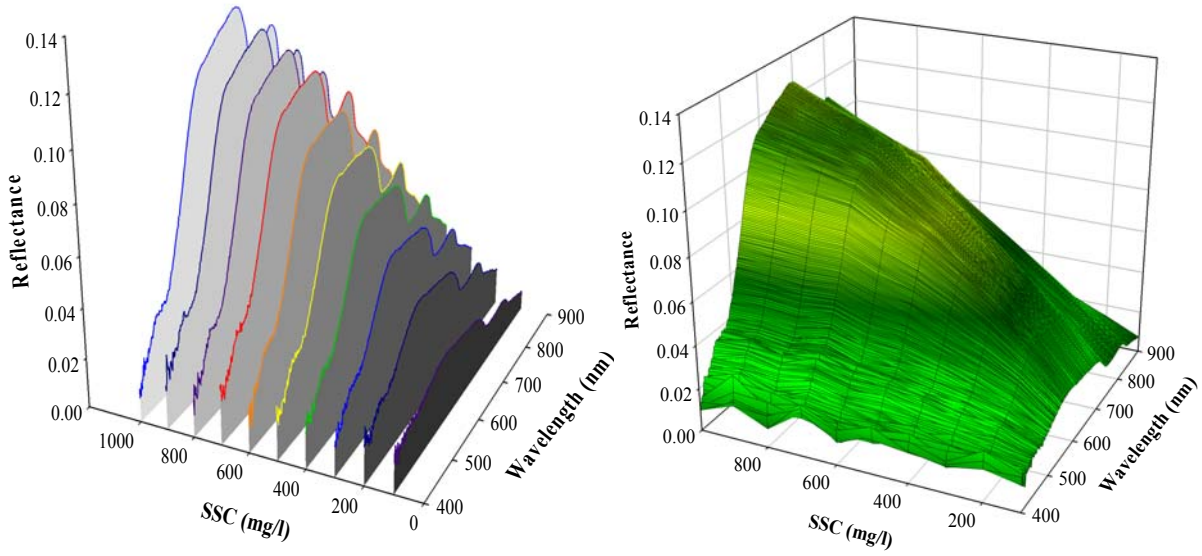

Figure 2.14 Spectral reflectance of water with varying concentration of silty red soil

The darker soil produced lower reflectance value than the light-coloured soil. In dry condition and as suspended sediments different soils can easily be distinguished from each other in the visible domain of 525-655 nm. It was observed from the figure 2.12 that the peak reflectance for each level and type of suspended sediment occurred in the visible domain and shifted towards longer wavelength with the increase in suspended sediment concentration. The peak is closely related to the amount of SSC. However, change in shift not only depends on the amount of SSC, but also on the type of the suspended material. The NIR wavelengths found to be more useful for estimation of suspended sediments. In cases of fine sand significant increase in reflectance was not observed with an increase in sediments concentration (Figure 2.15). This is because of texture and variation of grain size in fine sand. Different spectral reflectances were obtained for the different soil types of the same concentration because of the difference between the properties and characteristics of various soil types.

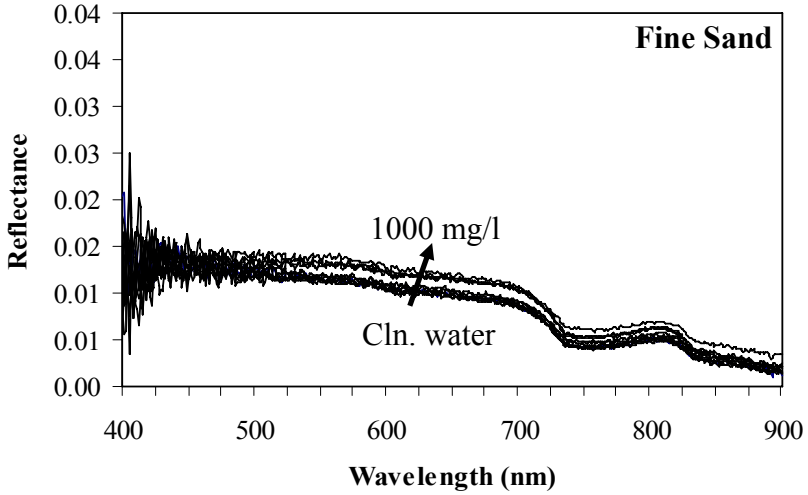

Figure 2.15 Spectral reflectance of water with varying concentration of fine sand (mg/l)

The linear relationship between NTU measured by PARTECH turbidity meter and SSC in mg/l is shown in figure 2.16.

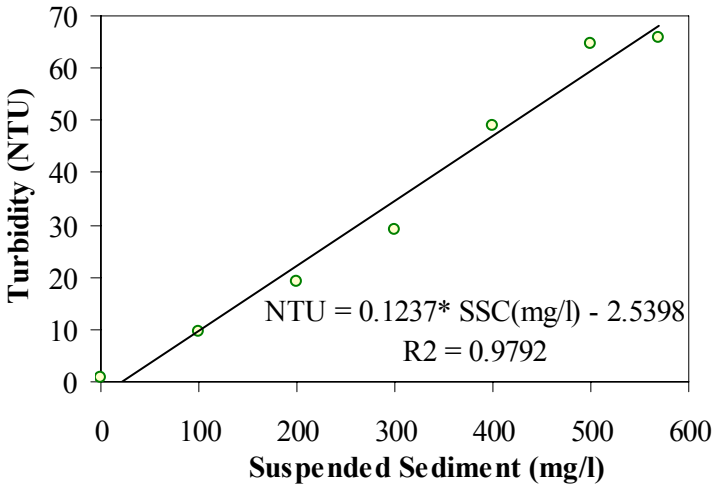

Figure 2.16 Relationship between SSC (mg/l) and Turbidity (NTU)

2.6.3.1 Distributions of suspended sediments with depth

Assessment of suspended sediment in water bodies is based mainly on assumption of uniform distribution of suspended sediments along the depth. Most of the sediment which is eroded from the land surface is in the form of fine particles which are transported in water courses as a suspended load. These fine sediments account for the turbidity often observed in rivers and their natural fall velocity in water is as low that the natural turbulence maintains them in suspension. However, the distribution of sediments is not uniform and varies with depth depending on sediment characteristics, precipitation, run-off, temperature, water flow, and wind speed.

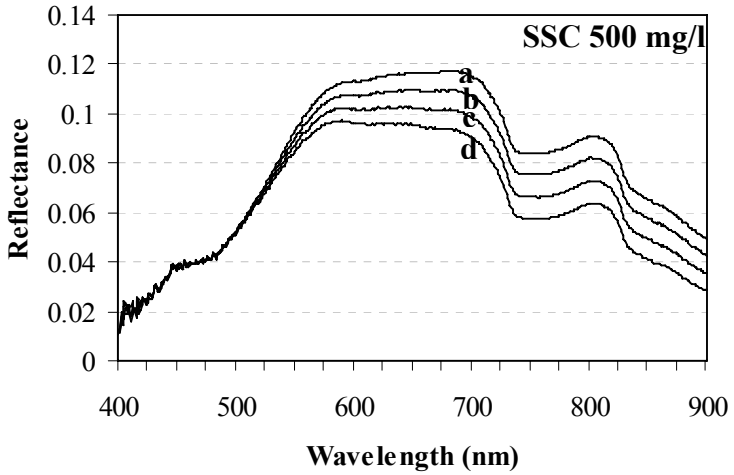

Figure 2.17 Spectral reflectance of water with constant concentration of clayey red soil (500 mg/l) a: Spectral reflectance after manual mixing 500mg/l clayey red soil b: spectral reflectance after 1 minute c: Spectral reflectance after 2 minutes d: Spectral reflectance after 3 minutes

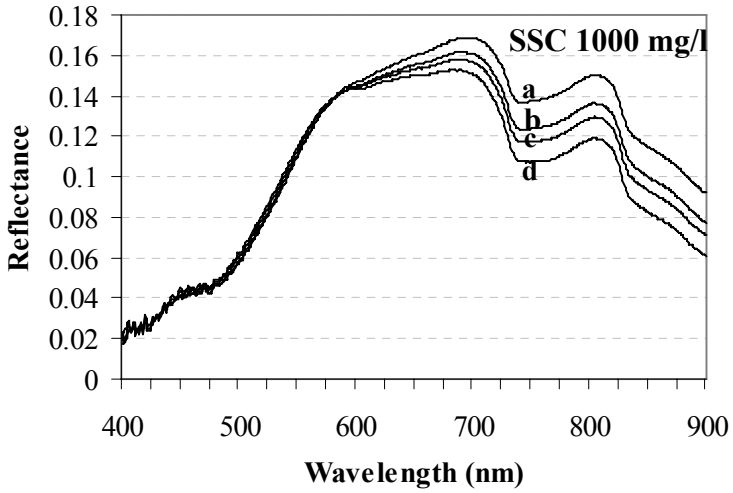

Figure 2.18 Spectral reflectance of water with constant concentration of clayey red soil (1000 mg/l) a: Spectral reflectance after manual mixing 1000mg/l clayey red soil b: spectral reflectance after 1 minute c: Spectral reflectance after 2 minutes d: Spectral reflectance after 3 minutes

The objective to perform the experiment was to investigate the effect of non-uniform distribution of suspended sediment on remotely sensed data. Sediments were mixed in water uniformly by manually stirring the water sample for a few minutes. The depth of water column was kept constant at 1 meter. Spectral reflectance of water is measured for the constant amount of sediments immediately after the mixing of sediments. Also for the same concentration of suspended sediments the reflectance signals was measured with time after 1, 2 and 3 minutes without stirring the water sample to investigate the effect of SSC distribution on reflectance value.

Suspended sediments settled with time in the water and reflectance value changed with the change in sediment distribution and caused error in accurate estimation of suspended sediments. With the time the reflectance value decreases for the same amount of sediments owing to settling of sediment with time. Sediment grain size is one of the major factors for the distribution of sediments. These results indicate that the sediment distribution with depth affects the reflectance values significantly.

2.6.3.2 Model development

The band ratioing technique and regression analysis were applied to develop band ratio models. The spectral data were partitioned into narrow bands each having 5nm width. In total 100 centered narrow bands were generated, including 25 bands in blue domain, 16 bands in green domain, 10 bands in yellow domain, 19 bands in red domain, and 30 bands in NIR domain. Each narrow band is referred to, by its central wavelength.

Table 2.2 Development of Narrow Bands

Ratio (Bi/Gj)	RrsBi/ RrsGj	i=1 to 25	j= 1 to 16
Ratio (Bi/Yj)	RrsBi/ RrsYj	i=1 to 25	j= 1 to 10
Ratio (Bi/Rj)	RrsBi/ RrsRj	i=1 to 25	j= 1 to 19
Ratio (Bi/NIRj)	RrsBi/ RrsNIRj	i=1 to 25	j= 1 to 30
Ratio (Gi/Yj)	RrsGi/ RrsYj	i=1 to 16	j= 1 to 10
Ratio (Gi/Rj)	RrsGi/ RrsRj	i=1 to 16	j= 1 to 19
Ratio (Gi/NIRj)	RrsGi/ RrsNIRj	i=1 to 16	j= 1 to 30
Ratio (Yi/Rj)	RrsYi/ RrsRj	i=1 to 10	j= 1 to 19
Ratio (Yi/NIRj)	RrsYi/ RrsNIRj	i=1 to 10	j= 1 to 30
Ratio (Ri/NIRj)	RrsRi/ RrsNIRj	i=1 to 19	j= 1 to 30

Figure 2.19 shows the relationship between ratios of spectral reflectance and SSC. This relationship is based on simple reflectance (Rrs) ratio between visible and near-infrared wavelengths plotted against suspended sediment concentration. The ratios of reflectance values in the sub-bands centered at Rrs848/Rrs548, Rrs803/Rrs708, Rrs793/Rrs713, Rrs783/Rrs673, Rrs773/Rrs663, and Rrs773/Rrs658 were found to be optimum for estimation of suspended sediment. The regression models were developed and correlation coefficients (r) between ratio of spectral reflectance and SSC were computed to describe the relationship between suspended sediment concentration and the reflectance. The above spectral reflectance ratios and suspended sediments were found to be well correlated for clayey red soil, silty red soil, kaolin, and kaolin (50%) and silty red soil (50%). The computed r value was greater than 0.90 in all cases. However, in case of fine sand the computed r value range was 0.55-0.70. The rational is because the fine sand texture and grain size affect the spectral reflectance.

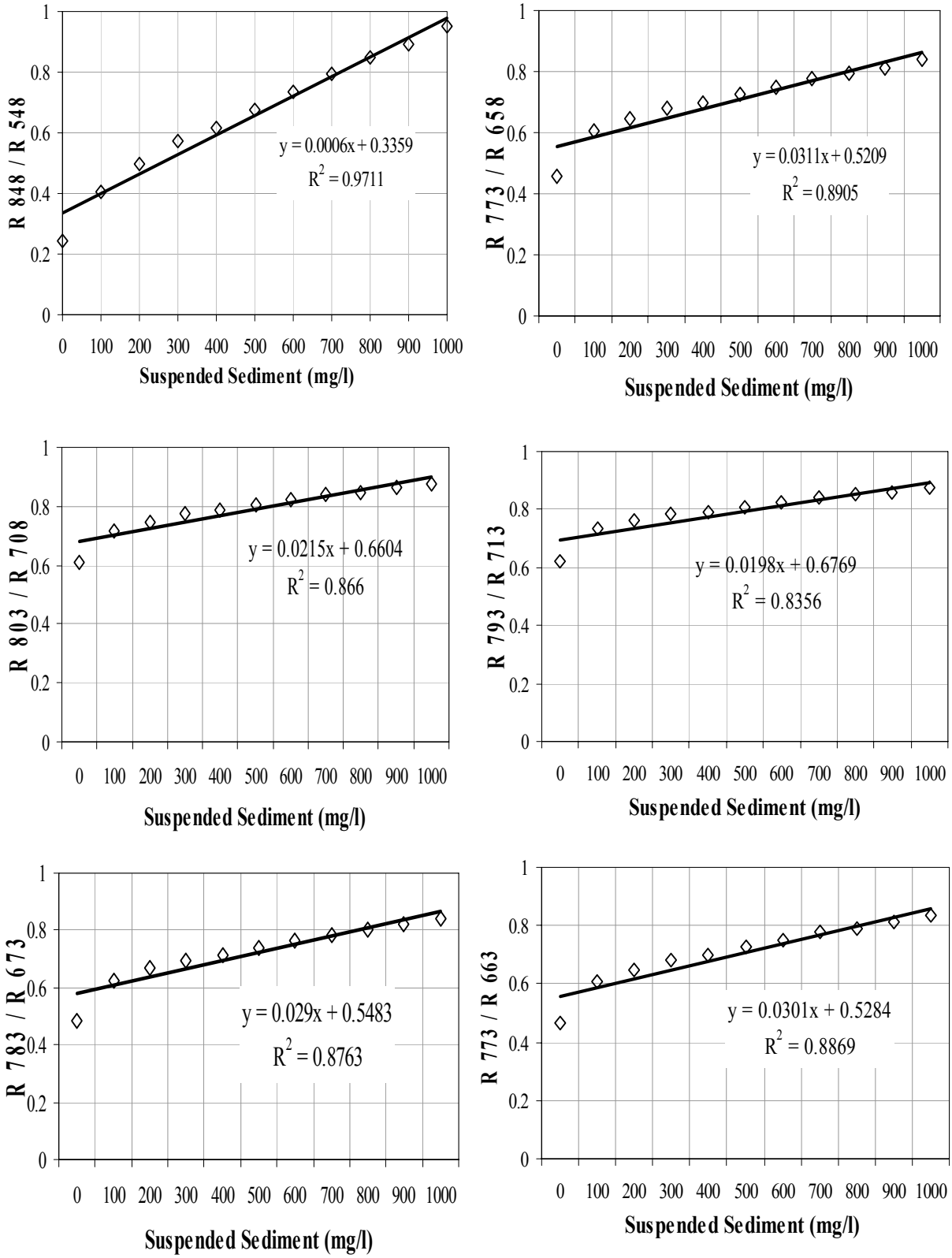

Figure 2.19 Band ratio models (Ratio of reflectance plotted against SSC)

2.7 Relationship between Simulated ALOS Data and SSC

In order to investigate the applicability of satellite data to measure precisely the SSC, the spectroradimeter laboratory data between 400 to 900 nm were integrated to spectral width of ALOS/AVNIR-2 sensor: Band 1 (420 to 500 nm), Band 2 (520 to 600 nm), Band 3 (610 to 690 nm) and Band 4 (760 to 890 nm). The integration to the satellite bands was approximated by the following summation:

$$\textit{Band averaged reflectance (\%)} = \Sigma Ri / n$$

Where Ri is the reflectance in the ith spectral band of the spectroradiometer and n is the number of spectroradiometer bands integrated per satellite band width.

Numerous researchers have analyzed the relationship between SSC and remotely sensed data, especially Landsat multispeatral scanner (MSS) and Thematic Mapper (TM). In case of simulated ALOS data the maximum reflectance was observed in the visible domain (Band 1, 2, and 3 of ALOS/AVNIR-2) and high absorption is in the NIR (Band 4). With the increase in the suspended sediments spectral reflectance increase and peak reflectance shifts towards longer wavelengths. The qualitative nature of the spectral curves are similar in all cases, however, there is considerable variance in the magnitude of spectral reflectance. The simulated ALOS/AVNIR-2 bands, individually and in combination, was used with regression techniques to examine the relationship between reflectance and SSC to provide solution for the field application of remotely sensed data for assessment of suspended sediments. The correlation coefficients (R^2) were computed between SSC and simulated AVNIR-2 band (Table 2.3).

Table 2.3 Correlation between simulated ALOS/AVNIR-2 bands and SSC

TM Bands	R^2
1	0.90
2	0.97
3	0.98
4	0.99

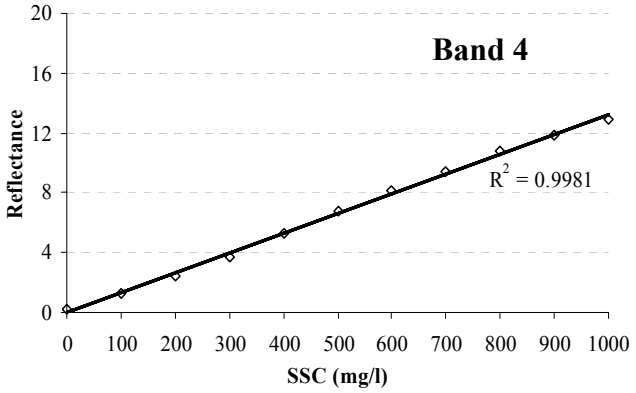

Figure 2.20 Correlation between simulated AVNIR-2 Band 4 and SSC

The NIR region (Band 4) seems to be more useful than the visible region for measuring the SSC in water. The spectral reflectance, in the NIR domain (Band 4), as a function of varying SSC in water is shown in figure 2.20. The selection of the best regression equation for measuring SSC is made by comparing the correlation coefficients. The reflectance of band 4 can be used to develop a linear regression model of the following form for estimation of SSC.

$$SC\ (mg/l) = (R\ (Band\ 4) - 0.0102\ )/\ 0.0132$$

2.7 Relationship Between Area Bounded by the Curve and SSC

The relationship was developed between the area bounded by the spectral curve with varying concentration of suspended sediment concentration. In case of clean water the area bound by the curve in the blue domain was highest, followed by the green, red and NIR region. With the increase in suspended sediment concentration the area bounded by the curve in green and red domain tends to increase showing symmetric pattern. The area bounded by the curve in terms of ALOS/AVNIR-2 sensor is of following form:

$$Band1 = \int_{420}^{500} R(\lambda)d\lambda \qquad Band2 = \int_{520}^{600} R(\lambda)d\lambda$$

$$Band3 = \int_{610}^{690} R(\lambda)d\lambda \qquad Band4 = \int_{760}^{890} R(\lambda)d\lambda$$

The linear relationship between the area bounded by the curve in the blue (Band 1), green (Band 2), red (Band 3) and NIR domain (Band 4) and SSC is shown in figure 2.21. Integral of Band 4 (760-890 nm) is well correlated with varying concentration of suspended sediments. The equation for estimation of SSC is of the following form:

$$SSC = \int_{760}^{890} R(\lambda)d\lambda - 0.0052$$

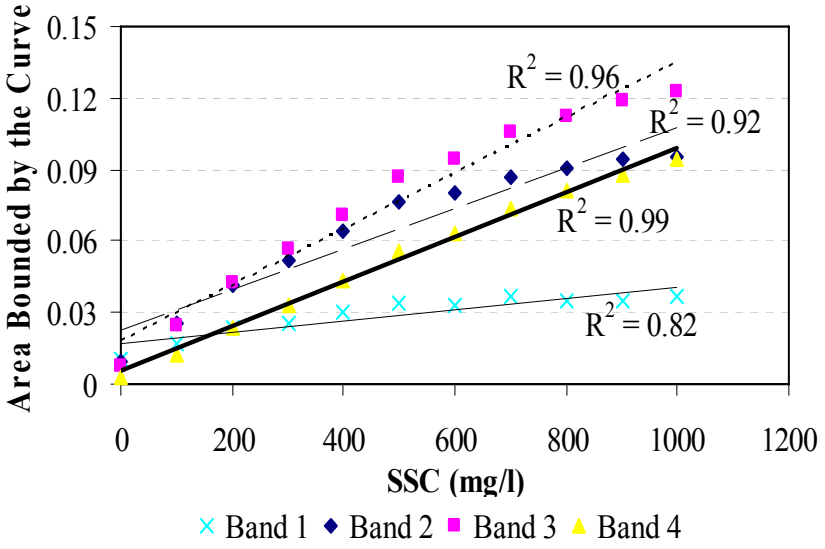

Figure 2.21 Integral of spectral reflectance with varying SSC of silty red soil

2.8 Relationship Between First Derivative of Reflectance and SSC

In the present research work the hyperspectral data of varying concentration of suspended sediments and correlation between first derivative and SSC is comprehensively analyzed. Derivative spectra indicate the rate of change of reflectance with respect to wavelength ($dR(\lambda)/d\lambda$), which is the slope of the reflectance curve at wavelength λ. Derivative analysis has been applied by researchers in studying the spectral characteristics of chlorophyll and suspended sediments in water (Han, 2005). Derivative analysis of reflectance signatures of water with varying of SSC allows correlating the spectral pattern with suspended sediments concentration.

The spectral data were partitioned into narrow bands each having 5nm width. The derivatives were computed by dividing the percentage reflectance difference between last and first percentage reflectance value of each narrow band by the wavelength interval separating them. The derivative spectra seem visually separable below SSC concentration of 500 mg/l with peak separation occurring at 827 nm (Figure 2.22). However, above 500mg/l, the curves seem visually identical.

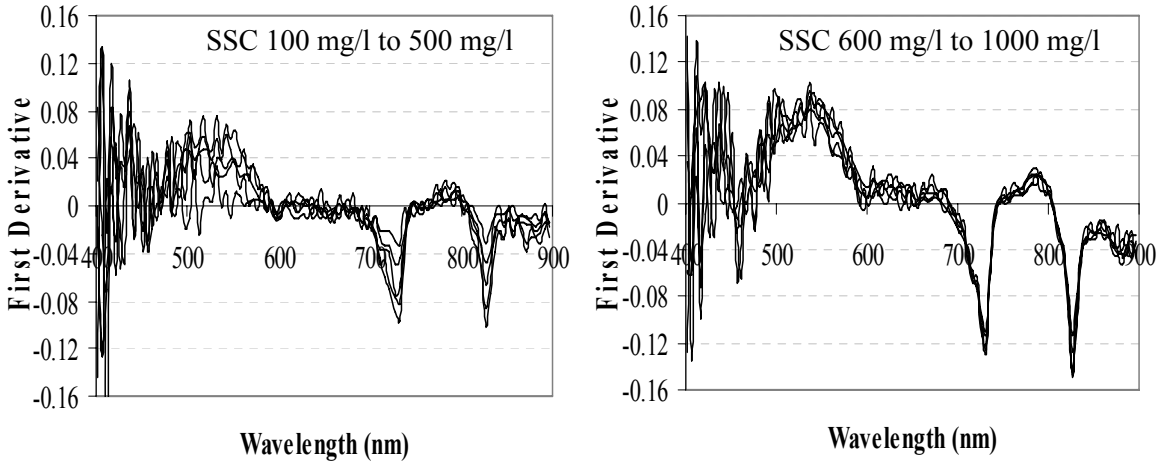

Figure2.22 First derivative spectra with varying SSC

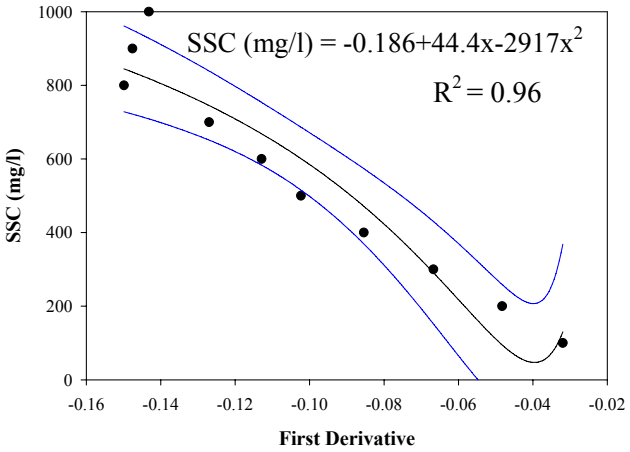

Figure 2.23 Correlation between SSC and first derivative at 827nm

The derivatives tended to be positive in visible domain and shift towards negative in the NIR domain. The regression model was developed in order to examine the relationship between first derivative at 827nm and SSC (Figure 2.23). The first derivative at 827 nm is proved to be better for estimation of SSC. The inverse second order equation of the following form can be used to estimate the SSC.

$$\mathbf{SSC\ (mg/l) = a + bx + cx^2}$$

Where a, b and c are regression coefficients and x is the derivative reflectance of the selected wavelength.

2.10 Effect of SSC on Depth of Light Penetration

2.10.1 Introduction

The incident energy on the water surface is reflected, absorbed, and/or transmitted. The transmitted, absorbed and scattered energy vary with quality and quantity of suspended sediments in water bodies. In remote sensing techniques the reflected energy is measured, carrying some information of the object from which it is reflected. Reflectance is function of many influencing factors that caused the change in reflectance signals. Different channels have their own properties and show different spectral characteristics. Rational feature selection is imperative for analysis and information extraction of hyperspectral data. Research on processing, analysis and information extraction of hyperspectral data should be strengthened to determine more useful information, make full use of the advantage and potential of hyperspectral remote sensing technology and promote the development of new and important technology (Mazar, 1988).

The optical properties of water are functions of underwater irradiance, such as the vertical attenuation coefficient for downward irradiance or irradiance reflectance. While dealing with suspended sediments, the characteristics of the sediments including size, shape and texture of the particles must be taken into consideration. In order to investigate the relationship between the SSC and depth of light penetration experiments were conducted in controlled condition. It is imperative to quantify the effect of SSC on light penetration in water bodes and the threshold concentration of SSC to ignore the influence of bottom reflectance on remote sensing signals.

.

2.10.2 Material & methodology

The experiments were conducted indoor in a black painted room at Center for Advanced Land Management Information Technologies (CALMIT), University of Nebraska- Lincoln, USA. Four Li-Cor Underwater Quantum Sensors were used to establish the relationship between upwelling and downwelling irradiance. One sensor was placed above the water surface facing upward towards the illumination source to measure the total downwelling irradiance (E_{do}) and second sensor was placed above water surface facing downward to measure the reflectance from the water surface (R). Third and fourth sensor was placed first at the depth of 30 cm and then 60 cm from the water surface, with one facing upward to measure the downwelling irradiance (E_d) beneath the surface and the other facing downward to measure the upwelling irradiance (E_u). The quantum instrument

record amounts of photosynthetically active radiation (PAR- 400 to 700 nm) in the water, measure photosynthetic photon flux density (PPFD) in micromoles per second per meter squared ($\mu mols^{-1}m^{-2}$). The quantum sensors were placed first at the depth of 30 cm and then 60 cm from the water surface, with one facing upward to measure the downwelling irradiance (E_d) beneath the surface and the other facing downward to measure the upwelling irradiance (E_u). The optical properties of water are functions of underwater irradiance, such as the vertical attenuation coefficient for downward irradiance or irradiance reflectance.

The measurements E_{do}, underwater downwelling irradiance at depth (E_d), upwelling irradiance from the tank bottom and water column (E_u) and PAR reflectance form the water surface R, in conjunction with variable SSC, allowed us to examine the energy budget for PAR in the water.

2.10.3 Result and discussion

The effect of depth and SSC on upwelling and downwelling irradiance was examined. E_u is a complex parameter because it should be dependent on the total radiation incident to the surface, SSC in the water column and any reflective effect of the bottom itself (Han, 1994). When electromagnetic energy reaches the surface water body, it may be reflected, absorbed, or transmitted. The interrelationship among these three processes can be expressed as below.

$$\mathbf{Ei = Ea + Et + Er}$$

Where Ei is the incident energy; Ea is absorbed energy (100-Et-Er); Et is transmitted energy (E_d/E_{do}); and Er is reflected energy (R- E_u/E_{do}).

The interrelationship involving PAR transmittance, reflectance, and absorption (in percent) with varying SSC at the depth of 60cm is shown above in figure 2.24.

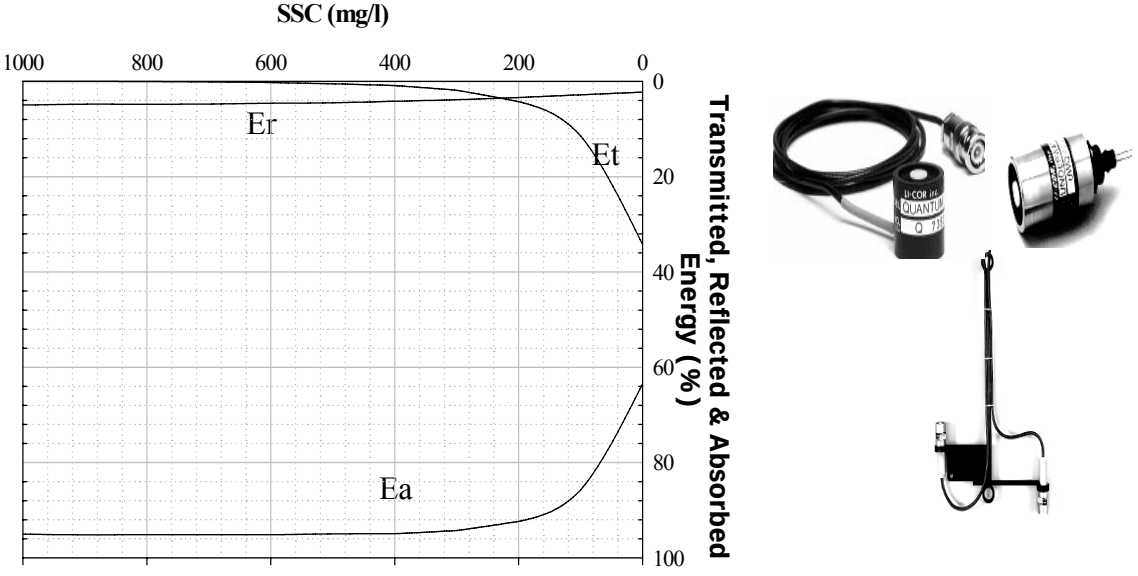

Figure 2.24 PAR Budget with varying SSC

The transmitted energy tends to decrease with the increase in SSC with the zero value above SSC of 400mg/l. However, the absorbed energy behaved oppositely showing increasing trend with the increase in suspended sediments. The change in absorption energy is more from 0 to 200 mg/l SSC and almost remain constant through the entire rang. Both the downwelling and upwelling radiance below the water surface decreased with increasing SSC. With the increase in suspended sediment concentration, the effect of upwelling radiance from the bottom decreased. At the SSC of 400 mg/l, there is no bottom effect if the water depth is more than 60cm. However, at the depth of 30 cm, the bottom effects the upwelling signals even with SSC of 1000 mg/l.

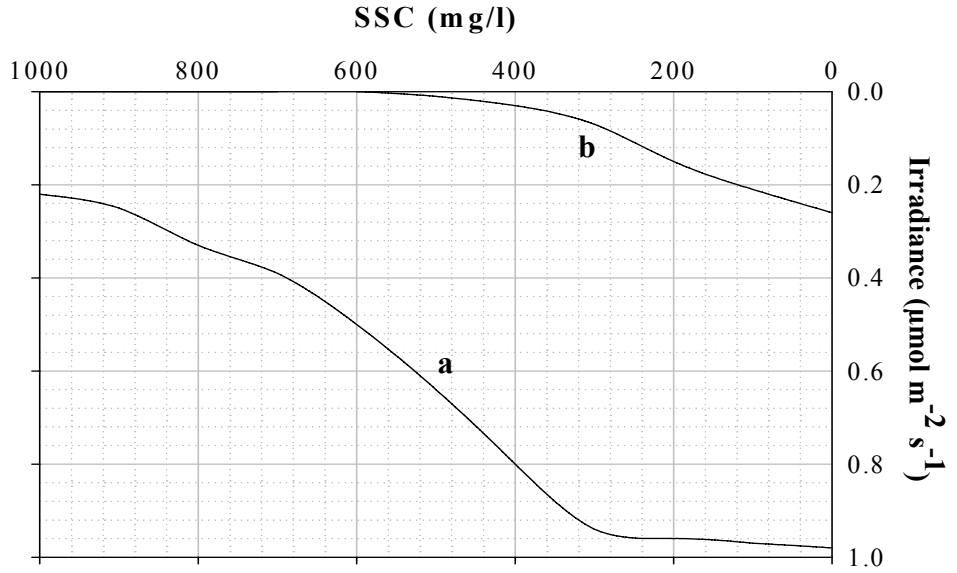

Figure 2.25 Upwelling irradiance (Eu) at 30 cm (Curve a) & 60 cm (Curve b) depth from water surface with varying SSC

It is worth mentioning that most of the incident energy in visible domain (400-700 nm) on the water surface is either absorbed, transmitted or reflected in other directions. The reflectance from the water surface in laboratory under controlled conditions is only 2% of the total incident light and increased to about 4 % at SSC of 1000 mg/l. The diffuse attenuation coefficient (k) is derived from the Beer-Bouger Law and can be calculated using the following equation.

$$k = [ln\ (E_{do} - E_d)]\ /d$$

Where E_{do} is the downwelling radiance at the surface, E_d is the radiance at depth and d is the distance between the sensor at depth and the sensor at the surface.

The diffuse attenuation coefficient k quantifies the "quenching" of light as it passes from the water surface to the quantum sensor at the depth of 60 cm. The relationship between SSC and k is important because the level of turbidity of a water body can be measured by means of computing k, instead of measuring SSC. The results of relationship between SSC and k are summarized graphically as figure 2.26. Suspended sediment concentrations can be estimated by extension coefficients using a linear regression model of the form;

K=*9E-05 (SSC)+0.021*

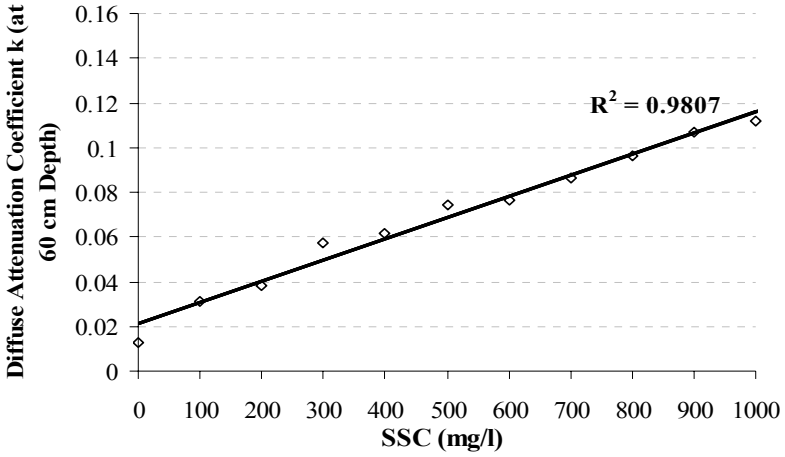

Figure 2.26 Relationship between SSC and extinction coefficient

2.11 Relationship between Varying Concentration of Chlorophyll - a and Spectral Reflectance

2.11.1 Introduction

A great number of attempts have been made to estimate chlorophyll-a and suspended sediment concentrations using remotely sensed reflectance from a water area in order to monitor its overall trophic state and primary productivity (Ritchie et al. 1990,Gitelson 1993, Arenz et al. 1996, Choubey 1998, Thiemann and Kaufmann 2000).

Phytoplankton, which is often a substantial part of suspended matter, is one of the major water quality parameter. Estimating phytoplankton biomass and distribution through quantifying and mapping chlorophyll concentration has been one of the major applications of remote sensing of coastal waters (Johnson 1978, Khorram 1985, Harding et al. 1994). The qualitative and quantitative characteristics of spectral signatures are influended by the type and concentration of the chlorophyll. Hyperspectral sensors have been considered as the future sensors to measure chlorophyll concentration in water (Richardson 1996).
Gitelson (1992) studied the behaviour of the reflectance peak near 700nm of algal water. It was found that the shift in peak position and an increase of the peak magnitude occurred as chlorophyll concentration increased. Gitelson concluded that the 700nm reflectance peak is important for the remote sensing of inland and coastal waters with regard to measuring chlorophyll. Han (1997) conducted research on characterizing the relationship between suspended sediment concentration (SSC) and reflectance in clear and algal laden waters. Han and Rundquist (1997) compared the near-infrared (NIR) and red ratio and the first derivative of reflectance in modeling chlorophyll concentration in a turbid Midwestern reservoir. In order to investigate the effect of chlorophyll concentration on spectral reflectance, experiments were conducted in the laboratory under controlled conditions.

2.11.2 Material & methodology

The experiments were conducted indoor in a black painted room at Center for Advanced Land Management Information Technologies (CALMIT), University of Nebraska- Lincoln, USA. Spectral reflectance measurements were made from a boat using Ocean Optics USB2000 Spectroradiometers (2048 channels, 370–1000 nm). Data were collected in the spectral range of 400-900 nm with a sampling interval of 0.3 nm and a spectral resolution of 1.5 nm. For each chlorophyll-a concentration, four spectral reflectance measurements were collected such as: i) Above surface nadir view; ii) Above surface at 45^{o} to the water surface; iii) below water nadir view; and iv) below water 45^{o}. The depth of the water was kept constant to 60 cm. The concentration of chlorophyll-a was measured fluorometrically. Initially the chlorophyll-a concentration was 801.3 µg/l. The water was then diluted and the chlorophyll-a concentration changed to 506.6 µg/l. Again diluted to 258.9, 78 and 0.4 µg/l and spectral signatures were collected. The water tank is also black coated to reduce the influence of extraneous reflectance. A Hach 2100P turbidity meter was used to measure turbidity (NTU) at each level of chlorophyll-a concentration.

2.11.3 Result and discussion

The presence of chlorophyll-a in water effects the spectral signals showing increasing trend with the increase in concentration. As depicted in the graph the 2.27 that the red peak near 700 nm is the best predictor of chlorophyll-a concentration. The read peak shifts from 0.5 percent in clear water to about 2% at chlorophyll-a concentration. It is observed that the visible domain 400-500 nm and red domain 650 to 715 nm is useful range for monitoring chlorophyll-a concentration in water bodies. However, these results based on controlled experiments and similar kind of response is expected in field conditions.

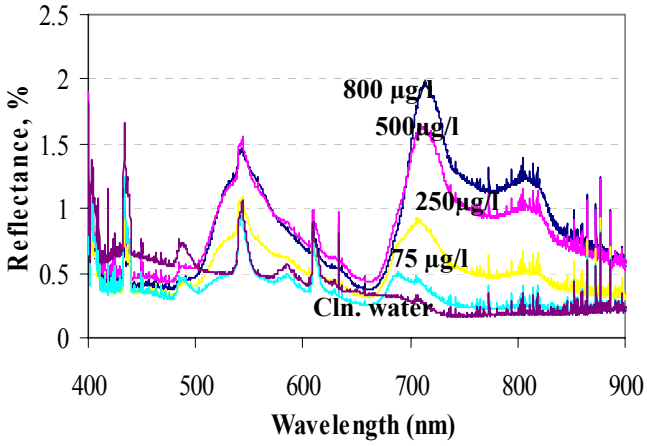

Figure 2.27 Reflectance at different concentration of Chlorophyll-a along wavelength

The presence of chlorophyll-a in water change the optical properties of water and spectral reflectance. The relationship between turbidity at different Chlorophyll-a concentration is given below.

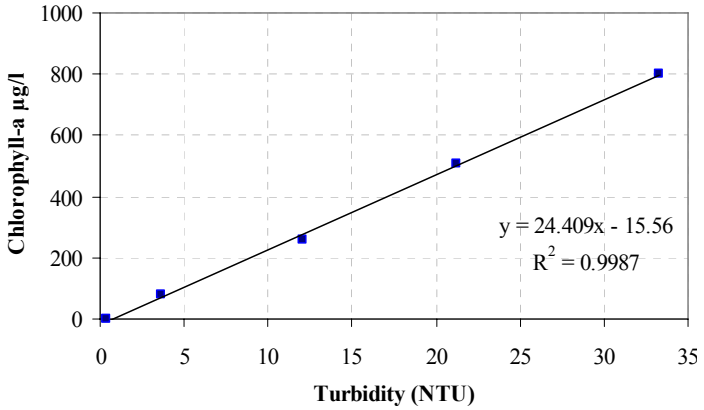

Figure 2.28 Relationship between Turbidity and Chlorophyll-a concentration

To quantify the concentration of Chlorophyll-a in water bodies the regression model was developed. The models are based on the simple relationship between the red and green domain. The rational is because the Chlorophyll-a is sensitive at wavelength near 675 nm. The presence of Chlorophyll-a is also very well correlated with red peak. The established models show good relation with Chlorophyll-a concentration. The relationship between peak in red domain near 715 nm show r^2 value of 0.99. This high correlation leads to predict that peak in red domain is useful in monitoring Chlorophyll-a concentration in water bodies.

The second model also shows a good correlation with r^2 value of 0.99. The purpose of this section is to demonstrate the relationship between remotely sensed signals and Chlorophyll-a concentration. The field application of developed algorithms is explained in detailed in chapter 4.

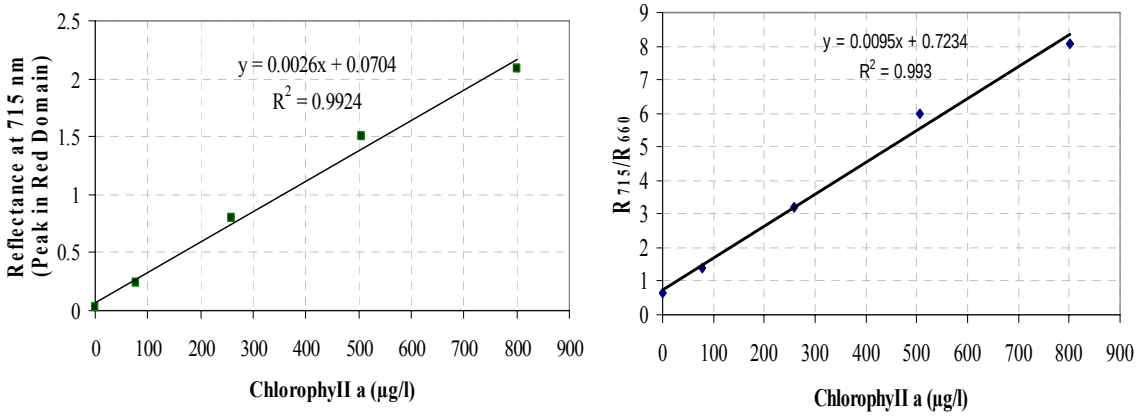

Figure 2.29 Regression models for chlorophyll-a estimation

2.12 Concluding remarks

In this chapter characteristic of equipment, factors effecting hyperspectral measurements in controlled conditions, the effect of suspended sediment amount and type

on spectral reflectance, effect of light penetration on SSC was addressed comprehensively. On the basis of experimental results obtained from the present study it can be concluded that the intensity and spectral distribution of reflectance varied with type, texture, grain size and concentration of suspended sediments in surface water. Spectral reflectance for different types and concentration of SSC are unique. With the increase in SSC, the reflectance signal increase uniformly with scattering in the visible domain and absorption in the near-infrared domain. It was observed that the reflectance in the red and near-infrared (NIR) wavelength 700-900 is a useful range for determining the amount of suspended sediments. However, the wavelength range 525-665 provides information about sediments type.

Band ration models allow the accurate quantification of suspended sediments. The relationship is based on the simple reflectance ratio between near-infrared and visible domains. The ratios of reflectance values in the sub-bands centered at 848/548, 803/708, 793/713, 773/663, 783/673, and 773/658 were found to be optimum for estimation of suspended sediment in surface water. The results of the estimation of suspended sediment by using hyperspectral band ration models are encouraging. To develop more generalized model for predicting suspended sediment concentration, similar studies are needed to express and quantify the integrated effect of all such parameters on spectral reflectance. The chapter leads to the following useful findings 1) In the visible domain, with increase in SSC, there is small increase in reflected energy compared to a large increase in energy absorbed; 2) Between 700 to 900 nm (NIR) the reflectance increases more uniformly with increased SSC. Thus, the optimum wavelength for measuring SSC is NIR (Band 4 of ALOS). However, visible wavelength (Band 2) is useful for qualitative point of view to characterizing and differentiating suspended sediments. 3) The shape and magnitude of the spectra reflected from water is strongly influenced by type and amount of suspended sediments. 4) The spectroradimeter data, integrated to into the band width of ALOS, allow accurate assessment of SSC. 4). The first derivative proved to be effective in estimating SSC; 5) The diffuse attenuation increase with the increase in SSC and the relationship is linear; and 6) At a depth of 60 cm, in the visible domain, there was no bottom effect when suspended sediment concentrations were above 400mg/liter. To develop more generalize model for predicting suspended sediment concentration, effect of suspended sediments distribution with depth and application of remotely sensed data with different environmental condition needs evaluation. It is further concluded that sustainable water resources management in an organized and coordinated way will be key measures to sustain the economic development. In the future, therefore, it will be important to incorporate sediment assessment as an integral part of water resources and environmental planning, development and management. Without this approach the problems of the water & environmental sector are going to compound in the future. Effect of suspended sediments distribution with depth and application of remotely sensed data with different environmental condition needs to be explored for future research.

CHAPTER 3

EFFECT OF FIELD CONDITIONS ON REMOTELY SENSED DATA

3.1 Introduction

Remote sensing is a tool and technique that provides a platform for large-scale synoptic observations and continuous monitoring of water bodies. This global capability is accomplished through hyperspectral or multispectral measurements of radiometric quantities. The necessary requirement and concern in application of remotely sensed data is that the radiometric data meet the overall objectives of the study. The optical data collection involves several continuous activities and the quality of collected data set depends on accurate methodology and influencing environmental factors. However, accuracy of remotely data depends upon a clear definition of what is being measured, on the conditions under which it is being measured, and on an unbroken traceability chain with known uncertainty at each step (Milton, 2006). A few systematic studies for radiance measurements have been made in natural waters (Mobley, 1989). The spectral reflectance is widely used for qualitative and quantitative assessment of constituents in water bodies. The vague understanding of data collection techniques and assumptions may lead to errors in the collected data. Scientists have explored a variety of techniques for collecting data by means of radiometer or spectroradiometer.

Rundquist (2004) compared the spectral data collected over cropland vegetation by means of machine-positioning versus hand positioning of the sensor and quantify the difference between acquired spectral data. Hooker et al. (2002) evaluated above and in-water methods for determination of water leaving radiance. Their fundamental premise was that it is difficult to remove the effect the surface waves, wind and other influencing parameters associated with above-water spectral measurements. Hooker and Maritorena (2000) took into account: a) calibration, (b) in situ sensor stability, (c) data collection method, and (d) data processing as source of uncertainty arising from in-water optical data collection deployment systems in the Case-1 environment.

Field spectroscopy is a useful tool to understand the process and application of remotely sensed data. However, after the years of research, the techniques and approaches for remotely data collection are insufficient to address and overcome the filed problems. The collection of accurate spectra in the field requires an awareness of the influences of the various sources of illumination, atmospheric characteristics and winds. Moreover, much of the research has been focusing on sea water and in coastal environment. A little intension has been given to the inland fresh water systems. Any application of remotely sensed data to monitor problem should be based on establishing a link between the information required and measurements. The meaningful application of remotely sensed data demands for high radiometric accuracy.

3.2 Purpose of the Study

The need to understand the spectral nature, influencing parameters and correct data collection techniques is crucial for monitoring of water bodies. Rundquist (2001)

suggested that the best research projects are those that deal with one relatively simple concept, problem, question, or hypothesis. The purpose of this chapter is to demonstrate the effect of field conditions of remotely sensed data. Series of experiments were carried out in field conditions to demonstrate the effect of various parameters on spectral signatures.

3.3 Effect of Sky Condition on Spectral Signatures of Varying Concentration of Suspended Sediments

In order to elucidate the solar effect on spectral signatures, the experiment was carried out in field condition. In lab condition the illumination condition and environmental factors are controlled and the influence parameters may not affect the spectral signals reflected from the target. However, in field conditions the environmental factors and sky condition affects the experimental readings and it is imperative to consider any change in influencing parameters. The experiment was performed in a black coated water tank under clear sky and partially cloudy sky conditions. The water tank is coated black to minimize the bottom effect and extraneous reflectance. ASD Field Spec FR spectrometer is used to collect the spectral signature from the water surface with varying concentration of suspended sediments. The sieved silty soil samples were weighted to produce fifty concentrations of suspended sediments in each case ranging from 20 to 1000 mg/l. The depth of water column was 60 cm and was kept constant for all experiment. The soil sediments were kept in suspension by means of a mechanical diffuser and manually stirring at regular intervals.

Reflectance was calculated as a simple ratio between target and reference panel using following equation.

$$R(\lambda) = \frac{L(\lambda)}{S(\lambda)} \times Cal(\lambda)$$

Where L (λ) is the radiance measured from the water surface, S (λ) is the radiance from the reference panel measured under the same illumination conditions and Cal (λ) is the calibration factor for the reference panel. The reference plaque was a Labsphere white Spectralon of dimensions 12.5cm x 12.5cm.

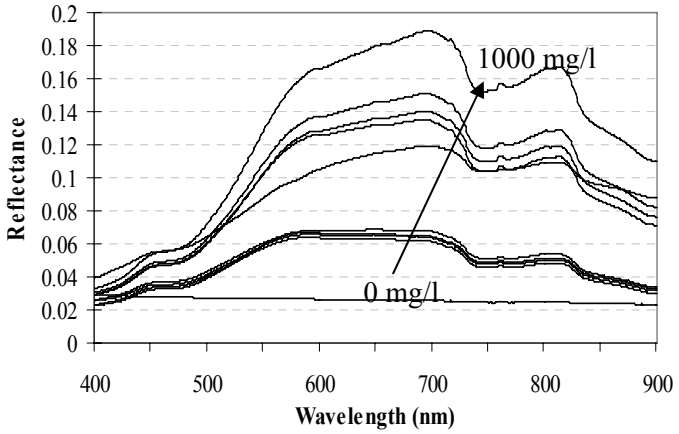

Figure 3.1 Spectral reflectance of water with varying concentration (mg/l) of silty red soil under clear sky condition

Figure 3.1 illustrate the spectral signature of silty red soil in the field under clear sky condition. As depicted from the graph that with the increase in suspended sediment, the spectral reflectance tends to increase. The spectral reflectance of silty red soil under natural conditions is more as compared to the spectral reflectance in lab conditions. The reason is that the spectral signatures are very much associated with the illumination source. To investigate the effect of illumination source and environmental factors, the spectral reflectance of silty red soil in lab, under clear sky condition and under partial cloudy sky is compared.

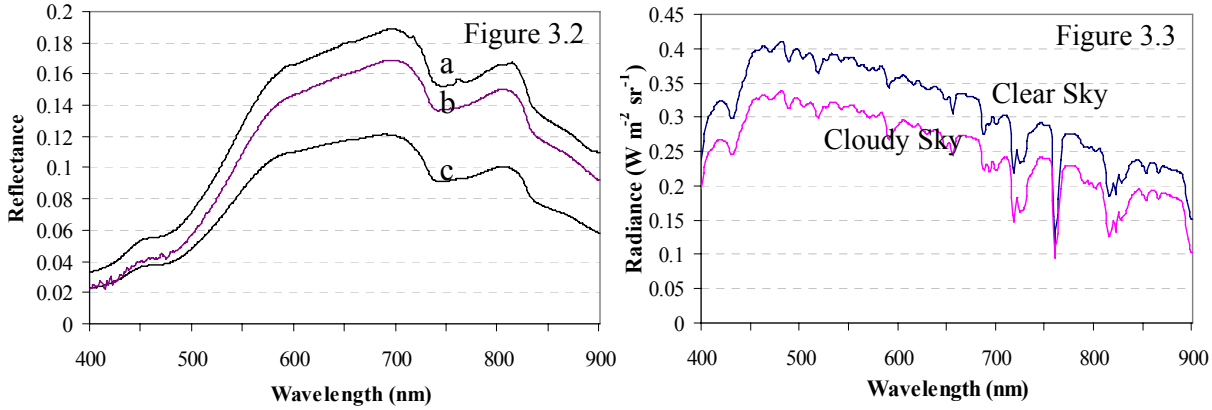

Figure 3.2 Spectral reflectance of water with silty red soil (1000 mg/l) a: Under clear sky condition b: In laboratory under controlled condition c: Under partial sky condition

As evident from the graph that the spectral reflectance under clear sky condition is more as compared to the reflectance under partial sky condition and in laboratory. The illumination source has effect on the reflectance signals and influences the result of the remotely sensed experiments. Figure 3.3 is the graphical representation of radiance acquired from the white reference panel under clear sky condition and under partial cloudy sky. It is good practice to take into account the illumination source and change in illumination angle.

3.4 Comparison between Percentage Reflectance and Remote Sensing Reflectance

ASD Field Spec FR spectrometer is normally used to collect the percentage reflectance in case of water bodies. Reflectance, % is a simple ratio between target and reference panel using following equation.

$$\%\ R(\lambda) = \frac{L(\lambda)}{S(\lambda)} \times Cal\ (\lambda) \times 100$$

Where L (λ) is the radiance measured from the water surface, S (λ) is the radiance from the reference panel measured under the same illumination conditions and Cal (λ) is the calibration factor for the reference panel. The reference plaque was a Labsphere white Spectralon of dimensions 12.5cm x 12.5cm.

In optical remote sensing the terminology, Remote sensing reflectance "R_{rs}" is widely used. The term R_{rs} is the ratio between total upwelling radiance from the water surface $L_U(\lambda)$ and downwelling irradiance $E_d(\lambda)$. It is not possible to measure directly the R_{rs} by

using a single spectroradiometer without irradiance sensor. However, it is possible to measure the R_{rs} by adopting the following methodology.

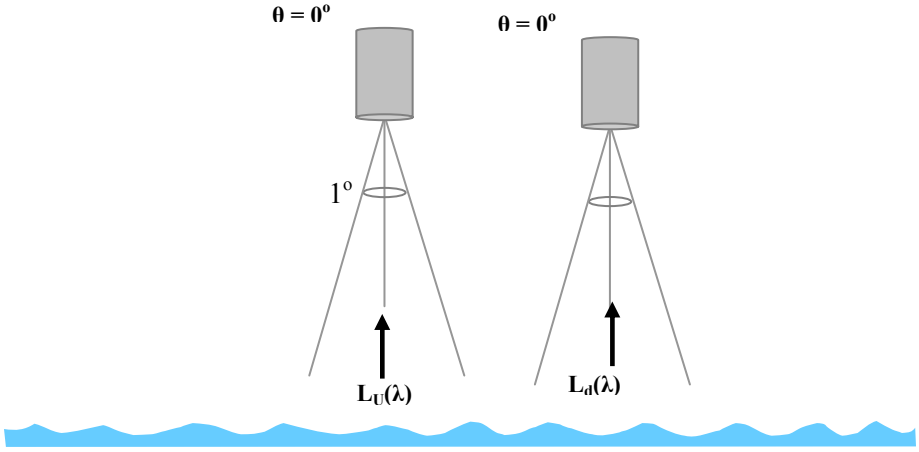

Figure 3.3: In situ remote sensing reflectance, R_{rs} measurement procedure

i) $L_u(\lambda)$; upwelling radiance spectrum is measured when the sensor views vertically downward to the water surface ($\theta = 0$)

ii) $L_d(\lambda)$; downwelling radiance spectrum is measured when the sensor views a Lambertian Spectralon plate, with a reflectance factor Rc ≈ 99%

The dowelling irradiance $E_d(\lambda)$ is calculated by using the following equation:

$$E_d(\lambda)(\mathrm{Wm}^{-2}\mathrm{nm}^{-1}) = \frac{\pi}{R_c} \times L_d(\lambda)$$

The graphical representation of R,% and R_{rs} is shown in graph 3.4. As clear from the graph that the R,% is more than the remote sensing reflectance R_{rs}. One should have basic and applied knowledge of both the terms and experimental methodology depending on the objective of the research work. For delineation of water bodies, percentage reflectance is widely used by researcher. However, the methodology and measurement protocols depend on field apparatus and research objectives. For comparison purpose between satellite data and in situ hyperspectral reflectance data, it is suggested to process and analyze the data with remote sensing reflectance.

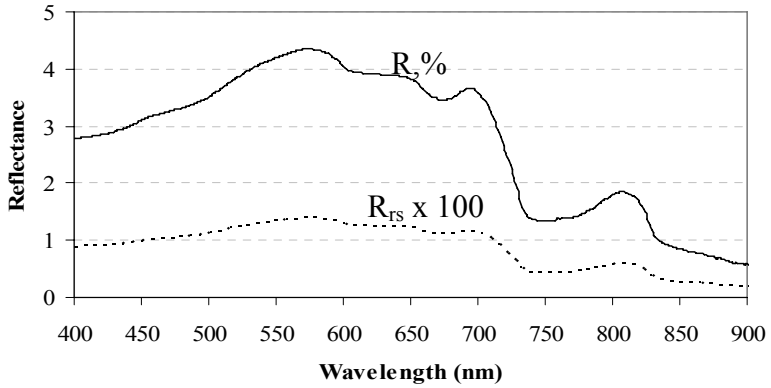

Figure 3.4: Comparison between R, % and remote sensing reflectance, R_{rs}

3.5 Quantitative Relationship between Upwelling Irradiance and Dowelling Irradiance in Water

The quantitative relationship between upwelling irradiance just below the water surface and downwelling irradiance on the water surface in the visible domain was investigated in chapter 2. In other words, it is relationship between the dowelling and upwelling light energy. The under water quantum sensor was used to measure the amount of photosynthetically active radiation (PAR-400 to 700 nm) in the water. Photosynthetically Active Radiation (PAR), can be measured in energy units (watts m^{-2}) or as Photosynthetic Photon Flux Density (PPFD), which has units of quanta (photons) per unit time per unit surface area. The units most commonly used are micromoles of quanta per second per square meter (µmol s^{-1} m^{-2}).

In field conditions, a small amount of total energy is reflected from the water surface and depends on the water constituents present within the water body and other influencing environmental factors. With TSS (mg/l) concentration of 27.8 and turbidity of 18.2 NTU, 7% of the total downwelling irradiance is reflected from the water. However, with TSS (mg/l) concentration of 8.6 and turbidity of 2.0 NTU, only 1% of the total downwelling irradiance is reflected from the water.

It is worth mentioning that even this reflected energy is enough to delineate the water bodies. The remote sensing theory lies on that fact that most of the incoming energy is absorbed, transmitted or reflected in other directions. Less than 10% of the incoming energy is the actual signals carrying information about the water body.

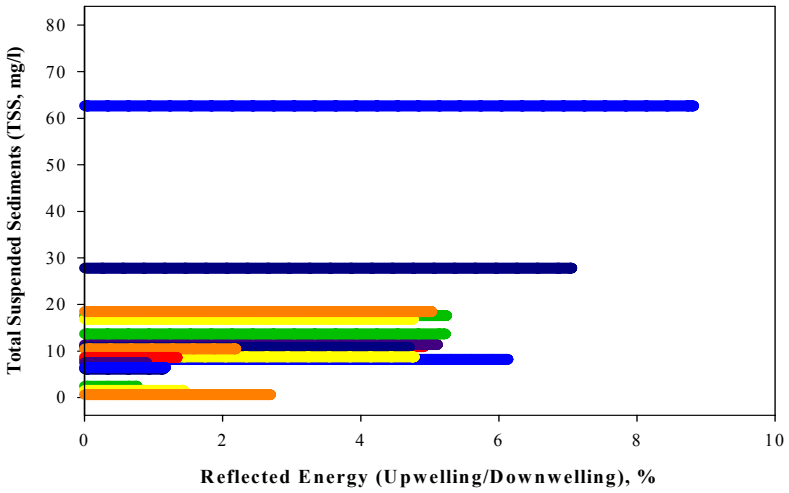

Figure 3.5: Relationship between TSS and percentage reflected energy

3.6 Environmental Factors Influencing the Hyperspectral Reflectance

Environmental factors in combination and individual affect the remote sensing reflectance. The influence of some environmental factors on remote sensing reflectance in the filed was thoroughly examined and explained. A little change in field circumstances affects the signals received by the sensor. The spectral signature of river water acquired under clear sky condition, the river water out side in black coated water tank under same

field conditions and the same water sample in the lab conditions show entirely different response as shown in figure 3.6-a. The spectral reflectance of river water was taken by pointing the senor at the height of 1 meter from the water surface. The water sample was taken out of the river in the black coated water tank at the same site and the spectral signal was acquired keeping the same procedure. Finally the spectral signature of same water sample was taken in the laboratory under controlled conditions.

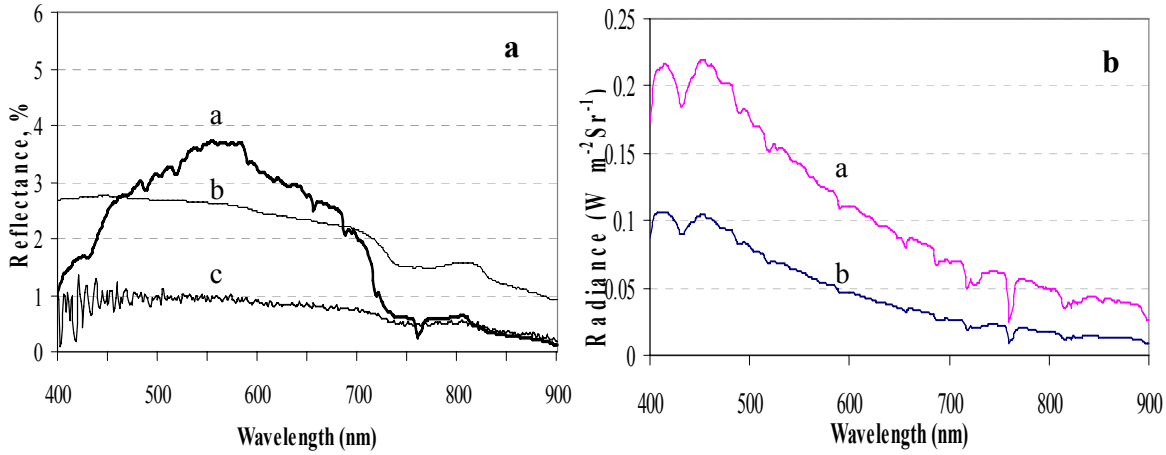

Figure 3.6-a Spectra of river water a): In River b): In black tank under same field conditions c): In Lab; Figure 3.6-b Radiance by pointing the sensor towards a): sun and b): sky

It was observed that the spectral signature acquired under field conditions in the black coated water tank was more as compared to the signals in the laboratory. The difference of spectral reflectance acquired at the river and in the laboratory was almost negligible in the NIR domain but the reflectance is about 3 times more in the visible domain. Figure 3.6-b depicts the radiance spectra acquired by pointing the sensor towards sky and sun. The change in experimental setup and viewing geometry influence the results. The results help to conclude the experimental environment contributes to the spectra significantly. It is not possible to avoid such errors in the results; however, by adopting proper methodology and measurement protocols it is possible to minimize the effects. Each environmental factor has its own influence on the remote sensing signals. It is dire need to take into account the influencing parameters and measurement protocols for accurate assessment of water bodies.

3.6.1 Effect of water surface waves on reflectance

Effect of waves on above water surface hyperspectral reflectance is significant and is a major source of error in the measurements. To examine the effect of waves on the spectral signature, experiment was made out in the field. The wooden frame was designed to make the water surface smooth. Firstly the spectra were acquired from the river water with unsmooth surface under natural field condition with clear sky. Secondly, at the same site, the wooden frame was placed and the spectra of water with in the frame were taken. The purpose is to compare the spectra of water surface with waves and without waves at the same site and under same conditions.

It was observed (Figure 3.7) that with the waves on the surface the spectral reflectance is about 2 times more as compared to the smooth surface. The effect of waves on the spectral signals is almost constant through the entire wavelength and disturbs the signals received by the sensor. It can be concluded that under windy conditions and waves on the water surface, the spectrum average and ratio of bands may decrease the effect of waves on the observed spectral signals.

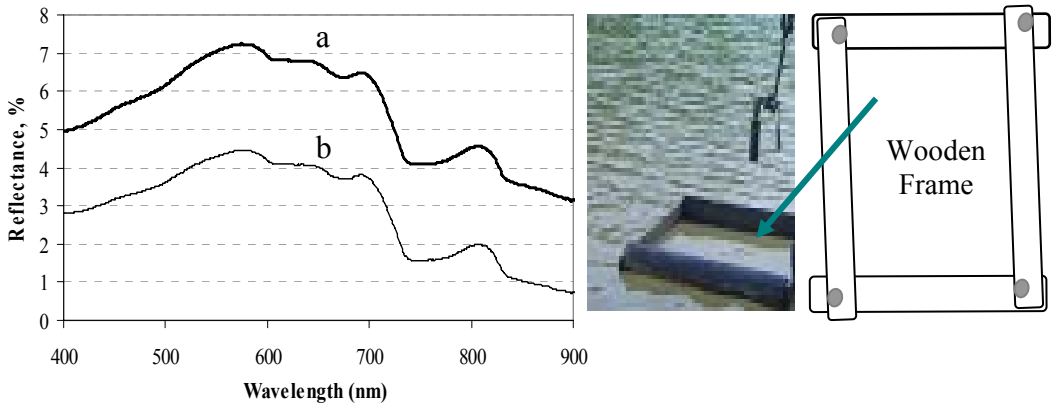

Figure 3.7 Comparison of river water reflectance a): With waves b): Smooth Surface in wooden frame

3.6.2 Effect of sensor height above the surface

The sensor height above the water surface in field conditions affects the signals significantly. However, it is much associated with the surface roughness and wind during the time of experiment.

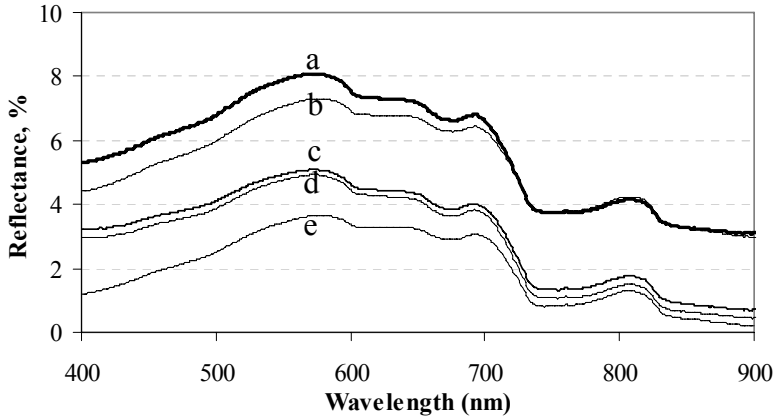

Figure 3.8 Spectral reflectance with different sensor height above the water surface a): 1.5 meter above the water surface b): 1 meter above c): 0.5 meter above d): just above the water surface e): below the water surface

The spectral signals were obtained from the river water surface under clear sky conditions. The wind speed was about 5m/s. Figure 3.8 illustrates the effect of sensor height above the water surface. It is examined that with the increase in sensor height above

the water surface, the spectral reflectance also increases. However, the increasing trend is more in the visible domain as compared to NIR region. The difference is reflectance is owing to many influencing parameters including surface reflection effects, wind speed, water constituents and illumination intensity and geometry. With the same FOV, the change in height affects the remote sensing signals.

3.6.3 Effect of field of view (FOV) on reflectance

The effect of FOV was explained by using 1degree and 25 degree FOV with the sensor height of 1 meter above the water surface. It is noticed that the effect of FOV for the same height above the water surface is negligible in the NIR domain. However, a slight difference was observed in the green domain. It can be concluded that FOV have almost no effect on the spectral signature. The advantage is that with large FOV, the large area can be observed and helps to assess the water bodies effectively and efficiently. The FOV changes with different fore optics and distance from the water surface. As explained above that with the same FOV the spectral reflectance is influenced with the change in sensor height above the water surface.

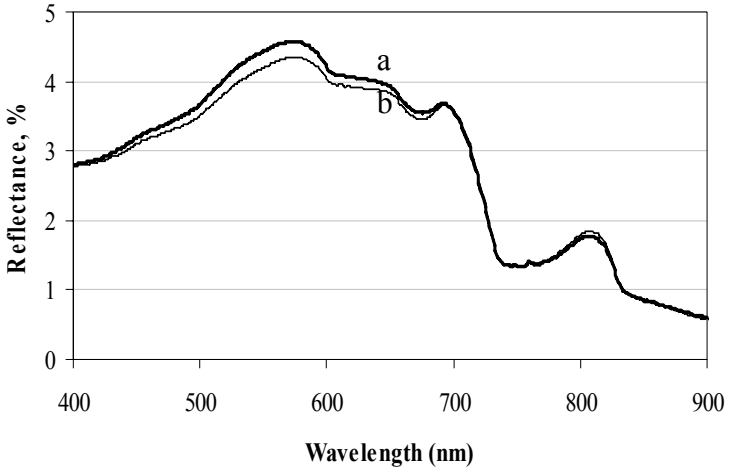

Figure 3.9 Effect of FOV on spectral signature a): FOV 25 degree b): FOV 1 degree

3.7 Under Water Light Field Condition

It is important to develop the relationship between change in magnitude of spectral signatures with water depth. Dawson (1983), and Jupp (1988) have invoked assumptions such as the light attenuation is exponential with depth and that water quality remains consistent within the image. The intensity of light decease with depth. However, it depends on type of water and environmental conditions. For monitoring water bodies and understanding the behavior of under water light filed condition; the parameter that controls the propagation of light through water, i.e., the diffuse attenuation coefficient $K_d(z,\lambda)$, needs to be known precisely. It is defined in terms of the exponential decrease with depth of the ambient downwelling irradiance $E_d(z,\lambda)$. This coefficient of downwelling irradiance, $E_d(z,\lambda)$, which comprises photons heading in all downward directions as written as follow (Mobley, 1994):

$$K_d(z,\lambda) = \frac{1}{E_d(\lambda)} \frac{dE_d}{dz}$$

Where,

$K_d(z,\lambda)$ diffuse attenuation coefficient (m^{-1})
$E_d(\lambda)$ downwelling irradiance (Wm^{-2})
dz Water depth (m)

Kd (z,λ) depends on inherent optical properties of aquatic medium and are not altered significantly by changes in the incident radiation field such as a change in solar elevation (Kirk, 1994). The underwater data at northwestern coast of Roatan Island in the Sandy Bay Marine Reserve were acquired by a field crew from the Center for Advanced Land Management Information Technologies, University of Nebraska–Lincoln. The instrument was a hand-held wand (appropriately named WANDA) comprising of: (a) an upward looking Ocean Optics sensor (hyperspectral sensor with 2048 bands, 1 nm bandwidth) with a cosine collector; (b) a downward looking Ocean Optics sensor. An upward looking Ocean Optics and a quantum sensor were also installed on the roof of the boat to simultaneously collect downwelling irradiance with the sensors on the wand. A vertical profile of downwelling irradiance was acquired by a diver lowering WANDA through the water column at approximately 0.5-m depth intervals. To avoid boat shadow, readings were taken approximately 20 m away and on the sunny side of the boat.

The water around Roatan Island is classified as Case I based on Morel and Prieur (1977), which implies that the concentration of phytoplankton is high compared to non-biogenic particles. Case I waters can range from very clear (oligotrophic) to very turbid (eutrophic), depending on the phytoplankton concentration. As clear from the figure 3.10 that the downwelling irradiance decrease with the increase in depth showing symmetric trend.

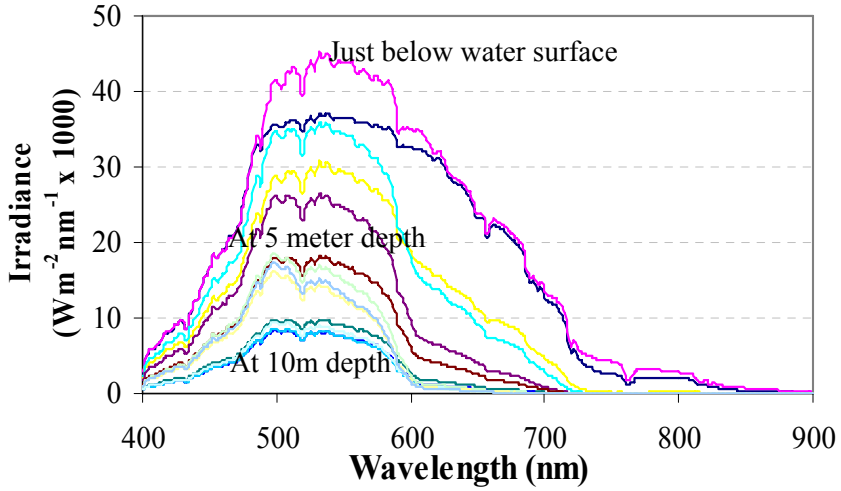

Figure 3.10 Relationship between downwelling Irradiance and wavelength at different dpeths

The spectra changed quantitatively; however, the qualitative nature of the spectra remained similar. The spectral behavior proof the assumption to consider the water body vertically homogenous for monitoring by means of remote sensing. Figure 3.11 demonstrate the relationship between diffuse attenuation coefficient K_d and wavelength. The $K_d(m^{-1})$ tends to increase with the wavelength in the visible domain. With the increase in depth, irradiance decrease and thus the value $K_d(m^{-1})$ of increased exponentially.

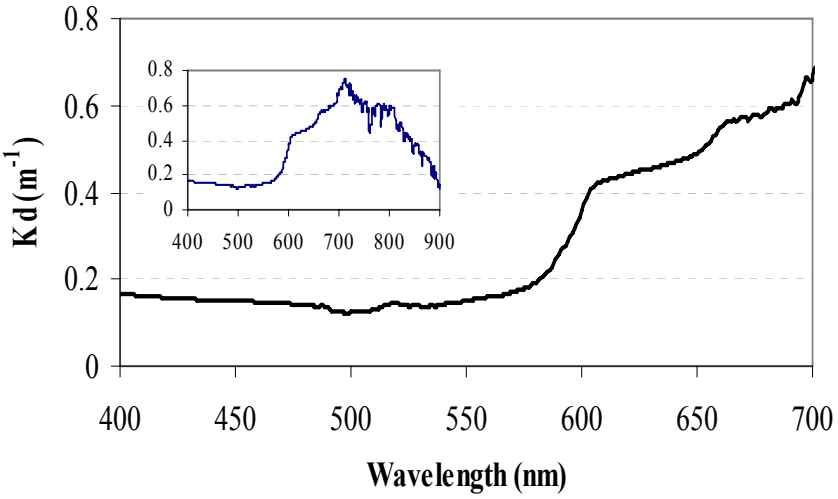

Figure 3.11 Relationship between K_d and wavelength

3.8 Comparison of Above Water Surface and Subsurface Reflectance Measurement

3.8.1 Introduction

Above-water surface and subsurface spectral comparison, relationship and the change in above and subsurface reflectance ratio with wavelengths have not been investigated in literature. The present section of the thesis is intended to demonstrate quantitatively the difference between the above and in-water spectral reflectances collected on variety of river waters. Many authors have concentrated to delineate the spectral differences, not on the methods of data collection. Doxaran et al. (2004) focused on estimation of surface reflection effects on upwelling radiance field measurements in turbid waters. The purpose of this paper is to elucidate the above-water and subsurface spectral behavior qualitatively and quantitatively.

3.8.2 Theoretical background

The optical properties considered here are above-water surface total upwelling radiance $L_t(\lambda)$, above-water surface spectral water leaving radiance $L_w(\lambda)$, the upwelling radiance just below the water surface (Subsurface) $L_u(\lambda)$, the dowelling irradiance incident on the water surface $E_{inc}(\lambda)$, and the reflectance quantity, also sometimes called water-leaving reflectance $R(\lambda)$.

The above surface upwelling radiance $L_w(\lambda)$ cannot be directly measured with commonly available instruments. The measured above surface upwelling radiance in the

sensor viewing direction is the sum of the water-leaving radiance $L_w(\lambda)$, plus any incident sky radiance reflected by the water surface. The total radiance entering the sensor can be expressed as (Mobley 1999);

$$L_t(\lambda) = L_w(\lambda) + L_r(\lambda)$$

L_r is the surface-reflected part of the incident sky radiance L_s. Lr is related to the sky radiance L_s incident on the water surface through the following equation Mobley (1999);

$$L_r = \rho L_s$$

Where ρ is a proportionality factor that depends not only on direction, wavelength, and wind speed, but also on the sensor field-of-view and on the sky radiance distribution. The above and below- water upwelling radiances are related by (Morel and Gentili 1996);

$$\frac{L_w}{L_u} = \frac{1 - r_F}{n_w^2}$$

Where r_F is the Fresnel reflectance of the surface as seen from the water side and n_w is the refractive index of water. For r_F 0.02 to 0.04 and $n_w \approx 1.34$, the following approximation was proposed (Mobley 1999):

$$\frac{L_w}{L_u} \approx 0.544$$

3.8.3 Methodology

The research is based on the filed spectral reflectance measurements carried out at three different locations. The data were acquired during massive field campaigns at Altamaha River, Georgia, USA o, St. Marys River, Georgia, USA, and Monebe River, Kochi, Japan. The field spectral data in the USA was collected by a filed crew from the Center of Advanced Land Management Information Technologies (CALMIT), University of Nebraska-Lincoln. The data of Monobe River, Kochi, Japan was acquired by the field crew of Kochi University of Technology.

Spectral reflectance measurements were made from a boat using, a dual-fiber system, two inter-calibrated Ocean Optics USB2000 Spectroradiometers (2048 channels, 370–1000 nm). Data were collected in the spectral range of 400-900 nm with a sampling interval of 0.3 nm and a spectral resolution of 1.5 nm. Radiometer # 1, equipped with a 25^o field off view optical fiber, was pointed downward in the nadir direction to measure the total above surface upwelling radiance from the water $L_t(\lambda)$. Radiometer # 2, equipped with an optical fiber and a cosine collector (yielding a hemispherical filed of view) was pointed upward to simultaneously measure the above surface incident irradiance $E_{inc}(\lambda)$. In order to measure the subsurface upwelling radiance $L_u(\lambda)$ the optical fiber was mounted on a 2-m fixed black pole, and the tip of the optical fiber was kept just below the water surface (~3 cm). An average of 10 consecutive scans was used to collect the reflectance

spectra at each of the sampling station. The spectral reflectance data were collected close to solar noon, and changes in solar zenith angle were minimal during the period of scanning. All spectral measurements were taken over optically deep water. Data collection procedure was kept constant in all the cases. Percentage spectral reflectance R(λ) was computed as:

$$\%R(\lambda) = [L(\lambda)_t / E(\lambda)_{inc}] \times [E(\lambda)_{cal} / L(\lambda)_{cal}] \times R(\lambda)_{cal} \times 100$$

$R(\lambda)_{cal}$ is the reflectance of the Spectralon panel linearly interpolated to match the band centers of each radiometer.

The spectral reflectance of Monobe River, Kochi, Japan was collected by using a single Hyperspectral Field SpecPro FR Spectroradiometer. This portable spectrometer combines three spectrometers to cover the wavelength range from 350 to 2500 nm. Reflectance was calculated as a simple ratio between upwelling radiance from the target and upwelling radiance of reference panel.

3.8.4 Surface reflection effects

To examine the characteristic of spectral signatures associated with above and subsurface optical sensor deployment; the spectral data was collected at three different rivers under clear sky conditions.

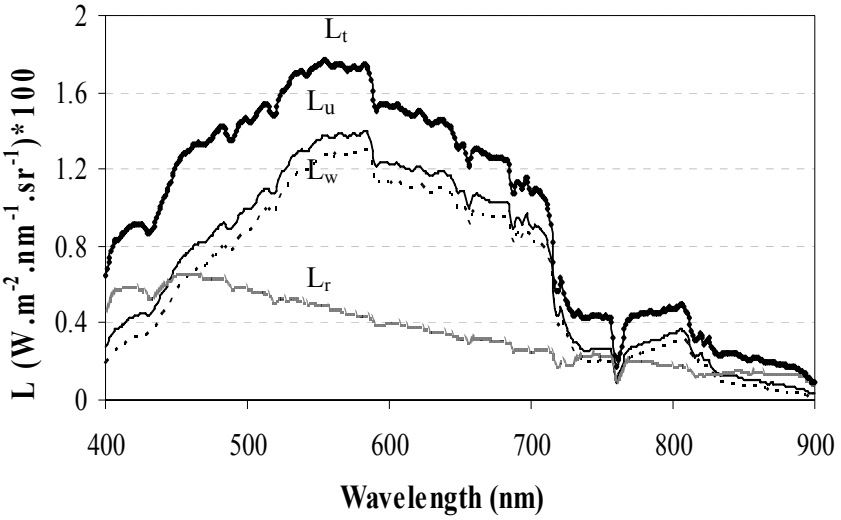

Figure 3.12 Comparison of the above water and subsurface upwelling radiance

Ancillary field data indicated low wind speed of about 3~ 5 m/s in all cases. Firstly the above-water surface and subsurface upwelling spectral radiance was compared. The upwelling above-water surface radiance $L_w(\lambda)$ was computed by equation (1). $L_s(\lambda)$ was measured by pointing the sensor towards zenith (detail in Doxaran 2001). $L_r(\lambda)$ was computed from $L_s(\lambda)$ by assuming $\rho \approx 0.022$. The comparison between measured and computed spectral radiance is presented in figure 3.12.

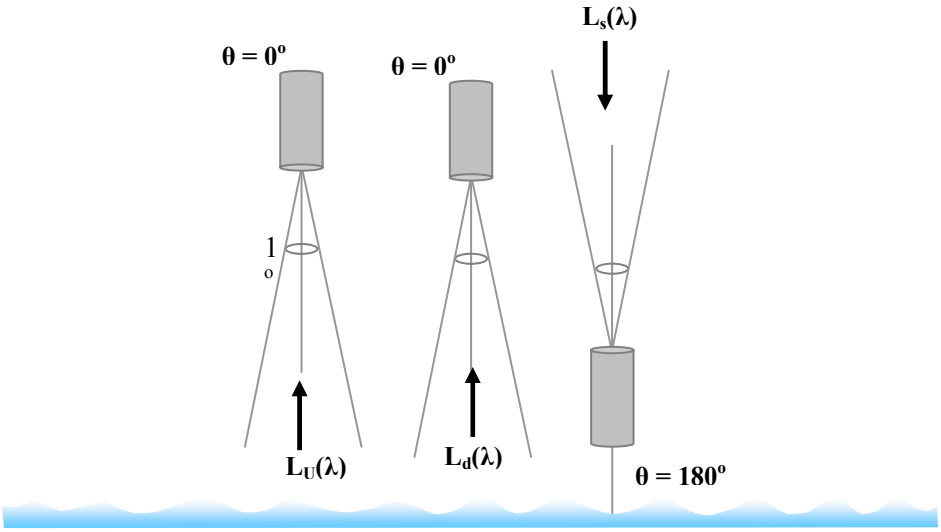

It is evident from the graph that there is a significant contribution of surface reflection effects in the upwelling radiance. The difference between above-water surface total upwelling radiance $L_t(\lambda)$ and above surface water-leaving radiance $L_w(\lambda)$ represents that the contribution of surface reflection effects was 70 % at 400nm, 40 % at 500 nm, 25% from 600 to 700 nm, and 40 to 70 % from 800 to 900nm. By comparing $L_t(\lambda)$ and $L_u(\lambda)$, it was seen that the difference was more in the visible domain with the maximum difference at 480nm and minimum at 655nm. The accurate retrieval of $L_w(\lambda)$ from the measured above water total upwelling signals is dependent on a proportionality factor ρ. Surface reflection effects are predominantly higher and the success of this correction is associated with the appropriate value of ρ. The ratio between computed $L_w(\lambda)$ and measured $L_u(\lambda)$ ranges between 0.6-0.9. It shows that the approximated value 0.054 as found in literature for the plane sea surface is not expected to be valid in case of inland water bodies. Moreover, the ratio is not constant and varies with the wavelength. The above-water surface and subsurface measured reflectances was compared and the collected datasets were plotted.

Figures 3.13-a, b & c illustrate the comparison between above-water surface and subsurface spectral data collected at Altamaha River, St. Marys River, and Monebe River respectively by adopting the same methodology as explained above. The change in solar zenith was not considered because the length of time difference between the two measurements, above- water surface and subsurface for the same point, was about 5 minutes and the collection of spectral data for all sampling points of individual river was accomplished within two hours.

For the purpose of spectral reflectance comparison and evaluation, the above-water upwelling radiances were not corrected for the surface reflection effects in the calculation of above-water surface spectral reflectances. As expected the above-water surface reflectances were more as compared to the subsurface reflectances. The maximum above surface reflectance was about 6% at Altamaha River, 4 % at St. Marys River and 4.5 % at Monobe River. The corresponding subsurface reflectance measurements were 4, 3.5 and 3.6 % respectively for the same sampling sites. The rational is because the surface reflection significantly influence the upwelling signals received by the sensor.

a: Altamaha River

Above water surface

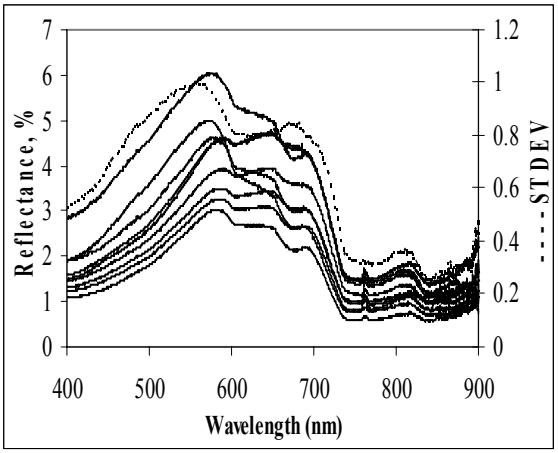

Below water surface/Subsurface

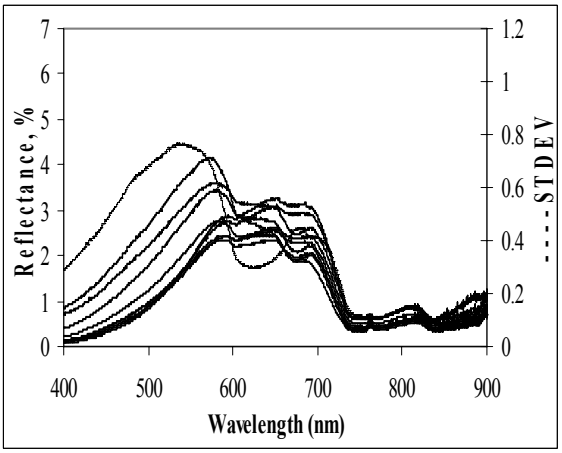

b: St. Marys River

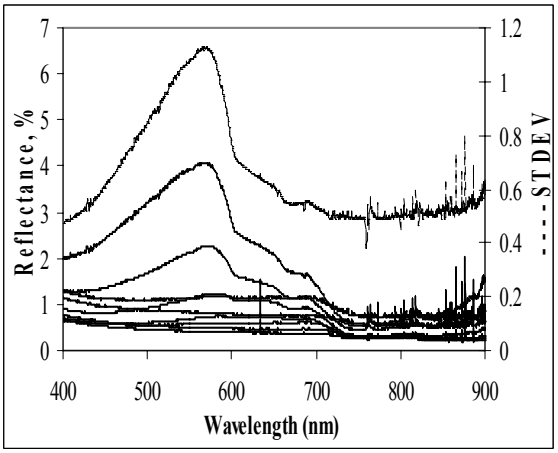

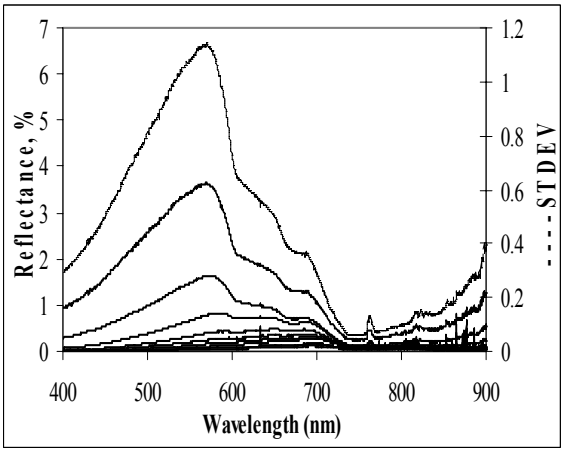

c: Monobe River

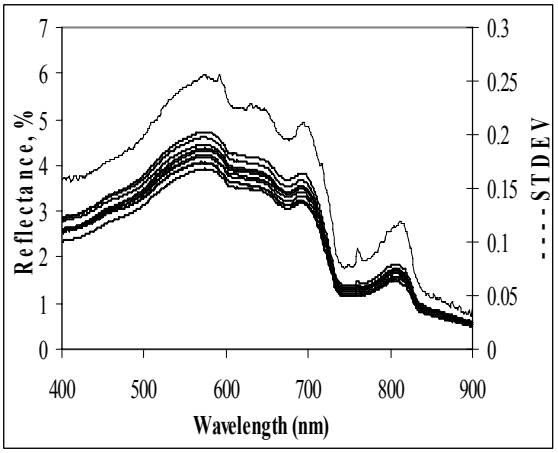

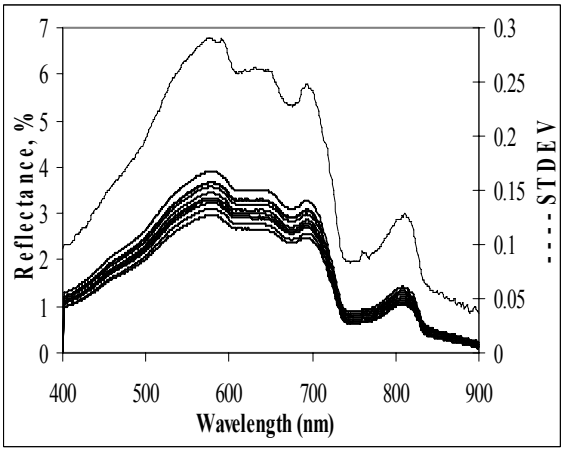

Figure 3.13- a,b,c: Comparison of above and subsurface spectral reflectances

Standard deviations (STDEV) were calculated for above-water and subsurface spectral reflectances. The reflectance variation was more in above-water reflectance measurements as compared to subsurface measurements of the same sampling stations. The minimal variation was noted in the red region for all the three rivers.

To describe the comparison elaborately, the sampling points of Altamaha River with maximum and minimum reflectance difference between above-water and subsurface reflectance measurements were plotted in figure 3.14. At the wavelength of 577 nm, maximum 6 % and minimum 3.6% above-water surface reflectance was observed at Altamaha River. The corresponding subsurface reflectances for the same sampling locations are 3 % and 2.7% respectively. The spectral reflectance difference of the sampling location with maximal reflectance is 3% and the same difference for the sampling point with minimal reflectance is 0.9 %.

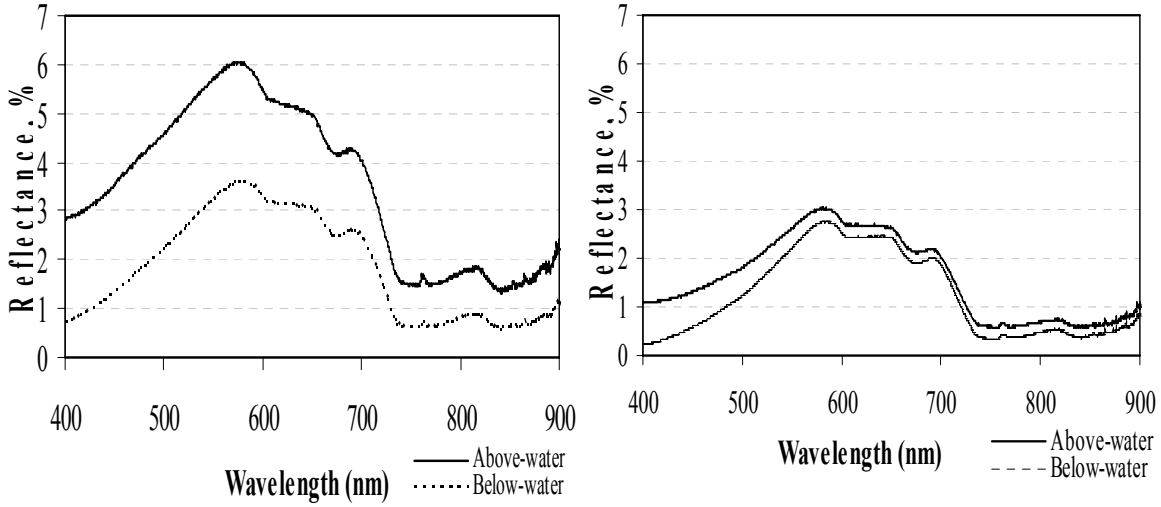

Figure 3.14: Comparison between sampling points with maximum and minimum reflectance difference at Altamaha River

The difference between above and subsurface reflectances are not same for all the sampling stations. It varies significantly from point to point and with wavelength. The difference between above-water and subsurface reflectance for the same sampling point varied with wavelength. The maximum difference was observed in the visible domain (400 nm -550 nm), that tends to decrease towards longer wavelength and becomes significant again in the NIR. The difference is almost constant in the blue and green domain; however, it was not consistence in the red region. In red domain the difference was minimal through the entire range. The comparisons showed that the difference between the above-water and subsurface spectral curves for the same sampling point is of quantitative nature. However, the qualitative nature of the curve is similar for all the cases. The similar kind of spectral behavior was noticed at all sampling points of the rivers. It leads to the conclusion that surface reflection has effect only on the magnitude of the reflectance, not on the nature and shape of the spectral signatures. The ratio between above and subsurface reflectance was also computed for the three rivers. It is interested to note that the ratio differs for all the sampling point at the same wavelength and for the same sampling point along the wavelength (Figure 3.15).

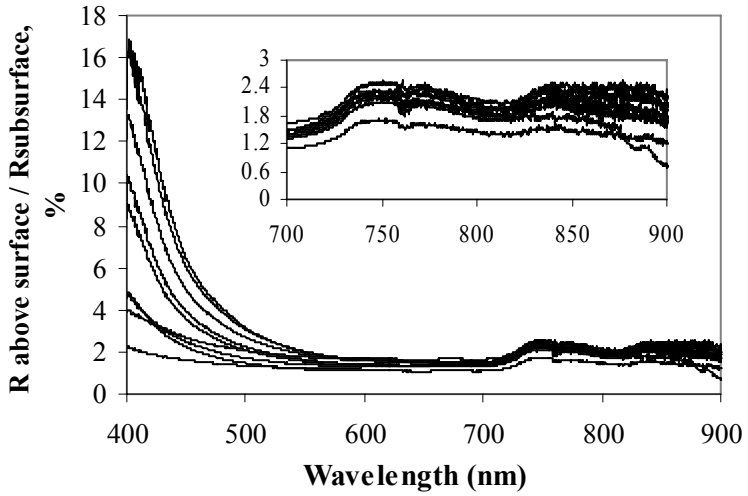

Figure 3.15: Correlation between above and subsurface reflectance ratio verses wavelength at Altamaha River

The maximum variation in the ratio was observed for the wavelength 400 to 500 nm. Standard deviation of the reflectance ratio were calculated for the datasets. All the STDEV in the visible range were between 5 to 2 % and 0.2 % in the NIR. The same response was observed at Monobe River. However, at ST Marry river, at some sampling points the reflectance ratio is more than 100 in the visible domain but the shows the almost same trend in the NIR. The spectral measurements of all the sampling points for one river were taken under the same conditions and simultaneously but, there is no symmetry in the above-water and subsurface reflectance ratios. The surface reflection effects are significant and the contribution of surface reflection effects is not same even for one water body. The above-water surface reflectance measurements were strongly influenced by surface reflection effects and researcher should avoid these effects during the collection of spectral data. However, in field it is rather difficult to grapple with such kind of influencing parameters.

The surface reflectance effects (caused by mainly sun glint, Illumination condition, viewing geometry) and water color add significant errors in the above surface optical measurements. Such error, if not removed, can prevent accurate assessment of water bodies by means of remotely sensed data. The functional dependency of ρ on various influencing parameters may lead to over- or underestimation of $L_w(\lambda)$. The perturbations in the above water spectral measurements are complex and presently there is no reliable method for its removal. However, in the subsurface reflectance measurement, there is no contribution of the surface reflection effects and one can easily overcome influence parameters naturally found in the field.

3.9 Effect of View Geometry on Multispectral Reflectance: ASTER Data

3.9.1 Introduction

The Advanced Spaceborne Thermal Emission and Reflection Radiometer (ASTER) sensor resides on the Terra platform, which was launched in December 1999.

The ASTER was developed through a cooperative project between Japan‘s Ministry of Economy Trade and Industry (METI) and NASA’S Earth Observing System (EOS) project. The orbit system of Terra is sun-synchronous with equatorial crossing at 10:30 am local time, and revisit time is every 16 days. All ASTER products are provided in Hierarchical Data Format (HDF-EOS). The first three spectral bands correspond to the Blue, Green, and Red portions of the electromagnetic (EM) spectrum. Bands 4, 5 and 7 correspond to different portions of the Near Infrared region of the EM spectrum. Band 6 corresponds to the Thermal Infrared portion of the EM spectrum.

3.9.2 ASTER sensor and products

The ASTER consists of three sensors (Table 2.1): the Visible and Near-infrared (VNIR) which has three bands with 15m spatial resolution including backward telescope for stereo, the Shortwave Infrared (SWIR) which has six bands with 30m spatial resolution, and the Thermal Infrared (TIR) which has five bands with 90m spatial resolution, each system was developed by a different Japanese company.

Table 3.1 : Major characteristics of ASTER sensor

Radiometer	Band	Wavelength (μm)	Spatial resolution
VNIR	1	0.52 - 0.60	15 meter
	2	0.63 - 0.69	
	3N	0.78 - 0.86	
	3B	0.78 - 0.86	
SWIR	4	1.600 - 1.700	30 meter
	5	2.145 - 2.185	
	6	2.185 - 2.225	
	7	2.235 - 2.285	
	8	2.295 - 2.365	
	9	2.360 - 2.430	
TIR	10	8.125 - 8.475	90 meter
	11	8.475 - 8.825	
	12	8.925 - 9.275	
	13	10.25 - 10.95	
	14	10.95 - 11.65	
Temporal Resolution:	Overpass Return Cycle: 16 days		
Area:	~60 km x 60 km		
Image Dimensions:	VNIR: 4200 rows x 4980 columns VNIR (3B): 4600 rows x 4980 columns SWIR: 2100 rows x 2490 columns TIR: 700 rows x 830 columns		

The Level 2 surface reflectance data set contains surface reflectance for each of the nine VNIR and SWIR bands at 15-m and 30-m resolutions, respectively. The results are obtained by applying an atmospheric correction to radiances reported by the ASTER sensor. The atmospheric correction algorithm used to retrieve the surface reflectance relies on a look-up table (LUT) approach. The atmospheric conditions are defined by the aerosol size distribution (or equivalently the aerosol type), the aerosol amount, surface pressure, and the sun-satellite geometry. The atmospheric correction removes effects due to changes in satellite-sun geometry and atmospheric conditions. The atmospheric correction algorithm is applied to clear-sky pixels only and the results are reported as a number between 0 and 1 (Aster User Guide, 2001).

3.9.3 ASTER data used

In this research work, ASTER-VNIR scenes of Indus River, Pakistan acquired on 2007/08/05, 2007/06/02, 2007/04/15, 2006/11/06, 2006/09/26, and 2005/06/11 was used. The coordinate system of the ASTER scenes is UTM 43N, and their datum is WGS84.

3.9.4 Comparison between 3N-NIR and 3B-NIR reflectance

The unique features of the visible and near-infrared (VNIR) subsystem of the Advanced Spaceborne Thermal Emission and Reflection Radiometer (ASTER) is the forth band (3B). The 3B band has near-infrared back-looking optical system of 27.6 degree from nadir and a detector, which enables stereoscopic images and obtained backward looking image 55 sec later than the corresponding nadir view. Data from the VNIR stereo system is effective to highlights the influence of observational geometry and surface roughness. However, in case of sun glitter, both the images show different behavior. In order to compare 3N-NIR and 3B-NIR images on water surface of Indus River, Pakistan the images acquired on different months of the years were examined.

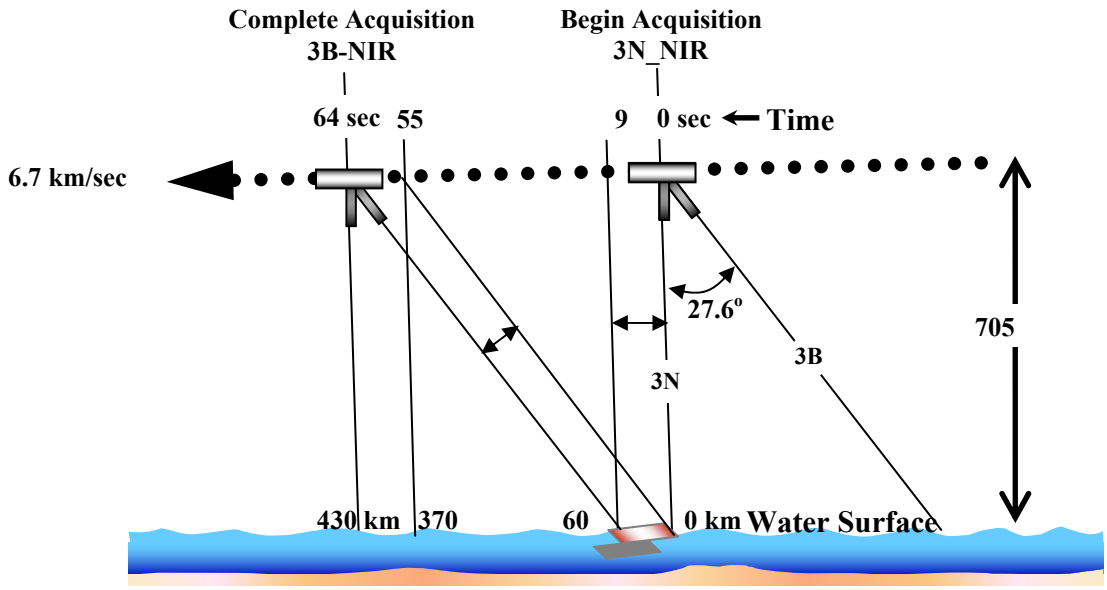

Figure 3.16 Acquisition cycle of VNIR-ASTER sensor

The prime objective is to quantify the difference between two types of remotely sensed data acquired with the time difference of 55 second. To elucidate the effect of viewing geometry on remote sensing signals, under different environmental conditions, graphs were plotted as shown in figure 3.17.

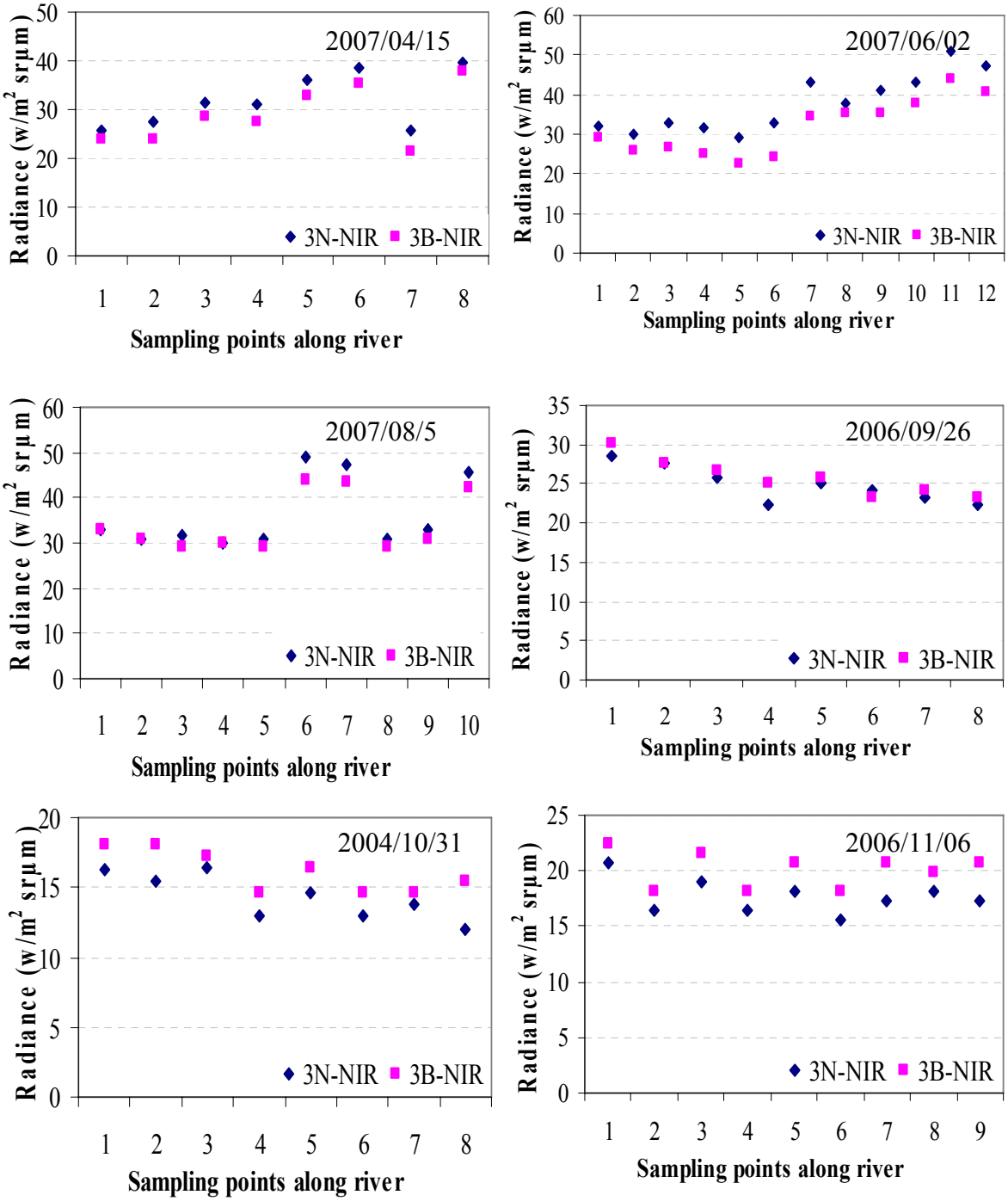

Figure 3.17 Comparison between 3N-NIR and 3B-NIR radiance at the sensor along different sampling points along the river reach

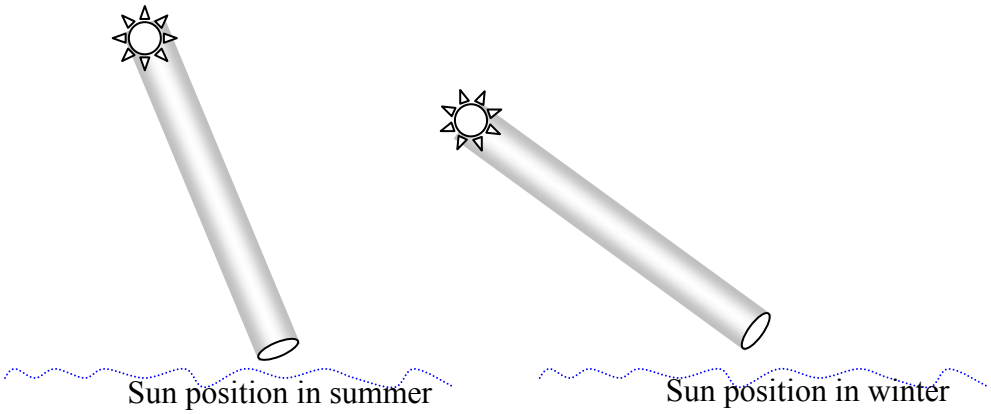

Figure 3.18 Sun position in summer and winter

The stereo feature of VNIR-ASTER allows coverage of selected research area for short period to monitor the change in signal owing to viewing geometry. It is also useful to monitor dynamic events such as to examine the effect of waves on spectral signals with different view geometry. As clear from the graph that there is slight difference between the radiance value acquired by two sensors. However, it is obvious that it depends on the month and indirectly with sun elevation. In summer the 3N-NIR value is more as compared to 3B-NIR sensor values but in winter the opposite behavior was observed. The atmospheric changes with seasonal differences, both sun position and river flow vary significantly during the annual cycle. The effect of sun position on radiance values of remotely sensed imagery is not significant; however, it affects the signals. Acquisition date is import in case of remote sensing and should be selected carefully to ensure maximum information content in remotely sensed data.

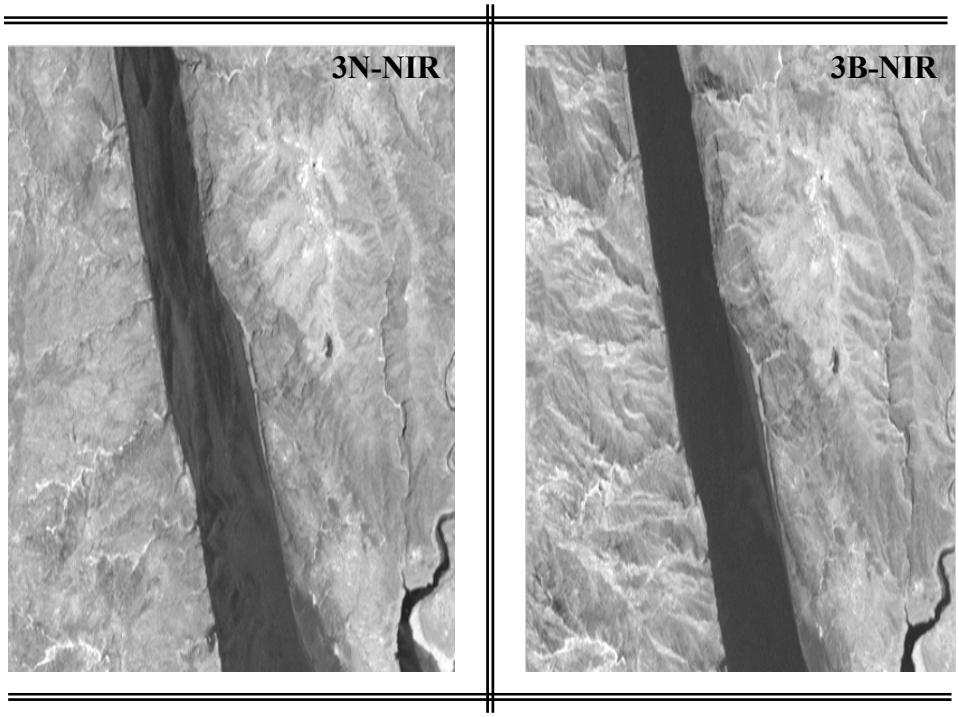

Figure 3.19 Comparison between 3N-NIR and 3B-NIR radiance image (2007/06/02)

It is noticed that the effect of water surface roughness is minimized by using 3B-NIR image as depicted in figure 3.19. In 3N-NIR image the water surface appears to be

rough showing water waves on the surface. In case of 3B-NIR the water surface seems to be smooth with no waves on the surface. In figure 3.18 it is clear that that difference between the radiance acquired by two sensors is almost constant along the river reach. To overcome the surface roughness 3B-NIR images is considered better. It can be conclude that the combination of band (3B-NIR and 3N-NIR) is useful to quantify the reflectance difference because of surface roughness. The selection of 3B-NIR image can be the solution to overcome the effects of surface roughness for studying water bodies.

3.10 Concluding Remarks

The work highlighted quantitatively and quantitatively the effect of different influencing parameters on remotely sensed data and demonstrates the feasibility of remote sensing for monitoring of water bodies. The experimental methodology and measurement protocols depend on field apparatus and research objectives. Each environmental factor has its own effect on the remote sensing signals. It is not possible to avoid errors in the results; however, by adopting proper methodology and measurement protocols it is possible to minimize the effects. The downwelling irradiance deceases with the increase in depth showing symmetric trend. The spectra changed quantitatively; however, the qualitative nature of the spectra remained similar. The remote sensing theory lies on that fact that most of the incoming energy is absorbed, transmitted or reflected in other directions. Only less than 10% (in case of subsurface irradiance) of the incoming energy is the actual signals carrying information about the water body. It is worth mentioning that even this little amount of reflected energy is enough to delineate the water bodies.

The selection of ASTER 3B-NIR image can be the solution to overcome the effects of surface roughness for studying water bodies. Under windy conditions and waves on the water surface, the spectrum average and ratio of bands may decrease the effect of waves on the observed spectral signals. The comparability between above surface and subsurface reflectance measurement demonstrates that in case of the above surface reflectance measurements there is significant contribution by the surface reflection effects and one should expect an error in estimating the optical characteristics of water bodies. A pronounced quantitative difference between the two measurements was observed. Above surface measurement, if not corrected for the erroneous effects may lead to errors in the findings. The above-water measurements are problematic because of inefficient methods for the removal of surface reflection effects from the total upwelling radiance signals. The retrieval of water leaving signals by assuming an approximate constant value ρ for all the sampling points leads to unsatisfactory result and doesn't seem to provide a solution to the problem. The subsurface deployment of sensor allows to avoid the surface reflection effects. It is strongly recommended that the subsurface spectral reflectance measurement is better option for the researcher who attempt to analyze water by using remotely sensed data. It is believed that the comparison results of this research study will be useful to quantify the perturbations between above and subsurface water reflectances.

CHAPTER 4

SUSPENDED MATTER MONITORING: APPLICATION OF HYPERSPECTRAL REMOTELY SENSED DATA

4.1 Introduction

Water quality is a general descriptor of water properties in terms of physical, chemical, and biological characteristics. Synoptic information on water quality parameters is difficult to obtain from a routine in situ monitoring network. The conventional measurement of water quality requires in situ sampling, expensive and time-consuming laboratory work. Moreover, the conventional sampling campaigns are point sampling techniques and do not provide either the spatial or temporal view of water quality needed for accurate assessment and management of water bodies. Therefore, the difficulty of overall and successive water quality sampling becomes a barrier in water quality monitoring, forecasting and management. Remote sensing could overcome these constraints by providing an alternative means of water quality monitoring over a greater range of temporal and spatial scales (Shafique et al., 2001).

Water quality assessment of coastal and inland waters using satellite data has been carried out since the first remote sensing satellite Landsat-MSS became operational (Thiemann and Kaufmann, 2000). Today, there are many satellites which have high enough resolution for use in water quality monitoring studies. Effectiveness of remotely sensed data in water quality assessment of different lakes and reservoirs has been attempted by various researchers (e.g. Lathrop and Lillesand, 1986; Ritchie et al., 1987; Harrington et al., 1992; Lavery et al., 1993; Reddy, 1993; Fraser, 1998; Nellis et al., 1998; Thiemann and Kaufmann, 2000).

From the remote sensing perspective, waters can generally be divided into two classes: case I and case II waters (Morel and Prieur 1977). Case I waters are those dominated by phytoplankton (e.g. open oceans) whereas case II waters are waters containing not only phytoplankton, but also suspended sediments, dissolved organic matter, and anthropogenic substances and their concentrations are not correlated with chlorophyll-a concentration, e.g. some coastal and inland waters (Nichol, 1993; Gin et al., 2003). Major factors affecting water quality in water bodies are suspended sediments, algae (i.e., chlorophylls), chemicals (i.e., nutrients, pesticides, metals), and colored dissolved organic matter (CDOM). Increases in water quality parameters such as chlorophyll-a, turbidity, total suspended solids (TSS), and nutrients are symptomatic of eutrophic conditions.

The remotely sensed techniques for accurate monitoring of water quality parameters depend on the substance being measured, its concentration, influencing environmental factors and the sensor characteristics. Numerous researchers (e.g., Dekker, 1993; Gitelson et al., 1993; Jupp et al.' 1994a; Jupp et al., 1994b) have developed empirical regression formulas for the prediction of lake water quality parameters from spectrometer data by employing spectral ratios, typically reflectance ratios, as the independent variables.

4.2 Purpose of the Study

The prime purpose of present research is to determine relationships between water quality parameters (WQP) and hyperspectral remotely sensed data. In this chapter attention has been paid for development of water quality models. In order to achieve this goal, hyperspectral measurement was made at 4 different rivers under different environmental conditions. The criterion that has been considered is the simplicity of the water quality model, accuracy, to overcome influencing factors, and the potential application of the developed model at different time and place.

4.3 Case Study of Monobe River, Japan

4.3.1 Introduction

The Monobe River, Kochi, Japan has its source at Mt. Akagioyama (1,436 m) in Tsurugi mountain range. The river is 68.12 km long and the basin area is 508.2 km^2 , in which, mountain forest is 461.8 km^2, flat land is 38.2 km^2 and water course is 8.2 km^2. The Monobe River has three dams and two head works, namely Nagase Dam, Yoshino Dam, Suita Dam, Godo Weir and Togo Weir from upstream to downstream (Nagashima S., 2003). The water of the river is clear, however, during the rainy seasons the water become muddy for two to three day due to heavy rain and soil erosion in the upstream catchment. The experiment was performed on the Monobe River at different times of the year. The objective of the study is to develop the relationship between spectral reflectance and suspended sediment concentration. Most of the time the field experiments were performed on Monobe River (33.636 N to 33.643 N, 133.719 E to 133.746 E) followed by the heavy rains and spectral data were acquired at four different sites along the river.

4.3.2 Material & method

Field SpecPro FR Spectroradiometer (Analytical Devices, Inc., Boulder, CO) was used to collect the above surface upwelling radiance from the water surface. This portable spectrometer combines three spectrometers to cover the wavelength range from 350 to 2500 nm, however, for the purpose of this study the spectral range of 400 to 900 nm was used. The spectrum range of 400 to 900 nm is considered to be useful for studying water bodies by means of remote sensing. The average of 25 spectrums is used in the collection of water samples. The measurements protocol as discussed in chapter 2 has been carefully adopted to improve the data accuracy.

The turbidity and chlorophyll-a concentration was collected by using YSI-6600 multi-parameter water quality logger. The YSI multi-parameter sonde allows filed measurement of 8 different parameters simultaneously with long battery life. The YSI-6600 with user friendly data management and analysis software EcoWatch is useful instrument for in-situ water quality monitoring. It is also equipped with a temperature and conductivity sensor. The concentration of suspended sediments (mg/l) was prime parameter in our case and the concentration was validated by using PARTECH turbidity meter in mg/l in order to verify the homogeneity of suspended sediments. The measurements collected by both the equipments were found to be almost same.

4.3.3 Result & discussion

The reflectance spectra of river water acquired at different times of the year is depicted in figure 4.1. As shown in the figure there is a variation in the spectral shape and magnitude. The rational is because the spectral data were acquired in different field campaigns with varying amount of suspended sediments concentration and environmental conditions. For brevity, the spectral data with high suspended sediment concentration is demonstrated for the purpose of SSC model development.

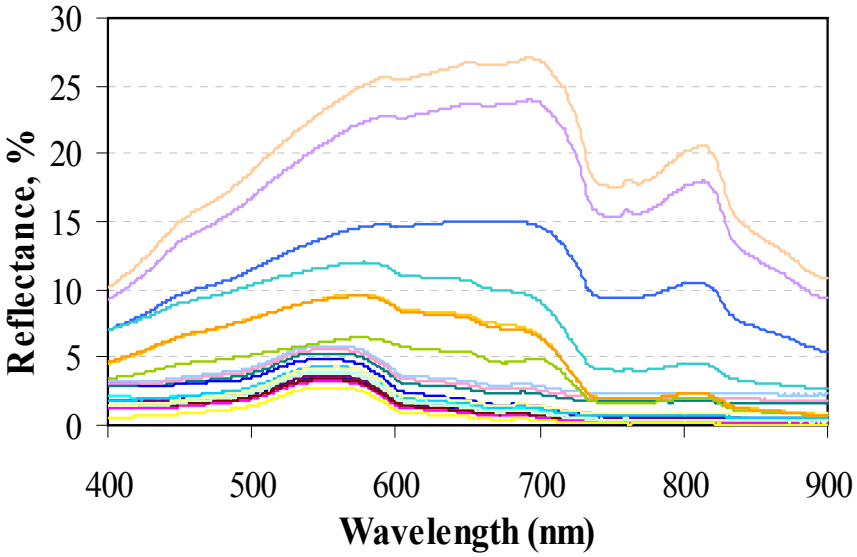

Figure 4.1 Spectral reflectance of Monobe River water

The study of suspended sediments in river waters by means of remote sensing is complex and involves many factors that must be carefully taken into account. The intensity and spectral shape varies with sediments type, texture, grain size and concentration of suspended sediments in surface water. It is evident from the figure 4.1 that the spectral shape shows increasing trend with the increase in suspended sediment concentration. Figure 4.2 illustrate a good example of relationship between suspended sediment concentration and spectral reflectance. The graphs showed that the water colour and amount of suspended sediments present in water body affects the spectral signals significantly. Other water quality parameters like chlorophyll also have also influence on spectral magnitude and shape. It is observed that the spectral shape of Monobe River is almost same although the signals were acquired at different times of the year. Most of the time the field campaign is carried out followed by heavy rain. So, the major constituent in the river water is suspended sediments. The fine sediments brought by the feeding streams affect the spectral magnitude; however, it is observed that the type of sediments is almost same in all cases. In some case a peak reflectance near 700 nm was observed in the spectra. The red peak in the spectral signature predicts the presence of chlorophyll in the water body. In case II water, the separation of suspended sediments signals from chlorophyll is difficult task and demands for careful investigation of the acquired spectra. The spectral behavior was examined and band ratio models were developed for estimation of suspended sediments in the river water.

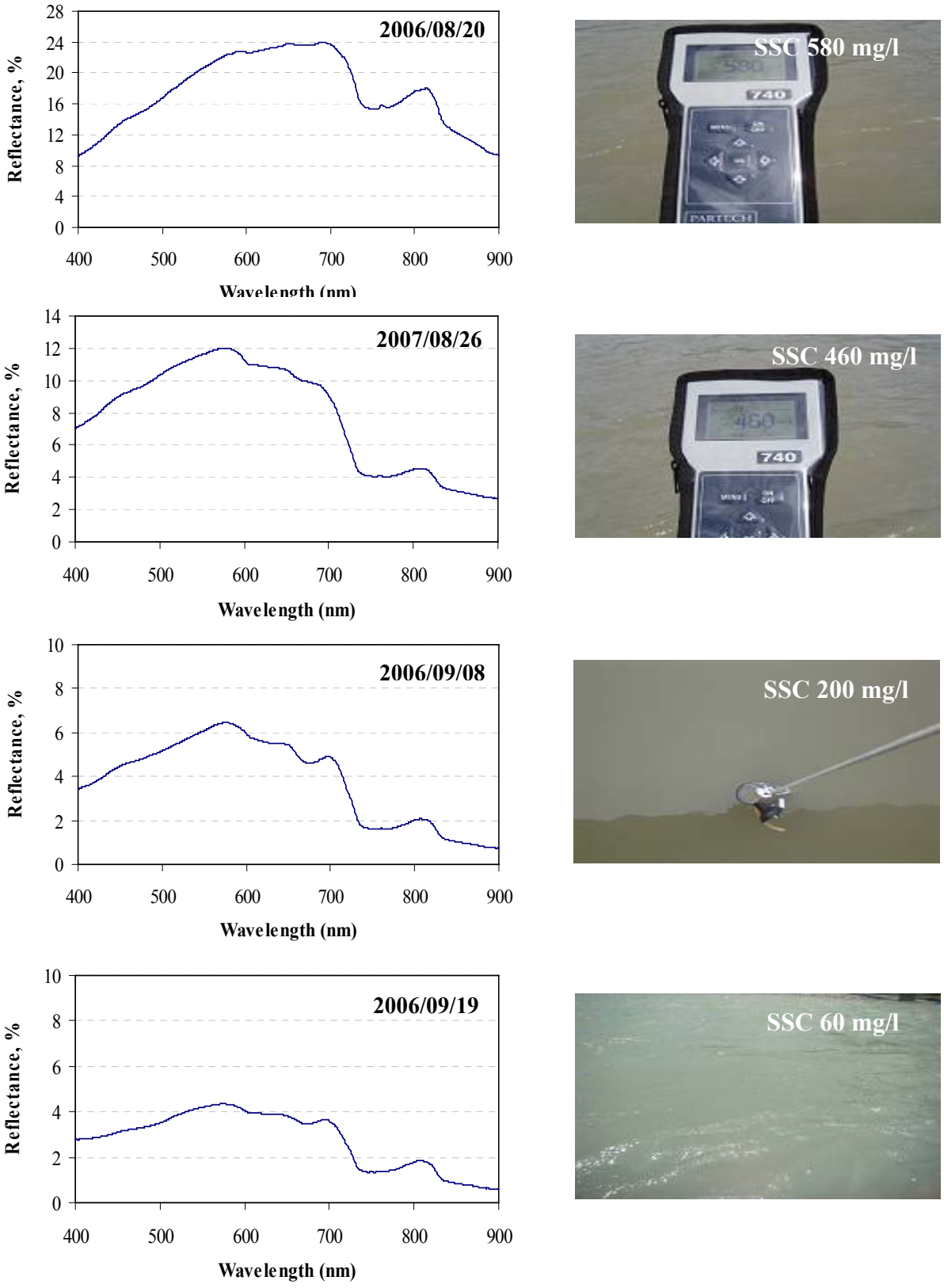

Figure 4.2 Spectral shape in relation with SSC acquired at Monobe River

4.3.3.1 Suspended sediment algorithm

Band ratio model was developed to define the relationship between SSC (mg/l) and spectral reflectance. In chapter 2, based on experiments, it was explained thoroughly that the ratio of NIR and red is best predictor of SSC in water. Han (1997) conducted research on characterizing the relationship between suspended sediment concentration (SSC) and reflectance in clear and algal laden waters. The author pointed out that the linearity in the SSC–reflectance relationship increased with wavelengths between 400nm and 900 nm. Han and Rundquist (1997) compared the near-infrared (NIR) and red ratio and the first derivative of reflectance in modeling chlorophyll concentration in a turbid Midwestern reservoir. They observed that the first derivative was correlated better with the chlorophyll than the NIR/red ratio. However, in our case the simple ratio between NIR and red domain was used. The reason for selection of wavelength 815, 615 and 560 nm is that the selected wavelengths correspond to central range of Band 4, Band 3 and Band 2 of ALOS-/AVNIR sensor.

As illustrated in figure 4.3 that the ratio of NIR and red domain (815/650) are not well correlated with SSC. In case of lab experiments the NIR/Red ratio was strongly correlated. In field conditions the situation vary significantly. The ratio of NIR/Green domain has better correlation with SSC. The wavelength have unique feature for each component in water body. The red domain near 700 nm represents the presence of Chlorophyll. The green domain is considered to be the representative of total suspended sediments (TSS) in water bodies. Based on research work and detailed investigation of laboratory and fields experiments, the 2 band ratio algorithm is suggested. The 2 band and 3 band approach not only minimize the effect of influencing parameters, but also improve the accuracy of developed model for SSC estimation.

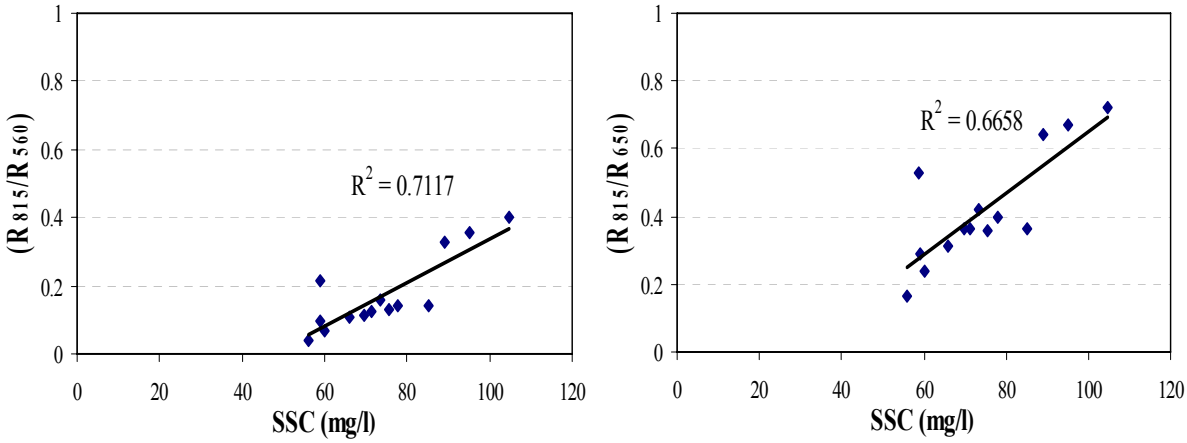

Figure 4.3 Relationship between reflectance ratio and SSC

The two band algorithm $(R_{815}+R_{650})/(R_{650}/R_{815})$ is strongly recommended for the prediction of SSC in water bodies. The suspended sediments in water bodies are different in type, texture, size and characteristics. The red and NIR region represents the suspended sediment concentration of different size of sediments. The Red wavelength penetrates deeply in water body and represents concentration of different suspended sediments ranging from very fine to medium size. However, the NIR domain represents the

sediments near water surface representing very fine texture. The addition of red and NIR wavelengths show the spectrum features of low and high concentrations of the suspended sediments and provides solution for the estimation of different sizes of sediments within the water body. However, the red domain is also influenced by the presence of chlorophyll. The addition of two wavelengths may lead to add the influence of chlorophyll and the resultant reflectance not only represent the suspended sediments but also represent the concentration of chlorophyll. To cope with this situation the resultant wavelength ($R_{815}+R_{650}$) is divided by the red wavelength. This approach helps to minimize the influence of the chlorophyll on SSC. The developed model $(R_{815}+R_{650})/R_{650}$ predicts the amount of SSC and the influence of chlorophyll is also minimized. More precisely, by adopting this approach the influence of chlorophyll is minimized, however, the spectral signals disturb. The actual representative of suspended sediment in water bodies is NIR domain. The reason is that NIR absorbs in the water. If there is any reflectance in this range, it means that the suspended sediments present in the water body and caused scattering. To deal with this situation and to develop model more accurately, the best approach is to multiply developed model with the NIR wavelength. The developed model for estimation of suspended sediments in water body is of following form:

$$(R_{815}+R_{650})/(R_{650}/R_{815})$$

$$\frac{(R_{815}+R_{650})}{R_{615}}\times R_{815}$$

$$\left[\frac{R_{815}}{R_{650}}+1\right]\times R_{815}$$

$$SSC(mg/l)=14.2\times[(R_{815}+R_{615})/(R_{615}/R_{815})]+73$$

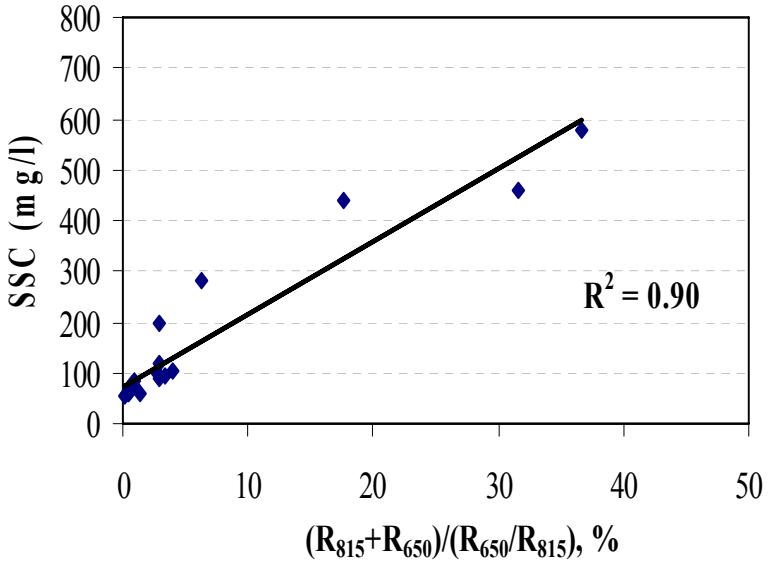

Figure 4.4 Relationship between developed model & SSC (mg/l)

The application of suspended sediments by means of remote sensing provides information about the sediments near the water surface. In order to examine the distribution of sediments along depth, the water profile of Monobe River was collected during heavy rain and under normal conditions at different times of the year. It was observed that during flash floods the vertical distribution of suspended sediments in the first 10 meter depth from the surface was almost same. However, under normal conditions when the velocity of water is slow, the vertical distribution of sediments varies slightly and in some case varied significantly along the depth. The graphical representation is shown in figure 4.5. The sediment distribution along depth depends on many factors including sediment type, concentration, water flow and wind speed. However, by assuming vertical homogenous distribution of sediments, there will not considerable affect on estimation of suspended sediments concentration in case of river waters.

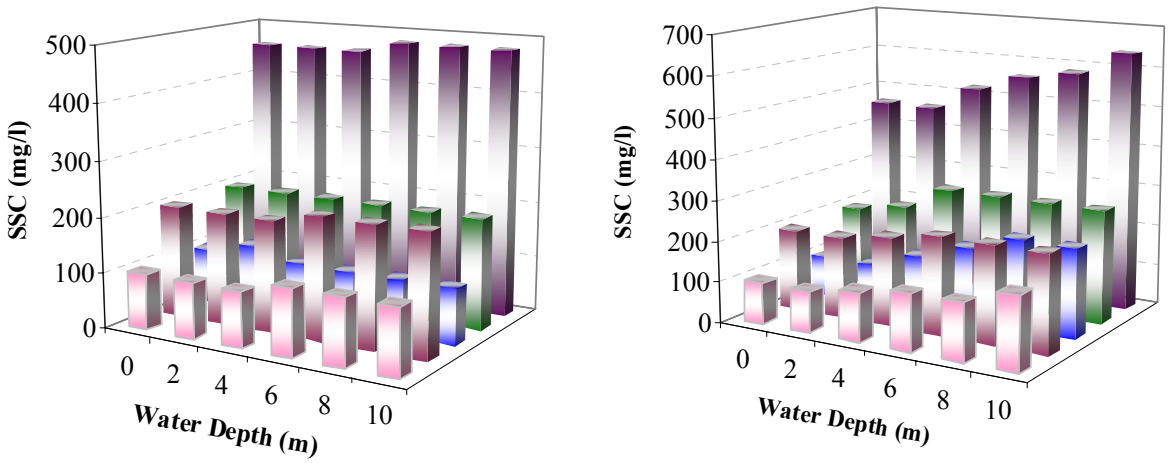

Figure 4.5 Vertical distribution of sediments along water depth

4.3.3.2 Chlorophyll-a assessment

A great number of attempts have been made by numerous researchers to monitor chlorophyll concentrations spatially and temporally using remotely sensed reflectance in water bodies. Most of remote sensing studies of chlorophyll in water are based on empirical relationships between radiance/reflectance in narrow bands or band ratios and chlorophyll. However, the feasibility of regression algorithms usually depends on the influencing environmental factors. Fraser (1998) correlated first derivative of reflectance with the chlorophyll-a among 22 fresh to alkaline lakes in Nebraska and found that the first derivatives at 429 nm and 695nm were correlated significantly with chlorophyll-a. The first derivative at 690 nm is useful in estimating chlorophyll concentration in the presence of other water constituents (Han and Rundquist 1997). The first-order derivative is able to remove pure water effects while the second derivative can remove suspended sediment effects (Goodin et al. 1993). However, it was found that the reflectance peak in red domain is well correlated with chlorophyll concentration. This simple approach estimates the concentration accurately and at different time and place. Figure 4.6 illustrate the relationship between reflectance peak at 685nm and chlorophyll-a concentration showing satisfactory results.

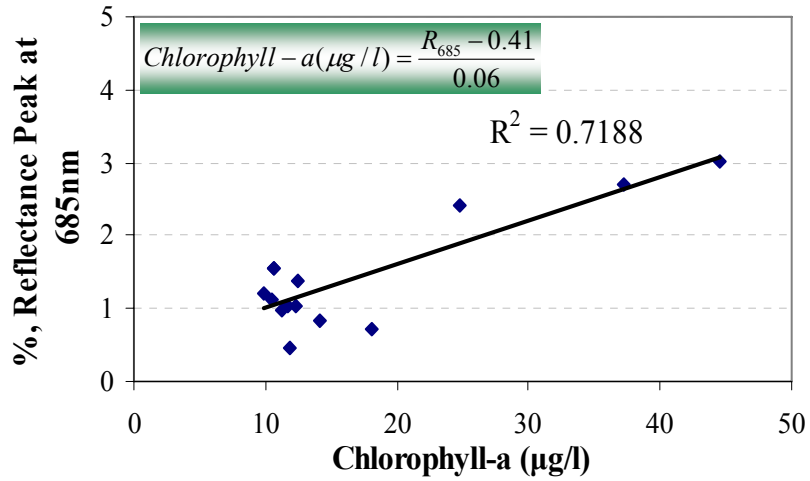

Figure 4.6 Relation between reflectance peak and chlorophyll-a concentration

4.4 Case Study of Altamaha River and St. Marys Rive, USA

4.4.1 Introduction

The Altamaha River in Georgia, USA drains one of the largest basins on the east coast. The watershed area of the river including its tributaries is 36,260 sq km. There is no dam on the river. The St. Marys River is in the southeastern United States. The river is approximately 144 km long. It rises in the southeastern Okefenokee Swamp, and flows into the Atlantic Ocean near St. Marys, Georgia and Fernandina Beach, Florida. The objective of this part of the thesis is to assess the potential of remotely sensed data for estimation of water quality parameters in Case 1 & Case 2 waters. The research work demonstrates an example for effective and efficient application of remotely sensed data for monitoring total suspended sediments (TSS), chlorophyll-a, colored dissolved organic matter (CDOM), secchi depth, and turbidity in water bodies. Regression models were developed for collected above-water surface and subsurface datasets and the homogeneity of developed models were tested. The developed algorithms were successfully applied for estimation of water quality parameters in river waters.

4.4.2 Material & method

The assessment of water quality parameters is based on the field measurements, laboratory examination and data analysis of the collected spectral reflectance data. The data were acquired during massive field campaigns at Altamaha River (31.307 N to 31.335 N, 81.244 W to 81.475W), Georgia, USA on 11th March, 2007 and St. Marys River (30.710 N to 30.761 N, 81.398 W to 81.779 W), Georgia, USA on 12th March, 2007. Spectral reflectance measurements were made from a boat using, a dual-fiber system, two inter-calibrated Ocean Optics USB2000 Spectroradiometers (2048 channels, 370–1000 nm). Data were collected in the spectral range of 400-900 nm with a sampling interval of 0.3 nm and a spectral resolution of 1.5 nm. Radiometer # 1, equipped with a 25^{o} field off view optical fiber, was pointed downward in the nadir direction to measure the total above surface upwelling radiance from the water $L_t(\lambda)$. Radiometer # 2, equipped with an optical

fiber and a cosine collector (yielding a hemispherical filed of view) was pointed upward to simultaneously measure the above surface incident irradiance $E_{inc}(\lambda)$. In order to measure the subsurface upwelling radiance $L_u(\lambda)$ the optical fiber was mounted on a 2-m fixed black pole, and the tip of the optical fiber was kept just below the water surface (~3 cm). To match their transfer functions, the inter-calibration of the radiometers was accomplished by measuring the upwelling radiance (L_{cal}) of a white Spectralon (Labshere, Inc., North Sutton, NH) reflectance standard, simultaneously with incident irradiance (E_{cal}). An average of 10 consecutive scans was used to collect the reflectance spectra at each of the sampling station. The spectral reflectance data were collected close to solar noon, and changes in solar zenith angle were minimal during the period of scanning. All spectral measurements were taken over optically deep water. Data collection procedure was kept constant in all the cases. Data collection and management were performed using a data management program, CDAP, written by Mr. B. Leavitt, CALMIT, University of Nebraska-Lincoln.

Percentage spectral reflectance R(λ) was computed as:

$$\%R(\lambda) = [L(\lambda)_t / E(\lambda)_{inc}] \times [E(\lambda)_{cal} / L(\lambda)_{cal}] \times R(\lambda)_{cal} \times 100$$

$R(\lambda)_{cal}$ is the reflectance of the Spectralon panel linearly interpolated to match the band centers of each radiometer.

The dual-fiber approach results in fast measurement and minimal error due to variation in irradiation condition. One critical issue with regard to the dual-fiber approach is that the transfer functions of both radiometers must be identical. The Ocean Optics instruments were tested under laboratory conditions; over a 4 hour period the standard deviations of the ratio of the two transfer functions did not exceed 0.004 (Rundquist, 2004). The dual-fiber system methodology allowed to collect data under variable illumination conditions (usually prohibitive for the single-instrument technique) without requiring absolute calibration of the radiometers. (Dall'Olmo, 2005).

4.4.3 In situ measurements

The in situ water quality parameter data was collected. Duplicate measures were made for Chl-a, total suspended solids (TSS), and CDOM. Average values for each replicate pair are used for analysis. There are three primary analytical approaches for laboratory analysis of Chl-a concentration in field samples: spectrophotometry, fluorometry, and high-performance liquid chromatography (APHA, 1998). In situ chlorophyll-a is currently assessed by using fluorometry. TSS was determined gravimetrically using pre-ashed and tared filters. Filters and retained particulate matter were dried (60 °C for at least 24 h) and reweighed. CDOM absorption was estimated using second filtrate fractions (first fractions discarded from the TSS procedure). Absorption of filtrate at 440 nm was measured with a 10 cm quartz cuvette and Geneysis 5 spectrophotometer. Absorption estimates were converted to m^{-1} as in Bricaud 1981. The measured parameters are tabulated as below in table 1. Turbidity and salinity was measured by using turbidity and salinity meters.

Table 4.1: Measured water quality parameters at Altamaha River & St. Marys River

Sampling points	Salinity (ppt)	Depth (m)	CDOM 440 (m^{-1})	Chl-a (µg/l)	TSS (mg/l)	Turbidity (NTUs)	Secchi Depth (m)
Althamaha River							
ALT1	28.6	5.9	0.2	4.8	25.8	18.2	1.1
ALT2	28.9	6.4	0.2	6.0	28.6	21.8	0.78
ALT3	21.2	6.0	0.7	5.1	17.6	15.5	0.93
ALT4	11.2	6.5	1.1	5.7	16.8	7.5	0.9
ALT5	7.6	6.1	1.4	5.7	18.4	9.78	0.77
ALT6	3.6	5.8	1.7	4.1	10.9	15.8	0.76
ALT7	1.6	7.6	2.7	5.3	11.3	18	0.58
ALT8	0.5	7.0	3.8	3.8	10.8	20	0.55
ALT9	0.1	6.7	4	2.9	8.2	13.7	0.57
St. Marys River							
ST1	30.9	16.1	0.3	2.4	13.6	2.4	1.87
ST2	30.3	15.8	0.5	4.5	8.7	1.2	1.81
ST3	25.8	9.7	1.3	4.3	10.4	2.3	1.57
ST4	20.5	5.4	2.1	3.9	8.6	2	1.43
ST5	15.7	7.3	2.5	5.4	7.5	2.4	1.31
ST6	9.8	6.4	4.1	4.2	6.1	2.4	1.08
ST10	4.7	8.8	5.5	3.5	6.4	3.7	0.82
ST7	1.6	9.8	6.3	4.3	2.4	4	0.92
ST8	0.5	7.9	8	2.2	1.5	3.8	0.87
ST9	0.1	9.8	8.2	3.8	0.65	1.9	0.81

4.4.4 Result & discussion

Numerous researchers have applied remote sensing as a tool to measure water quality parameters and developed some algorithms in this endeavour. The band ratioing technique has proven to be advantageous because it tends to allow compensation for variations from atmospheric influences. The decision involving which bands to use is not always straightforward (Jensen 2005). The four bands which are mostly correlated with water quality parameters are the blue, green, red and NIR domains. However, the procedures develop for data analysis depends on resolution of remotely sensed data, ancillary field data, time constraints and over all objective of the study. To investigate the water quality parameters in both rivers, the subsurface spectral signature were acquired as shown in figure 4.7.

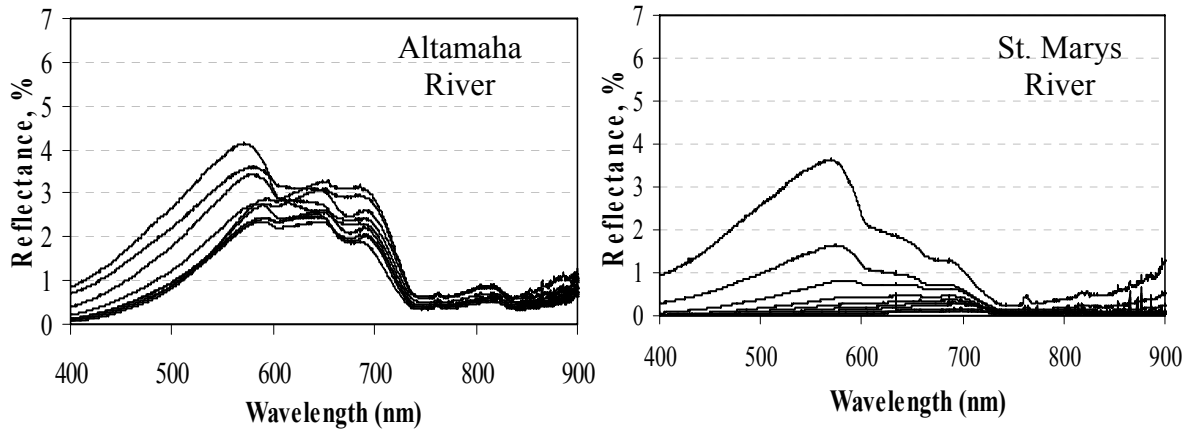

Figure 4.7 Subsurface spectral signature of river water

It is observed that the spectral signals were high at Altamaha River as compared to St. Marys River. The rational is that TSS, Chl-a and turbidity is significantly high at the Altamaha River. In both rivers, the reflectance was highly variable in the visible domain. The spectra are quite similar in shape with diverged magnitude for different sampling points. The reflectance peak in green domain was 4.2% and 3.6% for Altamaha River and St. Marys River respectively and less than 1% in red domain for both rivers. The averages of acquired spectral reflectance at both the river are depicted in figure 4.8.

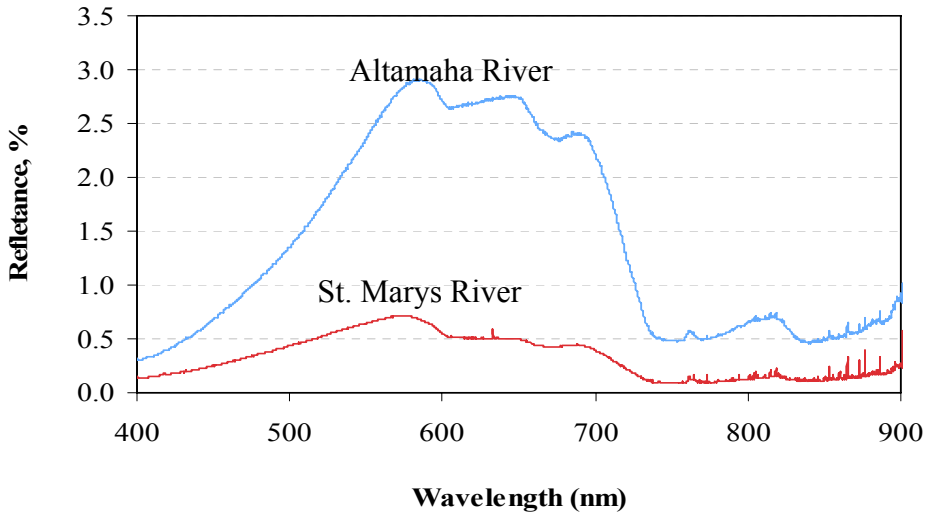

Figure 4.8 Average spectral reflectance of Rivers

As clear from the graph that the difference of averaged spectral reflectance of Altamaha River and St. Marys River is noticeably high in blue and green domain and tends to decrease in the red and NIR domain. The challenge in application of remote sensing in such condition is to develop model that is applicable on both the rivers. The model was developed for subsurface spectral reflectance and validated for above-water spectral reflectance. The developed model showed good correlation and can be successfully applied on Case-2 waters. Both the rivers fall under the category of Case-2

waters. Chl-a concentration and TSS were not related (Figure 4.9) with the determination coefficient of linear relationship $r^2 < 0.08$ & 0.07. It depicts that Chl-a was not the only characteristic controlling water quality, confirming that the waters belonged to typical Case-2 water group.

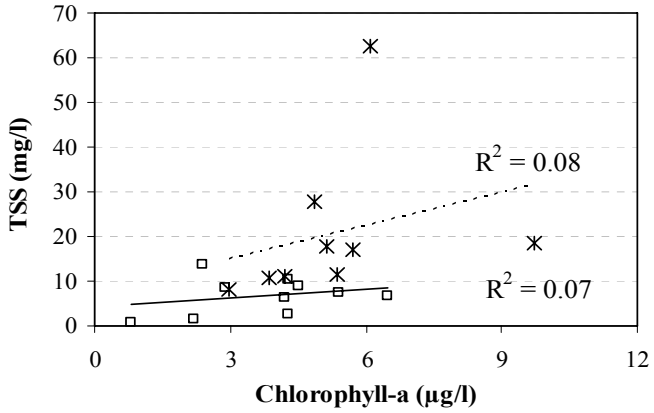

Figure 4.9 TSS plotted versus Chl-a for both rivers

The ability to monitor water quality parameters in Case 2 waters requires high resolution remotely sensed data, elucidation of quantitative and qualitative change in reflectance spectra and the diverse nature of optical constituents present in the water body. Case 1 algorithms rely on an assumed covariance of constituents, whereas the techniques for relating Case 2 constituents to reflectance signals often require multivariate, non-linear models (IOCCG, 2000). The St. Marys River, at the eastern border of Florida and Georgia, has high level of CDOM as compared to Altamaha River. In spectrum a subdued reflectance peak was observe in red domain near 700 nm. The scattering response was observed in blue and green regions. The scattering return was largely due to ultra fine clay-detritus aggregates (~ 16 µm diameter) that occur in these coastal plain rivers (Carlough, 1994).

Regression models were developed for estimation of water quality parameters for both the rivers. The advantage of the developed regression model is that the same model ca be applied on both the rivers. The models were developed for subsurface water reflectance and validated fro above surface water reflectance. The relationship between CDOM and salinity was also developed. Turbidity and secchi depth is optical property of water and is strongly related with water constituents present in the water bodies. The amount of TSS present in the water body defines the water category. Chl-a is commonly measured in water quality monitoring campaigns for costal and inland water bodies (Morrow, 2000; Jordan 1991). A basic principle of using band ratios is to select two spectral bands that are representative of absorption/scattering features of chlorophyll-a (Gin et al. 2002). Band ratio technique is used for model development. The description of the developed models is explained as follow and graphical representation is shown in figure 4.10.

Total Suspended Sediments (TSS)

Total suspended sediments showed good correlation with NIR/Green band ratio. In hyperspectral remote sensing, the spectral reflectance at 850 and 550 nm is useful for

estimation of TSS. The NIR domain (750~900nm) absorbs in the water and any reflectance in this range is because of suspended sediments present in the water body. However, the reflectance peak in green domain represents the amount of TSS present in the water body. The reflectance ratio R_{850}/R_{550} shows correlation coefficient $r^2 = 0.73$ for Altamaha River and 0.74 for St. Marys river.

$$TSS(mg/l) = m(R_{850}/R_{550})^2 - n(R_{850}/R_{550}) + l$$

Value of empirical coefficients for Althamaha River :

m = 186.5, n = 250.6, l = 61

For St. Marys River:

m = 6.4, n = 17.4, l = 13

Chl-a

The chlorophyll-a is an indicator of the abundance of phytoplankton in the water. The pronounced scattering/absorption features of chlorophyll-a are: strong absorption between 400–500nm (blue) and at 680nm (red), and reflectance maximums at 550 nm (green) and 700nm (NIR) (Han, 1997). The scattering and absorption characteristics of chlorophyll-a can be studied when more than one band is used (Dekker et al. 1991). Keeping in view the absorption and scattering relationship the reflectance ratio of R_{700}/R_{670} is applied. The correlation coefficient r^2 was 0.88 for Altamaha River and 0.71 for St. Marys river.

$$Chl-a(\mu g/l) = m(R_{700}/R_{670})^2 - n(R_{700}/R_{670}) + l$$

Value of empirical coefficients for Althamaha River:

m = -819.5, n = 1592.2, l = 767.5

For St. Marys River:

m = -56.5, n = 112, l = 50.6

CDOM

Colored Dissolved Organic Matter (CDOM) is the visible portion of the organic matter present in the aquatic environment. The colour characteristic is reflected in the many names given to CDOM in literature such as Gelbstoff (Kale 1996), Gilvin (Kirk, 1980), and Aquatic Humus (Dekker 1993). The presence of chlorophyll, TSS and CDOM usually dominate the water colour. The increase in the CDOM concentration affects the reflectance values in the blue and green region of the spectrum. CDOM absorption is characterized by a strong absorption in the blue wavelength region, exponentially declining towards longer wavelengths. To achieve a satisfactory degree of CDOM concentration retrieval the relationship between absorption by CDOM at 440 nm and reflectance ratio (R_{440}/R_{575}) showed good correlation.

$$CDOM(m^{-1}) = m(R_{440}/R_{575})^2 - n(R_{440}/R_{575}) + l$$

Value of empirical coefficients for Altamaha River:

m = 98.2, n = 59.3, l =8.6

For St. Marys River:

m = 104, n = 59.5, l = 8.5

The relationship between CDOM and Salinity was developed with high degree of correlation.

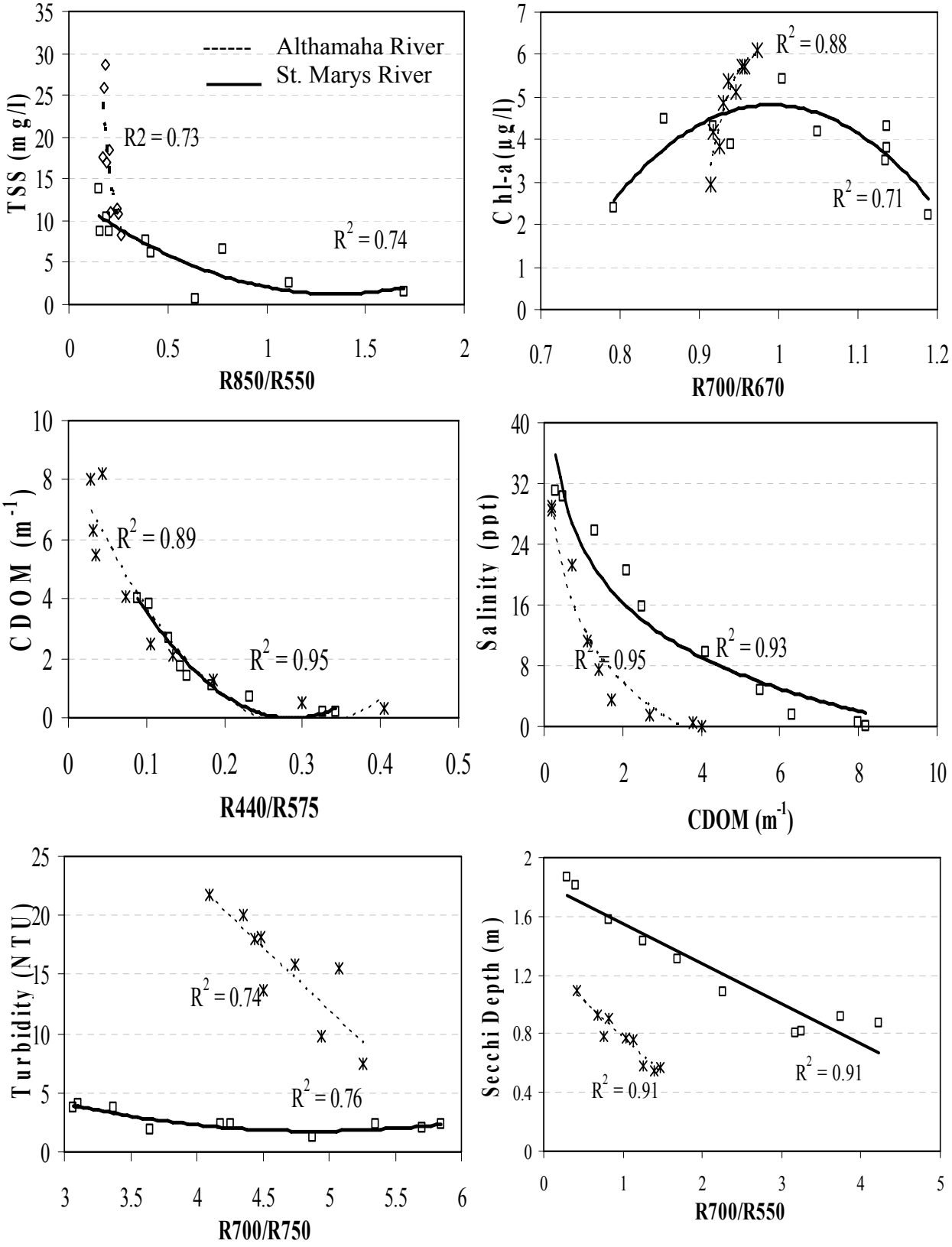

Figure 4.10 Regression models for estimation of water quality parameters

$$Salinity(ppt) = a\ln(CDOM, m^{-1}) + b$$

Value of empirical coefficients for Althamaha River:
a = -10.2, b=12.7
For St. Marys River:
a = -10.3, b=23.4

Turbidity & Secchi depth

Turbidity and secchi depth define the optical transparency of the water and correlates strong with the amount of TSS present in the water bodies. The secchi depth is the visual conventional method, however, in case of turbidity meters the intensity light scattered by the particles provides a turbidity measurement which can be used to determine water quality. The ratio of R_{700}/R_{750} provides information about the turbidity and the ratio of red and green domain R_{700}/R_{550} provides information about the secchi depth.

$$Turbidity(NTU) = m(R_{700} / R_{750})^2 - n(R_{700} / R_{750}) + l$$

Value of empirical coefficients for Althamaha River:
m = 0.65, n =16.8, l = 79.6
For St. Marys River:
m = 0.65, n = 6.3, l = 17.2
0.74, 0.76

$$SD(m) = m(R_{700} / R_{550}) + n$$

Value of empirical coefficients for Althamaha River:
m = -0.27, *n* = 1.8
For St. Marys River:
m = -0.5, *n* = 1.27

4.5 Case Study of Apalachicola Bay Florida , USA

4.5.1 Introduction

Monitoring and modeling of water quality parameters in water bodies is one of the most scientifically relevant and commonly used application of remote sensing. The complex composition and distribution of optically active constituents in water bodies hinder the successful application of remote sensing in water studies. The operational monitoring and useful application of remote sensing in water bodies demands for improved in methodology and new algorithms development. Remote sensing in case II waters has been far less successful. Many scientists have pointed out that this is due mainly to the complex interactions of four optically active substances in case II waters: phytoplankton, suspended sediments, coloured dissolved organic matter (CDOM), and water (Novo et al., 1989; Quibell, 1991; Goodin et al., 1993; Han et al., 1994; Lodhi et al., 1997; Doxaran et al., 2002; Gin et al., 2002).

Most of the satellite sensors record data in only a few broad spectral bands, the resolutions of which are too coarse to detect much of the spectral 'fine structure' associated with optically active substances in water (Goodin et al. 1993).The successful

quantification of water quality parameters using remote sensing is affected not only by the type of waters under investigation, but also by the sensor used (Liu et al. 2003).

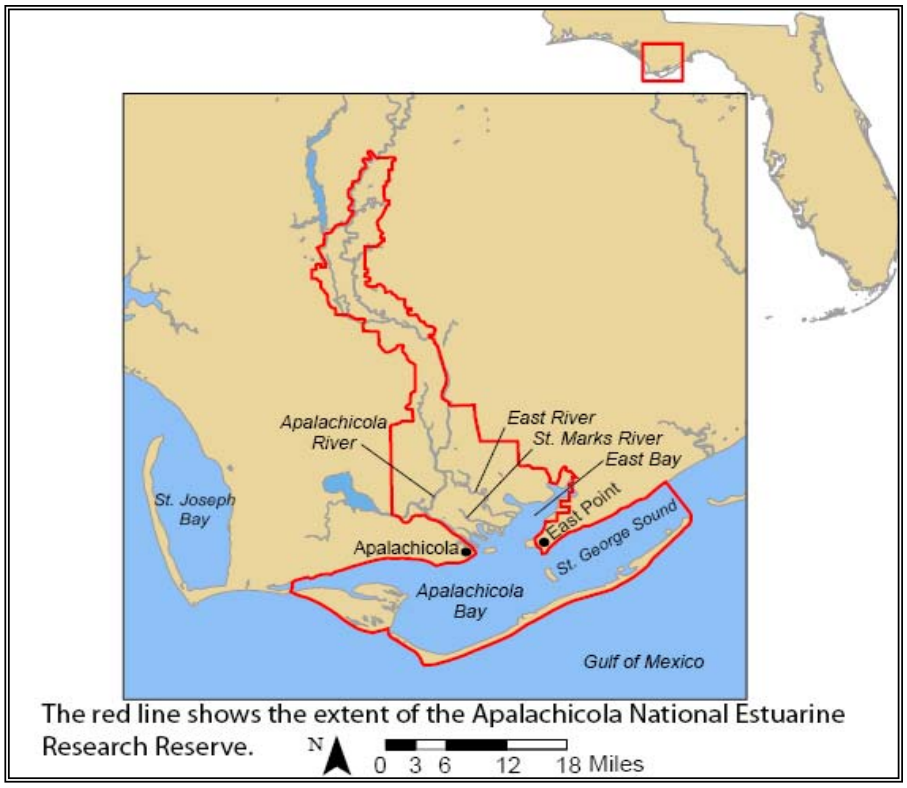

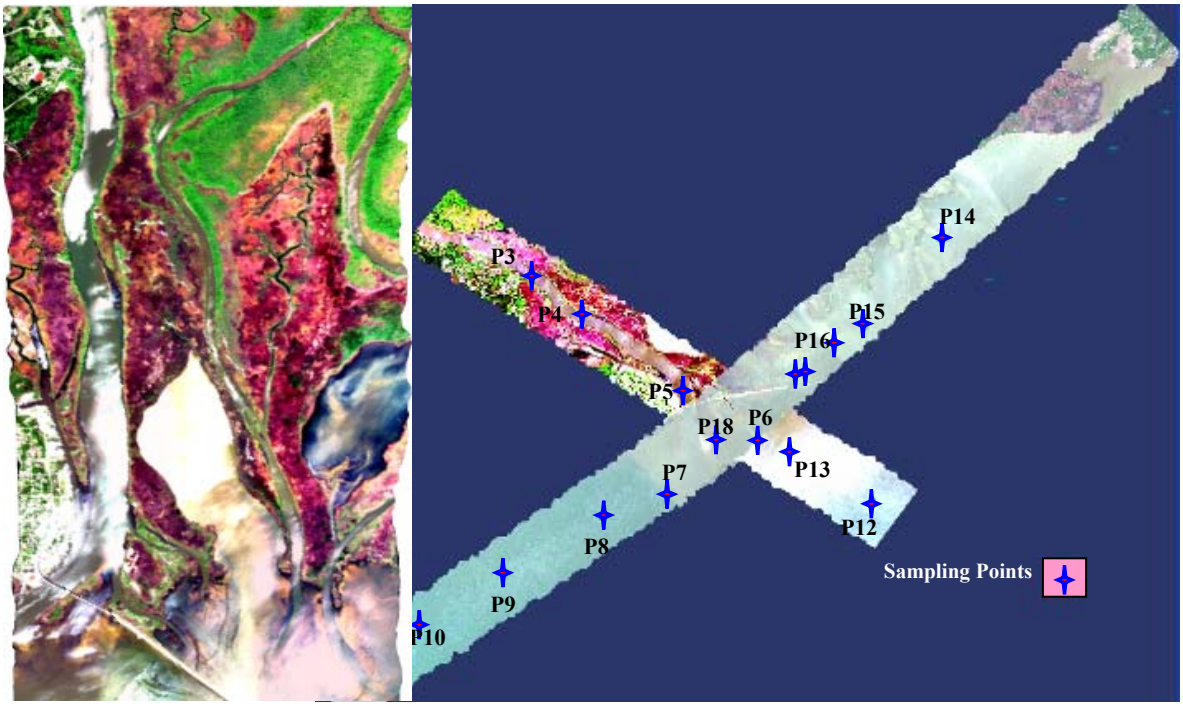

Figure 4.11 AISA image of the Apalachicola Bay, Florida

4.5.2 Material & Method

4.5.2.1 In situ measurements

Two independent in situ datasets were collected for model calibration and validation respectively. The ground truth data of Apalachicola Bay included water sampling for laboratory analysis (e.g. Chl- a and seston), on-site measurements (e.g. Secchi depth, water depth), weather observations (e.g. wind speed and sky condition) and upwelling radiance and downwelling irradiance hyperspectral data.

Table 4.2 Measured water quality parameters at Apalachicola Bay

Sampling Points	Chl- a (µg/l)	TSM (mg/l)	Secchi Depth (m)	Depth (m)
P1	21.1	27.7	0.35	1.65
P2	8.6	38.1	0.45	1.8
P3	3.4	2.5	0.55	2
P4	3.3	2.4	1.35	1.45
P5	3.2	3.1	1.3	1.38
P6	5.2	10.9	0.36	1.68
P7	3.6	4.9	-	2.32
P8	4.7	9.9	-	1.8
P9	6.4	12.5	-	2.04
P10	3.8	15.3	-	2.26
P11	17.4	18.8	0.34	1.13
P12	5.8	14.5	0.94	1.57
P13	4.8	13.6	0.72	1.78
P14	3.6	4.4	0.93	1.75
P15	4.9	5.5	0.92	1.73
P16	3.6	4.1	-	1.65

Two pairs of Ocean Optics USB 2000 hyperspectral radiometers was used (the dual headed system, i.e., upward looking and downward looking Ocean Optics sensor) for acquiring upwelling radiance (L_u) and downwelling irradiance (E_d) just above and below the water surface.

4.5.2.2 Airborne Imaging Spectroradiometer for Applications (AISA) Data

An aerial remote sensing platform for hyperspectral data collection was used. The instrument array included an AISA Eagle hyperspectral imager from Visible to Near Infrared (VNIR), a system which can provide high spatial and spectral resolution. The AISA Eagle is a solid-state, push-broom instrument that has the capability of collecting data within a spectral range of 390 to 1000 nm in up to 512 bands. The images are often acquired in 10 to 70 spectral bands depending on the aircraft speed, altitude and mission goals. The sensor has an Inertial Navigation System (INS) and (Differential Global Positioning System) DGPS in order to provide spatially accurate data. Pitch, roll, and yaw are encoded with the DGPS information to provide accurate locations of areas of interest

on the ground. The placement of the spectral bands may be configured by the user and the selected bandwidths can range anywhere from ~2nm to ~10nm. The AISA Eagle pre-processing software provides for the automatic geometric correction, rectification, mosaicking, and calculation of at-platform radiance by applying calibration coefficients referenced to well-characterized spectroradiometric targets (Mishra, 2007). The algorithm uses the DGPS and attitude information from the INS to perform geometric, georeferencing and mosaicking operations (Makisara *et al*., 1994).

AISA Eagle data used for the present study were acquired between 0330 and 0430 h (CST) on 3rd and 4th April 2006 when the solar zenith angle was close to 70°. Ground data indicated low wind (~ 3 m s^{-1}), high visibility (40 km), and clear skies. The sensor altitude was (2.073 km), and the image was acquired at nadir at a spatial resolution of 2 m and spectral resolution of 62 bands. The site selected from flight lines covered an area of approximately 1.6 km^2 in the vicinity of Apalachicola Bay (Figure 1). The image data were converted to at-platform radiance by applying the calibration coefficients provided by AISA processing software 'Caligeo' for subsequent processing. When extracting aquatic information, it is useful to eliminate all upland and terrestrial features (Jensen et al., 1991); thus all upland features, as well as boats, piers, and clouds, were masked out of the image. The "land-mask" restricts the spectral range of brightness values (BVs) to aquatic features and allows for detailed feature discrimination. Radiance values of the NIR band were used to prepare the binary mask which was subsequently applied to all the bands of AISA Eagle image.

4.5.3 Atmospheric correction

The radiance received by a sensor, $L_t(\lambda_i)$, at the top of atmosphere (TOA) in a spectral band centered at a wavelength, λ_i can be divided into the following components (Gordon *et al*., 1983):

$$L_t(\lambda_i) = L_r(\lambda_i) + L_a(\lambda_i) + T(\lambda_i)L_g(\lambda_i) + t(\lambda_i)L_w(\lambda_i)$$

where,

$L_r(\lambda_i)$ & $L_a(\lambda_i)$ = radiances generated along the optical path in the atmosphere by Rayleigh and aerosol scattering respectively;

$L_g(\lambda_i)$ = contribution arising from the specular reflection of direct sunlight from the sea surface or the sun glint component;

$L_w(\lambda_i)$ = desired water leaving radiance;

T = direct atmospheric transmittance; and

t = diffuse atmospheric transmittance of the atmosphere.

In the case of oceanic remote sensing, the total signal received at the sensor altitude is only 8% to 10% of the signal corresponding to the oceanic water reflectance (Gordon and Morel, 1983). The goal of atmospheric correction is to remove the contributions of scattering in the atmosphere and reflection from the water surface from the TOA radiances measured by a sensor in the visible region of the spectrum. AISA Eagle data were atmospherically corrected by using FLAASH (Fast Line-of-sight

Atmospheric Analysis of Spectral Hypercubes), a first-principles atmospheric correction algorithm for visible to shortwave infrared (SWIR) hyperspectral data.

FLAASH atmospheric correction uses MODTRAN code and typically consists of three steps (Matthew *et al*., 2003). The first is the retrieval of atmospheric parameters, most notably an aerosol description (the visibility or optical depth) and the column water amount. The second step in the correction is the solution of the radiative transfer equation provided below, for the given aerosol and column water vapor, and transformation to reflectance. FLAASH uses the standard equation for spectral radiance at the sensor level, L, in the solar wavelength range (neglecting thermal emission) from a flat Lambertian surface or its equivalent (Vermote *et al*., 1994).

$$L = \frac{A\,R_{rs}}{(1 - R_{rs}^{e}\,S)} + \frac{B\,R_{rs}^{e}}{(1 - R_{rs}^{e}\,S)} + L_a$$

where,
R_{rs} = pixel surface reflectance,
R_{rs}^{e} = surface reflectance averaged over the pixel and a surrounding region,
S = the spherical albedo of the atmosphere,
L_a = the radiance backscattered by the atmosphere, and
A and B = the coefficients that depend on atmospheric and geometric conditions

Each of these variables depends on the spectral range of the selected channel (the wavelength index has been omitted for simplicity). The first term in above equation corresponds to radiance that is reflected from the surface and travels directly into the sensor. The second term corresponds to radiance from the surface that scattered by the atmosphere into the sensor, resulting in a spatial blending, or adjacency, effect.

The solar zenith and azimuth angles were calculated in the algorithm from the AISA flight date, time, latitude, and longitude and were used to predict incident solar irradiance at the top of the atmosphere. A scale factor file for the input radiance image was provided to the algorithm. The input atmospheric and aerosol models were chosen to be tropical and maritime respectively with initial visibility of 40 km. Then 820 nm band was selected as the water absorption feature, and the aerosol scale height and CO_2 mixing ratio were kept as default, which is 2.0 km and 390 ppm respectively.

ENVI 4.3 is a digital image processing software, was used to process the AISA data. The image was first geometrically rectified to UTM (Universal Transverse Mercator) projection (Zone 16; Datum: WGS84). The geometrically and radiometrically corrected AISA image was used in the analysis.

4.5.4 Result & discussion

The subsurface water spectral reflectance were acquired at 16 points during the massive field at Apalachicola Bay, Florida. The field, laboratory and remotely sensed data were analyzed in a systematic manner. In order to compare the above water and subsurface spectral reflectance, at some points above water surface radiance reflectance was also collected. The collected spectrum shows that the qualitative nature of the acquired signals are same, however, the quantitative nature vary from point to point in the water body.

The acquired spectra of the Apalachicola bay, represents first reflectance peak in the green domain near 550 nm and the second reflectance peak in the red domain showing turbid water with low CDOM. The peaks near 700 nm clearly proof the presence of chlorophyll in the bay. The water of bay is considered as Case-2 water with turbid water and low level of CDOM. The spectral feature of subsurface and above surface spectral radiance reflectance is shown in figure 4.12.

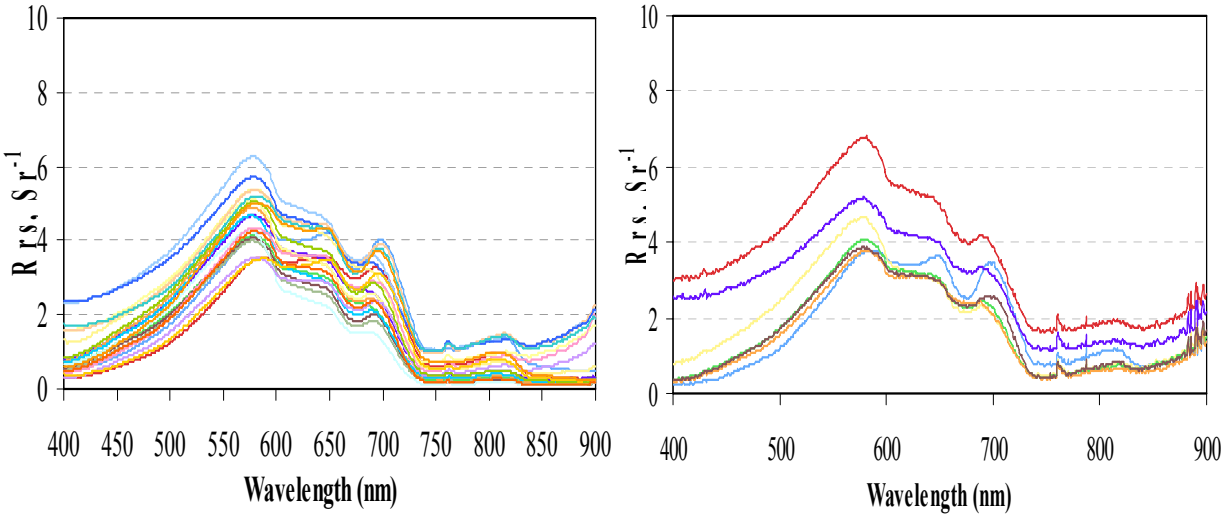

Figure 4.12 Spectral reflectance of selected sampling points of Apalachicola Bay

The processed atmospherically corrected AISA spectra of the selected sampling points under consideration are shown in figure 4.13. The AISA spectra showed the similar kind of behavior like in situ hyperspectral reflectance. However, at some sampling points the noise was observed in the blue domain and in NIR domain. In order to compare the acquired spectra in more detail the graphs were plotted showing spectra of above water surface, subsurface and AISA spectra.

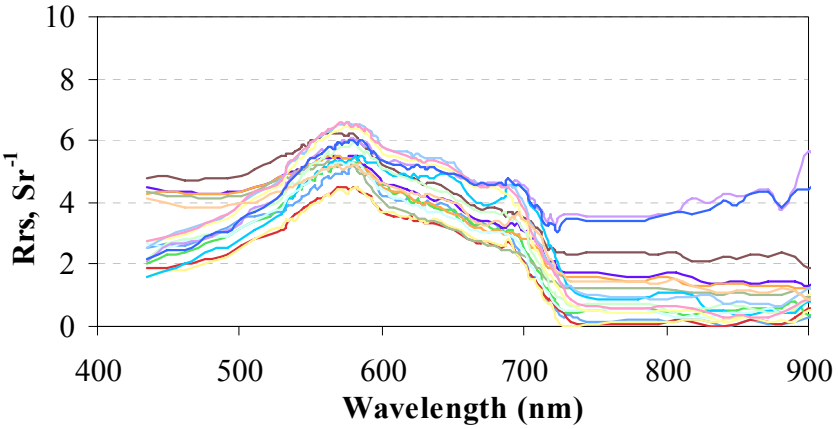

Figure 4.13 AISA spectrum of selected sampling points of Apalachicola Bay

The study of graphs lead to the result that the shape and magnitude of three spectral acquired by different ways for the same sampling point is almost same. The similar kind of trend was observed in all the case. The small variation in the magnitude is

because of atmospheric influence in case of AISA data. It is also observed that that in right graph there is significant difference in visible domain. Although the AISA data is atmospherically corrected but it is difficult to remove the overall influence of the atmosphere. However, by using band ratioing technique, the atmospherically corrected data by using FLAASH model or any other available atmospheric correction model may successfully applied for water quality monitoring.

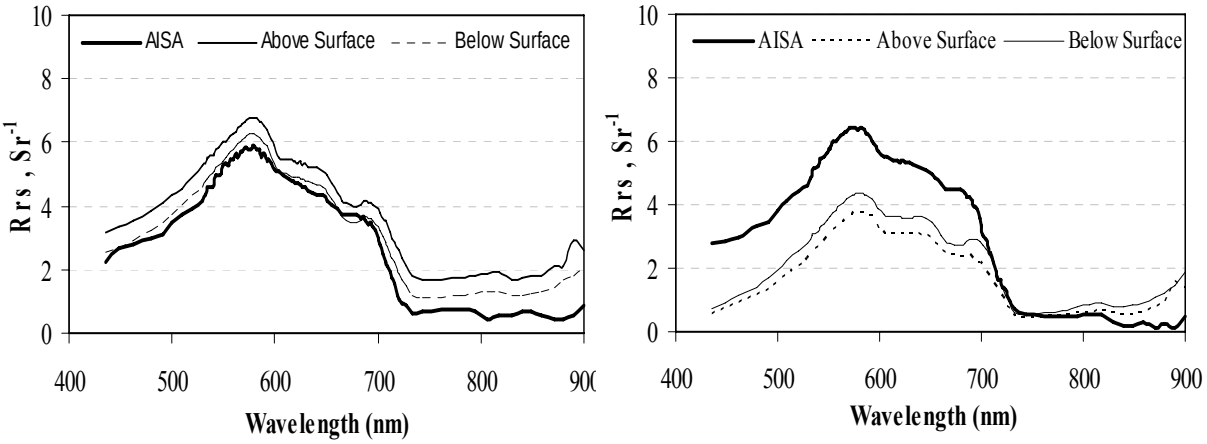

Figure 4.14 Comparison of collected spectral reflectance

In order to study the usability of remote sensing for assessment of spatial distribution of water quality in case II waters, regression models were developed for estimation of TSS and chlorophyll-a concentration. Empirical relationships between spectral properties and water quality parameters are established. All bands were tested for relationships with water quality parameter until it was found which bands and parameters correlated with the highest certainty. As it was observed in case of Althamaha River, the NIR and green ratio is the best predictor of TSS. In case of Apalachicola bay the same ratio also, proves to be effective. The applicability of the same model for three different water bodies shows it successful application under different environmental conditions.

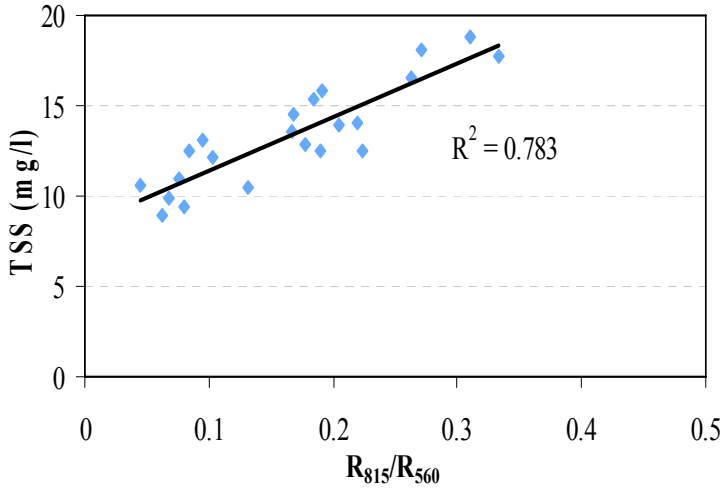

Figure 4.15 Regression models for TSS estimation

$$TSS(mg/l) = m(R_{815}/R_{560}) + n,\ m = 29.9,\ n = 8.4$$

In case I waters, concentrations of chlorophyll-a can be quite satisfactorily estimated with satellite images by using an empirical model and interpreting the received radiance at different wavelengths (Gordon and Morel 1983). However, in case II waters owing to complexity of the water constituents the retrieval of Chl-a is difficult task and needs advance techniques and approaches. Gitelson (1992, 1995) studied the behavior of the reflectance peak near 700nm and concluded that the 700nm reflectance peak is important for the remote sensing of inland and coastal waters with regard to measuring chlorophyll. Han, 2005 pointed out that he spectral regions 630–645 nm, 660–670 nm, 680–687nm and 700– 735 nm were found to be potential regions where the first derivatives can be used to estimate chlorophyll concentration. Three types of independent variables were tested: single spectral band, ratios of spectral bands, and combinations of multiple bands to develop linear regression equations and r^2 values were computed.

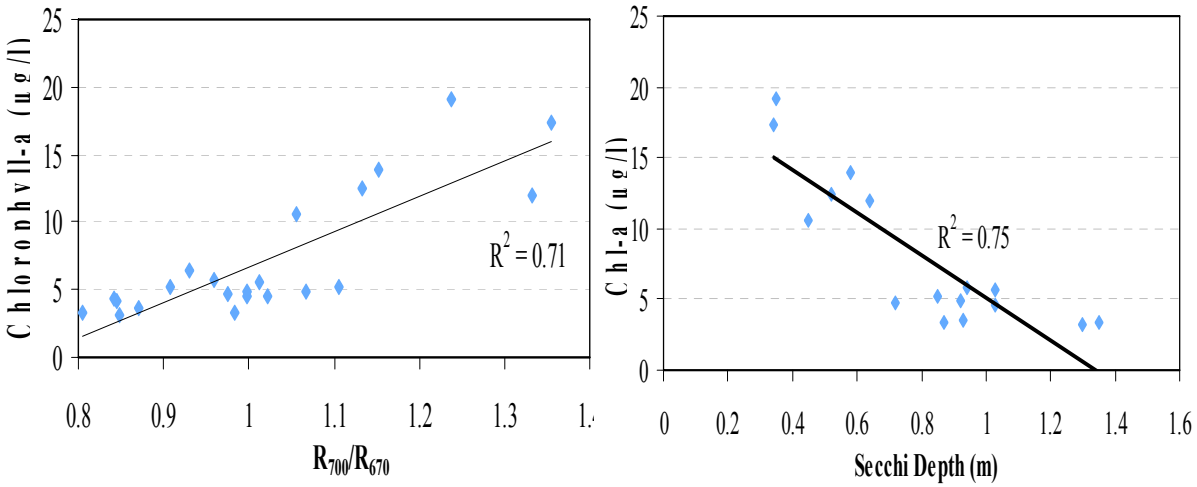

Figure 4.16 Regression models for Chl-a estimation

$$Chl-a(\mu g/l) = m(R_{700}/R_{670}) + n$$

m = 26, n = 19.3

Chl-a (µg/l)= m (Secchi depth, m)+n

m = -15, n = 20.15

It was observed that the ratio of R_{700}/R_{670} is well correlated with chlorophyll-a concentration. Also, it was observed that the chlorophyll-a was strongly correlated with secchi depth showing the effect of chlorophyll-a on optical properties of water.

4.6 Concluding remarks

Application of hyperspectral data allows to discriminate between water quality parameters and to develop a better understanding of light, water and substances interactions. Remote sensing is a power tool to monitor the water quality potentially up to several times per year and offer valuable data on the seasonal variability of water quality. Hyperspectral remote sensing allows accurate and potential use of entire range of

electromagnetic spectrum recorded in extremely narrow wavebands for monitoring water quality on multiple sites in water bodies. The study of suspended sediments in water by means of remote sensing is complex and involves many factors that must be carefully taken into account. The assessment of suspended sediments by means of remote sensing provides information about the sediments near the surface. During flash floods the vertical distribution of suspended sediments in the river is almost same in the first 10 meter depth from the surface. However, under normal conditions when the velocity of water is slow, the vertical distribution of sediments varies slightly and in some case significantly along the depth. The proposed 2 band model approach is considered to be the best predictor of SSC. It was found that the reflectance peak in red domain is well correlated with chlorophyll concentration and the ratio of NIR and green domain is best predictor of TSS. The optical depth is found to be strongly correlated with Chl-a and TSS concentration. The developed algorithms can be successfully applied for water quality monitoring. Empirical and semi-empirical algorithms are easy to use; however, the coefficients used in empirical algorithms are derived from data sets that do not necessarily represent all natural variations. The performance of such algorithms is always subject to compatibility between the waters under study and the waters from which data were obtained for algorithm development. The clear vision and understanding of relationship between water quality parameters and optical measurements made by means of remote sensing techniques is imperative for monitoring water bodies. This study demonstrates that the hyperspectral remote sensing technique can be a useful tool for monitoring the distributions of water quality parameters in water bodies.

CHAPTER 5

OPTICAL MODELING

5.1 Introduction

The Integration of remotely sensed data, in situ data, and optical models is widely touted by researchers to develop the relationship between water quality parameters and inherent optical properties (IOPs) of water bodies. IOPs are the fundamental parameters of hydrological optics. The inherent optical properties of relevance for monitoring water bodies are the absorption coefficient *a* (which determines the exponential rate of decay of flux per unit path length of light in the medium, and per unit incident flux, due to the process of absorption), and the scattering coefficient *b*, which defines similarly the exponential rate of decay of the flux due to scattering.

The inherent optical properties are the properties of the medium itself and are not affected by the ambient light field. Remote sensing of water quality relies on the strong relationship among the remotely estimated radiance scattered out of the water, the inherent water column absorption and scattering properties, and the amount and type of water quality constituents that absorb and/or scatter light. The waters in which phytoplankton and its accompanying substances are the principal components for variations in optical properties of the water is referred as Case 1 (Morel 1980). In many coastal and inland water bodies, a number of constituents, such as yellow substances (colored dissolved organic mater) and suspended material can be present in large concentrations, and vary independently of phytoplankton concentration. Such waters are referred as Case 2 (Sathyendranath 2004). Remote sensing provides an extremely valuable tool for characterizing the coastal optical environment and assessing the spatial variability of coastal reflectance patterns (Gould 1997). The spectral characteristics of different water bodies and at different sampling points of the same water body are not same. Optically active components in the water bodies influence the qualitative and quantitative nature of the spectral signatures. The main components responsible for change in spectral signals are yellow substance, phytoplankton pigments, and inorganic suspended matters and water itself. The quantitative derivation from hyperspectral data of useful geophysical parameters (mainly SSM concentration, and CHL concentration) necessitates models of the IOPs and of the radiative transfer (Forget 2001).

A rigorous understanding of the qualitative and quantitative characteristics of bio optical models is necessary for accurate modeling. The water quality parameters took into consideration in the present research work are colored dissolved organic matters (CDOM), total suspended matters (TSM), and phytoplankton. Dissolved organic matters cause absorption, suspended particles predominantly case scattering, while phytoplankton contributes to both scattering and absorption (Elisabeth 2001).

5.2 Purpose of the Study

The prime purpose of this section of the dissertation is to investigate the relationship between IOPs and spectral reflectance. The reflectance was modeled by

integrating IOPs and the comparison of model-derived reflectance spectra and in situ spectral reflectance is demonstrated. The effect of change in WQPs on absorption and scattering of light is described in detail. The chapter illustrates the inversion of reflectance spectra in terms of three parameters, total suspended matter, Chlorophyll concentration and yellow substance absorption coefficient at 440 nm. Furthermore, the useful outcomes of the research will improve the performance of IOPs algorithms, and extend their domain of applicability.

5.3 Bio Optical Theory

As defined by the Mobley (1994), the inherent optical properties (IOP's) specify the optical properties of natural waters. Consider a small volume ΔV of water, of thickness Δr, illuminated by a narrow collimated beam of monochromatic light of spectral radiant power $\Phi_i(\lambda)$, W nm^{-1}, as schematically depicted in Fig. 5.1. Some part of the incident power $\Phi_i(\lambda)$ is absorbed $\Phi_a(\lambda)$ within the volume of water, some part $\Phi_s(\theta, \lambda)$ is scattered out of the beam at an angle θ, and the remaining power $\Phi_t(\lambda)$ is transmitted through the volume with no change in direction. Let $\Phi_s(\lambda)$ be the total power that is scattered into all directions.

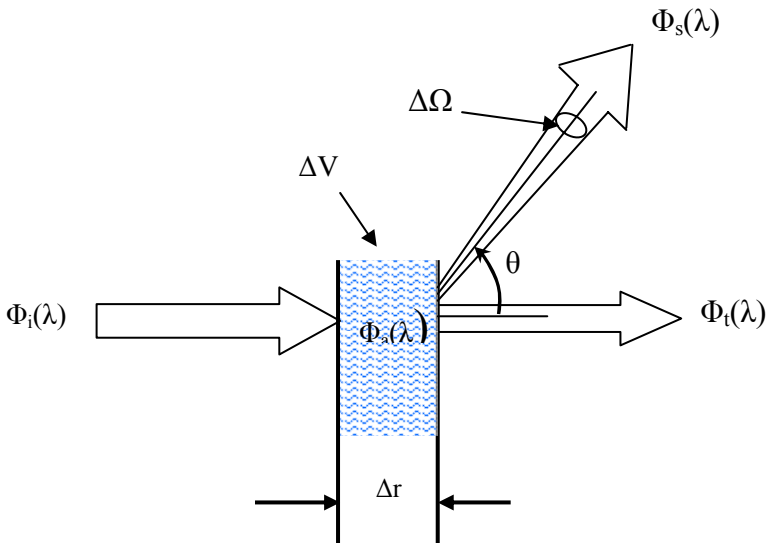

Figure 5.1 Geometry used to define inherent optical properties (Mobley, 1994, 2004).

Assuming that no inelastic scattering occurs, i.e. assume that no photons undergo a change in wavelength during the scattering process. By the law of conservation of energy;

$$\Phi_i(\lambda) = \Phi_a(\lambda) + \Phi_s(\lambda) + \Phi_t(\lambda)$$

The spectral absorptance $A(\lambda)$ is the fraction of incident power that is absorbed within the volume:

$$A(\lambda) = \frac{\Phi_a(\lambda)}{\Phi_i(\lambda)}$$

Likewise, the spectral scatterance B(λ) is the fractional part of the incident power that is scattered out of the beam;

$$B(\lambda) = \frac{\Phi_s(\lambda)}{\Phi_i(\lambda)}$$

and the spectral transmittance T((λ));

$$T(\lambda) = \frac{\Phi_t(\lambda)}{\Phi_i(\lambda)}$$

Clearly, $A(\lambda) + B(\lambda) + T(\lambda) = 1$

The inherent optical properties employed in hydrologic optics are the spectral absorption and scattering coefficients, which are respectively the spectral absorptance and scatterance per unit distance in the medium. From figure 4.1, the spectral absorption coefficient $a(\lambda)$ is defined as;

$$a(\lambda) = \lim_{\Delta r \to 0} \frac{A(\lambda)}{\Delta r} \quad (m^{-1})$$

The spectral scattering coefficient $b(\lambda)$ is;

$$b(\lambda) = \lim_{\Delta r \to 0} \frac{B(\lambda)}{\Delta r} \qquad (m^{-1})$$

The spectral beam attenuation coefficient $c(\lambda)$ is defined as;

$$c(\lambda) = a(\lambda) + b(\lambda)$$

The angular distribution of the scattered power, with $B(\theta,\lambda)$ being the fraction of incident power scattered out of the beam through an angle θ into a solid angle $\Delta\Omega$ centered on θ, as shown in Fig. 4.1. The angle θ is called the *scattering angle*; its values lie in the interval $0 \leq \theta \leq \pi$. Then the angular scatterance per unit distance and unit solid angle, $\beta(\theta,\lambda)$, is;

$$\beta(\theta;\lambda) = \lim_{\Delta r \to 0} \lim_{\Delta\Omega \to 0} \frac{\Phi_s(\theta;\lambda)}{\Phi_i(\lambda)\Delta r \Delta\Omega}$$

The spectral power scattered into the given solid angle $\Delta\Omega$ is just the spectral radiant intensity scattered into direction θ times the solid angle:

$$\Phi_s(\theta;\lambda) = I_s(\theta;\lambda)\Delta\Omega$$

Moreover, if the incident power $\Phi_i(\lambda)$ falls on an area ΔA, then the corresponding incident irradiance is:

$$E_i(\lambda) = \Phi_i(\lambda) / \Delta A$$

And $\Delta V = \Delta r \Delta A$ is the volume of water that is illuminated by the incident beam. The expression becomes:

$$\beta(\theta;\lambda) = \lim_{\Delta v \to 0} \frac{I_s(\theta;\lambda)}{E_i(\lambda)\Delta V}$$

This form of $\beta(\theta,\lambda)$ suggests the name spectral volume scattering function and the physical interpretation of scattered intensity per unit incident irradiance per unit volume of water. Integrating $\beta(\theta,\lambda)$ over all directions (solid angles) gives the total scattered power per unit incident irradiance and unit volume of water, in other words the spectral scattering coefficient;

$$b(\lambda) = 2\pi \int_0^{\pi} \beta(\theta;\lambda) \sin\theta \, d\theta$$

This integration is often divided into forward scattering, $0 \leq \theta \leq \pi/2$, and backward scattering, $\pi/2 \leq \theta \leq \pi$ parts.

$$b = b_b + b_f$$

$$b_f(\lambda) = 2\pi \int_0^{\pi/2} \beta(\theta;\lambda) \sin\theta \, d\theta$$

$$b_b(\lambda) = 2\pi \int_{\pi/2}^{\pi} \beta(\theta;\lambda) \sin\theta \, d\theta$$

5.4 Modeling IOPs

Natural waters contain a continuous size distribution of particles ranging from water molecules of size ~ 0.1 nm, to small organic molecules of size ~ 1 nm, to large organic molecules of size ~ 10 nm, to viruses of size ~ 100 nm, to ..., to whales of size ~ 10 m, to submarines of size ~ 100 m. Each of the components of natural water, regardless of how they are classified, contributes in some fashion to the values of the optical properties of a given water body. (Mobely, 1994). Several workers have investigated the relation between subsurface reflectance R and the inherent optical properties for ocean, coastal and inland water systems (Gordon et al. 1975, Morel and Prieur 1977, Whitlock et al. 1981, Kirk 1991, Dekker et al. 1997a).

Inherent optical properties provide understanding of water environments and open new doors for detailed delineation of optical active constituents. Algorithms based on the fundamentals of IOPs are strongly advocated. The water column is assumed to be homogeneous in terms of its optical properties. Passive optical remote sensing becomes quite a challenge when the optical properties of the upper water column are significantly

stratified. The method developed and applied here relies on the concepts of model inversion technique, leading to analytical algorithms.

5.5 Absorption

Light passing through water is attenuated by water molecules and by various suspended and dissolved substances. The absorption coefficient a(λ) is written as the sum of contribution from pure water and optically active constituents (OACs) present in the water body.

$$a(\lambda) = a_w(\lambda) + a_y(\lambda) + a_{ph}(\lambda) + a_s(\lambda)$$

Where the subscript *w, y, ph* and *s* represents water, colored dissolved organic mater, phytoplankton and total suspended maters. The absorption, scattering and beam attenuation coefficients all have units of 1/length, and are normally expressed in m^{-1}. An absorption of 0.5 m^{-1} indicates that an average photon entering the water column has a chance of $e^{-0.5}$ or 40%, of being absorbed in the first meter.

5.5.1 Absorption by water

Determination of the spectral absorption coefficient *a(λ)* for natural waters is a difficult task. There exists no theoretical model which describes the absorption and scattering of pure water exactly. Therefore, it is necessary to rely on laboratory measurements. Many techniques have been employed in attempts to determine the spectral absorption coefficient for pure water, *aw(λ)*; these are reviewed in Smith and Baker (1981). The absorption of water at a temperature of 20°C is below $0.05 m^{-1}$ for wavelengths between 400 to 550 nm.

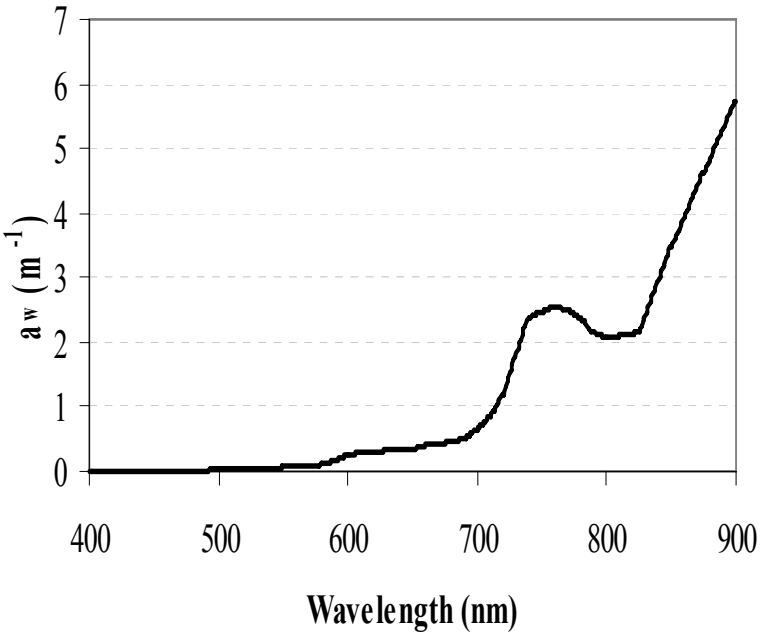

Figure 5.2 Absorption coefficient of pure water at a temperature of T = 20°C

There is a slight increase up to 0.1 m^{-1} till 580 nm, then the absorption increases rapidly to a value of 0.27 m^{-1} at around 610 nm. A second slight increase to 0.4 m^{-1} is at 665 nm before a local maximum is reached at 765 nm with 2.77 m^{-1} (Hakvoort, 1994, Albert, 2004)

The absorption by pure water $a_w(\lambda)$ are adopted from Smith and baker (1981) for the range of 400-800 nm and are deduced from Hale and Query (1973) for the range 800-900 nm (Forget 1999). The absorption of incident light on the water surface is maximum in the red and NIR domain and minimum in the blue region (Figure 4.2).

5.5.2 Absorption by phytoplankton

Phytoplankton cells are strong absorbers of visible light and therefore play a major role in determining the absorption properties of natural waters. The concentration of the main phytoplankton pigment, chlorophyll-a, is often taken as an index of phytoplankton biomass, although two major colour phytoplankton groups – green and brown – also contain chlorophylls-b and -c, respectively (Boney 1983). If no separation of the species is necessary, the phytoplankton absorption is estimated by the mean specific absorption coefficient of phytoplankton a^*ph multiplied by the total concentration of phytoplankton C_{ph} ;

$$a_{ph}(\lambda) = a^*_{ph}(\lambda) * C_{ph}$$

The specific absorption coefficient a^*ph was investigated for example by Prieur and Sathyendranath (1981), Sathyendranath et al. (1987) for oceanic and coastal sea water. Absorption by chlorophyll is characterized by strong absorption bands in the blue and in the red domain, with peaked around 440 nm and 675 nm, respectively, for chlorophyll *a* and very little absorption in the green, only about 40% at 550nm compared to the value at λ_o = 440 nm. No absorption by phytoplankton occurs from 750 nm onwards. Morel (1991) found that the power law;

$$a_p = 0.06 a^*_{chl}[Chl]^{0.65}$$

This was first proposed by Prieur and Sathyendranath (1981), was the best solution to estimate the absorption coefficient for his data set. C_{chl} is the concentration of chlorophyll-a in units of µg/l. The model of Bricaud et al. (1995) uses the parameterization of the specific absorption coefficient by means of C_{chl}. Based on extensive studies of more than 800 spectra; the model is of the following form;

$$a^*_{ph}(\lambda) = A(\lambda) \times C_{chl}^{-B(\lambda)}$$

Where A and B are positive empirical coefficients and are wavelength dependent and chlorophyll-a concentration C_{chl} in µg/l. The model of Bricuad, 1995 was adopted in this study. The rational is because the model takes the effect of varying pigment composition, depends on wavelength and shows satisfactory results in our case.

5.5.3 Absorption by suspended matters

Suspended matters, inorganic and organic detritus contribute mainly to scattering of light. In general, the absorption of the total suspended particles is very low and is negligible for the inorganic particles. Inorganic particles are due to suspended sediments brought by the feeding stream. Roesler ,1989 found an empirical exponential model for the absorption by detritus in coastal water;

$$a_s(\lambda) = a_s^*(\lambda_o) \cdot e^{-k_s(\lambda-\lambda_o)}$$

Where a_s^* is the specific absorption coefficient ($a_s^* = a_s/C$). C is suspended particle concentration (mgm^{-3}) and k_s is the constant. The reference wavelength λ_o is 400nm. The mean value of k_s = 0.011 nm^{-1} is reported for their data. Zimmerman & Maffione (2000) use the same model to describe the absorption by inorganic particles. They assigned a value of 0.001 m^2 mg^{-1} to a_s^* (400), which is an order of magnitude lower than values reported for phytoplankton and detritus.

Based on Prieur & Sathyendranath (1981), Buiteveld (1995) developed an inverse relationship between the absorption coefficient and wavelength. Buiteveld, 1995 model with slight modification is applied to quantify the absorption by suspended particles. The modified model is of the following form;

$$a_s(\lambda) = k_1 C_s^{k_2}(\lambda_0/\lambda)$$

Buiteveld (1995) assumed that inorganic particles hardly contribute to absorption and gave values of 0.016–0.025 for k_1 and k_2 1.04-1.22 for detritus. k_1 and k_2 are optimization parameters. Other researchers calibrated this model on data from about 20 Dutch lakes and report k_1-values for detritus of 0.001 up to 0.050. C_s is suspended particle concentration (mg/l). In our case the value of k_1 = 0.05 and k_2= 1.1 is used for analysis.

5.5.3 Absorption by CDOM

Both fresh and saline waters contain varying concentrations of colored dissolved organic matters. These compounds are generally brown in color, and in sufficient concentrations can color the water yellowish brown. For this reason the compounds are generically referred to as yellow matter or CDOM, colored dissolved organic matter. Other common names are gelbstoff and gilvin.

Yellow matter absorbs very little in the red, but its absorption increases rapidly with decreasing wavelength and can be significant at blue and ultraviolet wavelengths. Following the study of Morel and Prieur (1976), Bricaud et al. (1981) found that CDOM absorption shows an exponential decrease for increasing wavelengths and expressed this in the following relation.

$$a_y(\lambda) = a_y(\lambda_o)e^{-k(\lambda-\lambda_o)}$$

Where $a_y(\lambda_o)$ is the absorption coefficient at a reference wavelength. The reference wavelength of 440 nm, $a_y(440)$ = 0.2 $m^{-1}$and the exponential coefficient k is variable and the mostly the value = 0.014 nm^{-1} is used. In our case the value of 0.017 nm^{-1} is selected. Roesler *et al*. (1989) noted that the published mean value of k for yellow substances was

0.016 nm^{-1} with a standard deviation of 0.002nm^{-1}. Their conclusion is in agreement with the results of Kopelevich *et al*. (1989) based on over 400 spectra measured by various investigators in oceanic, coastal and fresh waters. They reported that *S* had a mean value of 0.017 nm^{-1} (with standard deviation, SD, of 0.001) in the spectral domain from 280 to 490 nm. For example, Hojerslev (1998) has reported a range in *k* of 0.008 to 0.042 nm^{-1}. It might be worth investigating whether these extreme values indicate difficulties with measurement, or some other source of absorption. Kopelevich *et al*. (1989) have reported that the mean slope decreases to 0.011 nm^{-1} for the spectral range from 500 to 680 nm.

Table 5.1 Measured absorption coefficient at λ = 440nm for selected waters due to CDOM, *ay(440)* (Mobley, 2004)

Water body	$a_y(440)$, (m^{-1})
Oceanic waters	
Sargasso Sea	~ 0
Off Bermuda	0.01
Gulf of Guinea	0.024-0.113
Oligotrophic Indian Ocean	0.02
Mesotrophic Indian Ocean	0.03
Eutrophic Indian Ocean	0.09
Coastal and estuarine waters	
North Sea	0.07
Baltic Sea	0.24
Rhone River mouth, France	0.086-0.572
Clyde River estuary, Australia	0.64
Lakes and rivers	
Crystal Lake, Wisconsin, USA	0.16
Lake George, Australia	0.69-3.04
Lake George, Uganda	3.7
Carrao River, Venezuela	12.44
Lough Napeast, Ireland	19.1

The above table gives measured values of *a*y(440) for selected waters. The selected model allows the determination of spectral absorption by yellow matter if the absorption is known at one wavelength, no model yet exists that allows for the direct determination of *a*y(λ) from given concentrations of yellow matter constituents.

5.6 Scattering

Scattering in natural water takes place due to the interaction of photons with water molecules and water constituents. Emission at the same wavelength as the incoming radiation is called elastic scattering and emission at another wavelength is called inelastic scattering. The influence of each constituent on the scattering process depends on wavelength, particle size, concentration, and refractive index. The theoretical aspects of

light scattering are treated extensively in van de Hulst (1981). Generally, the scattering coefficients are not the same as the diffuse scattering functions because of the incident angle of the radiance: forward scattered radiance contributes to the downwelling light, but also to the upwelling, and backscattered radiance contributes also to both, the up- and downwelling irradiance. In natural waters the scattering is not isotropic. Most light is scattered in forward direction and less is scattered backward or perpendicular to the incoming direction due to the shape and size of the particles in the water. However, it is assumed that backward and forward scattering are equal in magnitude and 50% of the total scattered light contributes to the backward scattering and the remaining 50% contributes to the forward scattering.

The total scattering coefficient *b* as the sum of contribution from pure water and optically active constituents present in the water body.

$$b\ (\lambda) = b_w(\lambda) + b_{ph}(\lambda) + b_s(\lambda) + b_y(\lambda)$$

Where the subscript w, y, ph and s represents water, colored dissolved organic mater, phytoplankton and total suspended maters.

The backscattering coefficient b_b (m^{-1}) is the relevant parameter for the reflected radiance and irradiance and therefore for remote sensing since this coefficient defines the amount of light scattered in an upward direction towards the sensor. The total backscattering coefficient b_b can be expressed in the same way as the scattering coefficient.

$$b_b(\lambda) = b_{bw}(\lambda) + b_{b\,ph}(\lambda) + b_{b\,s}(\lambda) + b_{by}(\lambda)$$

5.6.1 Scattering by water

The scattering of pure water is relatively high in the blue wavelength domain where the short wavelengths are of the same order of magnitude as the water molecules. The pure water scattering decreases exponentially towards the larger wavelength, approaching zero around 750 nm.

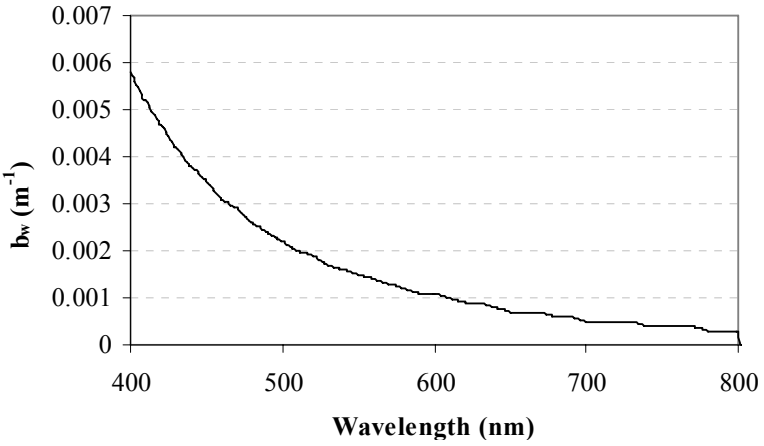

Figure 5.3 Scattering coefficient of pure water at a temperature of T = 20°C

Morel (1974) has studied and reviewed scattering by water. He has noted that scattering by pure water follows a λ^{-n} law, and that the appropriate value for *n* would be 4.32. Shifrin (1988) has also provided a detailed account of the study of molecular scattering by water, and concludes, based on both theoretical considerations and experimental data from different authors, that the appropriate value for *n* may lie between 4.05 and 4.35.

5.6.2 Scattering by phytoplankton

Theoretical studies and laboratory measurements have shown that phytoplankton have extremely low back-scattering coefficients (Bricaud *et al*., 1983).The influence of phytoplankton on the total scattering coefficient depends on the water type. For water with low concentration of inorganic suspended sediment the scattering is driven by the concentration of phytoplankton.

Gordon and Morel (1983) suggested that the scattering is correlated directly to the pigment concentration of chlorophyll-a C_{chl} (µg/l). Their empirically developed model is as follow:

$$b_{ph}(\lambda) = B \cdot C_{chl}^{0.62} (\lambda_o / \lambda)$$

The scattering coefficient of phytoplankton b_{Ph} in units of m^{-1}. The reference wavelength λ_0 is 550 nm and the mean value of B for case-1 water dominated by phytoplankton is 0.3. However, the developed model is valid in the range of phytoplankton concentration from 0.05 to 1 µg/l. Higher values are used for case-2 water to calculate the scattering coefficient in turbid water for example (Lee et al., 1998).

The backscattering coefficient of phytoplankton b_{bPh} can be determined by using the backscattering to scattering ratio b_{bPh}/b_P . Morel (1988) recognized an almost constant ratio of $b_{bPh}/b_P \approx 0.02$ slightly depending on the wavelength and the concentration of chlorophyll-a. Ahn et al. (1992) found lower values for phytoplankton cultures grown in the laboratory. Their backscattering to scattering ratio ranges from 0.0004 to 0.0045 at λ_0 = 550 nm.

In coastal regions, Sathyendranath et al. (1989) proposed that the scattering coefficient is indirectly proportional to the absorption of phytoplankton; $b_{Ph} \alpha 1/ a_{Ph}$ and the proportionality factor depends on the chlorophyll-a concentration. For the backscattering to scattering ratio Sathyendranath et al. (1989) & Tassan (1994) found a constant value of $b_{bPh}/b_P = 0.005$ in their measurements. Extensive and commonly used measurements were done by Petzold (1977) and suggested that the backscattering to scattering ratio of particles varies from 0.018 to 0.020 for turbid water. The integrated and modified model for measuring backscattering coefficient of phytoplankton in terms of chlorophyll-a concentration C_{chl} *(µg/l* is as below;

$$b_{ph}(\lambda) = (b_{bPh}/b_P) \cdot B \cdot C_{chl}^{0.62} (\lambda_o / \lambda)$$

$$b_{ph}(\lambda) = 0.005(0.12 * C_{chl}^{0.63} (a_{Ph}(550)/a_{Ph}(\lambda))$$

5.6.3 Scattering by suspended matters

Light scattered in the water is described by the co-called Mie theory, when the index of refraction is known. Mie theory allows to calculate the scattering efficiency Q_{scat}, if we assume that the particles are spherical and optically homogenous. The geometric cross section of the particle is $\pi D^2/4$, where D is the diameter of the particle. Calculations based on Mie theory are playing an increasingly important role in hydrologic optics, primarily because modern computers make it convenient to perform the necessary computations. Mie's solution is presented in terms of absorption and scattering efficiencies.

5.6.3.1 One particle Scattering Intensity

Let I_o be the intensity of the incident light. I is the intensity of scattered light in a point at a long distance r from the particle and k is the wave number defined by $k=2\pi/\lambda$, where λ is the wavelength in the surrounding medium. I must be proportional to I_o and r^{-2}.

$$I \propto I_o / r^2$$

We may write;

$$I = \frac{I_o F(\theta, \varphi)}{k^2 r^2}$$

Where $F(\theta, \varphi)$ is dimensionless function (F/k^2 is an area) of the direction but not of r. It also depends on the orientation of the particle with respect to the incident wave and on the state of polarization of the incident wave. The phase function is obtained when $F(\theta, \varphi)$ is divided by $k^2 C_{sat}$. The phase function has no physical dimension and its integral over all directions is 1.

Let the total energy scattered in all direction be equal to the energy of the incident wave falling on the area C_{sca}

$$C_{sca} = \frac{1}{k^2} \int F(\theta, \varphi) dw$$

Where $d_w = \sin\theta d\theta d\varphi$ is the element of solid angle and the integral is taken over all direction. The scattering cross section C_{sca} is obtained by multiplying the efficiency factor by the geometric cross section of the particle ($\pi D^2/4$). Let r be the distance from the center of the sphere and $k=2\pi/\lambda$. If natural light intensity I_0 (watt/m^2) is incident on the sphere, the scattered light in any direction has partial linear polarization. Its intensity (watt/m^2) is;

$$I = \frac{I_o (i_1 + i_2)}{2k^2 r^2}$$

In which i_1 & i_2 respectively represents the intensity of light vibrating perpendicular and parallel to the plane through the directions of propagation of the incident and scattered beams. The degree of polarization is $i_1 - i_2 / i_1 + i_2$.

5.6.3.2 Medium containing N particles per unit volume

The intensity scattered per unit volume in a given direction is simply N times the above mentioned intensities. The term "suspended matters" does not apply to a single type of material, but to a whole family of materials with their own individual characteristics. The diameter of suspended particles especially inorganic particles is generally much larger than the wavelength of visible light making them efficient scatterers. The suspended matter in the water column is treated as a collection of non-absorbing spherical particles, characterized by a refractive index *m,* relative to water. Light scattering in the water is described by Mie theory which allows us to calculate the scattering efficiency, Q_{scat} when the index of refraction is known.

If $|m-1| << 1$, the expression for the efficiency factor can be greatly simplified (van de Hulst 1957) and can be written

$$Q_{scat} = 2 - \frac{4\sin x}{x} - \frac{4\cos x}{x^2} + \frac{4}{x^2}$$

with $x=kD$ and $k=2\pi(|m-1| /\lambda)$, λ *is* being the light wavelength in the medium and D the particle diameter. The scattering cross section is obtained by multiplying the efficiency factor by the geometric cross section of the particle $(\pi D^2/4)$. Then integrating the scattering cross section over the particle size distribution one gets the total scattering coefficient for the particle system;

$$b_s = \int_{D_1}^{\infty} f(D) \frac{\pi D^2}{4} Q_{scat} dD$$

D_1 and ∞, are the lower and upper limits of the particle diameter under consideration. Much of the utility of Mie theory lies in the fact that it gives us an overall theoretical structure for the analysis and modeling of IOP's. The main assumption is that all the particles are assumed to be spherical particles, optical homogenous, and all have the same refractive index relative to water. $b_{bs}(\lambda)$ is modeled using Mie's theory (Van de Hulst, 1957) which has been of current use in ocean optics (Mobley, 1994).

For a collection of particles with size distribution $N(D)$ [$(N(D)dD$ is the number particles of diameter comprised between D and $D+dD$ per unit volume) and refractive index relative to m_p, $b_{bs}(\lambda)$ can be written as (Forgrt et al., 1999);

$$b_{bs} = \int_{D1}^{D2} Q_{bb}(D, m_p, \lambda) \frac{\pi . D^2}{4} N(D) dD$$

Q_{bb} designates the backscattering efficiency factor of a particle with characteristics D and m_p. m_p is a real number if sediment particles are non absorbing and is supposed independent of λ. Zaneveld and Pak (1973) emphasized that, *mp* must be considered as

"the value of the index of refraction reproducing the bulk scattering properties of the particles" rather than the value of a true average refractive index. The refractive index depends on the chemical composition of the particles, which in turn determines the particle density needed to derive the scattering coefficient per unit mass concentration. Q_{bb} was computed by the Mie intensity functions over the backscattering half-space (Forget, 1999). The value of Q_{bb} varies with Mie parameter $\alpha=\pi D/\lambda_m$, where λ_m is the light wavelength in the water ($=n\lambda$).

Table 5.2 Properties of typical particle types found in coastal waters (Babin, 2003)

Particle Type	Density ($x10^6$ g m^{-3})	Relative refractive index
Aragonite	2.83	1.22
Calcite	2.71	1.17
Chlorite	2.5	1.21
Gibbsite	2.42	1.18
Illite	2.8	1.18
Kaolinite	2.65	1.16
Montmorillonite	2.5	1.17
Opal	1.9	1.01
Quartz	2.65	1.16
Organic matter (dry)	1.38	1.16
Living organic matter (+water)	0.2-0.5	1.03-1.05

The particle size distribution can be considerably different at a particular time and location. The particle size distribution, which was not measured during the Rhone experiment, is modeled by the classical Junge hyperbolic law (Mobley 1994);

$$N(D)= kD^s$$

For a range of sizes $D_1 \leq D \leq D_2$ the above expression with the value of s = -4 seems to reproduces a wide variety of marine particle size distribution. However, departures of *s* about the value of -4 have already been observed (e.g., Campbell and Spinrad, 1987) following a thorough discussion by Stramski and Kiefer (1991). Above equation is probably valid over *a* wide range of particle diameters, typically 0.01–100 μm. Coefficient *k* depends on mass concentration *C* of suspended particles. Assuming spherical particles, as required by Mie's Theory, C can be expressed as

$$C = \int_{D_1}^{D_2} N(D)\rho_s \pi \frac{D^3}{6} dD$$

Where ρ_s is the sediment density, fixed to the typical value of 2600 kg/m^3. Putting value of *N(D)* in the above equation and integrating;

$$k = \frac{6C}{\pi\rho_s} g(s)$$

$$s \neq -4;\ g(s) = \frac{4+s}{D_2^{4+s} - D_1^{4+s}}$$

$$s = -4;\ g(s) = \frac{1}{\ln(D_2 / D_1)}$$

The spectral backscattering of sediments is written as;

$$b_{bs} = \frac{3C}{2\rho} . \frac{1}{\ln(D_2 / D_1)} \int_{D1}^{D2} Q_{bb} . D^{-2} dD$$

The backscattering to scattering ratio varies from 0.011 to 0.020. For river water with scattering coefficients of 10 to 20 m^{-1} the ratio can be two to three times higher (Albert, 2004). Q_{bb} is efficiency factor, ρ is the sediment density ,D_1 & D_2 are minimum and maximum suspended particles diameters, and C is the concentration of suspended sediments or total suspended sediments. The units of all parameters must be symmetric.

5.6.4 Scattering by CDOM

Coloured, dissolved organic matter (CDOM), Yellow substances, variously called "gelbstoff", "or "gilvin" consists of dissolved organic matter. The size of all CDOM components is smaller than the wavelengths of visible light. Hence, the scattering probability of CDOM is described by Rayleigh scattering proportional to λ^{-4} (Albert, 2004). The scattering and backscattering coefficient of CDOM is considered to be much smaller compared to the CDOM absorption coefficient. In optical oceanography the scattering probability of CDOM is neglected (Pozdnyakov and Grassl, 2003). The scattering and backscattering coefficient of CDOM is considered to be zero in our case and neglected fro further analysis.

5.7 Development of Modeled Spectral Reflectance

Numerous researchers have investigated the relation between subsurface reflectance ratio, R, and the inherent optical properties for ocean, coastal and inland water systems. The subsurface reflectance ratio, R, is dependent on the inherent optical properties (IOPs) of the medium, namely the spectral absorption coefficient a(λ) and backscattering coefficient $b_b(\lambda)$. The absorption and backscattering coefficients bring some complementary information on the water composition, because of their different sensitivity to the various optically significant materials in water. IOPs provide an improved capability to understand how physical processes influence the bio-optical

processes (Bissett *et al*., 2001; Arnone and Parsons, 2004).The relationship is expressed as (Gordon *et al*. 1975, Morel and Prieur 1977).

$$R(\lambda) = f \frac{\mathrm{b_b}(\lambda)}{\mathrm{a}(\lambda) + \mathrm{b_b}(\lambda)}$$

Where f is a coefficient varying with geometry of the light filed and also with water types (Sathyendranath and Platt, 1997). Value of f varies from 0.33 to 0.47 for R varying from 0% to 10% (Brando, 2000). The commonly adopted value of f is 0.33, which is valid for zenith sun and for large variety of natural waters (Kirk, 1994).

5.8 In situ Spectral Reflectance

Spectral reflectance measurements were collected using, a dual-fiber system, two inter-calibrated Ocean Optics USB2000 Spectroradiometers (2048 channels, 370–1000 nm). Data were collected from a boat in the spectral range of 400-900 nm with a sampling interval of 0.3 nm and a spectral resolution of 1.5 nm. Radiometer # 1, equipped with a 25^{o} field off view optical fiber, was pointed downward above and just below the water surface (~3 cm) in the nadir direction to collect the total subsurface upwelling irradiance from the water $E_u(\lambda)$. Radiometer # 2, equipped with an optical fiber and a cosine collector (yielding a hemispherical filed of view) was pointed upward to simultaneously measure the incident irradiance $E_d(\lambda)$ on the water surface.

$$\%R(\lambda) = [E_u(\lambda) / E_d(\lambda)] \times 100$$

where $E_u(\lambda)$ is the irradiance (flux per unit surface area) in the upward directions, or upwelling irradiance, at wavelength λ and depth z; and $E_d(\lambda)$ is the irradiance in the downward directions, or the downwelling irradiance, at the same wavelength and depth. For each sampling points above and below subsurface irradiance reflectance was collected.

5.9 Results & Discussion

The developed modeled in situ above surface and subsurface hyperspectral spectral signature was compared. The underlying assumption is that the in situ hyperspectral measurements and modeled reflectance spectral have similar magnitude and shape. The concept is depicted in the following equation forms the basis of optical modeling of water quality parameters by means of remote sensing.

$$R\,(\,Above \quad ,\, Subsurface \quad)_{Measured} = R\,(0-)_{Modeled} \begin{bmatrix} CDOM \\ Chl \quad - \quad a \\ TSS \\ water \quad itself \end{bmatrix}$$

The relationship between AOP and IOPs is illustrated in the figure 5.4. The relationship between measured $R(0-)$ and water quality parameters via the inherent optical properties (a & b_b) leads to develop the qualitative and quantitative relationship between the modeled and in situ above surface and subsurface reflectance spectra.

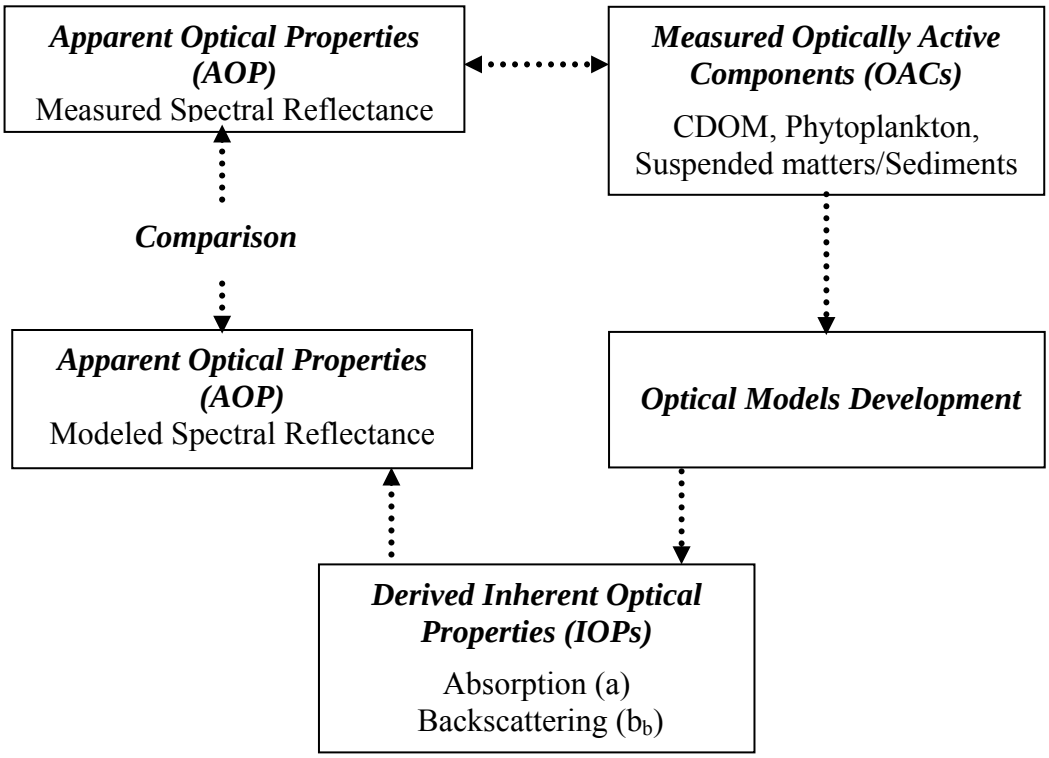

Figure 5.4 Schematic Diagram of relationship between AOPs , IOPs

On the basis of water quality parameters the inherent optically properties was derived by means of optically developed modeled. The developed modeled spectra seem to be in well agreement with the in situ measured spectral signals. The comparison between three kinds of spectral reflectance was demonstrated in the figure 5.5. It was observed that the spectral shape is almost same in all the cases. The modeled reflectance spectra actually represent the absorption and scattering properties of optically active constituents and strongly depend on the type and concentration of water constituents in the water bodies. The changes in water quality parameters not only change the spectral magnitude by also influence actively the spectral shape. As depicted in figure 5.5, the modeled spectral reflectance lies between the above and subsurface reflectance. The modeled spectral shows a systematic trend. The spectra attain the peak in the green domain, tends to decrease in the red region with again peak near 700 nm that depends on the chlorophyll concentration and finally absorbing fashion in the NIR regions. The developed spectra in actual is the response of water quality parameters and optical models. The behavior is based on a few assumptions, empirical parameters and analytical models. The spectral shape will remain constant however; the spectral magnitude may change depending on the input concentration and constituents. The application of optical models in turbid water is promising, however, in case 1 waters and optically complex water the applicability of the optical models demands for accurate in situ water quality measurements. It is noteworthy that the optical models don't take into account the variation of environmental factors. The optical model development approach is useful for delineation of water bodies.

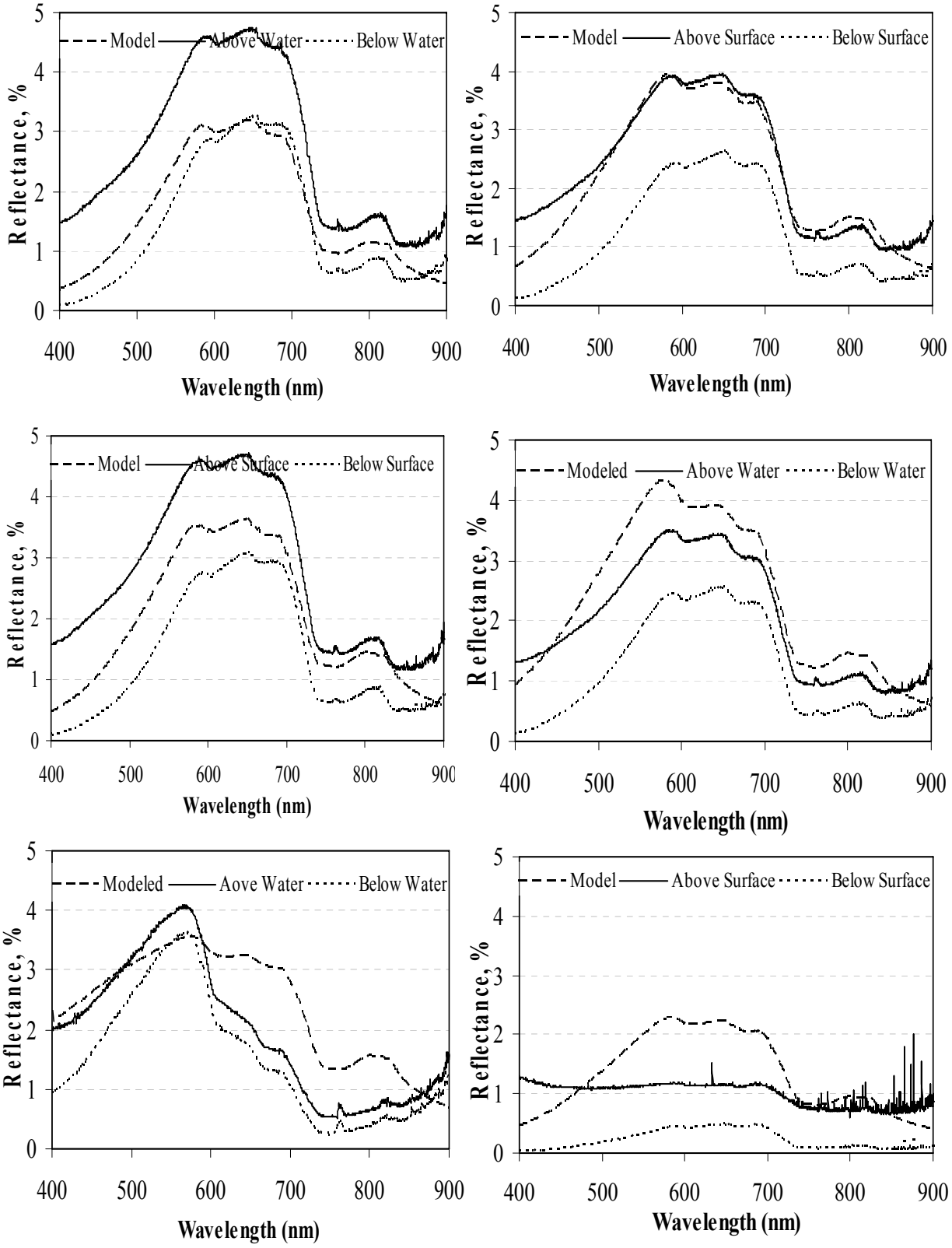

Figure 5.5 Comparison of modeled, above water and below water irradiance reflectance

If ground truth data is available, the developed models may apply to quantify the difference because of environmental factors including atmospheric effects in case of multispectral remote sensing. If ground data is not available, the developed approach may successfully apply to estimate the water quality parameters by comparing the spectra with in situ hyperspectral or multispectral remote sensing. The application of optical modeling for estimation of suspended sediments in explained in chapter 6. It is emphasized that an adequate knowledge optically active constituents is necessary for an understanding of inherent optical properties and for various field applications, including water quality monitoring by means of remote sensing. This knowledge is important not only for Case 2, Case 1 and optically complex waters but also for highly turbid waters whose optical properties have been considered to be dominated by suspended sediments and covarying materials.

5.10 Concluding Remarks

The goal of optical remote-sensing is to derive quantitative information on the types of substances present in the water and on their concentrations. The behavior of light is greatly affected by the nature of the medium through which it is passing. The inherent optical properties (IOPs) of water bodies are solely the properties of the medium and are fundamental to the understanding of the optical environment. Optical models that relate water quality parameters, IOPs to AOPs can play a significant role for monitoring water bodies, to estimate missing water quality parameters and to minimize the environmental influence on remotely sensed data. The integrated optical modeling approach is considered as a potential tool for monitoring and modeling water bodies. The optical modeling method and techniques is a useful tool for collection of information over large areas and has also been used for monitoring river water carrying heavy suspended sediments in the absence of ground truth data.

CHAPTER 6

APPLICATION OF MULTISPECTRAL REMOTE SENSING : A CASE STUDY OF INDUS RIVER – PAKISTAN

6.1 Introduction

Most of the problems in water resources and environmental sector are common in arid & semi-arid regions of the world. These are generally: water quality and quantity problem, soil erosion, inadequate storage and sedimentation in water bodies. It is universal truth that meager resources compel for their better utilization and preservation. Soil and water resource protection is crucial for productive and sustainable economies. Soil provides ecological capacity by delivering a range of functions including food and fiber production, biodiversity, environmental services, landscape and heritage, raw materials and physical platforms for the built environment. High concentrations of suspended sediment in river waters are a critical element in the economic feasibility of a project and could shorten the useful life of many reservoirs & dams. Assessment of suspended sediment volume carried by a river is vital for an adapted water resources management strategy. South Asia is one of the regions in the world where soil erosion by water and wind is a severe problem (Singh, 1992). The problem of soil erosion and sedimentation is more severe in developing countries, where the watershed management is not considered in the past. The design and sizing of many hydraulics structures require a pre-determined knowledge of the quality and quantity of suspended sediments carried by the water. This necessitates a comprehensive study of sediment carrying capacity of streams, the quantity of total sediment deposited in reservoirs, the particle size of the sediment, and the quantitative relation of sediment to the flow of water. Distribution of the suspended sediment concentration in the rivers is the key issues for analyzing the intensity of erosion in upstream watershed and its adverse effect on the downstream areas.

The loss of storage capacity in the United States reservoirs cost $ 100 million annually in dredging and related mitigation efforts (Julien, 1995). The most often cited estimates of the global suspended sediment discharge to the ocean range between 15×10^9 $t\cdot yr^{-1}$ to 20×10^9 $t\cdot yr^{-1}$ where the best estimate may be about $20\times\times10^9$ $t\cdot yr^{-1}$ (Walling, 1996), of which over 25% is considered to be trapped by dam reservoirs (Vorosmarty, 1997) . Identification of these sources and quantifying their effect is a major task for environmental technologist and water resources planners (Bhargava, 1991). In order to cope with demands for new information to underpin the development of sediment control and management strategies, particularly in those areas where sediment problem have attracted attention, there is dire need to explore new sources of data to complement traditional data collection techniques.

Arguments for the application of remotely sensed data for water resources and environmental monitoring is compelling. Global problems require global solutions and these in turn require information on a global scale. Information is the combination of knowledge and observation. Earth observation data must be combined with knowledge in order to improve the scientific understanding of the entire earth system. Earth observation from space offers unique opportunities to obtain information regionally and globally.

Remotely sensed data offer a unique perspective and are imperative for management and monitoring of earth resources from local to regional to global scale. Remote sensing techniques for monitoring coastal and inland waters have been under development since the early 1970's. The range of optical water quality properties that can be successfully estimated by remote sensing include total suspended matter, chlorophyll-a, suspended sediments, turbidity, colored dissolved organic matter (CDOM), and vertical attenuation coefficients of downwelling (K_d) and upwelling light. Remotely sensed data provide synoptic indication of the distribution of water colour and its associated physical properties in water bodies. The goal of environmental remote sensing is to obtain information on the nature and properties of the objects on the earth's surface and in the atmosphere. The common approach is to use the data from sensors which record the electromagnetic radiation reflected or emitted from those objects (Danson, 1995).

The application of remote sensing in water resources research and management mainly lies in one of the three categories: mapping of watersheds and features, indirect hydrological parameter estimation and direct estimation of hydrological variables (Melesse, 2007). Many applications in water resources and environmental monitoring require frequent coverage of the same area. With the availability of large volumes of remotely sensed data from multiple sensors, the application of remote sensing to water resources and environment has been increasing in recent years. The state-of-art satellite sensors are widely used in environmental applications, natural resources monitoring and management. The data from multiple sensors are acquired in multiple resolution (spatial, spectral, radiometric), multiple bandwidth, and in varying conditions, they need to be harmonized and synthesized before being used (Thenkabail, 2004). The remotely sensed techniques for accurate monitoring of water quality parameters depend on the substance being measured, its concentration, influencing environmental factors, and the sensor characteristics. Remote sensing provides a platform for monitoring and modeling of seasonal suspended sediment distribution patterns, which is not possible though traditional measurement campaign. The rate of scattering and backscattering from water body is a function of size, texture characteristics of the suspended sediments and is strongly affected by other optically active water components.

6.2 Objectives

The prime objective of this section of the thesis is to develop suspended sediment monitoring system with necessary data and accuracy by means of remotely sensed data. The feasibility and application of remotely acquired data is comprehensively analyzed. The model for estimation of suspended sediments was developed by integrating multispectral data (ALOS/AVNIR-2, ASTER and SPOT data), bio optical models and in situ suspended sediments data. To investigate the distribution of sediments at Tarbela dam, Indus River, Pakistan, integrated bio optical modeling inversion approach is suggested.

6.3 Research Study Area: Tarbela Dam, Indus River, Pakistan

6.3.1 Hydrology & water Resources

Currently, Pakistan is a water deficit country according to the criteria developed by John Waterbury, 1979. Pakistan is a country, which mostly comprises of arid, semiarid

and hyper arid regions and a belt of humid climate along the foothills of Himalayas. The mean annual rainfall distribution in Pakistan has a broad regional variation ranges between 125 mm in Southeast to 750 mm in the Northwest. About 70 percent of the annual rainfall occurs in the months of June to September. Indus delta represents the Climate arid tropical marine; mean daily maximum summer temperature between 34-40^{o}C and winter temperature between 19-20^{o}C; mean monthly summer rainfall 75 mm and winter less than 5 mm; relative humidity 67-68% in the morning and 30-35% in the afternoon. Acute shortage of fresh water is expected in the future due to imbalance between water availability and demands. Future prosperity will depend to a considerable extent on how well we harness and conserve freshwater resources.

The surface water resources of Pakistan mainly consist of flows of the Indus River and its tributaries. The catchment area extends over four countries-China, India, Pakistan and Afghanistan. The Indus rises in Tibet, in the snow-clad Kailas range of the Himalayas, about 5,500 m above mean sea level. The river slope from the headwaters to Attock is approximately 1/ 300; from Attock to Mithankot it is 1/4,000; and from Mithankot to the sea it averages 1/7,000 (Murakami M.,1995). The Indus River alone provides 65% of total river flows, while the contribution of River Jhelum and Chenab is 17 and 19 % respectively. The peak flow months are June to August during the Monsoon season. The flow during the summer season is 84% and during winter is 16% (Ishfaq A. 2002). During the 20th century, the Indus Basin irrigation system has been developed into one of the largest continuous and comprehensive irrigation systems of the world.

Table 6.1. Present Water Resources of Pakistan

Description	Quantity (10^9 m^3)
Surface water	169
Groundwater availability	46.7
Outflow to Sea (27-year average)	45
Canal diversions	130.4
Storage Reservoirs (Tarbela, Mangla & Chashma)	
a. Live Storage Capacity (Designed)	19.3
b. Storage Capacity (Year 2000)	16.6

6.3.2 Soil erosion & sedimentation

Soil erosion is a three phase process consisting of:

i) Detachment of individual particles from the soil mass. Rainfall impact of the soil is the most important detaching agent.

ii) Transport by erosive agents such as running water and wind. The river water caries large amount of suspended sediments brought by the feeding streams.

iii) When the water velocity is low a third phase, deposition occurs. The horizontal and vertical distribution of suspended sediments depends upon that of the particle size, shape, and density.

Sediment movement in rivers and reservoirs mainly depends on water flow and sediment characteristics. In a reservoir, there are two main patterns of flow motion: backwater flow and quasi-uniform flow. Under the condition of backwater flow, the water depth increases longitudinally and the flow velocity decrease accordingly. Sediment transport may have two patterns. One is sediment transport under open channel flow, where sediment particles diffuse to the whole section. As the flow velocity decreases longitudinally, deposition takes place. Such a kind of deposition is called back water deposition. The other is sediment transport by density current, which is formed by heavy sediment load with fine particles, and moves along the natural rivers. When the incoming sediment load is different from the sediment transport capacity of the flow, longitudinal deposition or erosion will occur (IRTCES, 2005).

Table 6.2 Land area affected by soil erosion by water and wind in South Asia (Lal, 2001)

Country	Water Erosion (Mha)	Wind Erosion (Mha)	Total land Area (Mha)
India	32.8	10.8	328.8
Iran	26.4	35.4	165.3
Pakistan	7.2	10.7	79.6
Afghanistan	11.2	2.1	65.3
Nepal	1.6	0	14.7
Bangladesh	1.5	0	14.4
Sri Lanka	1.0	0	6.6
Bhutan	0.04	0	4.7
Total	**81.74**	**59.0**	**679.4**

Sediments, which fill lakes, reservoirs, and dams, are one of the most important environmental problems throughout the world (Table 6.3).

Table 6.3 Sediment data of World Rivers (WAPDA, 1991)

River/Country	**Catchment Area (1000*km^2)**	**Annual Runoff (km^3)**	**Annual Sediment load (Million Tons)**	**Average Sediment Concentration (kg/m^3)**
Yellow/China	752.4	42.6	1,600	37.5
Ganges/ India, Bangladesh	955	344	1,451	3.91
Bramaputra/ Bangladesh	666	384	726	1.89
Yangtze/China	1700	933.6	490	0.52
Indus/Pakistan	969	175	470	2.68
Amazon/USA	5770	5710	363	0.06
Irrawady/Burma	430	427	299	0.70
Missouri/USA	1370	616	218	3.54

The rivers of Pakistan carry much sediment either as bed load or in suspension. Sedimentation in the three major reservoirs – Tarbela, Mangla, and Chashma in Pakistan is going to deplete their storage capacities by over 25 % by the end of the year 2010 (Kahlown, 2001). Much of the land in Pakistan is highly erodible because of sparse vegetal cover, steep slopes, and non-resistant soils and rocks. The Indus River is one of the largest sediment producing rivers in the world. The main source of sediment is from the glacial landscape and erosion from steep sided barren slopes. Melting glaciers and falling rocks leave behind large quantity of sediments each year.

6.3.3 Study Area

The Tarbela Dam is the largest earth and rockfill dam of the world across the river Indus in Pakistan. The total length of the Indus is about 2,900 km. The catchment area of the Indus River is 969000 km^2 with an annual runoff of 175 billion m^3 and annual sediment load of 470 million tons. Above Tarbela the catchment area is 169,650 km^2 with annual sediment load of 287 tons. Although the catchment area above Tarbela Dam accounts for only 17.5 percent of the total catchment area of the Indus, the annual sediment load above Tarbela accounts for 66 percent of the total sediment load of the river. The Indus River is one of the largest sediment producing rivers in the world. The main source of sediment is from the glacial landscape and erosion from steep sided barren slopes. Melting glaciers and falling rocks leave behind large quantity of sediments each year. The sediment load varies with discharge, seasonal differences and conditions of the watershed and river morphology. The river basin and catchment areas have significant effect on the grain size distribution of the suspended sediments. The river flow regime of the Indus is consistent from year to year.

Tarbela dam plays vital role in the national economy of Pakistan and its normal operation is imperative for the country. The length of Tarbela dam reservoir is 97 km with an area of 260 km^2. The large amount of sediment load carried by the Indus has shown a great threat to the dam due to serious sediment sedimentation in the reservoir. Heavy sediment load brought by the Indus River and its tributaries is major problem in the study area. About 94% of the catchment area of the Indus river is located in semi-arid to hyper-arid environment. A very large portion of the total sediment load is carried by the river during the summer time. The predicted rate of sediment inflow was 0.294 BCM (Billion Cubic Meter) per year meaning that the dam would silt up to 90% capacity in 50 years and thereafter continue to provide only about 1.2 BCM of live storage.

Table 6.4 Flow and sediment loads of the Indus catchment to Tarbela (WAPDA, 1998)

	Upper Catchment (Non-monsoon area), %	**Lower Catchment (Monsoon area), %**
Catchment Area	94	6
Annual flows	92	8
Annual sediment loads	96	4

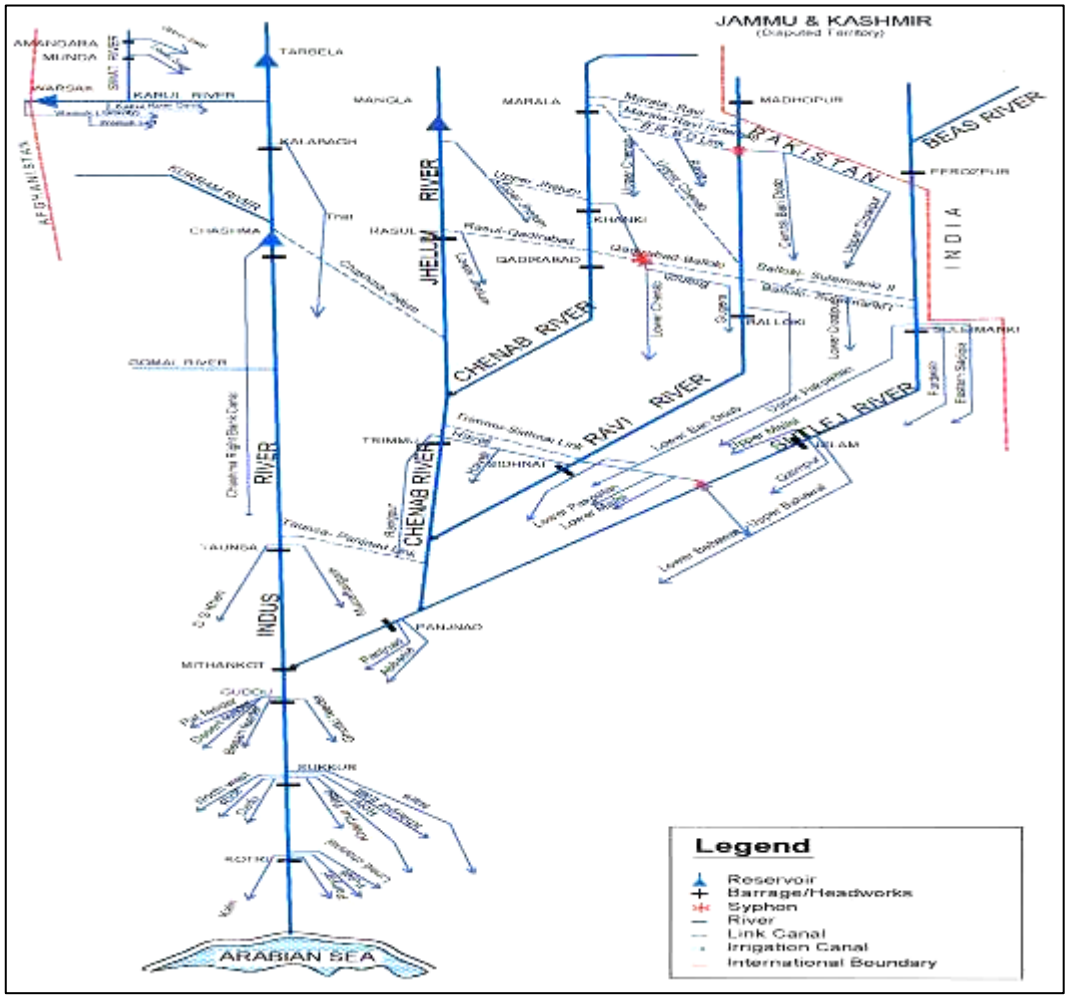

Figure 6.1 Schematic Diagram of Indus Basin Irrigation Network

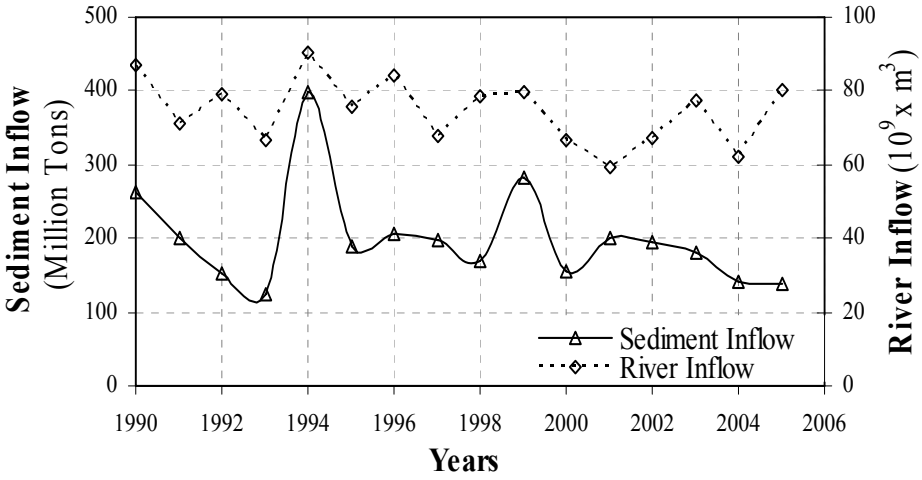

Figure 6.2 Annual sediment load computed from hydrograph survey

6.4 Hyperspectral SSC Model development –Lab Experiment

In order to investigate the effect of different concentration of suspended sediments on reflectance signals, experiment was performed in the laboratory. The spectral reflectance of collected soil samples from research study area with varying concentration of SSC were investigated in detail. The experiment was performed in the laboratory in a dark room under controlled conditions. Firstly the reflectance of dry soil with contact probe was collected. The spectral reflectance of water with varying concentration of suspended sediments (0 to 1000mg/l) was collected by means of 1 degree FOV.

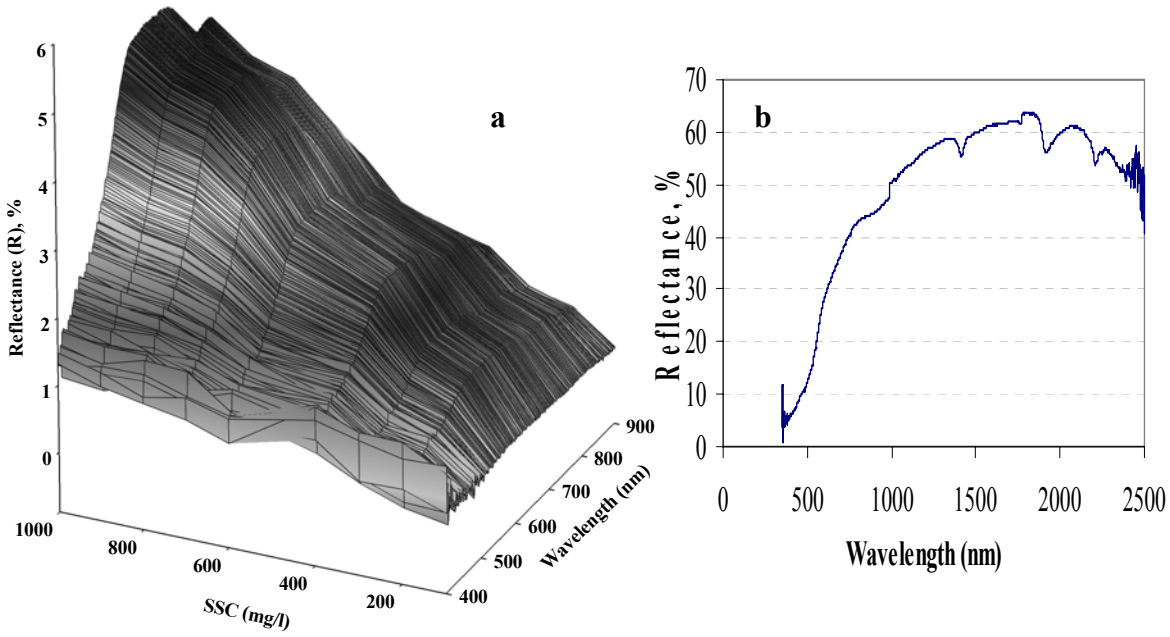

Figure 6.3a): Spectral reflectance of water with varying concentration of suspended sediments b): Spectral reflectance of collected dry soil

The reflectance increase with the increase in suspended sediments concentration and the peak reflectance shifts towards longer wavelength. To investigate the field application of collected hyperspectral reflectance, the acquired lab reflectance with varying concentration of suspended sediments was integrated to ALOS/AVNIR-2 band widths as shown in figure 6.4-a. The combination of ALOS/ AVNIR-2 bands 3 and 4 was selected to demonstrate the relationship between reflectance and suspended sediment concentration because SSC is strongly correlated with red and NIR domain. The 2 band multiplicative approach minimizes the influence of other parameters on spectral reflectance. The regression model was developed between the developed and SSC. As depicted in the figure 6.4-b a good correlation exists between the simulated data and SSC. The developed reflectance model $(B_4+B_3)/ (B_3/B_4)$ derived from series of laboratory and a field experiment is the best predictor of SSC. The subscripts 4 and 3 represent band 4 and band 3 of ALOS optical sensor AVNIR-2. The term (B_4+B_3) takes account of spectrum features of low and high concentrations of the suspended sediment. The term of (B_3/B_4) might reduce the chlorophyll interference to the low suspended sediment concentration.

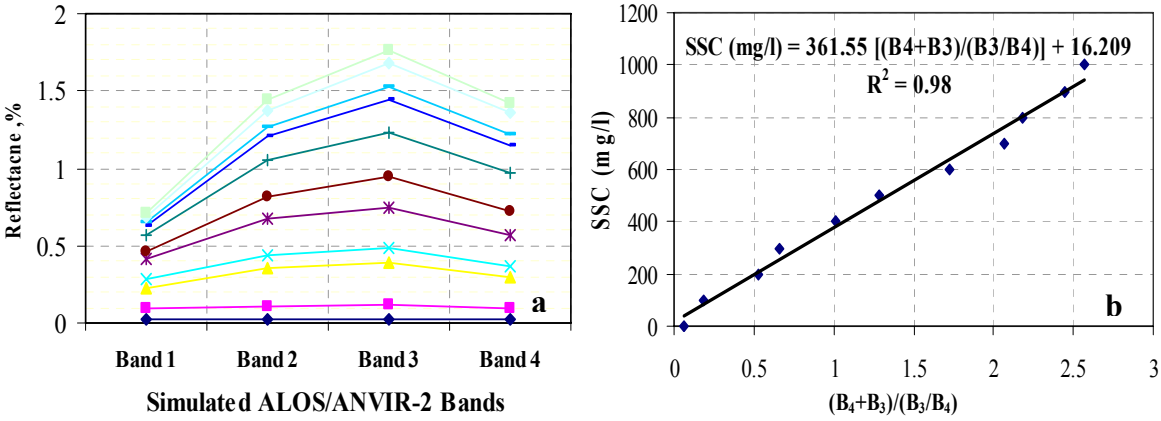

Figure 6.4 a): Relationship between simulated ALOS/AVNIR-2 bands and spectral reflectance; b): Relationship between SSC and developed reflectance model

6.5 Application of Multispectral Remotely Sensed Data for SSC Model Development

6.5.1 Introduction

Satellite and airborne optical sensors can provide the high spatial and temporal resolution data that is considered as a potential tool for monitoring and modeling inland and coastal waters. Satellites (ALOS, SPOT and ASTER etc.) have actual and potential role for assessment of water resources and to monitor water quality parameters in surface waters from space platforms. The ultimate justification for the effort and expense involved must lie in the applications envisaged. However, a successful application of remote-sensing in monitoring and modeling of water bodies demands for suitable sensors as well as complementary in situ experiments that are carefully designed.

Satellite-based remote sensing provides one option for relatively low-cost assessment of suspended sediment concentration in surface waters (Ritchie et al., 1987 & 1988). In the study of larger rivers like Indus River, Pakistan, in situ measurement can provide data at discrete points. However, the logistics and expense of traditional data collection methods can rarely produce the synoptic coverage, resolution and temporal detail necessary to delineate the water bodies. One solution of this problem can be remotely sensed data. The satellites can provide repetitive and synoptic coverage. Remotely sensed images provide regional coverage with the potential for monthly to daily coverage.

Current in situ techniques for measuring suspended sediments are time-consuming and do not give a synoptic view of a water body or, more significantly, a synoptic view of different water bodies across the landscape. There is dire need to develop technique and monitoring system for efficient and effective monitoring of water resources with significant suspended sediment problems so that soil conservation efforts can be concentrated in those watersheds with the most serious erosion and sediment yield problems. Ritchie and Cooper, 1988 pointed out that an algorithm for relating remotely sensed data to the sediment load developed for one year was applicable for several years.

Once developed, an algorithm should be applicable until some watershed event changes the quality (size, color, mineralogy, etc.) of suspended sediments delivered to the lake.

6.5.2 ALOS sensors/products

The Advanced Land Observing Satellite (ALOS) was launch on 26 January 2006. The Advanced Land Observing Satellite (ALOS) has two optical sensors called: Panchromatic Remote-sensing Instrument for Stereo Mapping (PRISM) for digital elevation mapping, and Advanced Visible and Near Infrared Radiometer type 2 (AVNIR-2) for precise land coverage observation. The third sensor called L-band Synthetic Aperture Radar (PALSAR) for day-and-night and all-weather land observation. The Advanced Visible and Near Infrared Radiometer type 2 (AVNIR-2) is a visible and near infrared radiometer for monitoring regional environment (land, coastal zones, and water bodies etc.). The AVNIR-2 is a successor to the AVNIR onboard the Advanced Earth Observing Satellite (ADEOS) launched in August 1996.

Table 6.5 ALOS/AVNIR-2 Characteristics

General features	Characteristics	
ALOS Characteristics		
Launch date	January 26, 2006	
Launch site	Tanegashima Space Centre, Japan	
Altitude	691.65 km	
Repeat cycle	46 days	
Design life	3-5 years	
AVNIR-2 Characteristics		
No. of bands	4	
Wavelength	Band 1	420-500 nm
	Band 2	520-600 nm
	Band 3	610-690 nm
	Band 4	760-890 nm
Spatial resolution	10 m	
Swath width	70km	

6.5.3 Data processing & analysis

Three ALOS images acquired on 6 October, 2006 were analyzed in this research study. These images encompass the Indus River, Tarbela Dam and surrounding area in the Pakistan. The month of October is the end of the high discharge and flood period in the Indus River. For each band the image digital numbers (DN) were converted to top of atmosphere (TOA) spectral radiance (L) by using the following equation.

$$L = DN * a + b$$

Where L is radiance ($Wm^{-2}Sr^{-1}\mu m^{-1}$), "a" is gain and "b" is offset. The vale of a and b can be retrieved from the scene header file. The TOA spectral radiance is converted into TOA reflectance for each band by using the following equation (Vermote, 1996).

$$R(i) = \frac{\pi L(i)}{\mu_s E_s(i)}$$

Where i = 1,2,3 and 4; $\mu_s = \cos(\theta)$, θ is the solar zenith angle, E_s ($Wm^{-2}\mu m$) is the solar TOA irradiance. The solar spectral irradiance values are not provides with the product. It can be computed using article from Thuillier 2003 and are as follow;

Table 6.6 Spectral Solar irradiance

Band	Band 1	Band 2	Band 3	Band 4
Central wavelength (nm)	460	560	650	820
Solar spectral irradiance $Wm^{-2}\mu m^{-1}$	1943.3	1813.7	1562.3	1076.5

The TOA measurements are then corrected for atmospheric effects. A reliable and robust atmospheric correction procedure was required to ensure that pixel values were comparable between a time series of images. The atmospheric correction is the process of retrieving the surface radiance and surface reflectance from the satellite radiances. The dark pixel subtraction technique was used to remove or reduces the atmospheric influence on water-leaving light signals. This approach was applied and confirmed by Hadjimitsis et al. (2004) in a study comparing a range of atmospheric correction procedures for reservoir water quality monitoring with Landsat, to provide a reasonable correction for cloud-free scenes. Hadjimitsis reported that systematic and robust atmospheric correction procedures of generic value remain problematic when working in inland waters with high spatial resolution platforms such as Landsat. He suggested that from an operational point of view, the darkest pixel approach was preferred over more sophisticated techniques that require atmospheric and meteorological data.

A darkest pixel subtraction approach is simple and feasible and may apply when no ground truth data corresponding with the image is available. The dark pixel subtraction is based on the assumption that an effective black body exists in the image, resulting in a pixel value of zero (Tyler, 2006). The minimum pixel value for that point in each band is because of atmosphere and subtracted from the corresponding band. In the upstream area of the Indus River, a small isolated clean water pond located in the mountains with the minimum pixel values was considered for the purpose of atmospheric correction. The resultant reflectance is the derived reflectance at the surface and it is atmospherically corrected. The reflectance value at the dam and along the river reach was computed for the 4 four band of AVNIR-2 sensor.

It was observed that the reflectance value along the river reach vary from point to point and strongly depends on the amount of suspended sediment concentration.

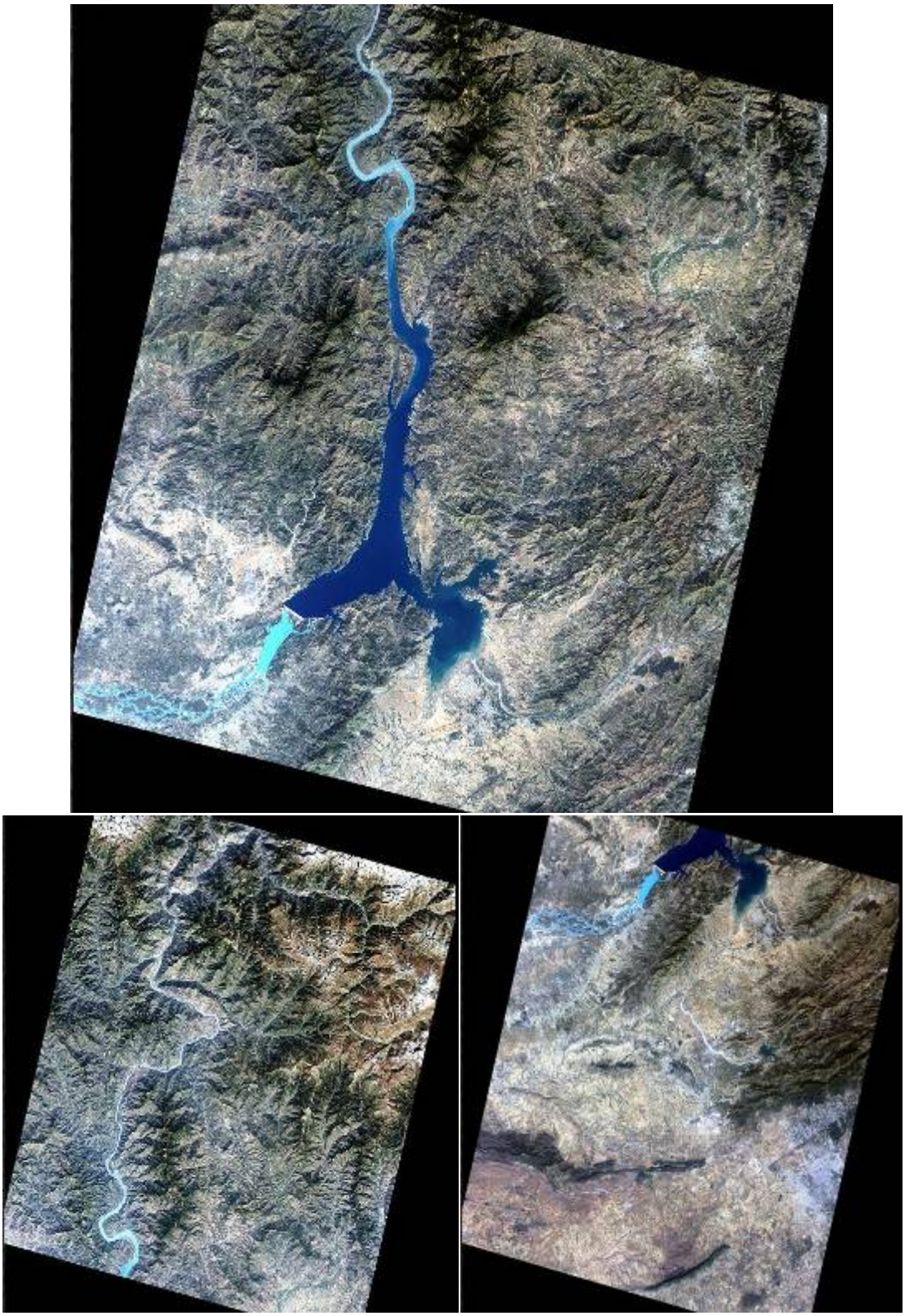

Figure 6.5 ALOS/AVNIR-2 Image of Tarbela Dam & Indus River, Pakistan
Acquisition Date: October 10, 2006

However, it was seen that the reflectance value near the dam body and 30 km upstream shows a quite different behavior with more value in the NIR domain. The rational is because the water velocity becomes slow in the reservoir near the dam body and the floating material may cause the different response of spectral signature acquired by the sensor. The reflectance along the river reach is illustrated in the figure 6.6.

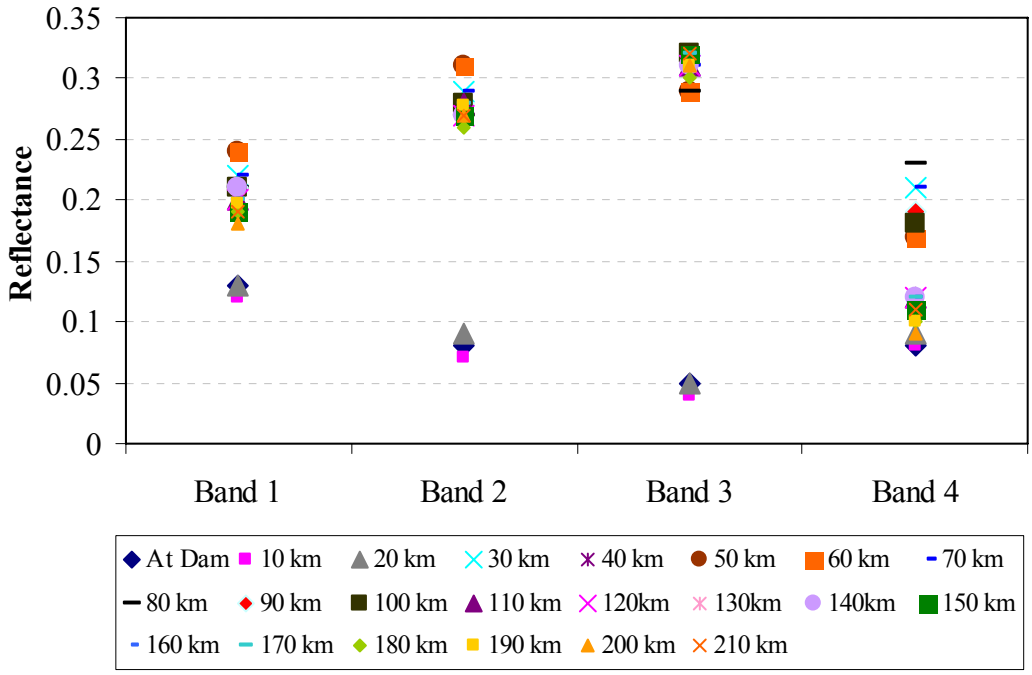

Figure 6.6 Reflectance value along the Indus River

The field application of remotely sensed data demands for ancillary field data. However, the problem in the research study area is that the suspended sediment concentration at only one sampling point 67 km upstream of the dam is known. There is no other data available for the research area. In order to cope with lack of data problem one option is to apply the laboratory based model developed under controlled conditions for the quantification of suspended sediments. It is worth mentioning that that the lab based model is not the solution of the problem. The field conditions are absolutely different from the laboratory conditions. In such situations only the remote sensing provides solution to engineers and resource managers.

6.6 Optical Model Inversion Techniques

To develop the monitoring system by means of remote sensing, the collection of appropriate ancillary field data sets is as important as the remotely sensed data. However, the model inversion technique may solve the problem of lack of data. The model inversion technique is proposed to estimate the suspended sediment along the river reach. Depending on the AVNIR-2 data and minimizing the difference between the modeled and actual AVNIR-2 reflectance value, the suspended sediment was computed. The basic concept is to consider AVNIR-2 reflectance value as the true values and minimize the

difference between modeled and ALOS-AVNIR-e data by changing the suspended sediment concentration.

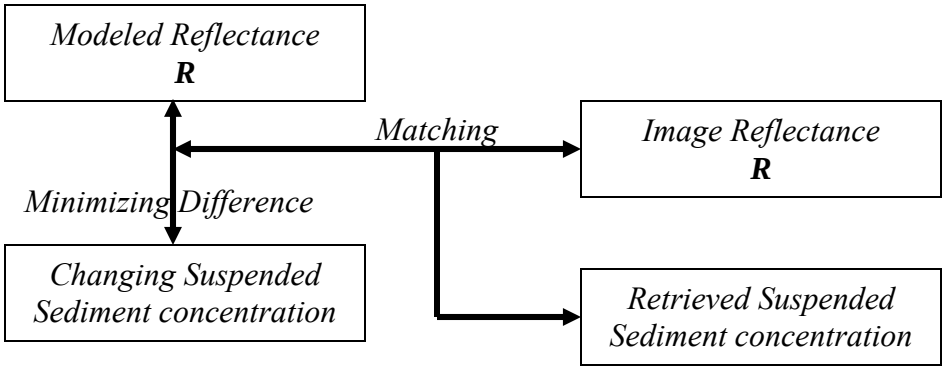

Figure 6.7 Concept diagram of model inversion technique

The environmental conditions are unknown. The only parameter known is suspended sediment concentration at one point. It is assumed that environmental factors have no effect on the spectral signatures. The above and below surface spectral reflectance is considered to be the equal. As illustrated in the chapter 3 the above and below surface spectral pattern is same and the minimum difference is in the red and NIR domain. The wavelength range of interest is red and NIR domain. By adopting the model inversion technique the suspended sediment along the river course is estimated and the proposed method is found to be effective and efficient. Often it is thought that these satellite sensor data are useless, because there is no concurrent massive in situ sampling available. The proposed technique makes remote sensing application for water quality monitoring much more flexible as archives of remote sensing data may now be accessed and processed to produce reliable concentration maps.

6.6.1 Modelled spectral reflectance

Mobley 1994 was prescient in stating that the development of remote sensing inversion algorithms for use in Case 2 waters scarcely has begun. As with other facts of the hydrologic optics of such waters, the remote sensing of case 2 waters will provide challenging research problems for a generation of scientists. In an effort to deal with case 2, turbid water the remote sensing spectra was modeled. The relationship between reflectance *R*, inherent optical properties (IOPs) of the medium, absorption coefficient a(λ) and backscattering coefficient $b_b(\lambda)$ is expressed as Morel 1977:

$$R(\lambda) = f\frac{\mathrm{b_b}(\lambda)}{\mathrm{a}(\lambda)+\mathrm{b_b}(\lambda)}$$

Where f is a coefficient and the commonly adopted value of f is 0.33, which is valid for zenith sun and for large variety of natural waters (Kirk, 1994). In the research study area during the flood season (June-October), the suspended matters in the water are mainly composed of sediments. The presence of chlorophyll in the water is neglected. So, the

absorption and scattering by chlorophyll is not taken in to account. The absorption coefficient a(λ) and backscattering coefficient $b_b(\lambda)$ is written as follow;

$$a(\lambda) = a_w(\lambda) + a_y(\lambda) + a_s(\lambda)$$
$$b_b(\lambda) = b_{bw}(\lambda) + b_{bs}(\lambda)$$

Where the subscript w, y, and s represents water, colored dissolved organic mater (CDOM), and total suspended sediments (TSS). The value of a_w and b_{bw} are taken from Smith and Baker (1981) for the range 400-800 nm.
a_y is modeled as follow;

$$a_y(\lambda) = a_y(\lambda_o)e^{-k(\lambda-\lambda_o)}$$

where λ_o is 400 nm, $a_y(\lambda_o)$ =0.3 m^{-1} and S=0.014 m^{-1}.

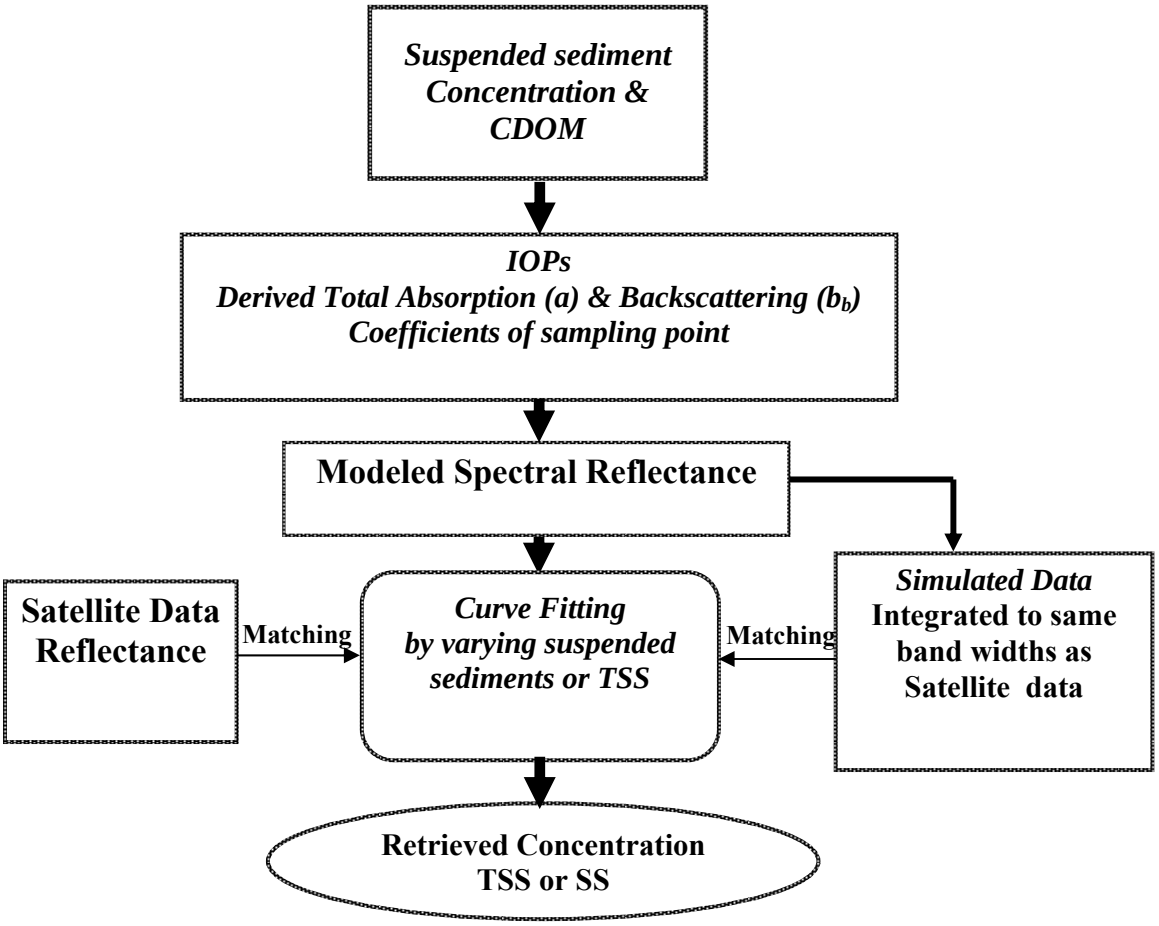

Figure 6.8 Diagram of modeled reflectance spectra development and retrieval of SSC

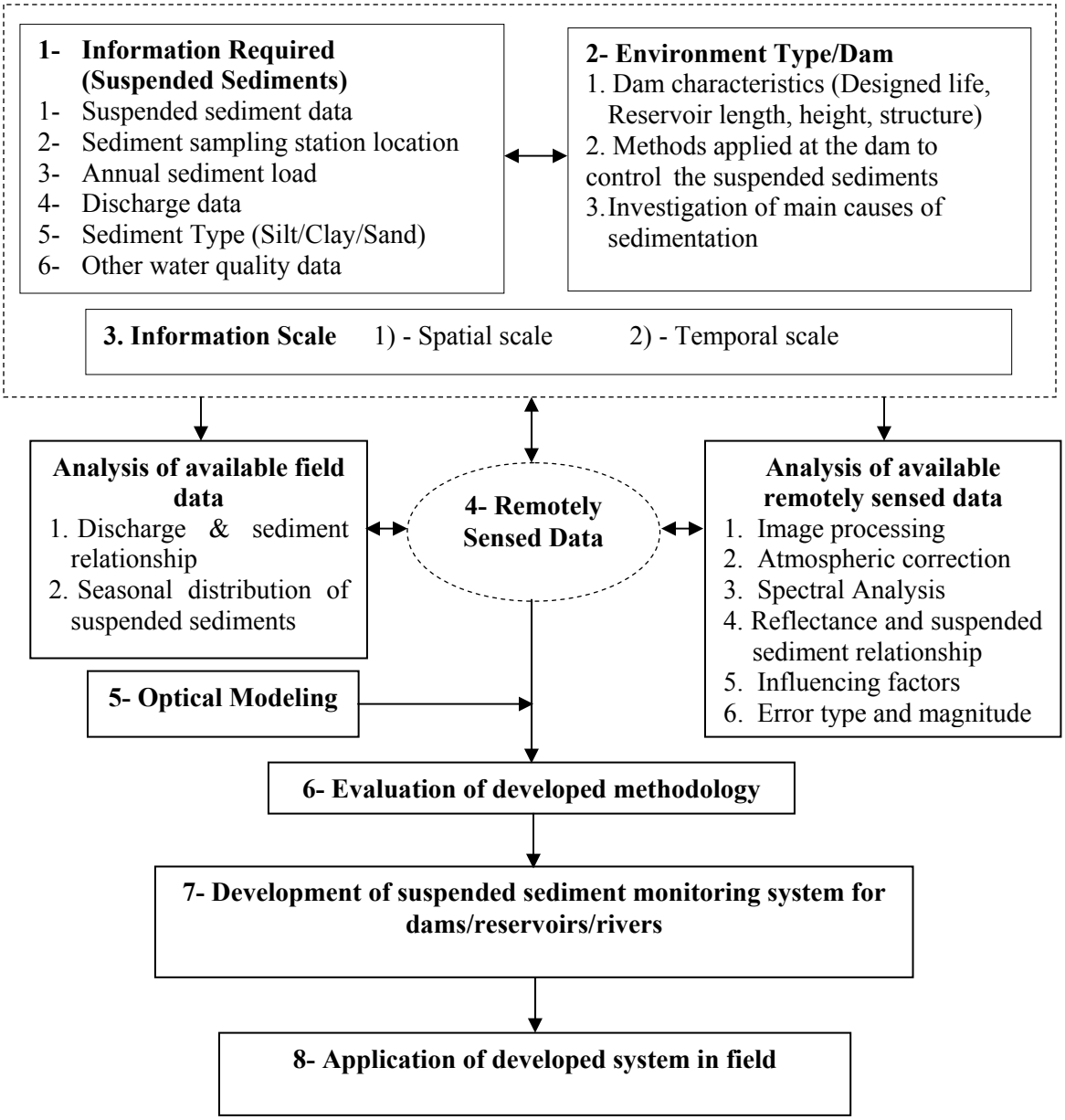

Figure 6.9 Framework for development of suspended sediment estimation model by means of remote sensing

Absorption by sediment is modeled as Buiteveld, 1995.

$$a_s(\lambda) = k_1 C_s^{\,k_2} (\lambda_0 / \lambda)$$

Where k_1 = 0.05, k_2 = 1.1 & λ_o= 400 nm and C_s is suspended sediment concentration (mg/l).

Light scattered by suspended sediment is modeled using the Mie theory. $b_{bs}(\lambda)$ is written as (Forget 1999);

$$b_{bs} = \frac{3S}{2\rho} \cdot \frac{1}{\ln(D_2 / D_1)} \int_{D1}^{D2} Q_{bb} . D^{-2} dD$$

Where C is suspended sediment concentration, ρ is the sediment density = 2600 kg/m^3. Q_{bb} is the backscattering efficiency factor of the suspended particle of refractive index m_r. the refractive index of sediment is taken as 1.125. D_2 and D_1 represents maximum and minimum diameter of the suspended particles (200 - 0.01 μm), which include variety of suspended particles.

The inherent optical properties and developed model is explained thoroughly in chapter 5.

6.6.2 Computation of modeled spectra and SSC by curve fitting

The developed modeled reflectance is simulated to ALOS/AVNIR-2 band widths: Band 1 (0.42-0.50 μm), Band 2 (0.52-0.60 μm), Band 3 (0.61-0.69 μm) and Band 4 (0.76-0.89 μm) for comparison purpose with ANVIR-2 data and computational purpose for SSC estimation. The developed modeled spectra are illustrated in figure 6.10-a and simulated modeled spectra are illustrated in figure 6.10-b.

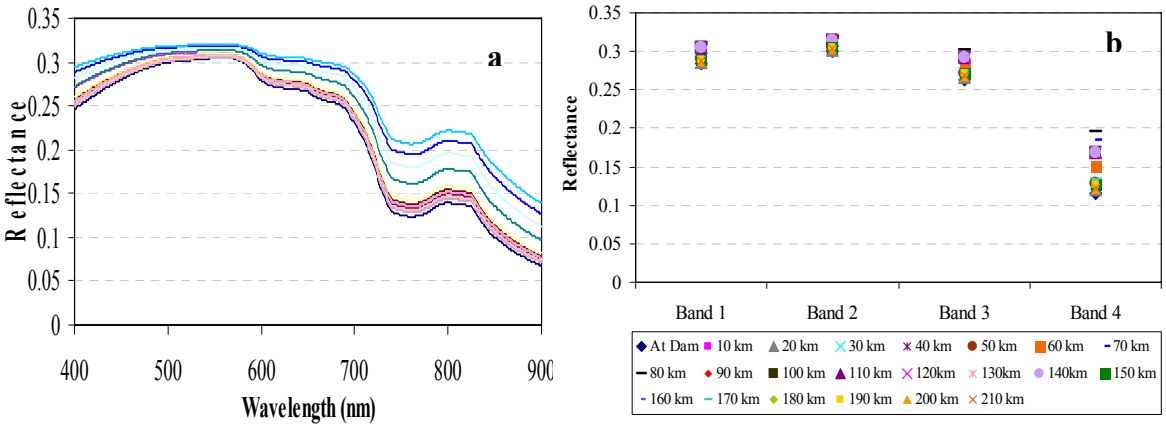

Figure 6.10 a): Developed modeled reflectance spectra along the river; b): Simulated modeled reflectance spectra in AVNIR-2 band widths along the river

The suspended sediment concentration (SSC, mg/l) of 250 mg/l at one point 67 km upstream of the dam body is known. Mobley, 2004 have mentioned different values for colour dissolved organic matters in coastal and estuarine waters. The average value of 0.3 m^{-1} for the river is assumed and kept constant for the along the river. With the SSC of 250 mg/l the modeled spectra was developed and simulated into AVNIR-2 band widths. The simulated modeled reflectance data and AVNIR-2 reflectance data at the same sampling point was compared as shown in figure 6.11. It was observed that the difference between

the two values was minimal in the green, red and NIR domain and overall showed well agreement.

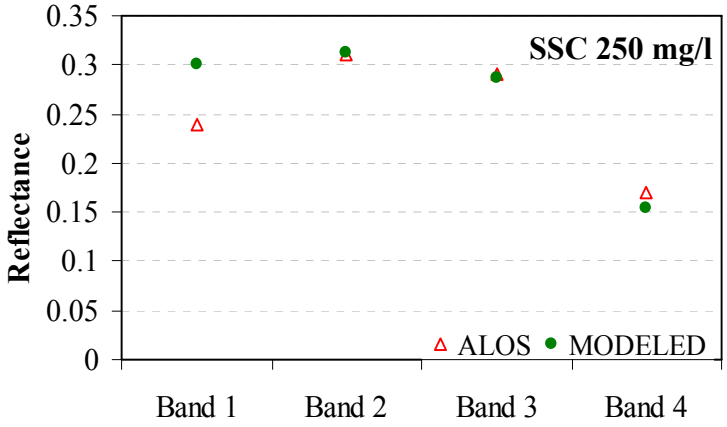

Figure 6.11 Comparison of modeled and ALOS/AVNIR reflectance data

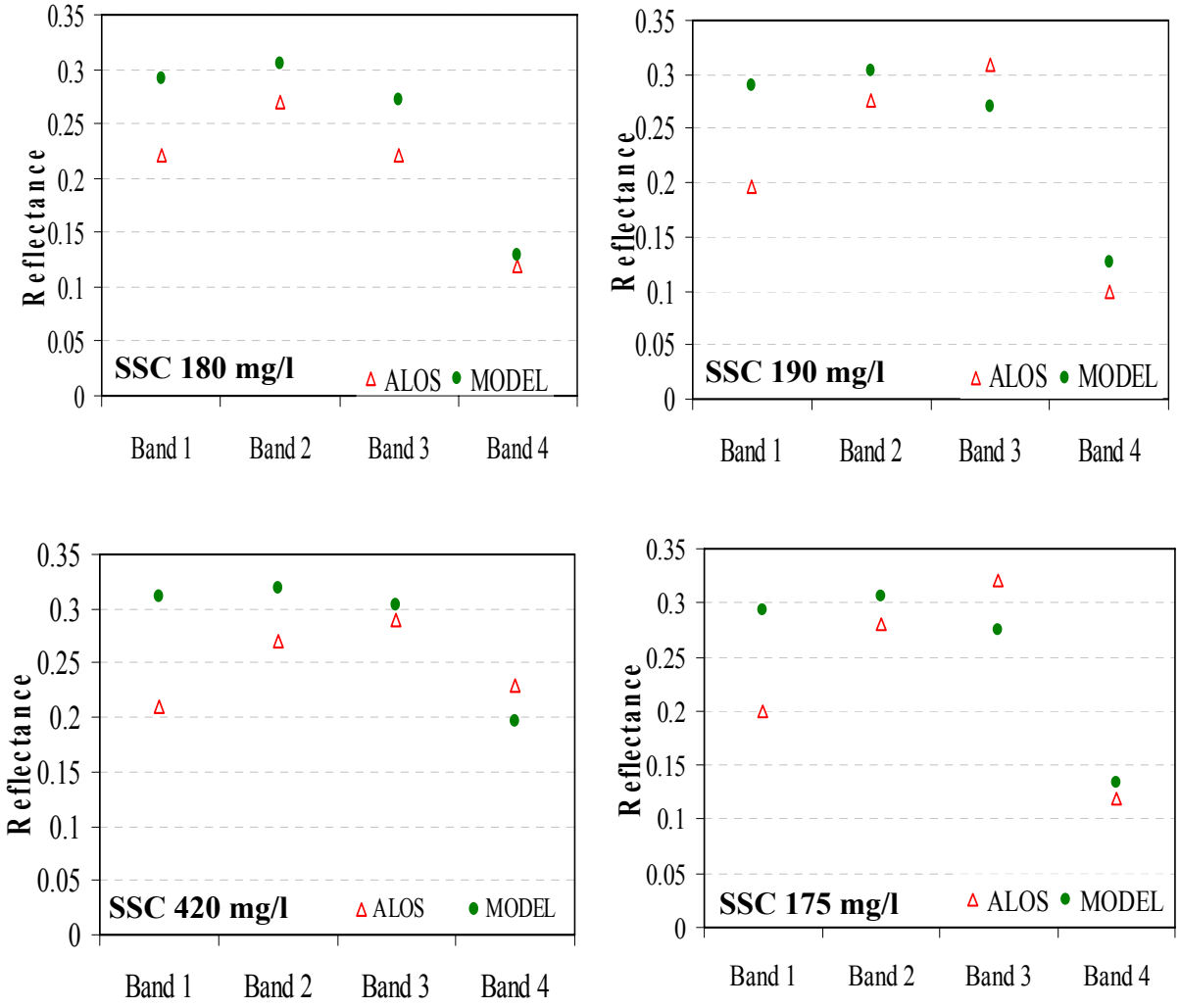

Figure 6.12 Comparison of modeled and ALOS/AVNIR reflectance data at different point along the river reach

However, in the Band 1 (blue domain) the difference was observed. The reason is that the chlorophyll concentration is unknown and chlorophyll has influence in the blue region. By considering the absorption and scattering by chlorophyll, the difference in the Band 1 values may minimized. It proves that the proposed approach is applicable for estimation of suspended sediments in turbid water bodies and amount of suspended sediments can be estimated. Similar approach is envisaged to compute the SSC and modeled spectra along the river reach. The input suspended sediment concentration at other points are assumed or estimated by lab based model and a modeled reflectance spectrum was generated. The developed spectrums were simulated to the same band widths of AVNIR-2 sensors. The procedure consists in minimizing the difference between AVNIR-2 data and modeled reflectance data, by varying the value of input suspended sediment concentration. The output value with minimum difference in the red and NIR domain is the suspended sediment concentration at the point and the resultant spectra represents the spectral shape and magnitude at that corresponding point. By adopting the same approach, the suspended sediment concentration along the river at every 10 km was retrieved. For the purpose of computation and simulation of data the spread sheet was developed in the Microsoft Office Excel. As obvious from the above graphs (Figure 6.12) that the proposed approach is applicable for estimation of suspended sediments in turbid water bodies.

Near the dam body, a different kind of relationship was observed. These were considerable difference in the Band1, Band 2 and Band 3 reflectance data (Figure 6.13). It is observed that the images values showed that the Band 3 value is less than Band 4 value. It helps us to point out that some floating material is on the water surface and may cause the difference in modeled and image values. However, it is worth to mention that the proposed technique is only applicable to turbid water when the image reflectance represents the water bodies. If any floating material is present on the water body, the proposed methodology will not provide accurate results. In such cases, by minimizing the difference in the NIR domain will lead to estimate the SSC in the water body.

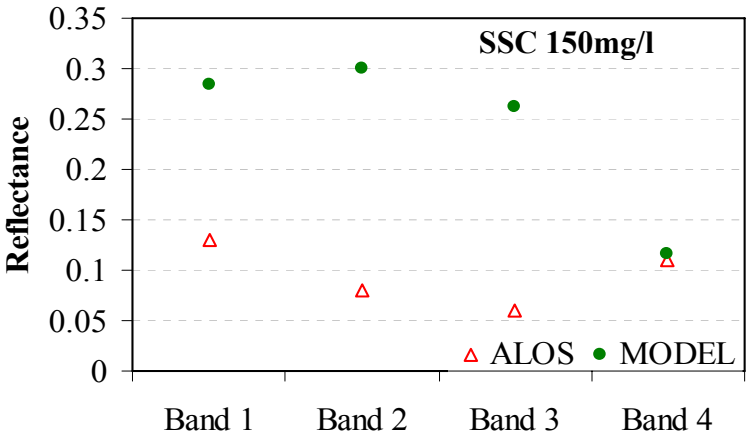

Figure 6.13 Comparison of modeled and ALOS/AVNIR reflectance data near dam 10 km upstream

The developed remote sensing methodology enables retrospective analysis of the AVNIR-2 sensor data of Indus River, Pakistan. By adopting the proposed methodology,

the satellites archives may become a valuable resource for water resources engineers and researchers to remotely monitor the water bodies in the absence of ground truth data. The proposed methodology is considered not to be susceptible to the lack of ground truth data and weather conditions. Based on the develop methodology, the satellite sensor data can become an independent measurement tool and the lack of sophisticated concurrent ground truth observations will not hamper the monitoring and modeling the water bodies.

6.6.3 SSC along the River Reach

The in situ suspended sediment concentration at the monitoring station 67 km upstream of the dam was 255 mg/l (sand 20%, silt 55% and clay 15%). The simulated model bands were compared with ALOS spectral signals of the same sampling station. By adopting the same approach, the suspended sediment concentration along the river at every 10 km was retrieved as depicted in figure 6.14. It is evident from the graphical presentation that the SSC vary along the river and the peak was observed at about 70 km upstream of the dam. In the range from 60km to 90km upstream of the dam, the amount of suspended sediments is significant and tends to decrease towards dam body. The velocity of the river inflow containing sediments decreases upon entering Tarbela reservoir, which reduces the sediment carrying capacity of the river water.

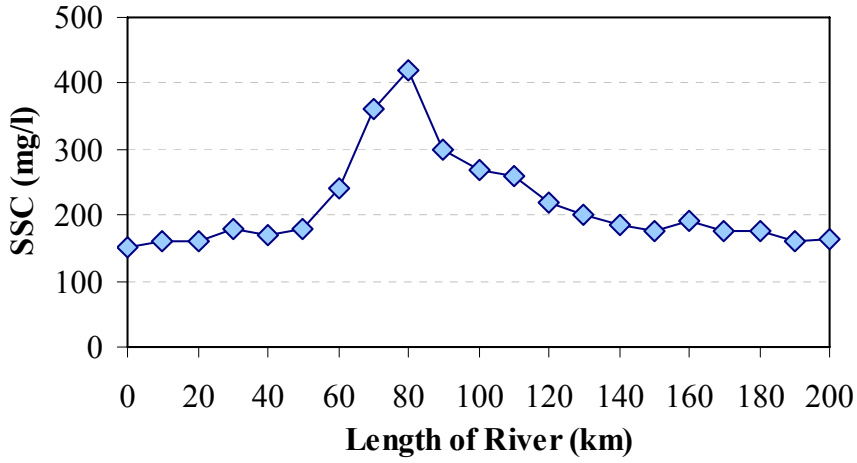

Figure 6.14 SSC along the river reach

The coarse sediment tends to deposit in the upper reaches of the reservoir, while the finer particles travel downstream towards the dam. The graphical demonstration of suspended sediment distribution reveals that heavy sediment load is settling upstream of the dam in the range from 60 km to 90 km, thus reducing the storage capacity of the dam. The periodic examination of the sediment deposits and distribution in the upstream and downstream of the dam is vital to enhance the mitigation efforts for reduction of sediments. The contribution of sediment load is significant from the upstream catchment area. The adopted methodology proved to be useful for quantification of SSC along the river reach. Integrated water resources management in an organized and coordinated manner is the solution to deal with management activities in the upstream area.

6.7 Simulated Image for SSC Model Development

The study of intensive literature demonstrate that the red and NIR region is best predictor of suspended sediment concentration. However, after the years of research the scientists and researchers are unsuccessful to develop global remote sensing model for estimation of SSC. The rational is because the environmental factors influence the remotely sensed signals and limits the utility of the data. Based on the data acquired during experimental work and massive field campaigns, the three band algorithm $(B_4+B_3)/(B_3/ B_4)$ is strongly advocated for the prediction of SSC in water bodies.

The AVNIR-2 Band 3 and Band 4 is considered to be predictor of different concentration and size of suspended sediments present in water bodies. The Band 3 penetrates deeply in water body and represents concentration of different suspended sediments ranging from very fine to medium size. However, the Band 4 the sediments near water surface representing very fine texture. The addition of Band 3 and Band 4 represents the spectrum features of low and high concentrations of the suspended sediments and provides solution for the estimation of different sizes of sediments within the water body. However, the influence of chlorophyll-a concentration on red domain (Band 3) is well documented in literature. The addition of two bands may lead to add the influence of chlorophyll and the resultant reflectance not only represent the suspended sediments but also represent the concentration of chlorophyll. To cope with this situation the resultant Band (B_4+B_3) is divided by the Band 3. This approach helps to minimize the influence of the chlorophyll on SSC. The developed model $(B_4+B_3)/(B_3)$ predict the amount of SSC and the influence of chlorophyll is also minimized.

More precisely, by adopting this approach the influence of chlorophyll is minimized, however, the spectral signals disturb. The actual representative of suspended sediment in water bodies is Band 4. The reason is that NIR region (Band 4) absorbs in the water. If there is any reflectance in this range, it means sediments are present in the water body and caused scattering. To deal with this situation and developing model more accurately, the best approach to multiply with the Band 4. The developed model for estimation of suspended sediments in water body is of following form:

$$(B_4 + B_3)/(B_3/B_4)$$

$$\frac{(B_4 + B_3)}{B_3} \times B_4$$

$$\left[\frac{B_4}{B_3} + 1\right] \times B_4$$

For the estimation of total suspended matter (TSS), it is proposed that the combination of 3 band (Band 4, Band 3 and Band 2) is best predictor of TSS. Model for estimation of TSS is developed in chapter 4 and the usefulness of Green domain is explained in detail. The model for prediction of TSS by using multispectral data is as below:

2 Band Model $(B_4 + B_3)/(B_3/B_4)$

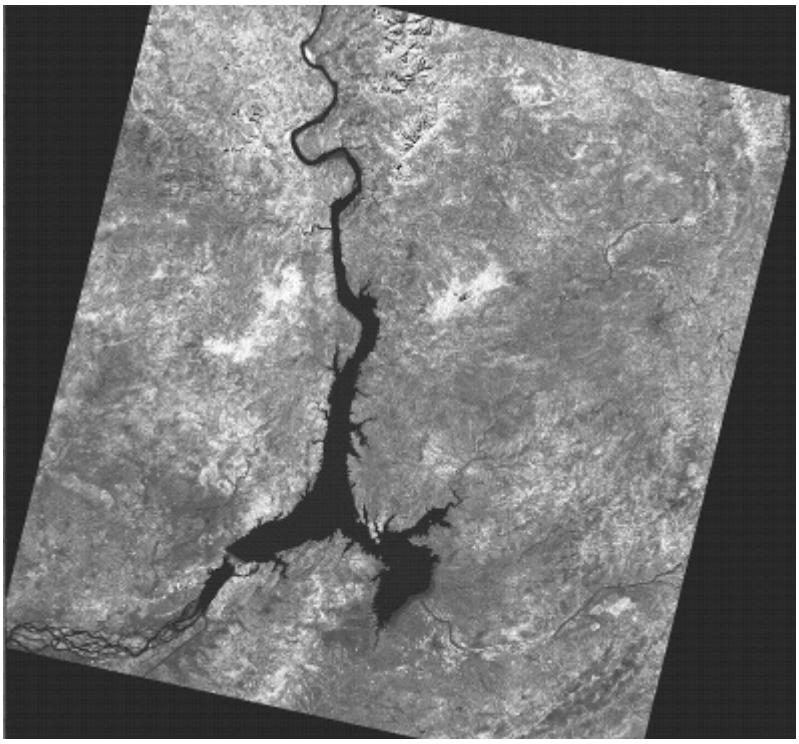

3 Band Model $(B_4 + B_3)/(B_3/B_2)$

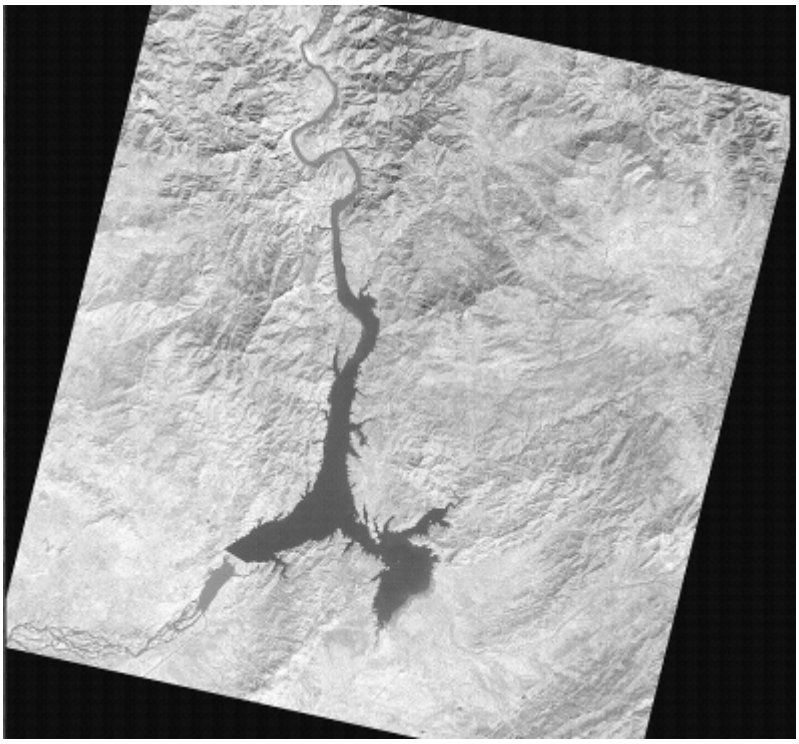

Figure 6.15 Simulated AVNIR-2 Images for SSC model development

$$(B_4 + B_3)/(B_3/B_2)$$

$$\frac{(B_4 + B_3)}{B_3} \times B_2$$

$$\left[\frac{B_4}{B_3} + 1\right] \times B_2$$

The simulated image was developed by adopting 2 bands and 3 bands algorithms by using ENVI 4.3 image processing software. The simulated images are shown in figure 6.15. The reflectance value of simulated image was plotted along the river reach is shown in figure 6.16.

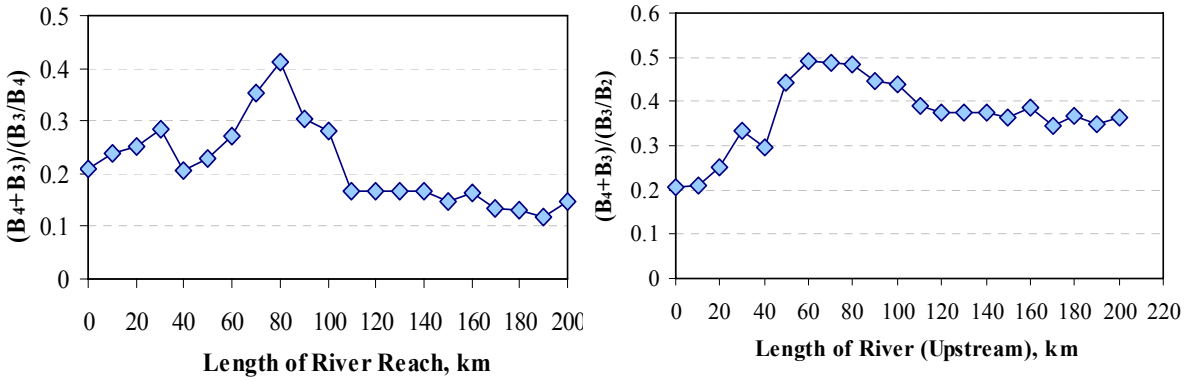

Figure 6.16 Simulated reflectance values along the river reach

6.7.1 SSC model development

Regression model was developed in order to quantify the suspended sediment along the river. As depicted in the figure 6.17, the correlation coefficient of 0.77 was obtained by applying the combination of two band model approach.

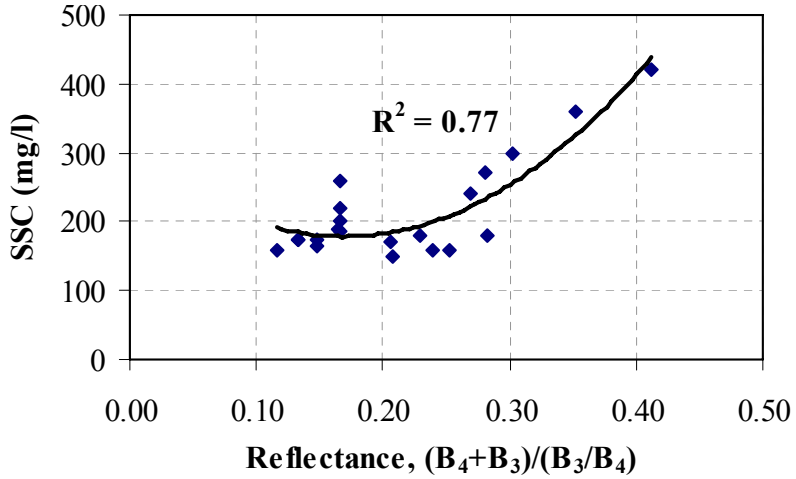

Figure 6.17 Relationship between SSC (mg/l) and reflectance

The developed model is of the following form;

$$SSC\ (mg\ /\ l) = m\left[(B_4 + B_3)/(B_3 / B_4)\right]^2 - n\left[(B_4 + B_3)/(B_3 / B_4)\right] + l$$

Where *m, n* and *l* are coefficient with values 4403, 1492 and 305 respectively.

6.8 Application of ASTER Data for Seasonal Distribution of SS along Indus River

In order to estimate the yearly and seasonally distribution of SSC, the Advanced Spaceborne Thermal Emission and Reflection Radiometer, ASTER-VNIR scenes of Indus River, Pakistan acquired on 07-06-02, 07-04-15, and 05-06-12 was used. The coordinate system of the ASTER scenes is UTM 43N, and their datum is WGS84. The scenes were atmospherically corrected. The characteristics of ASTER satellite is elucidated in Chapter 3, section 3.8.

By adopting the above explained model inversion technique, the Suspended sediment concentration along the river reach was quantified for the month April 2007, June 2007 and June 2005. The SSC April 2007, June 2007 & 2005 along the river reach is depicted in the above figure 6.18.

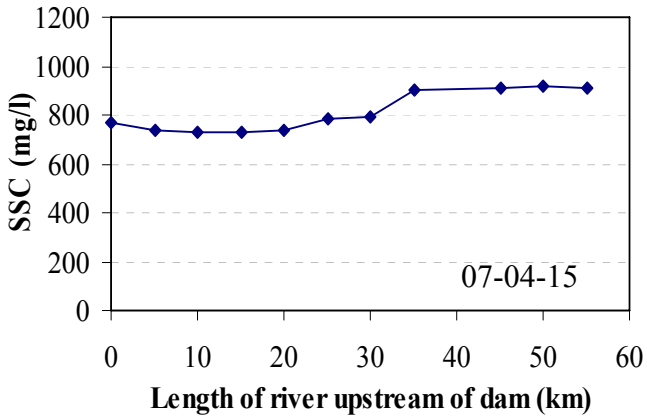

Figure 6.18 SSC along the river reach

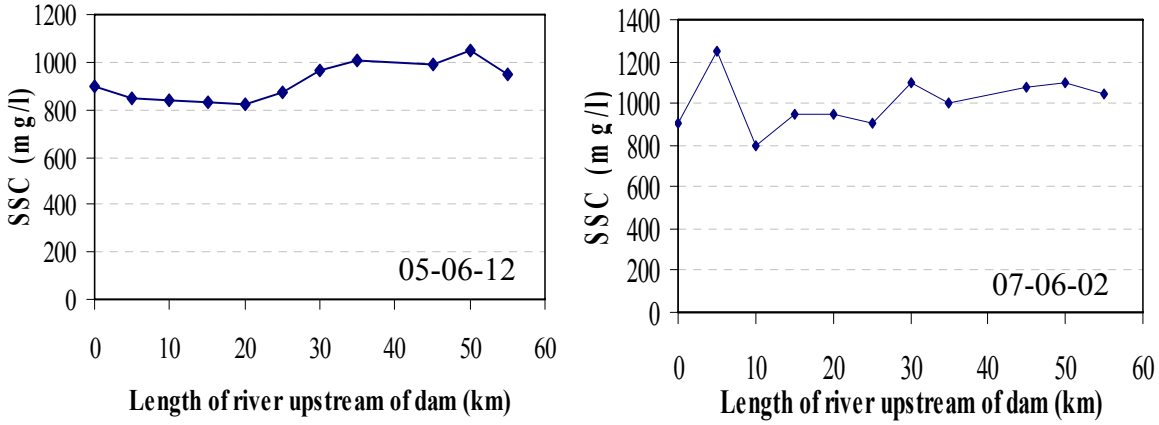

Figure 6.19 SSC along the river reach in flood season

The SSC for the image acquired on 07/06/02 & 05/06/12 represents high concentration of suspended sediments. The month of June is considered as flood season and river water carry heavy sediments load. To develop the model for estimation of suspended sediments by using ASTER data, the regression model was developed by adopting developed 2 band model approach. The relationship is illustrated in figure 6.20.

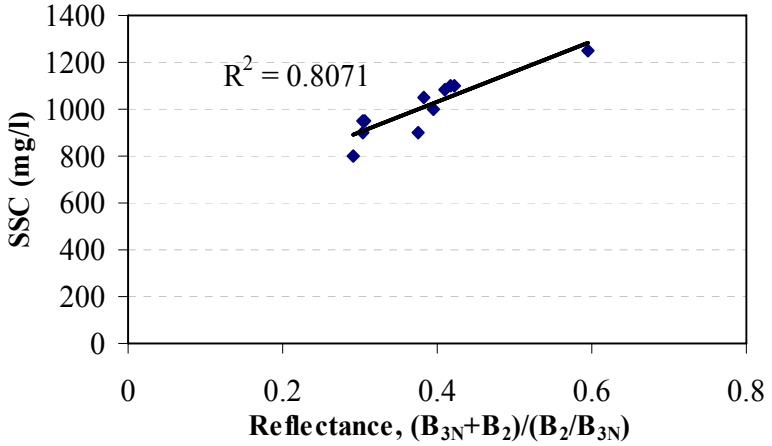

Figure 6.20 Relationship between SSC (mg/l) and reflectance

As obvious from the graph, the correlation coefficient is high. The regression model is of the following form;

$$SSC(mg/l) = m\left[(B_{3N} + B_2)/(B_2/B_{3N})\right] + n$$

Where the value of coefficient *m* is 1291 and *n* is 514.

6.9 Application of SPOT Data for Seasonal Distribution of SS along River

6.9.1 Introduction

In order to quantify the suspended sediment and evaluating the feasibility of SPOT data for estimation of suspended sediment, the SPOT image acquired on 10 May, 2005 was analyzed by using ENVI 4.3.

6.9.2 SPOT sensor & products

The SPOT (Systeme Pour l'Observation de la Terre) satellite system provides capability of applying high resolution multispectral imagery to a range of land use and land cover analyses. The SPOT satellite is equipped with two HRV (High Resolution Visible) linear array (pushbroom) sensors capable of operating in a panchromatic (PAN) mode with 10-m resolution, or a three-band multispectral (XS) mode with 20-m resolution.

Table 6.7 General features of SPOT

General features	Characteristics		
	SPOT 1,2,3	**SPOT 4**	**SPOT 5**
Launch Date	22nd February, 1986 22nd January, 1990 26th September, 1993	24 March, 1998	4 May, 2002
Altitude	822 km	822 km	822 km
Orbital Cycle	26days	26 days	26 days
Spectral Band and Resolution	1 Panchromatic (10m) 3 Multispectral (20 m)	1 Panchromatic (10m) 3 Multispectral (20 m) I shortwave Infrared (20 m)	1 Panchromatic (10m) 3 Multispectral (20 m) I shortwave Infrared (20 m)
Spectral range	P: 0.48-0.71 μm B1 (green):0.50-0.59μm B2 (Red):0.61-0.68μm B3 (NIR):0.78-0.89μm B4(SWIR):1.58-1.75μm	M: 0.61-0.68 μm B1(green):0.50-0.59μm B2 (Red):0.61-0.68μm B3 (NIR):0.78-0.89μm B4(SWIR):1.58-1.75μm	P: 0.50-0.73 μm B1(green):0.50-0.59μm B2 (Red):0.61-0.68μm B3 (NIR):0.78-0.89μm

6.9.3 Atmospheric correction

The digital numbers (DNs) was converted the into radiance units by using the equation 1;

$$L = DN/a + b$$

where L ($Wm^{-2}\ sr^{-1}\ \mu m^{-1}$) is the top of atmosphere (TOA) upwelling radiance and a ($W^{-1}m^2$ sr μm) is gain and b is offset.

The image was atmospherically corrected by using ENVI FLASH model. The FLASH is discussed in detail in chapter 4 section 4.5.3.

Table 6.8 Solar equivalent irradiances ($W/m^{-2}\mu m^{-1}$) for SPOT instruments

	SPOT 1		**SPOT 2**		**SPOT 3**		**SPOT 4**	
Spectral Band	**HRV 1**	**HRV 2**	**HRV 1**	**HRV 2**	**HRV 1**	**HRV 2**	**HRVIR 1**	**HRVIR 2**
P / M	1,680	1,690	1,705	1,670	1,668	1,667	1,568	1,586
XS1	1,855	1,845	1,865	1,865	1,854	1,855	1,843	1,851
XS2	1,615	1,575	1,620	1,615	1,580	1,597	1,568	1,586
XS3	1,090	1,040	1,085	1,090	1,065	1,067	1,052	1,054
SWIR							233	240

6.9.4 Spectral reflectance model

The modeled spectra were computed by using the following relationship;

$$Rrs\,(\lambda) = \frac{f}{Q}\,\frac{\mathrm{b}_{\mathrm{b}}(\lambda)}{\mathrm{a}(\lambda) + \mathrm{b}_{\mathrm{b}}(\lambda)}$$

Where f is a coefficient and the commonly adopted value of f is 0.33, which is valid for zenith sun and for large variety of natural waters, the value of factor Q (ratio of upwelling irradiance to upwelling radiance) as suggested by (Gordon et al. 1988, 1975), is ~ 3.4. The value of 3.14 is used for analysis. For many studies, Q is often arbitrarily chosen as a spectral constant. However, Carder et al.(1991), found that Q is not spectrally constant for the 1990 stations, and there was a trend for Q to increase with wavelength (an inverse trend compared with b_{bs}).

6.9.5 Distribution of SS along river

The SPOT image was acquired on 10 May, 2005 during that time the suspended sediment concentration at 67 km upstream of the dam was collected. The SSC was found to be 250mg/l (Table 6.9).The average reflectance value of SPOT XS2 was 10 % and XS3 is 7%. The concentration was found to be low because of dry season. However the month of June is considered to be rainy with many flash floods.

Table 6.9 In Situ Suspended Sediment Concentration Measurements

Date	Discharge (m^3/s)	SSC (mg/l)	% Average		
			Sand	Silt	Clay
10th May, 2005	3015	250	10.1	76.1	13.8

This scenario closely matches with the seasonal pattern of SSC in the river. The in situ suspended sediment measurements are shown in table 3. The SPOT reflectance (2 Band Model) along the river reach is shown in figure 6.21. The SSC along the river reach was estimated by using the model inversion technique and minimizing the difference between modelled and SPOT image reflectance data.

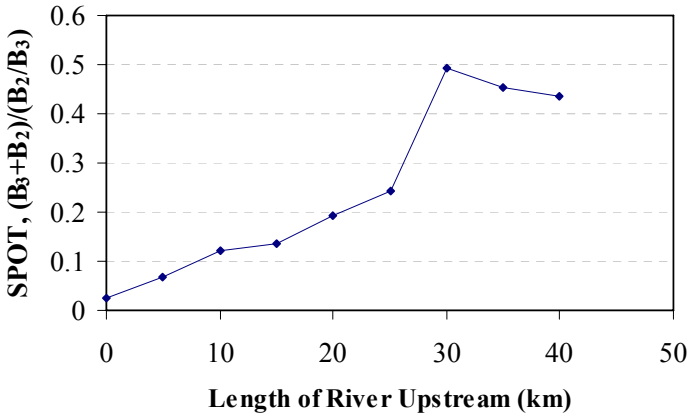

Figure 6.21 Reflectances along the river reach

The suspended sediment concentration along the river reach is illustrated in figure 6.22-a. The correlation coefficient between the 2 band model and SSC showed a high value of 0.96. The regression equation for estimation of suspended sediment is as follow;

$SSC(mg/l)=m[(B_3+B_2)/(B_2/B_3)]+n$, where value of *m* is 365, and *n* is 73.

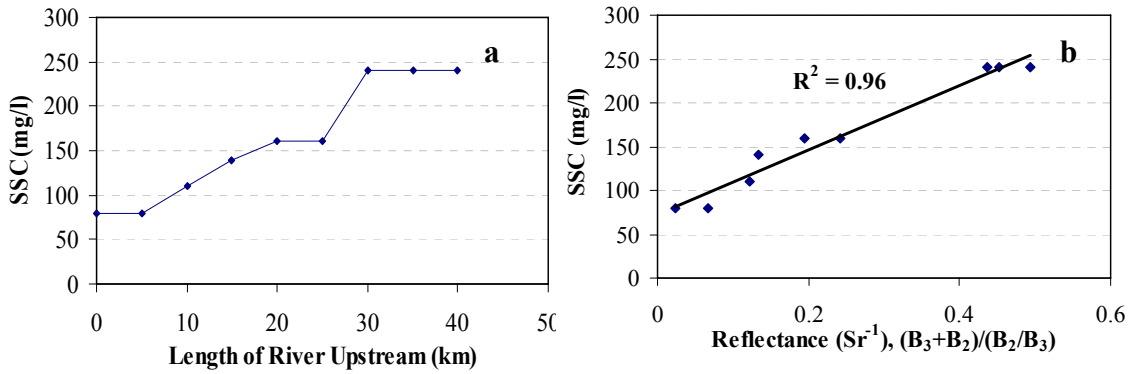

Figure 6.22 a): SSC along the river reach b): Relationship between SSC & 2 Band model

6.10 Concluding remarks

Remote sensing technologies have many actual and potential applications for assessing water resources and for monitoring and modeling of water quality parameters. The inversion technique is feasible to cope with lack of ground truth data problem. The integration of satellite data, in situ data, and theoretical model is an effective tool for monitoring erosion, deposition areas and sediment distribution in water bodies. If ground data is available, the inversion technique may apply for atmospheric correction. The research emphasises on the assessment of suspended sediments in water bodies by means of integrated remotely sensed approach. The proposed methodology is effective and efficient to deal with sediment management in large rivers. In developing countries the ground truth data is often minimal or unavailable. It is difficult for resource managers to plan strategy to cope with sedimentation and erosion problems. The usefulness of the research is to make possible to work with minimum data with high reliability and efficiently. In this reach work the concerned parameters was suspended sediments. If the concentration of one water quality parameter is known, the concentration of other parameters on the same sampling point may estimated by applying the same methodology. The integration of remotely sensed data and optical models is the solution to overcome lack of data problem. The research has shown the feasibility of multispectral data to estimate the suspended sediments in the surface water of rivers and reservoirs. It is imperative to incorporate sediment assessment as an integral part of water resources and environmental planning for sustainable development and management.

CHAPTER 7
CONCLUSIONS & RECOMENDATIONS

7.1 Conclusions

The dissertation highlighted the application of remotely sensed data for quantification of suspended matter in water bodies. The research work is comprised of controlled hyperspectral experiments in laboratory, field spectroscopy, optical modeling and multispectral remote sensing. It is believed that the outcomes of the research will play critical role in the development of multiple-use management strategies, and to implement monitoring system by means of remote sensing.

The controlled laboratory experiments consist of investigation of equipments characteristics and comprehensive analysis of different types and amounts of suspended sediments. Some useful measurement protocols are proposed to enhance the data reliability. Han (1994) investigated the spectral response of silt and clay loam as suspended sediments. However, the spectral response of five different types of soils with varying concentration of suspended sediments in laboratory and field conditions was investigated first time in detail. Spectral reflectance for different types and concentration of suspended sediments are unique. Magnitude and spectral shape varied with type, texture, grain size and concentration of suspended sediments in surface water. It was observed that the between 700 to 900 nm (NIR) the reflectance increases more uniformly with increased SSC and is considered to be a useful range for determining the amount of suspended sediments. The wavelength range 525-665 provides information about sediments type and is useful to identify the type of soil. The ratios of reflectance values in the sub-bands centered at 848/548, 803/708, 793/713, 773/663, 783/673, and 773/658 were found to be optimum for estimation of suspended sediment in surface water. The spectroradimeter data, integrated into the band width of ALOS/AVNIR-2 allow accurate assessment of SSC. The first derivative at 827nm wavelength is proved to be effective in estimating SSC.

Tolk et al. (2000) have pointed out that at a depth of 80 cm; there is no bottom effect above SSC of 100mg/liter. Bartolucci et al. (1977) mentioned that the river bottom has no influence on the spectral response of turbid river water (99 mg/l of suspended solids) when it is deeper than 30cm. One of the useful finding of this thesis is that if the water depth is more than 60 cm, in the visible domain, there was no bottom effect when suspended sediment concentration was above 400mg/liter. This threshold value of suspended sediments is different and contradicts with already published values in literature. On the bases of experiment and applied methodology it is strongly believed that the proposed value is correct.

The crux of this research is to highlight quantitatively and quantitatively the effect of different influencing parameters on remotely sensed data and demonstrates the feasibility of remote sensing for monitoring of water bodies. Each environmental factor has its own effect on the remote sensing signals. The remote sensing theory lies on that fact that most of the incoming energy is absorbed, transmitted or reflected in other directions. Only less than 10% (as subsurface irradiance) of the incoming energy is the actual signals carrying information about the water body and is detected by the sensor. The

effect of different environmental factors was examined thoroughly and findings are significant to minimize the error in the remotely sensed data. Under windy conditions and waves on the water surface, the spectrum average and band ratio technique may decrease the effect of waves on the observed spectral signals. This research includes an extensive investigation of above surface and subsurface reflectance measurements. The difference in reflectance measurements acquired above water surface and subsurface for the same sampling point was first time highlighted and documented in the thesis. The above-water measurements are problematic because of inefficient methods for the removal of surface reflection effects from the total upwelling radiance signals. It is strongly recommended that the subsurface spectral reflectance measurement is better option for the researcher who attempt to analyze water by using remotely sensed data. In case of multispectral remote sensing by using ASTER sensor, the selection of ASTER 3B-NIR image can be the solution to overcome the effects of surface roughness for studying water bodies.

Remote sensing makes it possible to monitor the water bodies effectively & efficiently and is most successfully used as part of a multidisciplinary approach to addressing natural resource questions. Numerous researchers have developed water quality algorithms. However, the work done in the present research work allows to discriminate between water quality parameters and to develop a better understanding of light, water and substances interactions. Water quality models developed as a result of massive field campaigns and collection of remotely sensed data enables to develop the regressions models that are applicable under different environmental conditions. The combination of ground truth data, in situ subsurface hyperspectral measurements and AISA data was successfully applied in this research and the thesis demonstrate the feasibility of remotely sensed data for water quality monitoring and modeling. One of the major finding of water quality monitoring by means of remotely sensed data is the development of multiplicative 2 band model for estimation of suspended sediments. The application of developed model for assessment of suspended sediment concentration is promising.

An important part of my research is to develop clear vision and understanding of relationship between water quality parameters and optical models. Integrated optical modeling technique was developed for monitoring and modeling of water bodies. The performance of such algorithms is always subject to compatibility between the waters under study and the waters from which data were obtained for algorithm development. The research work illustrates the quantitative and qualitative relationship between modeled spectra and acquired reflectance spectra. The relationship was not examined thoroughly in detail before. The developed technique is a useful tool for collection of information over large areas and to monitor river waters carrying heavy suspended sediments in the absence of ground truth data. Algorithms based on the fundamentals of hydrological optics are strongly advocated.

The major contribution of the research is to develop monitoring system for suspended sediment estimation in large rivers. The Indus River, Pakistan is selected as case study. The optical model inversion technique was developed and it is believed that the developed technique is feasible to cope with lack of ground truth data problem. The integration of satellite data, in situ data, and optical models is an effective tool for monitoring erosion, deposition areas, sediment distribution, and suspended matter in water bodies. The proposed system offers an ideal opportunity to consolidate various parameters such as chlorophyll, suspended sediments and CDOM. If ground data is available, the

inversion technique may apply for atmospheric correction. The research work proves the usefulness multispectral data to estimate the suspended sediments in the surface water of rivers and reservoirs. The present research work is successful example for the researchers to substantiate the utility of remotely sensed data for water quality monitoring and modeling of inland and coastal waters. The research work will prove to be the first step for application of remotely sensed data in the area where minimum or no ground truth data is available.

7.2 Accuracy and Precisions Limitations: *The expected accuracy and precision and on which influencing parameters we have to compromise*

It is not possible to avoid influencing effects on remotely sensed data; however, by adopting proper methodology and measurement protocols it is possible to minimize the effects.

Equipment calibration: The characteristics of equipment influence the spectral measurements and limit the practical use of the spectroradiometer. However, by adopting proper methodology and measurement protocols as explained in chapter 2, section 2.4, the error in the acquired data due to equipment may minimized.

The recommend warm up time: 120~ 150 minutes; Spectrum Average: Average of 20; Cable position: Straight; Field experiments under clear sky are recommended.

Surface Roughness effects: The effect of surface roughness/waves on hyperspectral data can not be removed. However, in case of hyperspectral remote sensing, the surface roughness can be minimized by collecting subsurface spectral measurements. Under waves it is difficult to acquire the subsurface data. In above surface spectral measurements, the surface roughnesses can me minimized by keeping minimum difference between the surface and the sensor. By applying band ratio technique and spectrum average technique, the effect may minimize. It is difficult to remove such kind of effects from hyperspectral data and one should have to compromise on such error. It is recommended that the field research should be carried out keeping in view the environmental conditions. Windy days should be avoided. In case of multispectral remote sensing, the surface roughness can be minimized by backward sensor image such as 3B-NIR/ASTER image and ALOS prism image.

Surface reflection effects: The surface reflection affects the hyperspectral signals significantly. The above surface reflectance measurements are influenced by surface reflections effects owing to sun glitter or slow wind. The effect of reflection from the total upwelling signals may minimized by subtracting the reflection effects as explained in chapter 3, section 3.7. However, reflections effects can not be removed and the approximately assumed value disturbs the signals. The subsurface spectral measurement helps to minimize the reflection effects.

Noise in collected data: The noise in collected data due to unknown environmental factors can be controlled. Accurate methodology allows us to overcome certain sources of errors that would remain unaccounted in formal sensitivity analyses.

Water quality models: The developed water quality models are useful for assessment of water quality parameters. However, the empirical coefficients may vary

from river to river, seasonally and due to environmental factors. The application of developed regression models with same empirical coefficients may not be so accurate globally. However, the selected wavelengths/bands may apply globally. The error in model itself leads to inaccurate estimation of parameters. There is often a need to tailor models for specific applications or for specific regions. If models are applied for purposes for which they were not designed, there is always a risk error.

Absorption & scattering: Absorption and scattering are also hydrological and environmental properties. Changes in concentration, size distribution and composition of particulate matter and/or dissolved constituents strongly influence the absorption and scattering. So, we have to assume that the water body is optically homogenous and one component is not influencing on absorption and scattering of other component present within the water body.

Atmospheric correction: In case of satellite data, the atmosphere is itself a source of error. Some already developed model such as FLAASH and simple technique like dark pixel technique and band ratioing is widely applied by the research to minimize the atmospheric influence. However, none of the technique completely remove the atmospheric effects. The researchers have to compromise on unknown effects in the data. We have to assume that after atmospheric correction, there is no influence of atmospheric effect on the acquired data.

Developed Monitoring technique: The developed monitoring technique is considered to be effective in case of turbid waters. If there are floating materials on the water surface, the proposed model inversion technique may lead to errors. In such conditions the only one band NIR should be took into account. It is recommended to test the developed algorithms for the specific application or region envisaged, before field application. However, in the present research work, the model was developed; the field application and validation will be carried out as postdoctoral research work.

7.3 Future Outlook

Adequate monitoring at appropriate time and space scales is imperative for water resources management. The evaluation of the developed monitoring system was not carried out owing to lack of ground truth data. The algorithms that have been optimized for local conditions will perform better than a general, global algorithm. The evaluation of the developed system needs investigation through massive filed campaigns in the research area.

To develop more generalize model for predicting suspended sediment concentration, effect of suspended sediments distribution with depth and application of remotely sensed data under different environmental condition needs evaluation.

There is dire need to develop new atmospheric correction techniques to minimize the influence of atmosphere on the remotely sensed signals.

The applicability of the remotely sensed data for suspended sediment estimation may enhance by coupling the remotely data with numerical models.

The effectiveness of developed water quality algorithms at another time and place needs investigation.

The research issues such as evaluation of influence of organic matters on spectral response of inorganic matters needs attentions. The accurate methodology and refine algorithms are needed to separate the spectral characteristics of suspended sediments from total suspended matters. The proposed research work may further enhance the application of remote sensing in monitoring water bodies.

7.4 Recommendations

Development of Suspended Sediment management system: The water quality and quantity "Q & Q" connection is vital for sustainable water resources development & management. Considerable research effort needs to be focused on development of economic, effective and efficient suspended matter monitoring system. Remote sensing is proved to be an effective tool and technique for monitoring and water bodies on repetitive basis.

Sustainable water resources management: Sustainable development demands a deeper knowledge of the interaction among economy, society and water resources. Water should be recognized as a tool for community development and peace building. In the future, it will be important to incorporate water quality monitoring as an integral part of water resources and environmental planning and management. Without this approach the problems of the water & environmental sector are going to compound in the future.

Technology bridge between developed and developing countries: There is dire need to develop the technological bridge between developed and developing countries. The universities in the developed countries may play a vital role to initiative the valuable research in the developing countries and to bridge the gap between developed and developing countries by understanding the real needs.

Institutional capacity building: Institutional capacity building is imperative and Japan International Cooperation Agency (JICA) capacity building program has important role in this aspect. Seminars, workshops and short training courses in the developed and developing countries is necessary. The research collaboration between developed and developing countries organizations is needed to cope with capacity building efforts.

Appendix

Absorption Coefficient

$$a(\lambda)=a_w(\lambda)+a_y(\lambda)+a_{ph}(\lambda)+a_s(\lambda) \qquad \textit{Equation 1}$$

Where the subscript *w, y, ph* and *s* represents water, colored dissolved organic mater, phytoplankton and total suspended maters.

Absorption by water: Table 1,

400-800nm Smith & Baker (1981), 800-900nm Hale & Query (1973)

Absorption by CDOM

$$a_y(\lambda) = a_y(\lambda_o)e^{-k(\lambda-\lambda_o)} \qquad \textit{Equation 2}$$

$a_y(440)$ = 0.2 $m^{-1}$and the exponential coefficient *k* is variable and the mostly the value = 0.014 nm^{-1} is used. In our case the value of 0.017 nm^{-1} is selected.

Absorption by phytoplankton

$$a^*_{ph}(\lambda) = A(\lambda) \times C_{chl}^{-B(\lambda)} \qquad \textit{Equation 3}$$

Where A and B are positive empirical coefficients and are wavelength dependent and chlorophyll-a concentration C_{chl} in µg/l. The values of A & B adopted from Bricuad, 1995 was given in Table 2.

Absorption by total suspended sediments (TSS) or Suspended Sediments (SS)

$$a_s(\lambda) = k_1 C_s^{\,k_2}(\lambda_0/\lambda) \qquad \textit{Equation 4}$$

C_s is suspended particle concentration (mg/l). In our case the value of k_1 = 0.05 and k_2= 1.1 is used for analysis.

Backscattering

$$b_b(\lambda) = b_{bw}(\lambda) + b_{b\,ph}(\lambda) + b_{b\,s}(\lambda) + b_{by}(\lambda) \qquad \textit{Equation 5}$$

Where the subscript w, y, ph and s represents backscattering due to water, colored dissolved organic mater, phytoplankton and total suspended maters.

Scattering by water: Table 1

Flow Chart of Model

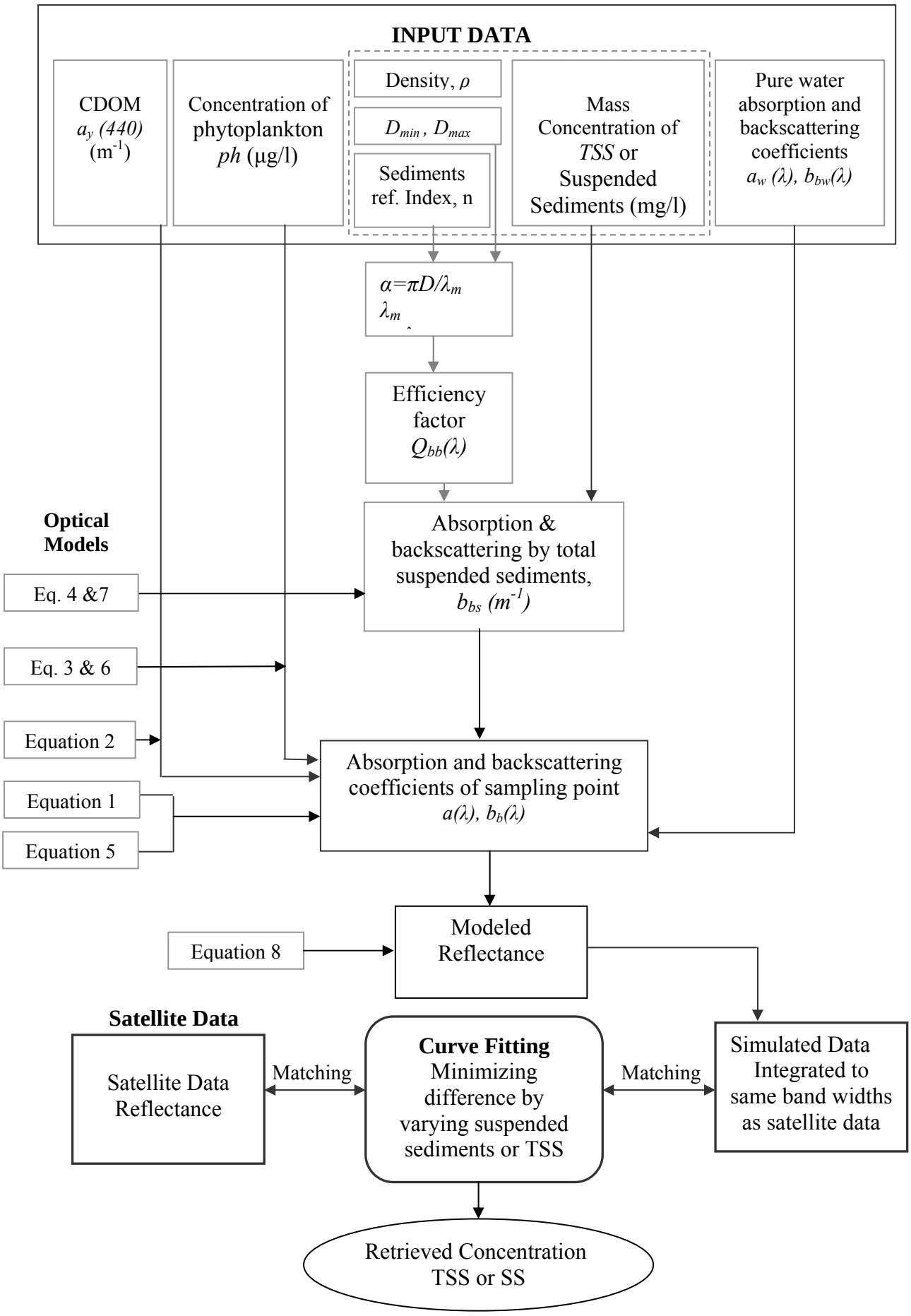

400-800nm Smith & Baker (1981), 800-900nm Hale & Query (1973)

Scattering by phytoplankton

$$b_{ph}(\lambda) = (\mathrm{b}_{\mathrm{bPh}}/\mathrm{b}_{\mathrm{P}}) \cdot B \cdot C_{chl}^{0.62}(\lambda_o/\lambda)$$
$$b_{ph}(\lambda) = 0.005(0.12 * C_{chl}^{0.63}(\mathrm{a}_{\mathrm{Ph}}(550)/\mathrm{a}_{\mathrm{Ph}}(\lambda)) \qquad \textit{Equation 6}$$

Scattering by total suspended sediments (TSS) or Suspended Sediments (SS)

$$b_{bs} = \frac{3C}{2\rho} \cdot \frac{1}{\ln(D_2/D_1)} \int_{D1}^{D2} Q_{bb} . D^{-2} dD \qquad \textit{Equation 7}$$

Q_{bb} is efficiency factor (Figure-I), ρ is the sediment density, D_1 & D_2 are minimum and maximum suspended particles diameters, and C is the concentration of suspended sediments or total suspended sediments. The units of all parameters must be symmetric.

Scattering by CDOM

CDOM have no role in scattering. Scattering by CDOM is neglected.

Modeled Spectral Reflectance

$$R(\lambda) = f \frac{\mathrm{b}_{\mathrm{b}}(\lambda)}{\mathrm{a}(\lambda) + \mathrm{b}_{\mathrm{b}}(\lambda)} \qquad \textit{Equation 8}$$

The commonly adopted value of *f* is 0.33

Or

$$Rrs(\lambda) = \frac{f}{Q} \frac{\mathrm{b}_{\mathrm{b}}(\lambda)}{\mathrm{a}(\lambda) + \mathrm{b}_{\mathrm{b}}(\lambda)}$$

The commonly adopted value of Q is 3.14 Sr.

Table 1: Absorption and scattering coefficients of pure water

λ	a_w	b_w	b_{bw}	λ	a_w	b_w	b_{bw}	λ	a_w	b_w	b_{bw}
400	0.0171	0.0058	0.0029	452	0.0147	0.0034	0.0017	504	0.0301	0.0021	0.0011
401	0.0170	0.0057	0.0029	453	0.0149	0.0034	0.0017	505	0.0312	0.0021	0.0010
402	0.0169	0.0057	0.0028	454	0.0150	0.0033	0.0017	506	0.0323	0.0021	0.0010
403	0.0168	0.0056	0.0028	455	0.0151	0.0033	0.0016	507	0.0334	0.0020	0.0010
404	0.0167	0.0055	0.0028	456	0.0152	0.0032	0.0016	508	0.0345	0.0020	0.0010
405	0.0166	0.0055	0.0027	457	0.0153	0.0032	0.0016	509	0.0356	0.0020	0.0010
406	0.0165	0.0054	0.0027	458	0.0155	0.0031	0.0016	510	0.0357	0.0020	0.0010
407	0.0164	0.0053	0.0027	459	0.0156	0.0031	0.0016	511	0.0370	0.0020	0.0010
408	0.0163	0.0053	0.0026	460	0.0156	0.0031	0.0016	512	0.0384	0.0020	0.0010
409	0.0162	0.0052	0.0026	461	0.0156	0.0031	0.0015	513	0.0397	0.0020	0.0010
410	0.0162	0.0052	0.0026	462	0.0156	0.0031	0.0015	514	0.0410	0.0020	0.0010
411	0.0161	0.0051	0.0026	463	0.0156	0.0030	0.0015	515	0.0424	0.0019	0.0010
412	0.0160	0.0051	0.0025	464	0.0156	0.0030	0.0015	516	0.0437	0.0019	0.0010
413	0.0159	0.0050	0.0025	465	0.0156	0.0030	0.0015	517	0.0450	0.0019	0.0010
414	0.0158	0.0050	0.0025	466	0.0156	0.0030	0.0015	518	0.0463	0.0019	0.0010
415	0.0157	0.0049	0.0025	467	0.0156	0.0029	0.0015	519	0.0477	0.0019	0.0010
416	0.0156	0.0049	0.0024	468	0.0156	0.0029	0.0015	520	0.0477	0.0019	0.0010
417	0.0155	0.0048	0.0024	469	0.0156	0.0029	0.0015	521	0.0480	0.0019	0.0009
418	0.0154	0.0048	0.0024	470	0.0156	0.0029	0.0015	522	0.0483	0.0019	0.0009
419	0.0153	0.0047	0.0023	471	0.0158	0.0029	0.0014	523	0.0486	0.0018	0.0009
420	0.0153	0.0047	0.0024	472	0.0160	0.0028	0.0014	524	0.0489	0.0018	0.0009
421	0.0152	0.0046	0.0023	473	0.0163	0.0028	0.0014	525	0.0492	0.0018	0.0009
422	0.0151	0.0046	0.0023	474	0.0165	0.0028	0.0014	526	0.0495	0.0018	0.0009
423	0.0150	0.0045	0.0023	475	0.0167	0.0027	0.0014	527	0.0498	0.0017	0.0009
424	0.0149	0.0045	0.0022	476	0.0169	0.0027	0.0014	528	0.0501	0.0017	0.0009
425	0.0148	0.0044	0.0022	477	0.0172	0.0027	0.0013	529	0.0504	0.0017	0.0009
426	0.0147	0.0044	0.0022	478	0.0174	0.0026	0.0013	530	0.0507	0.0017	0.0009
427	0.0146	0.0043	0.0022	479	0.0176	0.0026	0.0013	531	0.0513	0.0017	0.0008
428	0.0145	0.0043	0.0021	480	0.0176	0.0026	0.0013	532	0.0518	0.0017	0.0008
429	0.0144	0.0042	0.0021	481	0.0178	0.0026	0.0013	533	0.0524	0.0017	0.0008
430	0.0144	0.0042	0.0021	482	0.0180	0.0026	0.0013	534	0.0530	0.0017	0.0008
431	0.0144	0.0042	0.0021	483	0.0183	0.0025	0.0013	535	0.0535	0.0017	0.0008
432	0.0144	0.0041	0.0021	484	0.0185	0.0025	0.0013	536	0.0541	0.0016	0.0008
433	0.0144	0.0041	0.0020	485	0.0187	0.0025	0.0012	537	0.0547	0.0016	0.0008
434	0.0144	0.0040	0.0020	486	0.0189	0.0025	0.0012	538	0.0552	0.0016	0.0008
435	0.0145	0.0040	0.0020	487	0.0191	0.0024	0.0012	539	0.0558	0.0016	0.0008
436	0.0145	0.0039	0.0020	488	0.0194	0.0024	0.0012	540	0.0558	0.0016	0.0008
437	0.0145	0.0039	0.0019	489	0.0196	0.0024	0.0012	541	0.0567	0.0016	0.0008
438	0.0145	0.0038	0.0019	490	0.0196	0.0024	0.0012	542	0.0576	0.0016	0.0008
439	0.0145	0.0038	0.0019	491	0.0203	0.0024	0.0012	543	0.0585	0.0016	0.0008
440	0.0145	0.0038	0.0019	492	0.0209	0.0024	0.0012	544	0.0594	0.0016	0.0008
441	0.0145	0.0038	0.0019	493	0.0216	0.0023	0.0012	545	0.0602	0.0016	0.0008
442	0.0145	0.0037	0.0019	494	0.0223	0.0023	0.0012	546	0.0611	0.0015	0.0008
443	0.0145	0.0037	0.0019	495	0.0230	0.0023	0.0011	547	0.0620	0.0015	0.0008
444	0.0145	0.0037	0.0018	496	0.0236	0.0023	0.0011	548	0.0629	0.0015	0.0008
445	0.0145	0.0036	0.0018	497	0.0243	0.0022	0.0011	549	0.0638	0.0015	0.0008
446	0.0145	0.0036	0.0018	498	0.0250	0.0022	0.0011	550	0.0638	0.0015	0.0008
447	0.0145	0.0036	0.0018	499	0.0256	0.0022	0.0011	551	0.0646	0.0015	0.0007
448	0.0145	0.0035	0.0018	500	0.0257	0.0022	0.0011	552	0.0653	0.0015	0.0007
449	0.0145	0.0035	0.0018	501	0.0268	0.0022	0.0011	553	0.0661	0.0015	0.0007
450	0.0145	0.0035	0.0018	502	0.0279	0.0022	0.0011	554	0.0669	0.0015	0.0007
451	0.0146	0.0035	0.0017	503	0.0290	0.0021	0.0011	555	0.0677	0.0015	0.0007

λ	a_w	b_w	b_{bw}	λ	a_w	b_w	b_{bw}	λ	a_w	b_w	b_{bw}
556	0.0684	0.0014	0.0007	609	0.2890	0.0010	0.0005	662	0.4067	0.0007	0.0004
557	0.0692	0.0014	0.0007	610	0.2890	0.0010	0.0005	663	0.4100	0.0007	0.0004
558	0.0700	0.0014	0.0007	611	0.2912	0.0010	0.0005	664	0.4133	0.0007	0.0004
559	0.0707	0.0014	0.0007	612	0.2934	0.0010	0.0005	665	0.4167	0.0007	0.0004
560	0.0708	0.0014	0.0007	613	0.2957	0.0010	0.0005	666	0.4200	0.0007	0.0004
561	0.0718	0.0014	0.0007	614	0.2979	0.0010	0.0005	667	0.4233	0.0007	0.0004
562	0.0728	0.0014	0.0007	615	0.3001	0.0010	0.0005	668	0.4266	0.0007	0.0004
563	0.0738	0.0014	0.0007	616	0.3023	0.0009	0.0005	669	0.4300	0.0007	0.0004
564	0.0748	0.0014	0.0007	617	0.3045	0.0009	0.0005	670	0.4300	0.0007	0.0004
565	0.0759	0.0014	0.0007	618	0.3068	0.0009	0.0005	671	0.4322	0.0007	0.0003
566	0.0769	0.0013	0.0007	619	0.3090	0.0009	0.0005	672	0.4344	0.0007	0.0003
567	0.0779	0.0013	0.0007	620	0.3090	0.0009	0.0005	673	0.4367	0.0007	0.0003
568	0.0789	0.0013	0.0007	621	0.3101	0.0009	0.0005	674	0.4389	0.0007	0.0003
569	0.0799	0.0013	0.0007	622	0.3112	0.0009	0.0005	675	0.4411	0.0007	0.0003
570	0.0799	0.0013	0.0007	623	0.3123	0.0009	0.0005	676	0.4433	0.0006	0.0003
571	0.0830	0.0013	0.0006	624	0.3134	0.0009	0.0005	677	0.4455	0.0006	0.0003
572	0.0861	0.0013	0.0006	625	0.3146	0.0009	0.0005	678	0.4478	0.0006	0.0003
573	0.0893	0.0013	0.0006	626	0.3157	0.0009	0.0005	679	0.4500	0.0006	0.0003
574	0.0924	0.0013	0.0006	627	0.3168	0.0009	0.0005	680	0.4500	0.0006	0.0003
575	0.0955	0.0013	0.0006	628	0.3179	0.0009	0.0005	681	0.4556	0.0006	0.0003
576	0.0986	0.0012	0.0006	629	0.3190	0.0009	0.0005	682	0.4611	0.0006	0.0003
577	0.1017	0.0012	0.0006	630	0.3190	0.0009	0.0005	683	0.4667	0.0006	0.0003
578	0.1049	0.0012	0.0006	631	0.3201	0.0009	0.0004	684	0.4722	0.0006	0.0003
579	0.1080	0.0012	0.0006	632	0.3212	0.0009	0.0004	685	0.4778	0.0006	0.0003
580	0.1080	0.0012	0.0006	633	0.3223	0.0009	0.0004	686	0.4833	0.0006	0.0003
581	0.1134	0.0012	0.0006	634	0.3234	0.0009	0.0004	687	0.4889	0.0006	0.0003
582	0.1189	0.0012	0.0006	635	0.3245	0.0009	0.0004	688	0.4944	0.0006	0.0003
583	0.1243	0.0012	0.0006	636	0.3256	0.0008	0.0004	689	0.5000	0.0006	0.0003
584	0.1298	0.0012	0.0006	637	0.3267	0.0008	0.0004	690	0.5000	0.0006	0.0003
585	0.1352	0.0012	0.0006	638	0.3278	0.0008	0.0004	691	0.5166	0.0006	0.0003
586	0.1406	0.0011	0.0006	639	0.3289	0.0008	0.0004	692	0.5332	0.0006	0.0003
587	0.1461	0.0011	0.0006	640	0.3290	0.0008	0.0004	693	0.5498	0.0006	0.0003
588	0.1515	0.0011	0.0006	641	0.3312	0.0008	0.0004	694	0.5664	0.0006	0.0003
589	0.1570	0.0011	0.0006	642	0.3334	0.0008	0.0004	695	0.5830	0.0006	0.0003
590	0.1570	0.0011	0.0006	643	0.3357	0.0008	0.0004	696	0.5996	0.0005	0.0003
591	0.1667	0.0011	0.0006	644	0.3379	0.0008	0.0004	697	0.6162	0.0005	0.0003
592	0.1763	0.0011	0.0006	645	0.3401	0.0008	0.0004	698	0.6328	0.0005	0.0003
593	0.1860	0.0011	0.0006	646	0.3423	0.0007	0.0004	699	0.6494	0.0005	0.0003
594	0.1956	0.0011	0.0006	647	0.3445	0.0007	0.0004	700	0.6500	0.0005	0.0003
595	0.2053	0.0011	0.0006	648	0.3468	0.0007	0.0004	701	0.6710	0.0005	0.0003
596	0.2150	0.0011	0.0006	649	0.3490	0.0007	0.0004	702	0.6920	0.0005	0.0003
597	0.2246	0.0011	0.0006	650	0.3490	0.0007	0.0004	703	0.7130	0.0005	0.0003
598	0.2343	0.0011	0.0006	651	0.3547	0.0007	0.0004	704	0.7340	0.0005	0.0003
599	0.2439	0.0011	0.0006	652	0.3603	0.0007	0.0004	705	0.7550	0.0005	0.0003
600	0.2440	0.0011	0.0006	653	0.3660	0.0007	0.0004	706	0.7760	0.0005	0.0003
601	0.2490	0.0011	0.0005	654	0.3716	0.0007	0.0004	707	0.7970	0.0005	0.0003
602	0.2540	0.0011	0.0005	655	0.3773	0.0007	0.0004	708	0.8180	0.0005	0.0003
603	0.2590	0.0011	0.0005	656	0.3830	0.0007	0.0004	709	0.8390	0.0005	0.0003
604	0.2640	0.0011	0.0005	657	0.3886	0.0007	0.0004	710	0.8390	0.0005	0.0003
605	0.2690	0.0011	0.0005	658	0.3943	0.0007	0.0004	711	0.8756	0.0005	0.0003
606	0.2740	0.0010	0.0005	659	0.3999	0.0007	0.0004	712	0.9122	0.0005	0.0003
607	0.2790	0.0010	0.0005	660	0.4000	0.0007	0.0004	713	0.9488	0.0005	0.0003
608	0.2840	0.0010	0.0005	661	0.4033	0.0007	0.0004	714	0.9854	0.0005	0.0003

λ	a_w	b_w	b_{bw}	λ	a_w	b_w	b_{bw}	λ	a_w	b_w	b_{bw}
715	1.0220	0.0005	0.0003	768	2.5148	0.0004	0.0002	821	2.1396	0.0000	0.0000
716	1.0586	0.0005	0.0003	769	2.5104	0.0004	0.0002	822	2.1431	0.0000	0.0000
717	1.0952	0.0005	0.0003	770	2.5100	0.0004	0.0002	823	2.1466	0.0000	0.0000
718	1.1318	0.0005	0.0003	771	2.4934	0.0004	0.0002	824	2.1500	0.0000	0.0000
719	1.1684	0.0005	0.0003	772	2.4768	0.0004	0.0002	825	2.1500	0.0000	0.0000
720	1.1690	0.0005	0.0003	773	2.4602	0.0004	0.0002	826	2.2047	0.0000	0.0000
721	1.2390	0.0005	0.0003	774	2.4436	0.0004	0.0002	827	2.2593	0.0000	0.0000
722	1.3090	0.0005	0.0003	775	2.4270	0.0004	0.0002	828	2.3139	0.0000	0.0000
723	1.3790	0.0005	0.0003	776	2.4104	0.0003	0.0002	829	2.3686	0.0000	0.0000
724	1.4490	0.0005	0.0003	777	2.3938	0.0003	0.0002	830	2.4232	0.0000	0.0000
725	1.5190	0.0005	0.0003	778	2.3772	0.0003	0.0002	831	2.4778	0.0000	0.0000
726	1.5890	0.0005	0.0003	779	2.3606	0.0003	0.0002	832	2.5324	0.0000	0.0000
727	1.6590	0.0005	0.0003	780	2.3600	0.0003	0.0002	833	2.5871	0.0000	0.0000
728	1.7290	0.0005	0.0003	781	2.3378	0.0003	0.0002	834	2.6417	0.0000	0.0000
729	1.7990	0.0005	0.0003	782	2.3156	0.0003	0.0002	835	2.6963	0.0000	0.0000
730	1.7990	0.0005	0.0003	783	2.2934	0.0003	0.0002	836	2.7510	0.0000	0.0000
731	1.8635	0.0005	0.0002	784	2.2712	0.0003	0.0002	837	2.8056	0.0000	0.0000
732	1.9280	0.0005	0.0002	785	2.2490	0.0003	0.0002	838	2.8602	0.0000	0.0000
733	1.9925	0.0005	0.0002	786	2.2268	0.0003	0.0002	839	2.9149	0.0000	0.0000
734	2.0570	0.0005	0.0002	787	2.2046	0.0003	0.0002	840	2.9695	0.0000	0.0000
735	2.1215	0.0005	0.0002	788	2.1824	0.0003	0.0002	841	3.0241	0.0000	0.0000
736	2.1860	0.0004	0.0002	789	2.1602	0.0003	0.0002	842	3.0787	0.0000	0.0000
737	2.2505	0.0004	0.0002	790	2.1600	0.0003	0.0002	843	3.1334	0.0000	0.0000
738	2.3150	0.0004	0.0002	791	2.1500	0.0003	0.0002	844	3.1880	0.0000	0.0000
739	2.3795	0.0004	0.0002	792	2.1400	0.0003	0.0002	845	3.2426	0.0000	0.0000
740	2.3800	0.0004	0.0002	793	2.1300	0.0003	0.0002	846	3.2973	0.0000	0.0000
741	2.3900	0.0004	0.0002	794	2.1200	0.0003	0.0002	847	3.3519	0.0000	0.0000
742	2.4000	0.0004	0.0002	795	2.1100	0.0003	0.0002	848	3.4065	0.0000	0.0000
743	2.4100	0.0004	0.0002	796	2.1000	0.0003	0.0002	849	3.4612	0.0000	0.0000
744	2.4200	0.0004	0.0002	797	2.0900	0.0003	0.0002	850	3.4613	0.0000	0.0000
745	2.4300	0.0004	0.0002	798	2.0800	0.0003	0.0002	851	3.5093	0.0000	0.0000
746	2.4400	0.0004	0.0002	799	2.0700	0.0003	0.0002	852	3.5573	0.0000	0.0000
747	2.4500	0.0004	0.0002	800	2.0700	0.0003	0.0002	853	3.6053	0.0000	0.0000
748	2.4600	0.0004	0.0002	801	2.0700	0.0000	0.0000	854	3.6533	0.0000	0.0000
749	2.4700	0.0004	0.0002	802	2.0735	0.0000	0.0000	855	3.7013	0.0000	0.0000
750	2.4700	0.0004	0.0002	803	2.0770	0.0000	0.0000	856	3.7493	0.0000	0.0000
751	2.4789	0.0004	0.0002	804	2.0804	0.0000	0.0000	857	3.7973	0.0000	0.0000
752	2.4878	0.0004	0.0002	805	2.0839	0.0000	0.0000	858	3.8453	0.0000	0.0000
753	2.4966	0.0004	0.0002	806	2.0874	0.0000	0.0000	859	3.8933	0.0000	0.0000
754	2.5055	0.0004	0.0002	807	2.0909	0.0000	0.0000	860	3.9413	0.0000	0.0000
755	2.5144	0.0004	0.0002	808	2.0944	0.0000	0.0000	861	3.9893	0.0000	0.0000
756	2.5233	0.0004	0.0002	809	2.0978	0.0000	0.0000	862	4.0373	0.0000	0.0000
757	2.5322	0.0004	0.0002	810	2.1013	0.0000	0.0000	863	4.0853	0.0000	0.0000
758	2.5410	0.0004	0.0002	811	2.1048	0.0000	0.0000	864	4.1333	0.0000	0.0000
759	2.5499	0.0004	0.0002	812	2.1083	0.0000	0.0000	865	4.1813	0.0000	0.0000
760	2.5500	0.0004	0.0002	813	2.1118	0.0000	0.0000	866	4.2293	0.0000	0.0000
761	2.5456	0.0004	0.0002	814	2.1152	0.0000	0.0000	867	4.2773	0.0000	0.0000
762	2.5412	0.0004	0.0002	815	2.1187	0.0000	0.0000	868	4.3253	0.0000	0.0000
763	2.5368	0.0004	0.0002	816	2.1222	0.0000	0.0000	869	4.3733	0.0000	0.0000
764	2.5324	0.0004	0.0002	817	2.1257	0.0000	0.0000	870	4.4213	0.0000	0.0000
765	2.5280	0.0004	0.0002	818	2.1292	0.0000	0.0000	871	4.4693	0.0000	0.0000
766	2.5236	0.0004	0.0002	819	2.1326	0.0000	0.0000	872	4.5173	0.0000	0.0000
767	2.5192	0.0004	0.0002	820	2.1361	0.0000	0.0000	873	4.5653	0.0000	0.0000

λ	a_w	b_w	b_{bw}
874	4.6133	0.0000	0.0000
875	4.6190	0.0000	0.0000
876	4.6657	0.0000	0.0000
877	4.7124	0.0000	0.0000
878	4.7591	0.0000	0.0000
879	4.8058	0.0000	0.0000
880	4.8525	0.0000	0.0000
881	4.8992	0.0000	0.0000
882	4.9459	0.0000	0.0000
883	4.9926	0.0000	0.0000
884	5.0393	0.0000	0.0000
885	5.0860	0.0000	0.0000
886	5.1327	0.0000	0.0000
887	5.1794	0.0000	0.0000
888	5.2261	0.0000	0.0000
889	5.2728	0.0000	0.0000
890	5.3195	0.0000	0.0000
891	5.3662	0.0000	0.0000
892	5.4129	0.0000	0.0000
893	5.4596	0.0000	0.0000
894	5.5063	0.0000	0.0000
895	5.5530	0.0000	0.0000
896	5.5997	0.0000	0.0000
897	5.6464	0.0000	0.0000
898	5.6931	0.0000	0.0000
899	5.7398	0.0000	0.0000
900	5.7413	0.0000	0.0000

Table 2: Value of A & B for Absorption by Chlorophyll

λ	A	B	λ	A	B	λ	A	B	λ	A	B
400	0.0263	0.282	496	0.0249	0.341	592	0.0057	0.081	686	0.0124	0.124
402	0.0271	0.281	498	0.024	0.332	594	0.0056	0.088	688	0.0102	0.107
404	0.028	0.282	500	0.023	0.321	596	0.0056	0.093	690	0.0083	0.086
406	0.029	0.281	502	0.022	0.311	598	0.0055	0.095	692	0.0067	0.065
408	0.0301	0.282	504	0.0209	0.3	600	0.0054	0.092	694	0.0054	0.042
410	0.0313	0.283	506	0.0199	0.288	602	0.0054	0.088	696	0.0044	0.015
412	0.0323	0.286	508	0.0189	0.275	604	0.0055	0.086	698	0.0036	-0.016
414	0.0333	0.291	510	0.018	0.26	606	0.0055	0.082	700	0.003	-0.034
416	0.0342	0.293	512	0.0171	0.249	608	0.0056	0.076			
418	0.0349	0.296	514	0.0163	0.237	610	0.0057	0.071			
420	0.0356	0.299	516	0.0156	0.224	612	0.0059	0.069			
422	0.0359	0.306	518	0.0149	0.211	614	0.006	0.066			
424	0.0362	0.313	520	0.0143	0.196	616	0.0062	0.063			
426	0.0369	0.316	522	0.0137	0.184	618	0.0063	0.064			
428	0.0376	0.317	524	0.0131	0.173	620	0.0065	0.064			
430	0.0386	0.314	526	0.0126	0.162	622	0.0066	0.068			
432	0.0391	0.318	528	0.0121	0.151	624	0.0067	0.071			
434	0.0395	0.324	530	0.0117	0.139	626	0.0068	0.074			
436	0.0399	0.328	532	0.0113	0.129	628	0.0069	0.076			
438	0.0401	0.332	534	0.0108	0.119	630	0.0071	0.078			
440	0.0403	0.332	536	0.0104	0.109	632	0.0073	0.08			
442	0.0398	0.339	538	0.01	0.1	634	0.0074	0.084			
444	0.039	0.348	540	0.0097	0.09	636	0.0075	0.088			
446	0.0383	0.355	542	0.0093	0.081	638	0.0076	0.093			
448	0.0375	0.36	544	0.009	0.073	640	0.0077	0.098			
450	0.0371	0.359	546	0.0086	0.066	642	0.0078	0.105			
452	0.0365	0.332	548	0.0083	0.059	644	0.0079	0.113			
454	0.0358	0.366	550	0.008	0.052	646	0.008	0.119			
456	0.0354	0.367	552	0.0076	0.044	648	0.0081	0.123			
458	0.0351	0.368	554	0.0072	0.036	650	0.0083	0.124			
460	0.035	0.365	556	0.0068	0.027	652	0.0085	0.125			
462	0.0347	0.366	558	0.0065	0.016	654	0.0089	0.124			
464	0.0343	0.368	560	0.0062	0.016	656	0.0095	0.122			
466	0.0339	0.369	562	0.0059	0.013	658	0.0104	0.12			
468	0.0335	0.369	564	0.0057	0.01	660	0.0115	0.121			
470	0.0332	0.368	566	0.0055	0.007	662	0.0129	0.125			
472	0.0325	0.371	568	0.0054	0.007	664	0.0114	0.131			
474	0.0318	0.375	570	0.0053	0.005	666	0.0161	0.137			
476	0.0312	0.378	572	0.0053	0.011	668	0.0176	0.143			
478	0.0306	0.379	574	0.0052	0.018	670	0.0189	0.149			
480	0.0301	0.377	576	0.0052	0.022	672	0.0197	0.153			
482	0.0296	0.377	578	0.0052	0.028	674	0.0201	0.157			
484	0.029	0.376	580	0.0053	0.035	675	0.0201	0.158			
486	0.0285	0.373	582	0.0054	0.04	676	0.02	0.159			
488	0.0279	0.369	584	0.0055	0.05	678	0.0193	0.158			
490	0.0274	0.361	586	0.0055	0.056	680	0.0182	0.155			
492	0.0267	0.356	588	0.0056	0.065	682	0.0166	0.148			
494	0.0258	0.349	590	0.0056	0.073	684	0.0145	0.138			

Efficiency factor Q_{bb}

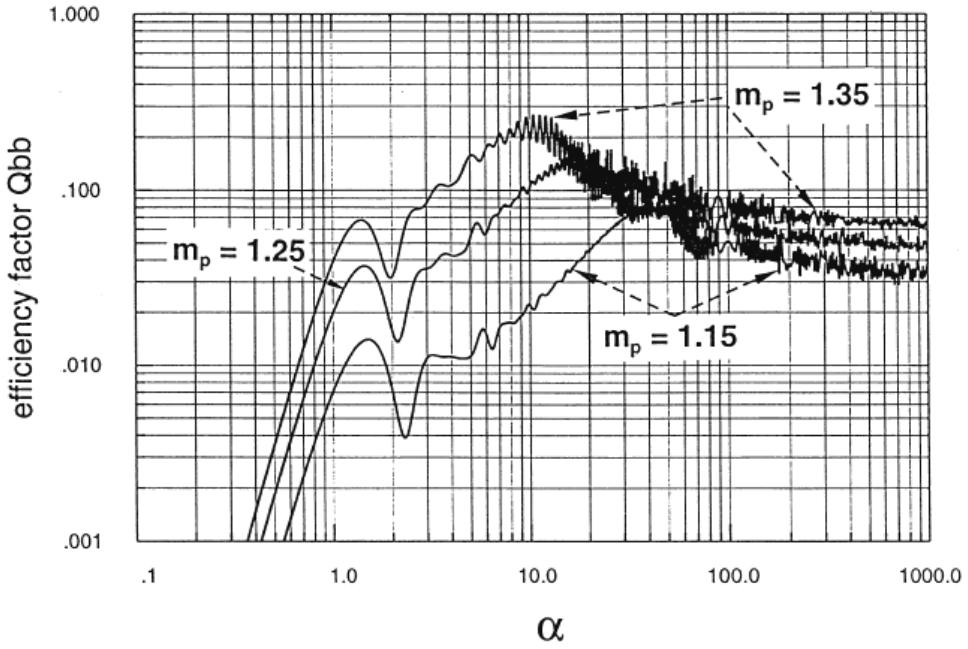

Figure I : Variation of the backscattering efficiency factor Q_{bb} of particle versus Mie parameter $\alpha=\pi D/\lambda_m$ for different sediment index m_p; Forget, 1999

Bibliography

Arenz R.F., Lewis, W.M. and Saunders, J.F. (1996), "Determination of chlorophyll and dissolved organic carbon from reflectance data for Colorado reservoirs", International Journal of Remote Sensing, 17, pp. 1547–1566.

American Public Health Association (1998), "Standard methods for the examination of water and wastewater", Section 1200 — chlorophyll (20th ed.), American Public Health Association.

Arnone, R.A., and Parsons, A.R. (2004), "Real-time use of ocean color remote sensing for coastal monitoring", In: Remote Sensing of the Coastal Environments.

Ahn Y.H. (1992), "Light backscattering efficiency and related properties of some phytoplankters. Deep-Sea Research, 39 (11/12):1835–1855, 1992.

Albert A. (2004), "Inversion technique for optical remote sensing in shallow water", PhD Dissertation, Hamburg university, 2004.

Bricaud A. et al. (1995), "Variability in the chlorophyll-specific absorption coefficients of natural phytoplankton: analysis and parameterization", Journal of Geophysical Research, 100 (C7):13321–13332, 1995.

Bissett, W.P. et al. (2001), "Resolving the impacts and feedback of ocean optics on upper ocean ecology. Oceanogr. 14: 30-53.

Bricaud, A., Morel, A., and L. Prieur (1983), "Optical efficiency factors of some phytoplankters", Limnology and Oceanography, 28, 816-832.

Bricaud, A., Morel, A. and Prieur, L. (1983), "Optical efficiency factors of some phytoplankters", Limnol. Oceanogr. **28:** 816-832.

Bissett, W.P. (2001), "Resolving the impacts and feedback of ocean optics on upper ocean ecology". Oceanogr. 14: 30-53.

Boney AD (1983), "Phytoplankton", The Institute of Biology's Studies in Biology no 52. Edward Arnold Publishers Limited, London, U. K.

Babin M, et al. (2003), "Light scattering properties of marine particles in coastal and open ocean waters as related to the particle mass concentration" Limnol. Oceanogr., 48(2), 2003, 843–859.

Bricaud, A., Morel, A. and L. Prieur (1981), "Absorption by dissolved organic matter of the sea (yellow substance) in the UV and visible domains", Limnology and Oceanography, **26**, 43-53.

Benny, A.H., Dawson, G.J. (1983), "Satellite imagery as an aid to bathymetric charting of the Red Sea", The Cartographic Journal 20, 5–16.

Bhargava, D. S., and Mariam, D. W. (1991), "Effects of suspended particle size and concentration on reflectance measurement", Photogrammetric Engineering and Remote Sensing, 57, 519–529.

Bhargava D.S. and D.W. Mariam (1991), "Light penetration depth, turbidity and reflectance related relationships and models", Journal of Photogrammetry & Remote Sensing, 46 (1991) 217-230.

Buntzen, R. R., (1996), "Analytical Spectral Devices FieldSpec Radiometric calibration for Tower I": SITAC in-house report, 1996.

Bricaud A., A. Morel, and L. Prieur (1981), "Absorption by dissolved organic matter of the sea (yellow substance) in the UV and visible domains", Limnology and Oceanography, 26 (1):43–53, 1981.

Bartolucci R. M., B. F. Robinson and L. F. Silva (1977), "Field measurements of the spectral response of natural waters", Photogrammetry Engineering and Remote Sensing, Vol 43, pp 595–598.

Curtiss B. and S.L. Ustin (1988), "Spectral changes in Ponderosa Pine associated with natural ozone exposure", Proc. U.S. Forest Service Forest Response Program Annual Meeting, Corpus Christi, Texas, February 23 - 26.

Chen Z., Hanson J. D. and Curran P. J. (1991), "The form of the relationship between suspended sediment concentration and spectral reflectance: its implication for the use of Daedalus 1268 data". Int. Journal of Remote Sensing, Vol.1 2, pp 215- 222.

Curtiss B. and Goetz, A. F. H. (1994), "Field Spectrometry: Techniques and Instrumentation", Presented at the International Symposium on Spectral Sensing Research, July 1994.

Choubey, V.K. (1998), "Laboratory experiment, field and remotely sensed data analysis for the assessment of suspended solids concentration and secchi depth of the reservoir surface water", International Journal of Remote Sensing, 19, pp. 3349–3360.

Carlough, L.A. (1994), "Origins, structure and trophic significance of amorphous seston in black water river", Freshwater Biology, 31:227-237.

Carder K. L. (1991), "Reflectance model for quantifying chlorophyll a in the presence of productivity degradation products", J. Geophys. Res. 96, 20,599-20,611 (1991).

Danson F. M. & Plummer S. E. (1995), "Advances in Environmental Remote Sensing", John Wiley & Sons Ltd., page 171, 1995.

Dekker, A.G., Malthus, T.J. and Seyhan, E. (1991), "Quantitative modeling of inland water quality for high-resolution mss systems", IEEE Transactions on Geoscience and Remote Sensing, 29, pp. 89–95.

Dekker, A.G. and S.W.M. Peters (1993), "The use of the Thematic Mapper for the analysis of eutrophic lakes: A case study in The Netherlands", Int. J. Remote Sensing 14: 799-822.

Dekker, A.G. (1997), "Operational tools for remote sensing of water quality: A prototype tool kit", Vrije Universiteit Amsterdam, Institute for environmental studies. BCRS Report 96-18.

Doxaran D., Jean-M Froidefond & P. Castaing (2003), "Remote-sensing reflectance of turbid sediment-dominated waters. Reduction of sediment type variations and changing illumination conditions effects by use of reflectance ratios", Applied Optics, Volume 42, Issue 15, pp. 2623-2634.

Doxaran D. et al. (2004), "Estimation pf surface reflection effects on upwelling radiance field measurements in turbid waters", Journal of Optics A: Pure and Applied Optics, 6(2004), 690-697.

Doxaran, D., Froidefond, J.M. and Castaing, P. (2002), "A reflectance band ratio used to estimate suspended matter concentrations in sediment-dominant coastal waters", International Journal of Remote Sensing, 23, pp. 5079–5085.

Dekker, A. G. (1997a), "The relationship between inherent optical properties and reflectance spectra in turbid inland waters", Remote Sensing Reviews, **15**, 59–74.

Dall'Olmo (2005), "Effect of bio-optical parameter variability on the remote estimation of chlorophyll-a concentration in turbid productive waters: experimental results", Applied Optics, Vol. 44(3),412-422.Bhargava, D. S., and Mariam, D. W. (1990), "Spectral reflectance relationships to turbidity generated by different clay materials", Photogrammetric Engineering and Remote Sensing, 56, 225–229.

Elisabeth H.S. (2001), "Modeling underwater light climate in relation to sedimentation, resuspension, water quality and autotrophic growth", E.P.H. Best & J.W. Barko (eds), Modelling Sediment Resuspension, Water Quality and Submersed Aquatic Vegetation. Kluwer Academic Publishers. Netherlands.

Engman E. T. and R. J. Gurney (1991), "Remote Sensing of Hydrology", University Press Cambridge, 1991.

Fischer J., and Kronfeld U. (1990), "Sun stimulated chlorophyll fluorescence 1: influence of oceanic properties". International Journal of Remote Sensing, Vol.1 1, 2125 - 2147.

Forget, P., Ouillon, S., Lahet, F., and Broche, P. (1999), "Inversion of reflectance spectra of non-chlorophyllous turbid coastal waters", Remote Sens. Environ. 68:264–272

Forget P. et al. (2001), "Reflectance sensitivity to solid suspended sediment stratification in coastal water and inversion: a case study", Remote Sensing of Environment 77 (2001) 92– 103.

Fraser, R.N. (1998), "Hyperspectral remote sensing of turbidity and chlorophyll a among Nebraska Sand Hills lakes", International Journal of Remote Sensing, 19, 1579–1589.

Gin, K.Y.et al., 2002, Application of spectral signatures and colour ratios to estimate chlorophyll in Singapore's coastal waters. Estuarine, Coastal and Shelf Science, 55, pp. 719–728.

Gin, K.Y.H., Koh, S.T. and Lin, I.I. (2003), "Spectral irradiance profile of suspended marine clay for the estimation of suspended sediment concentration in tropical waters", International Journal of Remote Sensing, 24, pp. 3235–3245.

Gin, K.Y.H. (2002), "Study of the effect of suspended marine clay on the reflectance spectra of phytoplankton", International Journal of Remote Sensing, 23, pp. 2163–2178.

Gordon, H. R., and A. Y. Morel (1983), "Remote assessment of ocean color for interpretation of satellite visible imagery: A review lecture notes on coastal and estuarine studies", 113 pp., Springer-Verlag, New York.

Gordon, H. R. et al. (1983), "Phytoplankton pigment concentrations in the Middle Atlantic Bight: comparison of ship determinations and CZCS estimates", Applied Optics, 22(1), 20-36.

Gordon, H. R., Brown, O. B., and Jacobs, M. M. (1975), "Computed relationships between the inherent and apparent optical properties of a flat homogeneous ocean. Applied Optics, 14, 417–427.

Goetz, A.F.H. and W.M. Calvin (1987), "Imaging spectrometry: Spectral resolution and analytical identification of spectral features", Imaging Spectros. II, G.Vane, Ed., Proc. SPIE, 834, 158-165.

Goetz, A.F.H. (1992b), "Principles of Narrow Band Spectrometry, in The Visible and IR: Instruments and Data Analysis in Imaging Spectroscopy: Fundamentals and Prospective Applications", F. Toselli and J. Bodechtel, Eds., pp. 21-32, Brussels and Luxembourg.

Gitelson, A. (1993), "Algorithms for remote sensing of phytoplankton pigments in inland waters", Advances in Space Research, 13, pp. 197–201.

Gitelson, A. (1992), "The peak near 700nm on radiance spectra of algae and water: relationship of its magnitude and position with chlorophyll concentration", International Journal of Remote Sensing, 13, pp. 3367–3373.

Gitelson, A. et al. (1995), "Remote estimation of chlorophyll concentration in polluted marine waters in Haifa Bay, Southeastern Mediterranean", Proceedings of SPIE, 2503, pp. 44–54.

Gitelson, A., G. et al., (1993), "Quantitative remote sensing methods for real-time monitoring of inland waters quality. International Journal of Remote Sensing 14:1269-1295.

Goodin, D. et al. (1993), "Analysis of suspended solids in water using remotely sensed high resolution derivative spectra", Photogrammetric Engineering and Remote Sensing, 59, pp. 505–510.

Gordon H. R. (1988), "A semianalytic radiance model of ocean color", J. Geophys. Res. 93, 10,909-10,924, 1988.

Goodin, D.G., et al., (1993), "Analysis of suspended solids in water using remotely sensed high resolution derivative spectra", Photogrammetric Engineering and Remote Sensing, 59, pp. 505–510

Gould R.W., R. A. Arnone (1997), "Remote sensing estimates of inherent optical properties in a coastal environment", Remote sensing of Environment, 61:290-301, 1997.

Hale, G. M., and Querry, M. R. (1973), "Optical constants of water in the 200nm to 200 μm wavelength region". Appl. Opt. 12:555–563.

Harding, L., Itsweire, E. and Esaias, W. (1994), "Estimates of phytoplankton biomass in the Chesapeake Bay from aircraft remote sensing of chlorophyll concentrations, 1989–92", Remote Sensing of Environment, 49, pp. 41–56.

Han L.& D. C. Rundquist (1994), "The response of both surface reflectance and the underwater light filed to various levels of suspended sediments: preliminary results", Photogrammetric Engineering & Remote Sensing, Vol. 60, No. 12, 1463-1471.

Han L. (1997), "Spectral reflectance with varying suspended sediment concentrations in clear and algae-laden waters", Photogrammetric Engineering and Remote Sensing, 63, pp. 701–705.

Han L. and Rundquist, D. (1997), "Comparison of NIR/red ratio and first derivative of reflectance in estimating algal-chlorophyll concentration: a case study in a turbid reservoir", Remote Sensing of Environment, 62, pp. 253–261.

Han L., 2005, "Estimating chlorophyll-a concentration using first-derivative spectra in coastal water", International Journal of Remote Sensing, Vol. 26, No. 23, 10 December 2005, 5235–5244.

Hooker S. and Maritorena S. (2000), "An Evaluation of Oceanographic Radiometers and Deployment Methodologies", Journal of Atmospheric and Oceanic Technology, American Meteorological Society, Volume 17, 811-830.

Hooker S. (2002), "An evaluation of above- and in-water methods for determining water-leaving radiances", Journal of Atmospheric and Oceanic Technology, American Meteorological Society, Volume 19, 486-515.

Harrington, J. A., Schiebe, F. R., and NIX, J. F. (1992), "Remote sensing of Lake Chicot, Arkansas: monitoring suspended sediments, turbidity and Secchi depth with Landsat MSS data", Remote Sensing of Environment, 39, 15–27.

Hakvoort J.H.M., "Absorption of light by surface water", PhD thesis, Delft University of Technology, 1994. ISBN 90-407-1023-6.

Højerslev, N. K. (1998), "Spectral light absorption by gelbstoff in coastal waters displaying highly different concentrations", In: Proceedings, Ocean Optics XIV, S. G. Ackleson and J. Campbell (eds.), Office of Naval Research, Washington, DC.

Hadjimitsis D.G. et al. (2004), "An assessment of the effectiveness of atmospheric correction algorithms through remote sensing of some reservoirs", International Journal of Remote Sensing, 20, pp. 3651–3674, 2004.

IRTCES, (2005), "Fluvial Processes, International workshop", International Research & Training Center on Erosion and Sedimentation (IRTCES), China, September 11-19, 2005.

Ishfaq A. (2002), "Water and New Technologies", Global Change and Impact Studies Centre, Islamabad, Pakistan, p 1-25,41.

IOCCG, S. Sathyendranath (2000), "Remote Sensing of Ocean Colour and Other Complex Waters", International Ocean-Color Coordinating Group, IOCCG Report Number 3, 140pp.

Johnson, R. (1978), "Mapping of Chlorophyll a distribution in coastal zones", Photogrammetric Engineering and Remote Sensing, 44, pp. 617–624.

Julien, R.Y. (1995), "Erosion and sedimentation", Cambridge University Press, New York, pp. 279.

Jensen John R. (2000), "Remote sensing of the environment: An earth resource perspective", Pearson Education Inc., 2000.

Jupp, D.L.B. (1988), "Background and extensions to depth of penetration (DOP) mapping in shallow coastal waters", Proc. Symposium on Remote Sensing of the Coastal Zone IV. Gold Coast, Queensland, pp. 2.1–2.19.

Jordan, T.E., D.L. Cornell, J. Miklas, and D.E. Weller (1991), "Long-term trends in estuarine nutrients and chlorophyll, and short-term effects of variation in watershed discharge", Marine Ecology Progress Series, 75:121-132.

Jensen, J. R. et al.(1991), "Remote sensing offers an alternative for mapping wetlands", Geo Info. Sys., 1, 46-53.

Jensen, J.R. (2005), "Introductory Digital Image Processing, A Remote Sensing Perspective", Upper Saddle River, New Jersey: Prentice Hall.

Jupp, D.L., J.T.O. Kirk, and G.P. Harris (1994a), "Detection, identification and mapping of cyanobacteria using remote sensing to measure the optical quality of turbid inland waters", Australian Journal of Freshwater Research 45:801-828.

Jupp, D.L., et al., (1994b), "Monitoring optical water quality of the Hawkesbury River using airborne remote sensing. CSIRO Division of Water Resources, Consultancy Report No. 94/9.

Kalle, K. (1966), "The problem of the gelbstoff in the sea", Oceanography Marine Biology Annual Review 4: 91-104.

Kirk, J.T.O. (1980), "Spectral absorption properties of natural waters: contribution of the soluble and particulate fractions to light absorption in some inland waters of south-eastern Australia. Aust. J. Mar. Freshwater Res. 31: 287-296.

Kuo, C. Y., and Cheng, R. Y. K. (1978), "Laboratory requirements for in situ and remote sensing of suspended material", Technical report (NASA-CP-145367), Old Dominian University, Norfolk, Virginia, USA., pp. 29-31.

Khorram, S. (1985), "Development of water quality models applicable throughout the entire San Francisco Bay and Delta", Photogrammetric Engineering and Remote Sensing, 51, pp. 53–62.

Kubotera H. (2006) "The factors and assumed mechanisms of the hardening of red soils and yellow soils in subtropical Okinawa Island, Japan", JARQ 40 (3), 197 – 203.

Kirk, J. T. O. (1991), "Volume scattering function, average cosines, and the underwater light field", Limnology and Oceanography, 36, 455–467.

Kirk, J. T. O. (1994), "Light and Photosynthesis in Aquatic Eco- systems", Cambridge University Press, Cambridge, 509 pp, 1994.

Kahlown M.A. and Maheed A. (2001), "COMSATS 1st meeting on Water Resources in The South: Present Scenario and Future Proposals", Nov. 2001, Islamabad, Pakistan.

Kopelevich, O. V. (1989), "Light spectral absorption by yellow substance of ocean water", Okeanologiya **29:** 409-414.

Lodhi M. A, Rundquist C. and L. Han (1997), "The potential for remote sensing of loess soils suspended in surface waters", Journal of the American Water resources Association, Vol. 33, No. 1, 111–117,1997.

Loynachan T. E., et al. (1999), "Sustaining our soils and society", Alexandria: American Geological Institute, Soil Science Society of America, and US-DA, 66 pp, 1999.

Lavery, P., Pattiaratchi, C., Wyllie, A., and Hick, P. (1993), "Water quality monitoring in estuarine water using the Landsat Thematic Mapper", Remote Sensing of Environment, 46, 268–280.

Lal R. (2001), "Soil degradation by erosion. Land Degradation and Development", 12: 519 – 539, 2001.

Lee Z., et al.(1998) "Hyperspectral remote sensing for shallow waters.1.A semianalytical model. Applied Optics, 37 (27):6329–6338, 1998.

Liu Y., Islam, M.A. and GAO, J. (2003), "Quantification of shallow water quality parameters by means of remote sensing", Progress in Physical Geography, 27, pp. 24–43.

Lathrop, R.G. and T.M. Lillesand, (1986), "Use of Thematic Mapper Data to Assess Water Quality in Green Bay and Central Lake Michigan", Photogrammetric Engineering and Remote Sensing. 52(5): 671-680.

Mahmood K. (1987) "Reservoir sedimentation: impact, extent and mitigation", World Bank Technical Paper 71.

Mazar, A. S., Martin, M., Lee, M., and Dolomon, J. E. (1988), "Image processing software for imaging spectrometry data analysis", Remote Sensing of Environment, 24, 201–211.

Mobley C. (1989), "A numerical model for computation of radiance distributions in natural waters with wind roughened surfaces", Limnology and Oceanography, 34(8), 1473-1283.

Mobley, C.D. (1994), "Light and Water: Radiative Transfer in Natural Waters", Academic Press, San Diego.

Milton E., et al., 2006. Progress in Field Spectroscopy, IEEE.

Makisara, K. (1994), "A system for geometric and radiometric correction of airborne imaging spectrometer data", Int. Geosci. Remote Sens. Symp pp.851-853, ISBN: 0-7803-1497-2, California, USA, 8-12 August.

Mishra, D. R., S. Narumalani, D. Rundquist, M. Lawson, and R. Perk (2007), "Enhancing the detection and classification of coral reef and associated benthic habitats: A hyperspectral remote sensing approach", Journal of Geophysical Research, 112, C08014, doi:10.1029/2006JC003892.

Matthew, M. W. et al., (2003), "Atmospheric correction of spectral imagery: Evaluation of the FLAASH algorithm with AVIRIS data", Proc. SPIE Algorithms and Technologies for Multispectral, Hyperspectral, and Ultraspectral Imagery, IX(5093), 474-482.

Melesse A. M., et al., (2007), "Remote Sensing Sensors and Applications in Environmental Resources Mapping and Modeling", Sensors Journal, 7, 3209-3241, 2007.

Morrow, J.H. et al. (2000), "A bio-optical approach to reservoir monitoring in Los Angeles", Limnology and Lake Management-Archives for Hydrobiolia Special Issues, Advances in Limnology, 55:171-191.

Murakami M. (1995), "Managing Water for Peace in the Middle East:Alternative Strategies", The United Nations University Press, p 45-52.

Morel, A. (1974), "Optical properties of pure seawater. In: Optical Aspects of Oceanography", N. G. Jerlov and E. Steemann Nielsen (eds.), Academic Press Inc., New York, 1-24.

Morel, A. (1980), "In-water and remote measurement of ocean color. Boundary-Layer", Meteorology, 18, 177–201.

Mobley Curtis D. (2004), "Light and Water: Radiative Transfer in Natural Waters", Academic Press, USA.

Morel A. (1988), “Optical modeling of the upper ocean in relation to its biogenous matter content (case I waters)”, J of Geophysical Research, 93 (C9):10749–10768, 1988.

Morel A. and Louis Prieur (1977), “Analysis of variation in ocean color”, Limnology and Oceanography, Volume 22, Issue 4, 709-722, 1977.

Nazir Ahmad. (1993), “Irrigated Agriculture of Pakistan”, Shahzad Nazir Publishers Lahore.

Novo, E.M.M. et al. (1989), “The effect of viewing geometry and wavelength on the relationship between reflectance and suspended sediment concentration”, International Journal of Remote Sensing, 10, pp. 1357–1372.

Nichol, J.E. (1993), “Remote sensing of water quality in the Singapole–Johor–Riau growth triangle”, Remote Sensing of Environment, 43, pp. 139–148.

Novo, E. M. M., Hansom, J. D., and Curran, P. J. (1989 a), “The effect of sediment type on the relationship between reflectance and suspended sediment concentration”, International Journal of Remote Sensing, Vol. 1 0, pp. 1283 - 1289.

Nagashima S., 2003, Res. Rep. Kochi University, (Nat. Sci.) Volume 52, 2003.

Pozdnyakov D. and H. Grassl (2003), “Colour of inland and coastal waters - a methodology for its interpretation”. Springer Verlag Berlin/Heidelberg/New York, Praxis Publishing Ltd. Chichester, 2003.

Petzold T.J. (1977), “Volume scattering functions for selected ocean waters, pages 152–174. Light in the sea. Dowden, Hutchinson & Ross, Strouddberg, 1977.

Prieur L. and S. Sathyendranath (1981), “An optical classification of coastal and oceanic waters based on the specific spectral absorption curves of phytoplankton pigments, dissolved organic matter, and other particulate materials”, Limnology and Oceanography, 26 (4):671–689, 1981.

Quibell, G. (1991), “The effect of suspended sediment on reflectance from freshwater algae”, International Journal of Remote Sensing, 12, pp. 177–182.

Roesler C.S., M.J. Perry, and K.L. Carder (1989), “Modeling in situ phytoplankton absorption from total absorption spectra in productive inland marine waters. Limnology and Oceanography, 34 (8):1510–1523, 1989.

Ritchie, J.C., Schiebe f. R., & Mchenary J. R. (1976), “Remote sensing of suspended sediments in surface waters”, Photogrammetric Engineering and Remote sensing, 42, 1539-1545.

Ritchie, J. C., Cooper, C. M., and Yongquing, J. (1987), “Using Landsat multi spectral scanner data to estimate suspended sediments in Moon Lake, Mississippi”, Remote Sensing of Environment, 23, 65–81.

Ritchie J.C. and C. M. Cooper (1988), “Comparison of Measured Suspended Sediment concentration with Suspended Sediment Concentrations Estimated from Landsat MSS data”, Int. Jour. of Remote Sensing. Vol. 9, No. 3, pp. 379-387.

Ritchie, J.C., Cooper, C.M. and Schiebe, F.R. (1990), The relationship of MSS and TM digital data with suspended sediments, chlorophyll, and temperature in Moon lake, Mississippi. Remote Sensing of Environment, 33, pp. 137–148.

Ritchie, J.C. & F.R. Schiebe (2000), “Remote Sensing in Hydrology and Water Management”, Water Quality In: G.A. Schultz and E.T. Engman (eds.) Springer-Verlag, Berlin, Germany, pp. 287-303, 351-352.

Richardson L., (1996), "Remote sensing of algal bloom dynamics", BioScience, 46, pp. 492–501.

Rong-Rong Li, Yoram J. Kaufman, Bo-Cai Gao, & Curtiss O. Davis (2003), "Remote Sensing of Suspended Sediments and Shallow Coastal Waters", IEEE Transaction on Geoscience and Remote sensing. Vol. 41, No. 3 PP. 559.

Rundquist D. (2001), "Field techniques in remote sensing: Learning by doing", Geocarto International, Vol.16, No. 1, March 2001.

Rundquist D., et al. (2004), "Collecting spectral data over cropland vegetation using machine positioning versus hand-held positioning of the sensor", Computers and Electronics in Agriculture, 43, 173-178.

Salisbury John W. (1998), "Spectral measurements field guide", Defense Technology Information Center , Report No. ADA362372, April 23, 1998.

Streck A. N., Rundquist D. and Connot J., (2003) "Spectral Signature of selected soils", Revista Brasileria de Agrometeorologia, Santo Maria, Vol. 11, No.1, pp. 181-184.

Sathyendranath S. (1989), "A three-component model of ocean colour and its application to remote sensing of phytoplankton pigments in coastal waters", International Journal of Remote Sensing, 10 (8):1373–1394, 1989.

Shifrin, K. S. (1988), "Physical Optics of Ocean Water", American Institute of Physics, New York, 285 p.

Sathyendranath S., L. et al. (1987), "Variations in the spectral values of specific absorption of phytoplankton", Limnology and Oceanography, 32 (2):403–415, 1987.

Sathyendranath, S., and T. Platt (1997), "Analytical model of ocean color". Appl. Opt. 36:2620–2629.

Shafique, N.A., B.C. Autrey, F. Fulk, and S.M. Cormier (2001), "Hyperspectral narrow wavebands selection for optimizing water quality monitoring on the Great Miami River, Ohio", Journal of Spatial Hydrology 1(1):1-22.

Stramski, D., Bricaud, A., and Morel, A. (2001), "Modeling the inherent optical properties of the ocean based on the detailed composition of the planktonic community", Appl. Opt. 40: 2929-2945.

Sathyendranath S. (2004), "A multispectral remote sensing study of coastal waters of Vancouver Island", Int. J. Remote Sensing, Vol. 25, NO. 5, 893–919, 2004.

Smith, R. C., and Baker, K. (1981), "Optical properties of the clearest natural waters", Appl. Opt. 20(2):177–184.

Singh G. et al. (1992), "Soil erosion rates in India", J. Soil Water Conservation, 47: 93 – 95. 1992.

Thenkabail, P.S.; Enclona, E.A.; Ashton, M.S.; Legg, C.; Jean De Dieu, M. Hyperion, IKONOS, ALI, and ETM+ sensors in the study of African rainforests. Remote Sensing of Environment 2004, 90, 23-43.

Thiemann, S. and Kaufmann, H. (2000), "Determination of chlorophyll content and trophic state of lakes using field spectrometer and IRS-1C satellite data in the Mecklenburg Lake District, Germany", Remote Sensing of Environment, 73, pp. 227–235.

Thuillier G. (2003), “The solar spectral irradiance from 200 to 2400 nm as measured by the solspec spectrometer from the Atlas and Eureca missions”, Solar Physics 214: 1–22, Kluwer Academic Publishers, Netherlands, 2003.

Tassan S. (1994), “Local algorithms using SeaWiFS data for the retrieval of phytoplankton, pigments, suspended sediment, and yellow substance in coastal waters”, Vol. 33, No. 12 / Applied Optics.

Tolk B. L., L. Han, D. C. Rundquist (2000), “The impact of bottom brightness on spectral reflectance of suspended sediments”, International Journal of Remote Sensing, Volume 21, Issue 11 July 2000 , pages 2259 – 2268.

Tyler A. N. et al. (2006), “Remote sensing of the water quality of shallow lakes: A mixture modeling approach to quantifying phytoplankton in water characterized by high-suspended sediment”, International Journal of Remote Sensing, Vol. 27, No. 8, 1521–1537, April 2006.

User Guide (2001), “Advanced Spaceborne Thermal Emission and Reflection Radiometer Higher-Level Product Version 2.0”, JPL D-20062, California Institute of Tech., 2001.

Vittorio E. Brando and A. G. Dekker (2003), “Satellite hyperspectral remote sensing for estimation estuarine and coastal water quality”, IEEE Transactions on Geoscience and remote sensing, Vol. 41, No. 6, 2003.

Vorosmarty, C. J., Meybeck, M., Fekete, B. and Sharma, K. (1997), “The potential impact of neo-Cartorization on sediment transport by the global network of rivers”, In: Proceedings of the Rabat Symposium, IAHS Publication No. 245,261-273.

Vermote, E. F. et al. (1994), “Second Simulation of the Satellite Signal in the Solar Spectrum (6S)”, 6S User Guide Version 6.0, 134 pp., NASA-GSFC, Greenbelt, Maryland.

Vermote E. F. et al. (1997), “Second simulation of the satellite signal in the solar spectrum: an overview”, IEEE Transactions on Geoscience and Remote Sensing, 35 (3), 675-686, 1997.

Van de Hulst, H.C. (1981), “Light Scattering By Small Particles”, Dover, New York.

Walling, D. E. and Webb, B. W. (1996), “Erosion and Sediment Yield: global overview”, Proceedings of the Exeter Symposium, July 1996, IAHS Publication No. 236, 3-19.

Whitlock, C. H. et al. (1981), “Comparison of reflectance with backscatter and absorption parameters for turbid waters”, Applied Optics, 20, 517–522.

WAPDA (1998), “Tarbela Dam Sediment management Study” Volume 2, March 1998.

Tarbela second periodic inspection (1991), Volume: 2, Sec: 20.5 (b), page 20-12.

Waterbury John (1979), “Hydropolitics of the Nile Valley”, Syracuse, N.Y., Syracuse University Press.

White W. R (2005), “Review of Current Knowledge, World water storage in man-made reservoirs”, Foundation for Water Research, FR/R0012, April 2005.

Zimmerman, R. C. (2000), “Radiative transfer and photosynthesis of aquatic vegetation in turbid coastal waters”, Hydrobiologia, 2000.